MALCOLM STUART PURDEY

Hydrogen Peroxide Sensing for Reproductive Health

Hydrogen Peroxide Sensing for Reproductive Health

by Malcolm Stuart Purdey

THE UNIVERSITY of ADELAIDE

A Thesis submitted for the degree of

Doctor of Philosophy

in the

Faculty of Science

School of Physical Sciences

December 2015

For Ainsley: my patient, beautiful, longsuffering wife.

If we knew what it was we were doing, it would not be called research, would it?

Albert Einstein

CONTENTS

LIST OF FIGURES

LIST OF SCHEMES

PUBLICATIONS

Journal Papers

These papers comprise full chapters in this thesis:

Purdey, M. S.; Connaughton, H. S.; Whiting, S.; Schartner, E. P.; Monro, T. M.; Thompson, J. G.; Aitken, R. J.; Abell, A. D., Boronate probes for the detection of hydrogen peroxide release from human spermatozoa. *Free Radical Biology and Medicine* **2015,** *81* (0), 69-76.

Purdey, M. S.; Thompson, J. G.; Monro, T. M.; Abell, A. D.; Schartner, E. P., A dual sensor for pH and hydrogen peroxide using polymer-coated optical fibre tips. *Sensors* **2015**, *15* (12), 31904-31913.

Purdey, M. S.; Abell, A. D., New BODIPY-based probes for the detection of hydrogen peroxide. **2015**, *In Preparation.*

These publications represent other work by the author described in this thesis:

Sutton-McDowall, M. L.; Purdey, M.; Brown, H. M.; Abell, A. D.; Mottershead, D. G.; Cetica, P. D.; Dalvit, G. C.; Goldys, E. M.; Gilchrist, R. B.; Gardner, D. K.; Thompson, J. G., Redox and anti-oxidant state within cattle oocytes following in vitro maturation with bone morphogenetic protein 15 and follicle stimulating hormone. *Molecular Reproduction and Development* **2015,** *82* (4), 281-294.

Sutton-McDowall, M. L.; Wu, L.; Purdey, M.; Brown, H. M.; Abell, A. D.; Goldys, E. M.; MacMillan, K. L.; Robker, R. L.; Thompson, J. G., Non-Esterified Fatty Acid-Induced Endoplasmic Reticulum Stress in Cattle Cumulus Oocyte Complexes Alters Cell Metabolism and Developmental Competence. *Biology of Reproduction* **2015**, *Available online,* doi:10.1095/biolreprod.115.131862

Zuber, A.; Purdey, M.; Schartner, E.; Forbes, C.; van der Hoek, B.; Giles, D.; Abell, A.; Ebendorff-Heidepriem, H., Detection of gold nanoparticles with different sizes using absorption and fluorescence based method. *Sensors and Actuators B: Chemical* **2016**, *227*, 117-127.

Schartner, E. P.; Henderson, M. R.; Purdey, M. S., Dhatrak, D.; Monro, T. M.; Gill, P. G.; Callen, D. F., Tumour detection in human tissue samples using a fibre tip pH probe. **2016**, *In preparation*.

Patent

Australian patent application 2015902890 – "*Detection of Gold Nanoparticles*" (Deep Exploration Technologies CRC Limited) – 21 July **2015**

Conference presentations

Conference paper:

Purdey, M. S.; Schartner, E. P.; Sutton-McDowall, M. L.; Ritter, L. J.; Thompson, J. G.; Monro, T. M.; Abell, A. D., Localised hydrogen peroxide sensing for reproductive health. *Proceedings of SPIE* **2015,** *9506*, 950614.

Invited talks:

Purdey, M. S.; Schartner, E. P.; Heng, S.; Zhang, X. Z.; Stubing, D. B.; Monro, T. M.; Abell, A. D.; Functionalisation of Optical Fibres for Biosensing Applications. *ANFF Research Showcase,* Canberra, ACT, Australia, November **2014**.

Purdey, M. S.; Schartner, E. P.; Sutton-McDowall, M. L.; Ritter, L. J.; Monro, T. M.; Thompson, J. G.; Abell, A. D.; A Non-invasive Sensor for Hydrogen Peroxide and pH. *Society for Reproductive Biology,* Adelaide, SA, Australia, August **2015**.

Conference posters:

Purdey, M. S.; Connaughton, H. S.; Whiting, S.; Thompson, J. G.; Aitken, R. J.; Abell, A. D.; Reactive Oxygen Species Detection in Human Spermatozoa with Aryl Boronates. *RACI National Congress,* Adelaide, SA, Australia, December **2014**.

Purdey, M. S.; Schartner, E. P.; Monro, T. M.; Aitken, R. J.; Thompson, J. G.; Abell, A. D.; Hydrogen Peroxide Sensing for Reproductive Health. *249th ACS Nation Congress,* Denver, CO, USA, March **2015**.

ABBREVIATIONS

4HNE	4-Hydroxynonenal
AA	Arachidonic Acid
ACN	Acetonitrile

APTES	3-(Aminopropyl)triethoxysilane
BODIPY	Boron Dipyrromethene
$CDCl_3$	Deuterated chloroform
$CHCl_3$	Chloroform
CPF1	Carboxy Peroxyfluor-1
CPF1-NHS	N-Succinimide ester of Carboxy Peroxyfluor-1
DCFH	2',7'-Dichlorohydrofluorescein diacetate
DCM	Dichloromethane
DHE	Dihydroethidium
DMF	Dimethylformamide
DMSO	Dimethylsulfoxide
DPI	Diphenyl Iodonium
EEPF1	2-Ethoxy(2-Ethoxyethoxy) Peroxyfluor-1
ETC	Electron Transport Chain
FCR2	Flavin Coumarin Redox sensor 2
FRET	Förster Resonance Energy Transfer
H_2O_2	Hydrogen Peroxide
HEPES	4-(2-Hydroxyethyl)piperazine-1-ethanesulfonic acid
HNO	Nitroxyl
HPLC	High Performance Liquid Chromatography
HRMS	High Resolution Mass Spectrometry
IVF	*In Vitro* Fertilisation
MeOH	Methanol
MitoPY1	Mitochondrial PeroxyYellow-1

MRI	Magnetic Resonance Imaging
MSR	MitoSOX Red
$NaCNBH_3$	Sodium Cyanoborohydride
NbzB	NitrobenzoylBODIPY
NbzF	NitrobenzoylFluorescein
NCR3	NicotinamideCoumarin Redox sensor 3
NEFA	Non-Esterified Fatty Acid
NMR	Nuclear Magnetic Resonance
NO	Nitric Oxide
NPF1	Naphthoperoxyfluor-1
NpFR1	Naphthalimide Flavin Redox sensor 1
$O_2^{\bullet-}$	Superoxide
^{-}OCl	Hypochlorite
$^{\bullet}OH$	Hydroxyl radical
$ONOO^-$	Peroxynitrite
PB1	PeroxyBODIPY-1
PBS	Phosphate Buffer Solution
PEG	Poly Ethylene Glycol
PET	Photoinduced Electron Transfer
PF1	Peroxyfluor-1
ROS	Reactive Oxygen Species
SE	Standard Error of the mean
SNARF2	Seminaphthorhodofluor-2
TBHP	Tert-Butyl Hydroperoxide

GLOSSARY OF FLUORESCENT PROBES

Carboxyperoxyfluor-1 (**CPF1**)

See **Chapters 2-4**, **6** and **7**

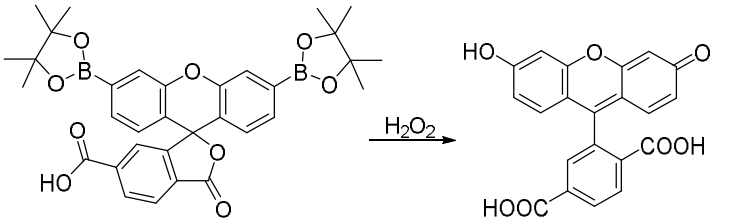

CPF1
Non-Fluorescent

Carboxyfluorescein
Exc. 485nm; Em. 525nm

2',7'-Dichlorohydrofluorescein Diacetate (**DCFH**)

See **Chapters 1** and **2**

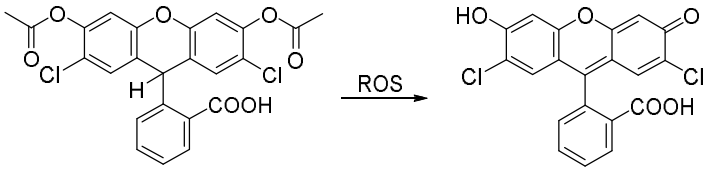

DCFH
Non-Fluorescent
(Acetates removed by intracellular esterases)

Dichlorofluorescein
Exc. 485nm; Em. 525nm

Dihydroethidium (**DHE**)

See **Chapters 1** and **2**

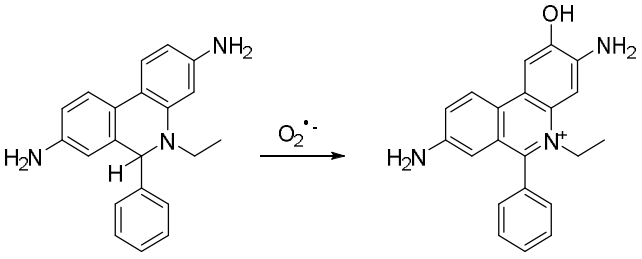

DHE
Non-Fluorescent

2-hydroxyethidium
Exc, 500 nm; Em. 580 nm

2(2-Ethoxyethoxy)ethoxy Peroxyfluor-1 (**EEPF1**)

See **Chapters 2**, **6** and **7**

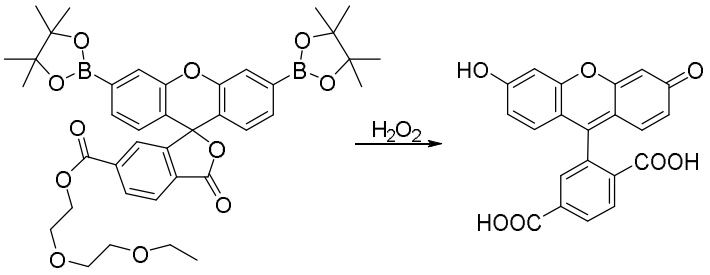

EEPF1
Non-Fluorescent
(PEG likely removed by intracellular esterases)

Carboxyfluorescein
Exc. 485nm; Em. 525nm

MitoSOX red (**MSR**)

See **Chapters 1** and **2**

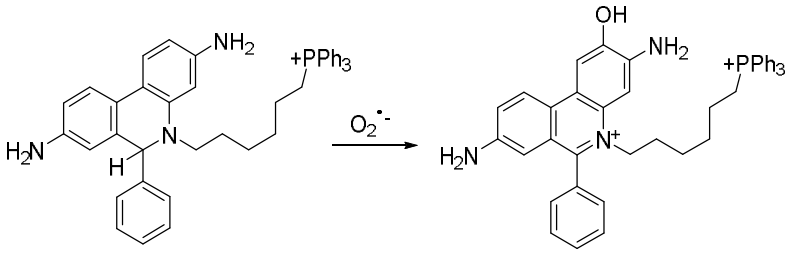

MSR
Non-Fluorescent

2-hydroxy Mitoethidium
Exc, 500 nm; Em. 580 nm

NitrobenzoylBODIPY (**NbzB**)

See **Chapters 5-7**

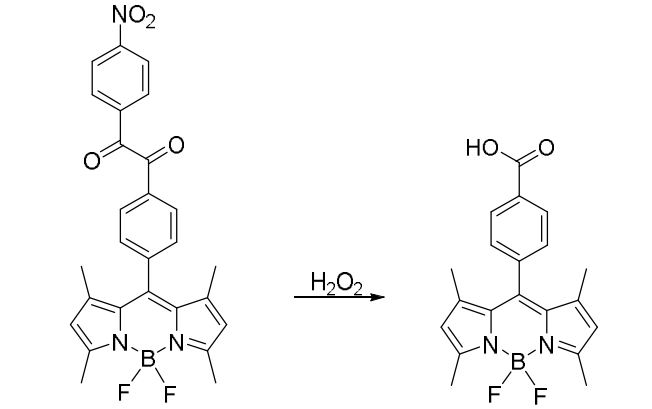

NbzB
Weakly fluorescent
Exc. 490nm; Em. 510nm

20
Exc. 490nm; Em. 510nm

Nicotinamide Coumarin Redox Sensor 3 (**NCR3**)

See **Chapters 6** and **7**

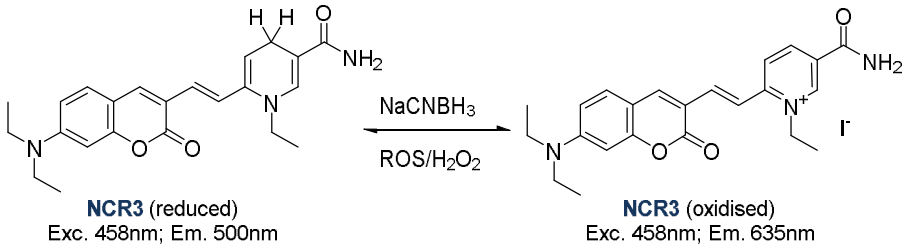

NCR3 (reduced)
Exc. 458nm; Em. 500nm

NCR3 (oxidised)
Exc. 458nm; Em. 635nm

Naphthoperoxyfluor-1 (**NPF1**)

See **Chapters 6** and **7**

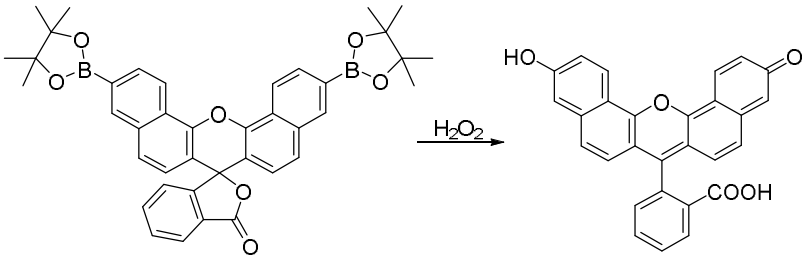

NPF1
Non-Fluorescent

Naphthofluorescein
Exc. 598nm; Em. 650nm

PeroxyBODIPY-1 (**PB1**)

See **Chapters 5-7**

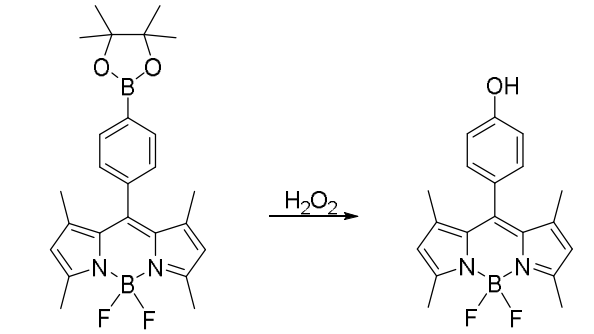

PB1
Exc. 490nm; Em. 510nm

19
Weakly Fluorescent

Peroxyfluor-1 (**PF1**)

See **Chapters 1-7**

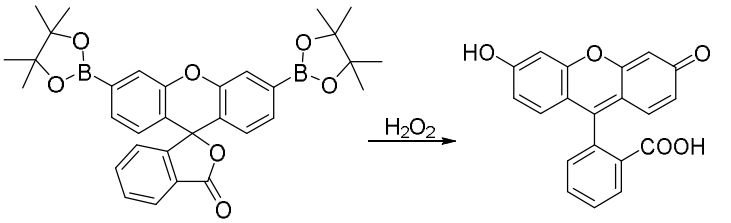

PF1
Non-Fluorescent

Fluorescein
Exc. 490nm; Em. 520nm

Seminaphtharhodafluor-2 (**SNARF2**)

See **Chapters 4** and **7**

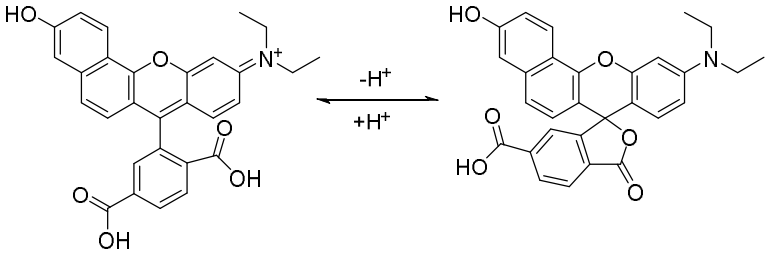

SNARF2 (Low pH)
Exc. 530nm; Em. 600 nm

SNARF2 (High pH)
Exc. 530nm; Em. 650 nm

ABSTRACT

The research presented in this thesis details the synthesis, surface functionalisation and photochemical studies of fluorescent probes for the detection of hydrogen peroxide (H_2O_2) in reproductive health.

Chapter 1

H_2O_2 is an important reactive oxygen species (ROS) that is detrimental to the health of spermatozoa and embryos. Fluorescent probes are commonly used for the detection of ROS and here examples with different mechanisms of detection are examined; such as turn-on probes, turn-off probes, Förster resonance energy transfer (FRET)-based and photoinduced electron transfer (PET)-based probes. Specific reference is given to the aryl boronate and benzil classes of probe, which show good selectivity for H_2O_2 over other ROS. The attachment of the fluorescent probe to an optical fibre as a non-invasive sensing platform is discussed. This then allows sensing in a sensitive biological environment, such as an embryo, without exposure to the probe in solution. Fibre tip sensors and microstructured optical fibre-based sensors are discussed for use in such biological environments. Finally, a summary is provided detailing the objectives of this thesis and the chapters in which these are addressed.

Chapter 2

Three aryl boronate probes [peroxyfluor-1 (**PF1**), carboxy peroxyfluor-1 (**CPF1**) and a novel probe 2(2-ethoxyethoxy)ethoxy peroxyfluor-1 (**EEPF1**)] were synthesised for use in the detection of H_2O_2 in human spermatozoa. The activity and selectivity of these probes was then compared to three commonly used commercial probes, 2',7'-dichlorohydrofluorescein diacetate (**DCFH**), dihydroethidium (**DHE**) and MitoSOX red (**MSR**). **PF1** and **EEPF1** were found to be effective at detecting H_2O_2 and peroxynitrite ($ONOO^-$) produced by spermatozoa when stimulated with menadione or 4-hydroxynonenal. Flow cytometry was used to demonstrate that **EEPF1** is more effective at detecting ROS in spermatozoa compared to **DCFH**, **DHE** and **MSR**. Furthermore, **EEPF1** distinguished poorly motile sperm from motile sperm as revealed by an enhanced production of ROS.

Chapter 3

A fibre-tip based probe constructed by encapsulating **CPF1-NHS** in a polyacrylamide matrix is reported for the detection of H_2O_2. This non-invasive platform avoids the need to introduce an organic fluorophore into a sensitive cell such as an embryo as discussed above. A number of derivatives of **PF1** were investigated, with carboxylated fluorophore **CPF1** proving to be the easiest to synthesise and characterise. **CPF1** was functionalised to glass slides

using layer-by-layer deposition of polyelectrolytes. This functionalised surface showed a fluorescent response to H_2O_2 comparable to solution-based measurements. Three surface functionalisation methods were then investigated for attachment to an optical fibre tip, specifically polyelectrolyte deposition, silane monolayer formation, and light-catalysed polymerisation of acrylamide. The most effective method of functionalisation was found to be light-catalysed formation of a polyacrylamide matrix with the **CPF1** embedded. These polyacrylamide fibre tip probes were then guided into microdroplets of bovine *in vitro* fertilisation (IVF) media using a micromanipulator. This was visualised under an optical microscope to detect the controlled release of H_2O_2. This fibre probe is thus compatible with imaging techniques used in IVF research laboratories.

Chapter 4

This chapter presents the development of a single optical fibre tip probe capable of detecting both the concentration of H_2O_2 and the pH of the associated solution. The sensor was constructed by embedding two fluorophores [**CPF1** and seminaphtharhodafluor-2 (**SNARF2**) for H_2O_2 and pH detection respectively] on the tip of an optical fibre using the previous developed polyacrylamide matrix methodology. The functionalised fibre probes reproducibly sensed pH with a resolution of 0.1 pH units. The probe also accurately detected H_2O_2 over a biologically significant concentration range, of 50-100 μM. This study revealed the importance of simultaneous detection of H_2O_2 and pH, where changes in pH were shown to affect the fluorescent response of **CPF1**. This new fibre probe offers potential for non-invasive detection of pH and H_2O_2 in biological environments using a single optical fibre.

Chapter 5

Two new cell-permeable boron-dipyrromethene (**BODIPY**) based fluorescent probes for the detection of H_2O_2 were designed and synthesised. The aryl boronate peroxyBODIPY-1 (**PB1**) gave rise to a decrease in fluorescence on reaction with H_2O_2, while the fluorescence of the benzil-based nitrobenzoylBODIPY (**NbzB**) probe increased on reaction with H_2O_2. The benzil probe **NbzB** exhibited a high degree of selectivity for H_2O_2 over other ROS. The aryl boronate **PB1** showed a greater change in fluorescence on reaction with H_2O_2 compared to **NbzB**, and **PB1** also detected H_2O_2 in bovine oocytes under oxidative stress. These results suggest that aryl boronates (i.e. **PB1**) and benzils (i.e. **NbzB**) have use in biological environments requiring higher sensitivity or selectivity to H_2O_2.

Chapter 6

The research discussed here extends the solution-based and fibre tip experiments to the detection of H_2O_2 in biological environments. Detection of H_2O_2 within cells is often frustrated

by autofluorescence in the green emission region. Contrastingly, the red emission region in biological systems shows a lower autofluorescence background signal. Therefore a red-emitting fluorescent probe for H_2O_2, naphthoperoxyfluor-1 (**NPF1**), was synthesised. However, when incubated with H_2O_2 in cuvette, **NPF1** showed a greater than 20-fold reduced fluorescent response to H_2O_2 compared with **CPF1**. This poor sensitivity suggests that **NPF1** should not be used for the detection of H_2O_2, but rather fluorophores with a greater fluorescent response should be utilised (e.g. **CPF1**). A reversible optical fibre-based sensor for H_2O_2 was then explored by attaching a reversible fluorescent probe for ROS (nicotinamide coumarin redox sensor 3, **NCR3**) to an optical fibre tip. The sensor was constructed using light-catalysed polymerisation to give a polymer matrix on the tip containing **NCR3**. This allowed the fibre tip to be reversibly oxidised by H_2O_2 and reduced by $NaCNBH_3$. The sensor exhibited good reversibility over at least seven cycles of oxidation and reduction, with consistent fluorescent ratios of its maxima at 500 and 635 nm. However, its fluorescence intensity decreased over time, suggesting that **NCR3** leached from the polymer into the buffer solution. This nevertheless represents the first example of a reversible fibre sensor for ROS and is as such an important first step towards a reusable optical fibre probe for H_2O_2.

DECLARATION

I certify that this work contains no material which has been accepted for the award of any other degree or diploma in my name, in any university or other tertiary institution and, to the best of my knowledge and belief, contains no material previously published or written by another person, except where due reference has been made in the text. In addition, I certify that no part of this work will, in the future, be used in a submission in my name, for any other degree or diploma in any university or other tertiary institution without the prior approval of the University of Adelaide and where applicable, any partner institution responsible for the joint-award of this degree.

I give consent to this copy of my thesis when deposited in the University Library, being made available for loan and photocopying, subject to the provisions of the Copyright Act 1968.

The author acknowledges that copyright of published works contained within this thesis resides with the copyright holder(s) of those works.

I also give permission for the digital version of my thesis to be made available on the web, via the University's digital research repository, the Library Search and also through web search engines, unless permission has been granted by the University to restrict access for a period of time.

Signed:

_____

Malcolm Purdey

Tuesday, 8 December 2015

ACKNOWLEDGEMENTS

Firstly, I would like to thank my supervisor, Prof. Andrew Abell. There are few things that can aid a PhD student more than a fantastic supervisor, and I could not have asked for a better supervisor than Andrew. I have learned enormous amounts through the course of this study, and certainly a vast proportion of that is due to Andrew's input. It was always reassuring to know that whenever I was stuck with an issue I could take it to Andrew and there would be a solution.

Thanks to Prof. Tanya Monro for the input into the project and for invaluable knowledge about optical fibres and sensor designs. In this area I would also like to acknowledge Dr. Erik Schartner for his endless assistance with optics, optical fibres and sensing in general. It also helped to have someone constantly there to top me up with fresh cynicism towards any given experiment when I may be running dry. There were a lot of good laughs had, as well as many valuable discussions and timely assistance.

I wish also to thank Prof. John Carver, for initial supervision of this project, and for further support even after his move to ANU in Canberra.

Importantly, I would like to acknowledge Cook Medical Australia, along with the ARC Linkage grant (LP 110200736) that supported this work. The outcomes have been fantastic and it was immensely helpful working so closely with industry.

For those post-docs in the Abell group; particularly Dr. William Tieu, Dr. Sabrina Heng and Dr. Niels Krogsgaard-Larsen, I thank profoundly for listening patiently to any issues I might be having. It would not be a stretch to call each of them unending sources of chemical wisdom, and I am extremely grateful for the number of hours chopped off my PhD studies due to helpful suggestions. A special thanks to Niels for extended periods of time listening to ideas and helping with aesthetics of figures and presentation of this thesis.

I also thank my contemporary and past PhD students, particularly Daniel Stubing, Michelle Zhang, Jacko Feng, Kelly Keeling and Tim Engler for making the lab a fun place to be all the time. I really don't think I would have finished all this if there weren't people to bounce ideas off and to empathise with on the tougher days.

I must thank Assoc. Prof. Jeremy Thompson and Dr. Mel Sutton-McDowall for direction and help with biological studies with embryos. Working with them enabled the whole project to be grounded in applications, as well as them just being fantastic people to work with.

The technical staff at IPAS and the Discipline of Chemistry also deserve a huge thanks. I would particularly like to mention the assistance of Dr. Herbert Foo, who was instrumental in helping with surface functionalisation and analysis.

I would further like to thank Prof. John Aitken, Haley Connaughton and Sara Whiting at the University of Newcastle for assistance with experiments in human spermatozoa.

It would be remiss of me to leave out thanking the superb lab placement students I supervised during my studies: Pang-Chong (Alex) Yun, Yvonne Yusa, Camilia Tan Huici, Alex “Bumpmaster” Jackson and Conner Sangster. Each were exceptional students and were extremely helpful in the lab. I enjoyed teaching them as much as they hopefully enjoyed learning!

I would also like to thank all involved in the formation of the Centre for Nanoscale BioPhotonics. It has been a pleasure to get to know everyone and the level of research taking place is certainly inspiring to students like me.

On a more personal note, there is again nearly too many people to thank! I will start by thanking my parents, Don and Annette Purdey, for all their support during all my studies throughout my entire life. I would especially like to thank Mum for her continued support, help and excellent proof-reading even after Dad passed away mid last year. It is truly inspiring to have parents of such incredible love and wisdom.

I must thank also my Grandad, Dr. J. Howard Bradbury, who really piqued my interest in science by his continued tireless work at the Australian National University for more than 25 years since his retirement. He remains a profound input into my studies, and the only difficulty I now have is continuing on such a legacy of academic excellence and personal integrity.

If I were to name all the other family and friends I would wish to thank and reasons why, I believe it would take at least as many pages as the research presented here! Suffice it to say that I feel blessed to have such amazing brothers, sisters, parents (& in-laws), and friends. I can’t thank you all enough for putting up with me in this amazing yet lengthy journey.

Finally, it is no surprise that I thank my wife Ainsley. This last three and a half years has been full of joy and sorrow, and I can’t thank you enough for the constant support and friendship that you’ve shown me. There is no other way to put it – this PhD would not have been the same without you. I entered this program not yet married, and exited it married to

the best woman ever, complete with a beautiful daughter Elsie who is a constant joy! Thank you so very much, you are simply the best!

I also can’t help but acknowledge God who led me here and continues to prod me with new thoughts and ideas. He is incessantly consistent and perfectly reliable, I never thought I wanted to end up where I am, but He had much better ideas.

Chapter 1
INTRODUCTION

If I have seen further than others, it is by standing on the shoulders of giants.

Isaac Newton

Chapter 1: Introduction

1.1 REACTIVE OXYGEN SPECIES AND HYDROGEN PEROXIDE

Reactive oxygen species (ROS) are responsible for oxidative stress that can damage and destroy cells.[1-7] The ROS generally described in biological systems are hydrogen peroxide (H_2O_2), superoxide ($O_2^{\bullet-}$), nitric oxide (NO), hydroxyl radicals ($^{\bullet}OH$), peroxynitrite ($ONOO^-$), alkyl peroxides and hypochlorite (^-OCl). There is a complex relationship between the production and decay of these ROS within cells (**Figure 1**).[8-10] ROS are produced in cells by regulated enzyme processes such as NO synthase and NAD(P)H oxidase isoforms,[11] or in excessive amounts by leakage of electrons from the electron transport chain in mitochondria[12,13] and excessive stimulation of NOX and NAD(P)H oxidases.[11,14]

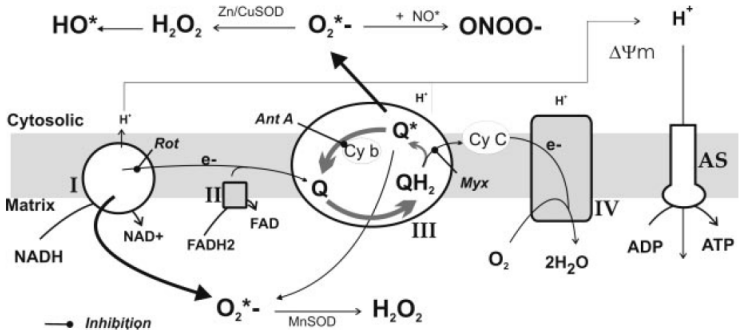

Figure 1. The formation of reactive oxygen species (ROS) within mitochondria is complex.[13] Superoxide ($O_2^{\bullet-}$), nitric oxide (NO), peroxynitrite ($ONOO^-$), hydrogen peroxide (H_2O_2) and the hydroxyl radical ($^{\bullet}OH$) are shown here.

ROS can cause DNA damage in sperm to adversely affect their function.[2-5] Furthermore, oxidative stress is detrimental to embryonic development and is an indicator of health risk.[7] However, the relationship of ROS to developmental biology is complex, as healthy embryos also release ROS at key stages of development[7] and may benefit from limited exposure to external ROS.[15] Thus the ability to visualise ROS near and within reproductive cells is critical to understanding their health.

H_2O_2 is a ROS of particular interest in cell stress and reproductive health.[7,16,17] Within cells, H_2O_2 shows much greater longevity compared to many other ROS such as OH or $ONOO^-$.[18] H_2O_2 can permeate out of a cell and is involved in cell signalling processes in other biological contexts.[19-22] Furthermore, H_2O_2 is particularly damaging to mammalian sperm function as indicated in several independent studies.[23-25] Therefore it is extremely important to visualise H_2O_2 in biological environments while excluding other ROS.

H_2O_2 is typically detected in using fluorescent probes,[26] electrochemical probes[27,28] or magnetic resonance imaging (MRI) contrast agents.[29] Although electrochemical methods

can be sensitive to less than 0.1 μM, it relies upon the use of an enzyme to catalyse the breakdown of H_2O_2 to dissolved O_2 that is then measured by the electrode.[27,28] This is undesirable as it is an indirect measurement of H_2O_2. MRI contrast agents are useful for the detection of H_2O_2 in whole organs or bodies.[29] However, fluorescent probes detect H_2O_2 with greater spatial resolution within cells than contrast agents[29] and are highly sensitive and selective for H_2O_2[30] without addition of external enzymes such as used in electrochemical detection of H_2O_2.

1.2 FLUORESCENT PROBES

Species of interest in biology such as ROS or other biomolecules, metal ions, proteins or molecular interactions are too small to directly visualise using optical or electron microscopes. In order to visualise these species or processes, fluorescent tags or probes are commonly used. For example, fluorescent compounds such as **Alexafluor 488** (**Figure 2**)[31] can be tagged to a protein.[32] The fluorescence of the tagged protein then allows the associated interaction of the protein within a cell to be detected by a fluorescence microscope. This technique can be employed using other fluorophores such as nanodiamonds or quantum dots,[33,34] and also proteins such as green fluorescent protein.[35]

Other small molecule fluorescent compounds can be used to probe for specific ions or molecules.[36] For example, the photoswitchable **SP2** (**Figure 2**) can be used to detect Zn^{2+} ions.[37] It is a non-fluorescent compound, however the ring-opened spiropyran ring binds Zn^{2+} and the resultant complex is fluorescent. Spiropyrans can be switched off to a non-fluorescent form under irradiation with white light.[37-39] The reversibility of these compounds makes them reusable and an improvement on other ion chelators that irreversibly turn on fluorescence.

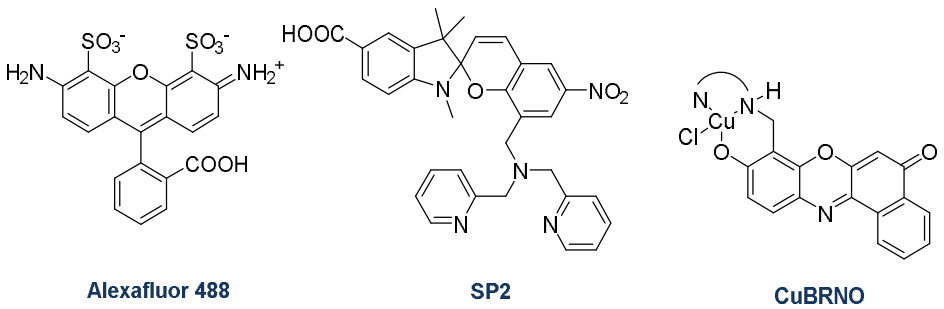

Figure 2. Different fluorophores for sensing purposes: tagging proteins (**Alexafluor 488**),[31] reversibly sensing zinc (**SP2**)[37] and detecting the nitroxyl species (**CuBRNO**).[40]

CuBRNO (**Figure 2**) is an example of a reaction-based turn-on fluorescent probe that reacts irreversibly and specifically with nitroxyl (HNO).[40] Before reaction with HNO it is non-fluorescent, and upon exposure to HNO it becomes highly fluorescent. The increase in

fluorescence of the reaction-based probe thus indicates the concentration of HNO in solution.

1.2.1 Principles of Fluorescence

Fluorescence is defined as a type of luminescent decay of an excited electron within a molecule. It is distinguished from phosphorescence by the time-scale over which this decay takes place. Fluorescence usually occurs within nanoseconds of excitation whereas phosphorescence may decay over seconds to hours.[41] The excitation of the molecule occurs by absorption of a photon (**Figure 3**). However, the energy absorbed from this photon can decay through a number of processes, of which fluorescence is only one. These can be non-radiative processes such as internal conversion, intramolecular charge transfer, conformational change, energy transfer or a photochemical transformation; in addition to radiative decay such as fluorescence or phosphorescence.[42] This radiative decay must by definition yield a photon of longer wavelength and hence lower energy than the photon absorbed by the molecule,[41] except for cases where two photons are absorbed and upconverted to a single higher energy photon.[43-45]

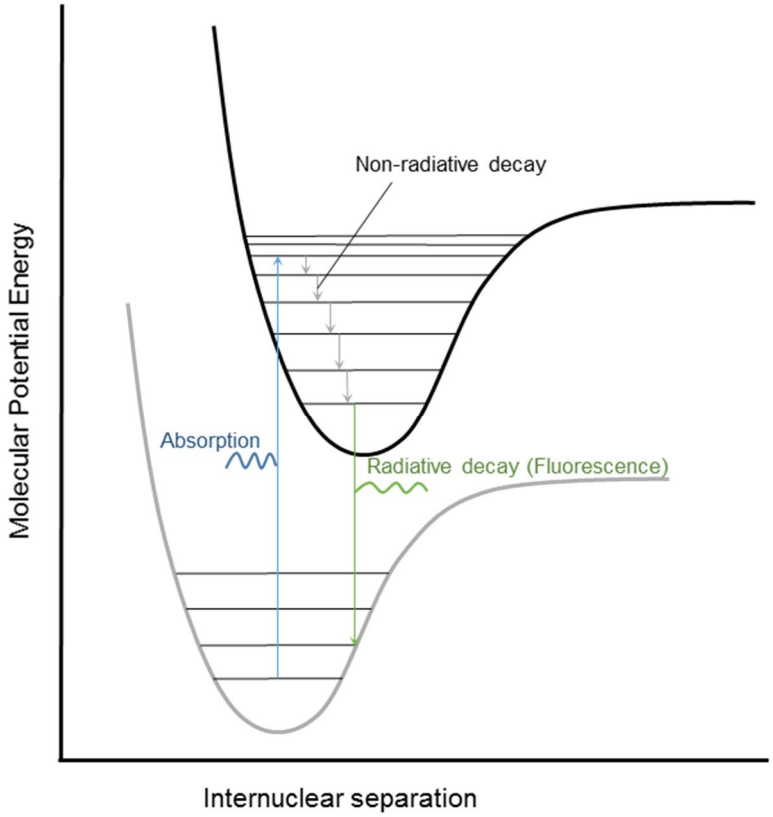

Figure 3. Franck-Condon energy diagram of fluorescence within a molecule.[42]

1.2.2 Common structures of Organic Fluorophores

The presence of a fluorescent compound can therefore be inferred by excitation of a sample and collection of the resultant emission spectrum. For example, a protein can be tagged with a fluorescent compound **Alexafluor 488** that will fluoresce at 519 nm upon excitation with 488 nm light.[46] The emission spectrum collected from this infers the presence of the protein and hence can be used to track its interactions within a cell. Biomolecules and ions are detected in a similar fashion.[26,47]

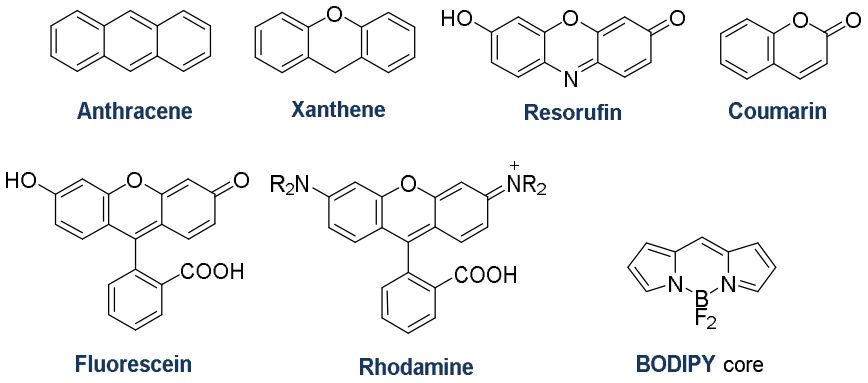

Figure 4. Standard organic fluorophores. Note that the R group in **rhodamine** can be many different alkyl groups leading to different rhodamines with shifted excitation/emission spectra. The **BODIPY** core shown here is the basis for many derivatives although this structure itself has not been synthesised.[48]

Common organic fluorophores that provide a basis for many fluorescent probes are shown in **Figure 4.**[26] Many fluorophores are based on the **anthracene** or **xanthene** scaffold.[49] For example, **fluorescein** is one of the most common fluorophores used for fluorescent tagging.[50] This scaffold is structurally very similar to the **rhodamine** and **resorufin** structures. **Fluorescein** is a common xanthene, many derivatives of which have been used in cell biology.[26,51] **Rhodamines** are very structurally similar to **fluorescein**, however vary from fluoresceins as they contain amino groups in place of phenols. Moreover, **rhodamines** have excellent photophysical properties for fluorescence assays.[52] **Resorufin** is a red-emitting fluorophore upon which many fluorescent probes are based.[40,53-55] A fluorophore of smaller molecular weight, **coumarin**, is a key fluorophore that emits in the blue region. This compound is often used for turn-on or resonance energy transfer probes.[56-60] A common fluorescent scaffold unrelated to **xanthene** is the boron dipyrromethene (**BODIPY**) core. Many substituted **BODIPY's** have been used in a diverse range of fluorescence applications.[61-65] **BODIPY**-based fluorophores are stable under physiological conditions and they have an ability to tune excitation and emission with very minor structural modifications.[48] However, **BODIPY's** are generally quite lipophilic and hence are often not very cell permeable, which can restrict uses *in vitro*.

1.2.3 Turn-on Fluorescent Probes

Biomolecules or ions can be detected using molecules that turn “on” fluorescence when interacting with them (**Figure 5**). The initial compound is non-fluorescent or weakly fluorescent in its “off” state, but upon reaction or interaction with the biomolecule/ion of interest fluorescence is turned “on”.[26] The resultant increase in the fluorescence can then be used to infer the presence or otherwise of the species targeted. **CuBRNO** mentioned previously (**Figure 2**)[40] is an example of a turn-on fluorescence probe. Turn-off probes work by a similar mechanism, however in this case the probe is initially in an “on” state being turned “off” upon reaction with the biomolecule/ion.

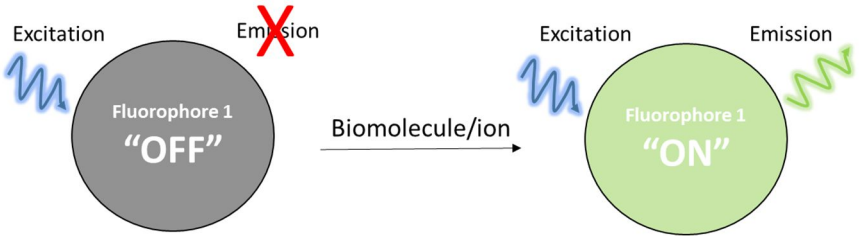

Figure 5. A turn-on fluorescent probe. The molecule initially in the "off" state does not fluoresce, however when it interacts with a biomolecule or ion, there is a conformational or configurational change, and the fluorescence is turned "on".

1.2.4 Förster Resonance Energy Transfer

In addition to utilising fluorescence in the design of fluorescent probes, intramolecular energy transfers are often exploited to enhance the usability of the fluorophore. Förster resonance energy transfer (FRET) is a process by which the energy absorbed by one fluorophore is transferred to a second fluorophore in a non-radiative energy transfer (**Figure 6**).[66,67] The excitation of this second fluorophore must match the emission of the first fluorophore, and the fluorophores must be separated by a Förster distance of no greater than 9 nm.[68]

The FRET principle has been exploited for use in fluorescent probes by the two states of a compound: an “off” state where FRET does not occur, and an “on” state where FRET does occur (**Figure 7**). The fluorophore is switched from the “off” to the “on” state by reacting or interacting with the desired biomolecule or ion. Hence a shift in the emission spectrum will be observed, from the spectrum of fluorophore 1 to fluorophore 2.[69] The ratio of the two emission maxima can thus be used to determine how much of the fluorescent probe has reacted with the biomolecule/ion, and how much remains unreacted. This can present an advantage over turn-on fluorescent probes *in vitro*, as it is difficult to determine how much of a turn-on probe is within a cell until it reacts with the target biomolecule/ion. By comparison, a FRET-based probe will fluoresce before and after reaction with the biomolecule/ion; thus its presence in a biological system can be detected before and after, not just following

reaction as is the case with turn-on fluorescent probes. An example of a FRET-based probe is **Cou-Rho-NO** (**Figure 8**), used to detect endogenous NO in macrophages.

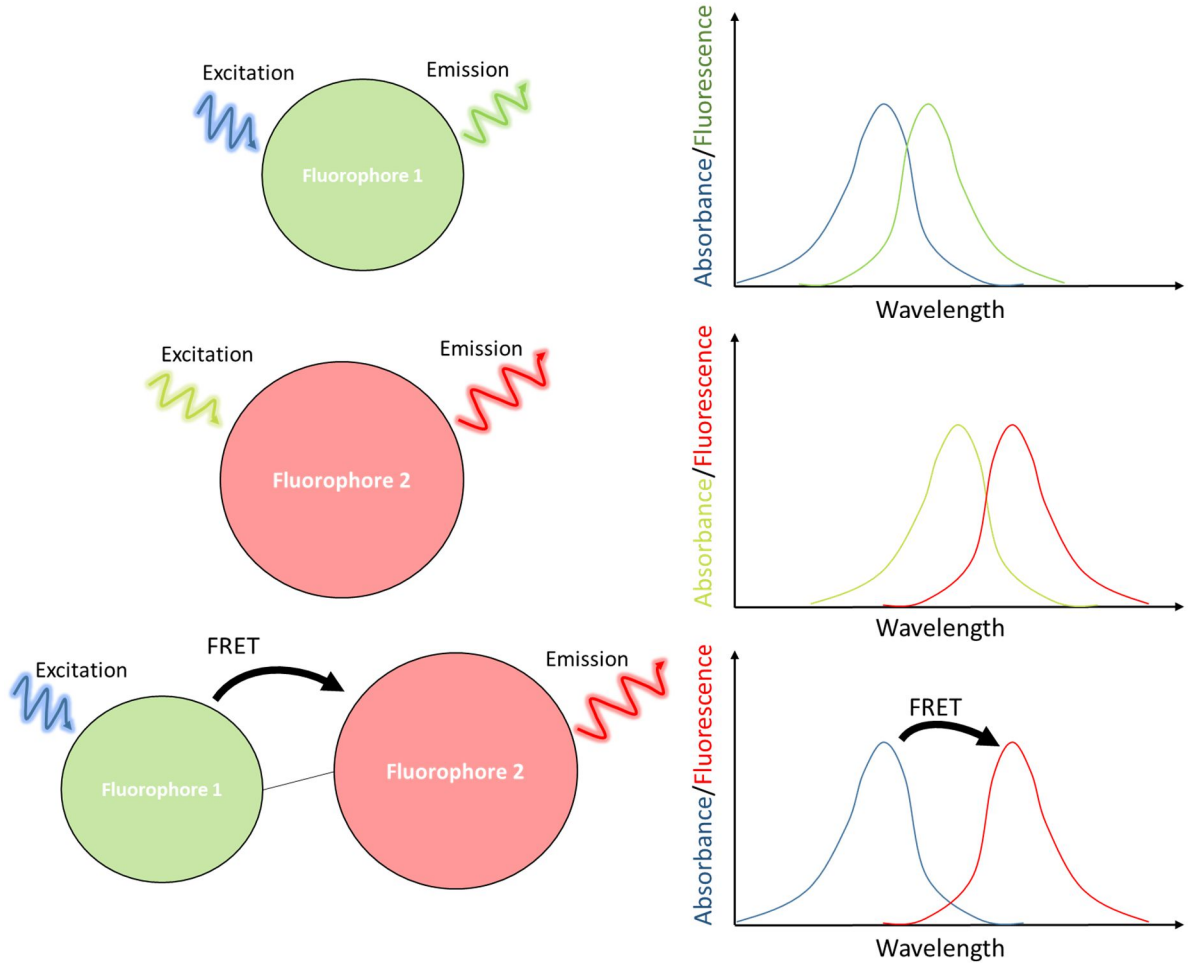

Figure 6. FRET between two example fluorophores 1 and 2. The emission wavelength of fluorophore 1 (top) overlaps the excitation wavelength of fluorophore 2 (middle). Therefore when they are covalently linked (bottom), excitation in the blue region leads to FRET and hence emission in the red.

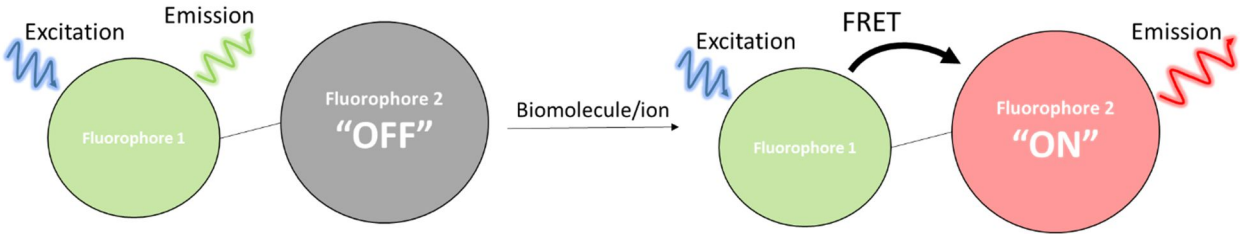

Figure 7. A FRET-based probe in "off" and "on" configuration. Reaction or interaction with the target biomolecule or ion changes it to the "on" configuration and hence induces a change in the fluorescence spectrum.

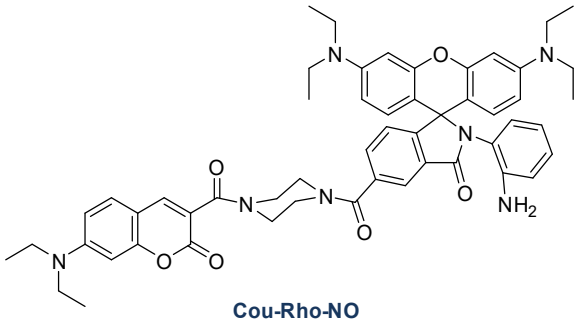

Figure 8. A **coumarin** and **rhodamine** FRET-based fluorescent probe for NO, **Cou-Rho-NO**.[70]

1.2.5 Photoinduced electron transfer

Photoinduced electron transfer (PET) is another mechanism of intramolecular energy transfer that is often responsible for fluorescence quenching.[41] PET involves both a donor, and an acceptor. The donor is excited by absorption of a photon, but rather than relaxing via fluorescence, the excited electron is transferred to an electron-poor acceptor. Thus the donor is oxidised and the acceptor is reduced (**Figure 9**). The paired donor and acceptor ions may then transfer charge, with the original donor and acceptor pair being regenerated. This is a non-radiative decay as discussed in section **1.2.1** that acts to quench the fluorescence of a molecule.

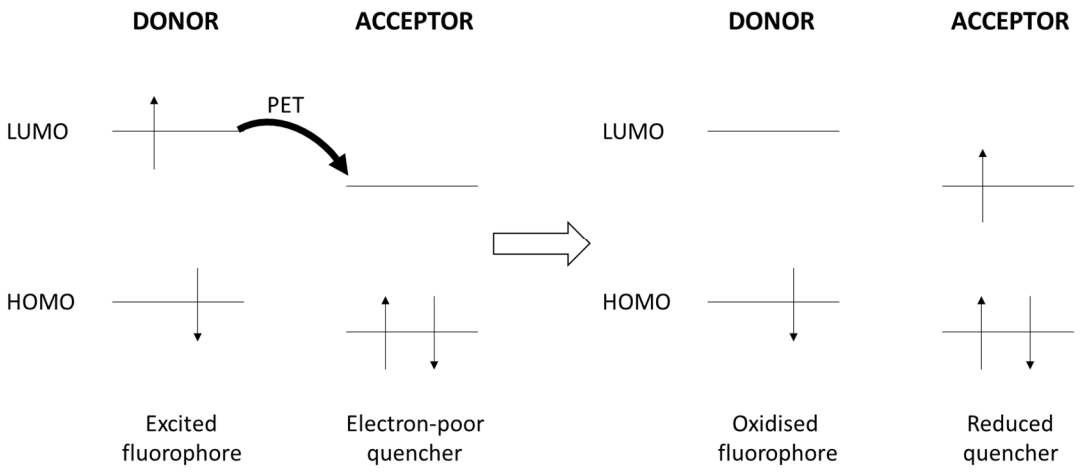

Figure 9. Jablonski diagram demonstrating the principle of photoinduced electron transfer (PET).[41]

Fluorescent probes can utilise this PET effect to give a turn-on fluorescence to detect a target species.[71] A PET-based probe will be quenched in its initial configuration, the "off" state of the probe. However, upon reaction with a biomolecule/ion of interest, PET will not take place with the acceptor (**Figure 10**). Hence, the fluorescence will no longer be quenched, giving an "on" state fluorophore. An example of a PET-based fluorescent sensor molecule is **MAMBO** (**Figure 11**), as it is non-fluorescent due to PET, but fluoresces upon reaction with NO.[72]

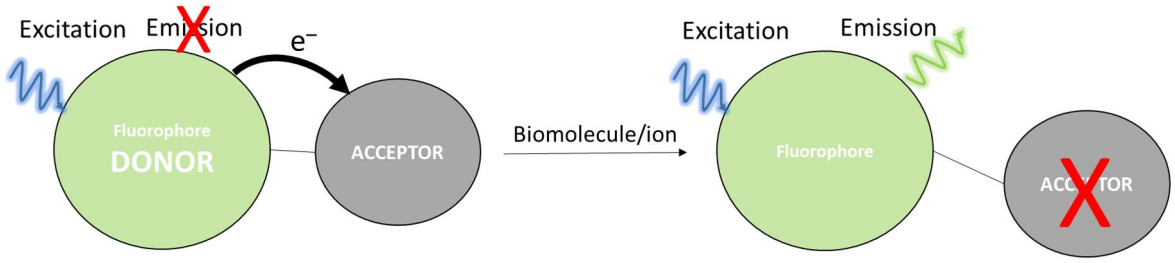

Figure 10. A turn-on probe utilising photoinduced electron transfer (PET) to distinguish off and on states. PET occurs from the fluorophore donor to the acceptor. This transfer of charge quenches fluorescence, however upon reaction with the biomolecule/ion desired, PET cannot take place and hence the fluorescence of the fluorophore is enhanced.

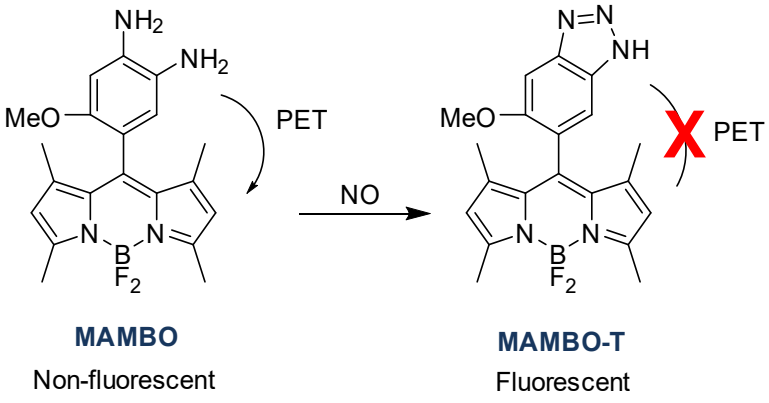

Figure 11. **MAMBO** is an example of a PET-based sensor for NO.[72] The diamino methoxy phenyl group donates an electron to the BODIPY core to quench fluorescence. Upon reaction with NO, no charge transfer takes place and the molecule fluoresces.

1.3 FLUORESCENT PROBES FOR REACTIVE OXYGEN SPECIES

There are three types of reaction-based fluorescence probes that can be used to infer the production of H_2O_2. Some probes react with other ROS such as $O_2^{\bullet-}$ or $^{\bullet}OH$ that are related to H_2O_2 (either produce H_2O_2 or are produced by H_2O_2).[73] Thus the presence or otherwise of H_2O_2 can be inferred, although not directly measured. Examples of such probes are MitoSOX red (**MSR**, **Figure 12**) and dihydroethidium (**DHE**, **Figure 12**) that are reported to react with $O_2^{\bullet-}$,[74-77] a precursor to H_2O_2 (**Figure 1**). However while **DHE** and **MSR** may be effective at detecting $O_2^{\bullet-}$, the presence of H_2O_2 is only inferred indirectly. Furthermore, there are doubts that the red fluorescence of DHE and MSR reliably indicates $O_2^{\bullet-}$ production.[78]

Secondly, there are probes that react with many ROS and as such these do not specifically detect H_2O_2. 2,7-Dichlorohydrofluorescein diacetate (**DCFH**, **Figure 12**) and

dihydrorhodamin (**DHR**, **Figure 12**) are examples of such probes that have been widely used for *in vitro* and *in vivo* studies.[74,79-81] More recent probes for ROS such as the Te-rhodamine (**2Me TeR**)[82] naphthalimide Flavin redox sensor 1 (**NpFR1**)[83] and Flavin coumarin redox sensor 1 (**FCR1**)[84] react with many ROS and are reduced by antioxidants for continual imaging *in vitro*. Although **DCFH** and **DHR** can be used to infer H_2O_2 production, the species detected may not accurately represent the concentrations of H_2O_2 present within the sample.

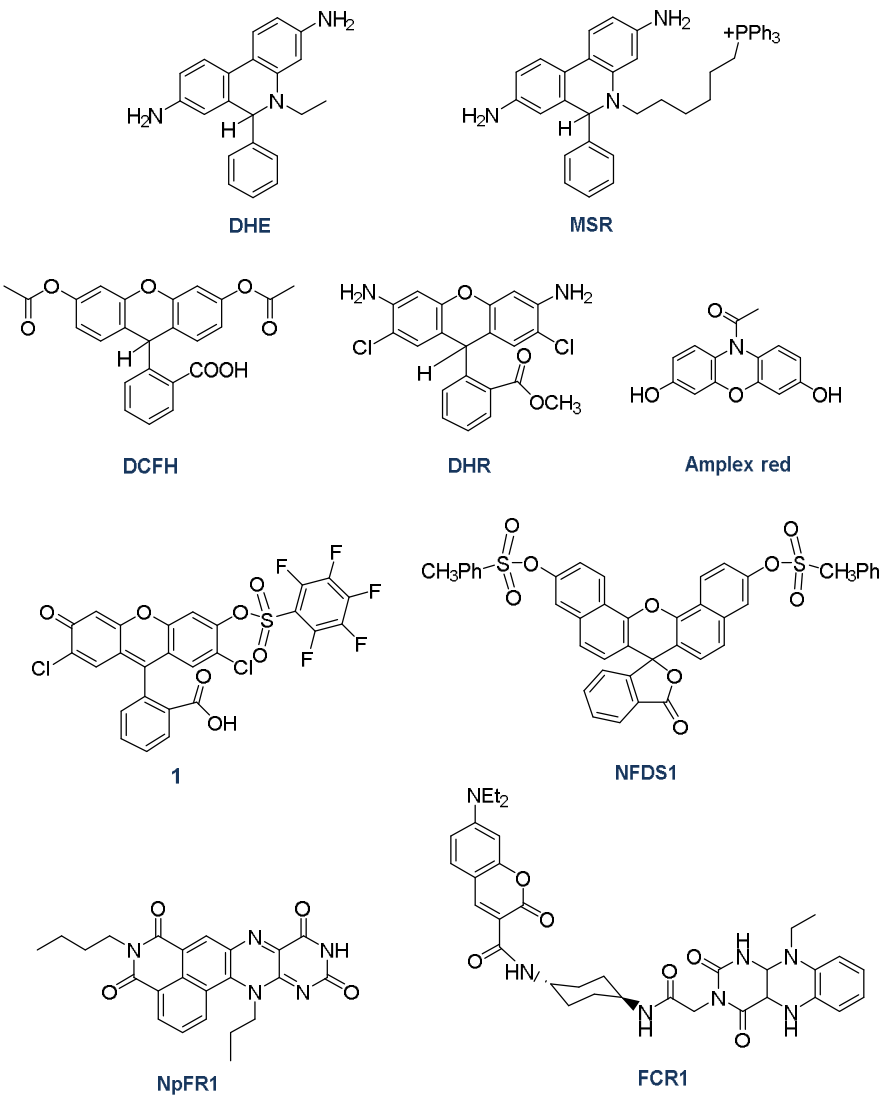

Figure 12. Various fluorescent probes for sensing ROS: Dihydroethidium (**DHE**) and MitoSOX red (**MSR**),[74-76] 2',5'-dichlorodihydrofluorescein diacetate (**DCFH**),[74,79,80] dihydrorhodamin (**DHR**),[27,28] **Amplex red**,[85] Perfluorobenzenesulfonyl fluorescein (**1**)[86] Naphthofluorescein disulfonate (**NFDS-1**),[87] naphthalimide flavin redox sensor 1 (**NpFR1**)[83] and flavin coumarin redox sensor 1 (**FCR1**).[84]

Amplex red (**Figure 12**) is a fluorescent probe that reacts selectively with H_2O_2 and is reported to have a very low detection limit of less than 100 nM under ideal assay conditions.[85,88] However, **Amplex red** requires the presence of the enzyme horseradish

peroxidase in order to react with H_2O_2. This presents a problem for biological studies, as the enzyme may not be internalised by the cell, thus reducing the ability to detect H_2O_2 within a cell. A derivative of **Amplex red** has been attached inside a microstructured optical fibre to attempt to create a remote sensor.[89] However, the requirement for pre-mixing the sample with horseradish peroxidase removes a capacity of this form of sensor such to be non-invasive.

There are also probes that react selectively with H_2O_2 over other ROS,[90] e.g. protein based fluorescent sensors,[91,92] perfluorobenzenesulfonyl fluorescein **1** (**Figure 12**)[86] and **NFDS-1** (**Figure 12**).[87] However, compound **1** was found to be unstable for long-term storage and photobleaches readily under intense light.[89] **NFDS-1** utilises the same sensing mechanism as fluorophore **1**, suggesting that it is not stable enough for long-term storage required for use in repeated biological experiments.

1.3.1 Aryl Boronate Esters

Aryl boronates react with H_2O_2 to form a phenol (**Scheme 1**).[93] Chang et al.[94] used a dipinacolatoboron fluoran structure to synthesise the first fluorescent probe for H_2O_2, peroxyfluor-1 (**PF1**, **Figure 13**). Although completely non-fluorescent, upon oxidation with H_2O_2, a highly fluorescent dye **fluorescein** (**Figure 4**) is produced. Similarly, other boronate esters are also essentially non-fluorescent and the resultant phenol upon reaction with H_2O_2 produces a large increase in fluorescence.[30] The design of **PF1** is ingenious in numerous ways: it incorporates a moiety specific to H_2O_2, is cell-permeable, and its product on reaction with H_2O_2 (**fluorescein**) is universal for use with any fluorescent microscope or fluorimeter. A further advantage of **PF1** is its relatively straightforward two-step synthesis[94] (**Scheme 2**), which is amenable to larger-scale production.

Other aryl boronate probes have since been synthesised for specific functions, such as fluorescence emission spectra in the yellow, orange or red.[54,95] Further probes have also been synthesised in order to decrease the detection limit for H_2O_2,[20,96] to target specific areas of the cell such as the mitochondria (**MitoPY1**, **Figure 13**)[97] and other organelles,[98] or for increased dye retention in cells (**PF6-AM**, **Figure 13**).[99]

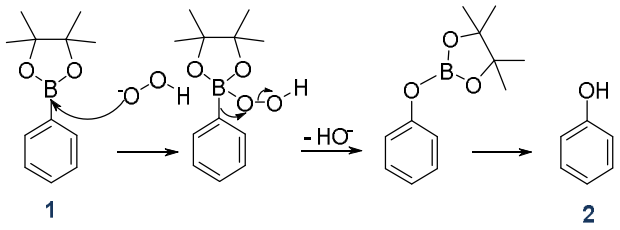

Scheme 1. Deprotection of boronate ester **1** by H_2O_2 to give phenol **2**.[30,93]

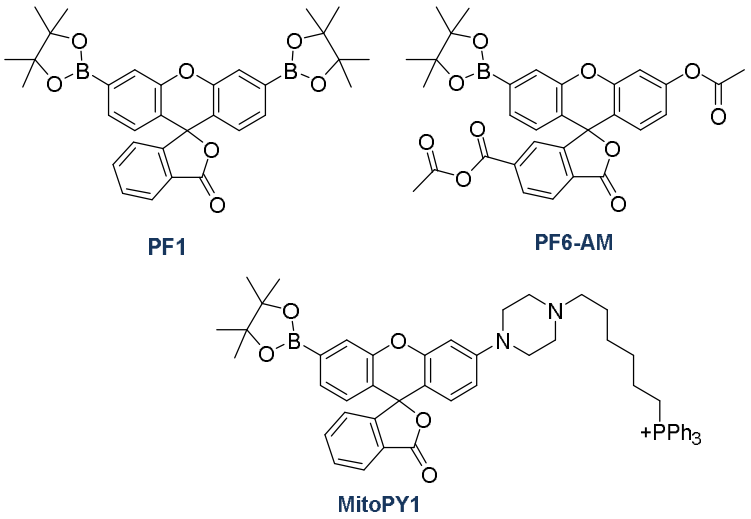

Figure 13. A selection of boronate ester probes: Peroxyfluor-1 (**PF1**),[94] **PF6-AM**[99] and **MitoPY1**.[97]

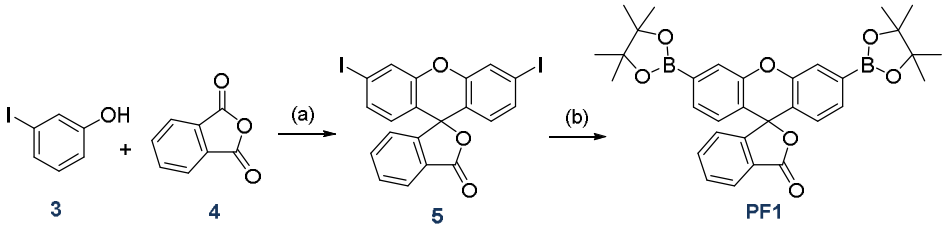

Scheme 2. Synthesis of PF1[94] under conditions: (a) $MeSO_3H$, 135 °C, 48 h. (b) Bis(pinacolato)diboron, $Pd(dppf)Cl_2$, KOAc, DMF, 80 °C, 2 h.

Although aryl boronates were originally reported to show selectively for H_2O_2 over other ROS,[94] cross-reactivity with peroxynitrite ($ONOO^-$) and hypochloric acid (HOCl) has subsequently been shown.[100,101] However H_2O_2 has a longer lifetime than the relatively transient $ONOO^-$.[18] This allows H_2O_2 to diffuse more readily throughout a cell and as such it may more frequently interact with the fluorescent probe than species such as $ONOO^-$. Physiological arguments such as this have been used to justify the lack of acknowledgement that aryl boronate probes react with $ONOO^-$, although the probes are being used only for H_2O_2 detection. However, a more recent study recognised this cross-reactivity and suggested the use of controls to distinguish between H_2O_2 and $ONOO^-$.[97]

1.3.2 Benzils

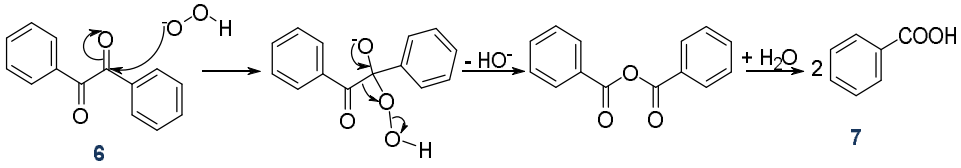

Scheme 3. Reaction of benzil (**6**) with H_2O_2 to produce benzylic acid (**7**).[102]

A Baeyer-Villager cleavage of the diketone in benzil is also specific for H_2O_2 (**Scheme 3**).[102] A fluorescent probe for H_2O_2 based on this reaction, **NbzF** (**Figure 14**), was reported with selectivity for H_2O_2 over other ROS including $ONOO^-$.[103] The design of NbzF incorporates the benzil moiety that reacts specifically with H_2O_2 to release a carboxy-**fluorescein**. This released **fluorescein** is highly fluorescent, in contrast to the very weak fluorescence from **NbzF** that is quenched by donor-excited PET (d-PET) effects.

Another benzil derivative, **NbzF-BG**, was created to covalently link to a SNAP protein in order to give a fluorophore-protein conjugate to measure localised H_2O_2 production within a cell.

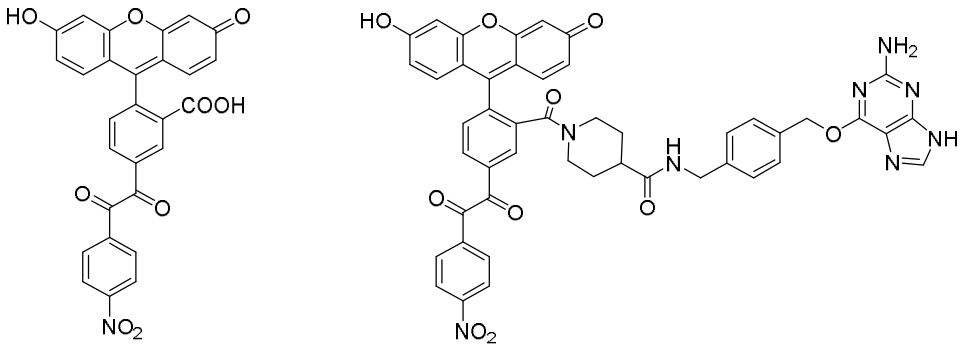

Figure 14. Fluorescent probes for H_2O_2 based on benzils: **NbzF**[103] and **SNAP-NbzF**.[104]

1.4 OPTICAL FIBRE SENSORS

Optical fibre based sensors are ideal for non-invasive sensing technologies as they are light, flexible, chemically inert, do not carry current and are immune to electromagnetic interference.[105] Such sensors work by coupling a light source into the fibre, with the reflected fluorescence from the sensing region collected by a spectrometer (**Figure 15**). A fluorophore can be immobilised to the sensing region to perform this task. The collected fluorescence reveals what is happening at the surface of the optical fibre. Thus a specific fluorophore can be immobilised to an optical fibre to create a sensor, for example the Zn^{2+} specific fluorophore **SP2** (**Figure 2**).[37]

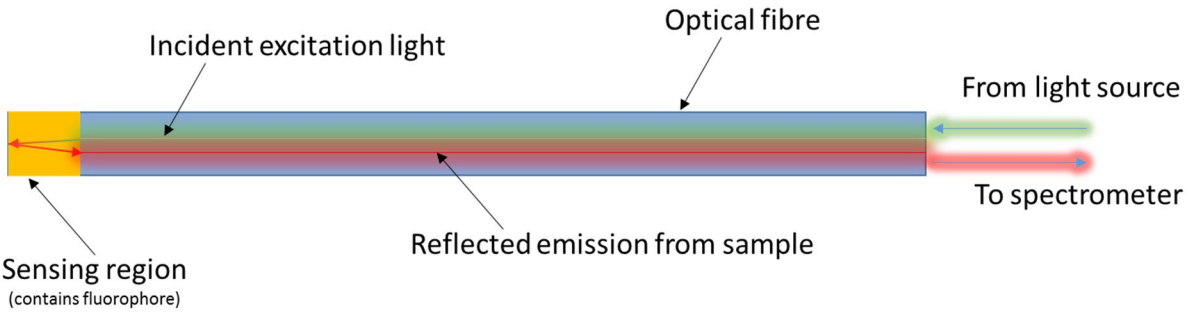

Figure 15. Example of an optical fibre as a fluorescence-based sensor in a tip-sensor configuration. The excitation is provided by a light source such as a laser or LED source and the emission spectrum is collected by a spectrometer for analysis.

Optical fibre sensors can be significantly more sensitive than cuvette-based measurements.[106] In addition to this, fibre-based sensors functionalised with a fluorescent sensor molecule present a non-invasive platform for bio-sensing that avoids the need for the fluorophore to be released into the solution with the target.[107] The use of an optical sensor also allows for spatial mapping of gradients around a cell, for time-based measurements and single point measurements at desired locations within a sample. **Figure 16** shows how an optical fibre would be used in a biological experiment. The sensing region placed near a cell such as an embryo allows detection of biomolecules, without releasing a fluorophore into the solution.

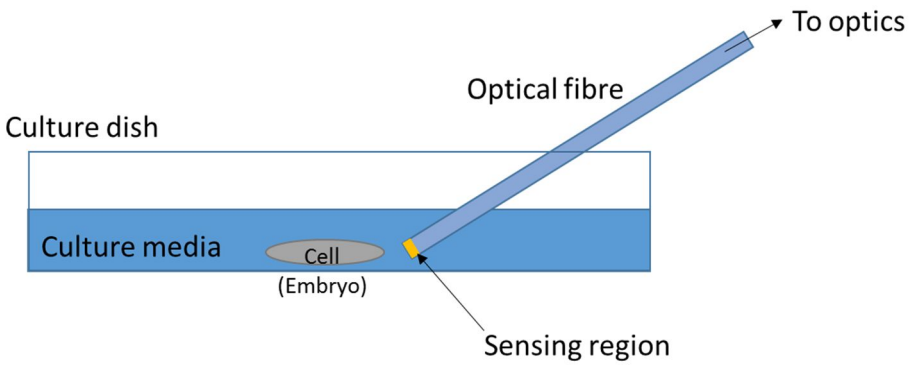

Figure 16. An example of using an optical fibre tip-probe for sensing near a cell. Similar sensors based on microstructured fibres can also be used in this way.

1.4.1 Fibre Tip Sensors

Several types of optical fibres can be used as remote fluorescence sensors.[108] Solid-core optical fibres can be functionalised on the tip of the fibre with a sensor molecule or particle.[109,110] The functionalised fibre tip can then be placed in the desired media, such as a biological environment shown in **Figure 16**. The coated tip will interact with the desired biomolecule/ion and the fluorescence can be detected through the external optics. For example, a pH sensor has been created by immobilising a pH-sensitive fluorophore to the tip

of the optical fibre.[107,111-113] These tip coatings can be created in various ways, either by depositing the fluorophore using sol-gel matrixes, covalently linking to the surface or embedding in an acrylamide matrix (**Figure 17**). The use of such fibre tip sensors for detection of H_2O_2 in biological systems has not been explored. Although a H_2O_2 sensor for fuel degradation has previously been reported,[114] it is not useful for H_2O_2 sensing in biological environments due to its non-compatibility with aqueous systems, and the general nature of the Prussian blue dye for multiple ROS.

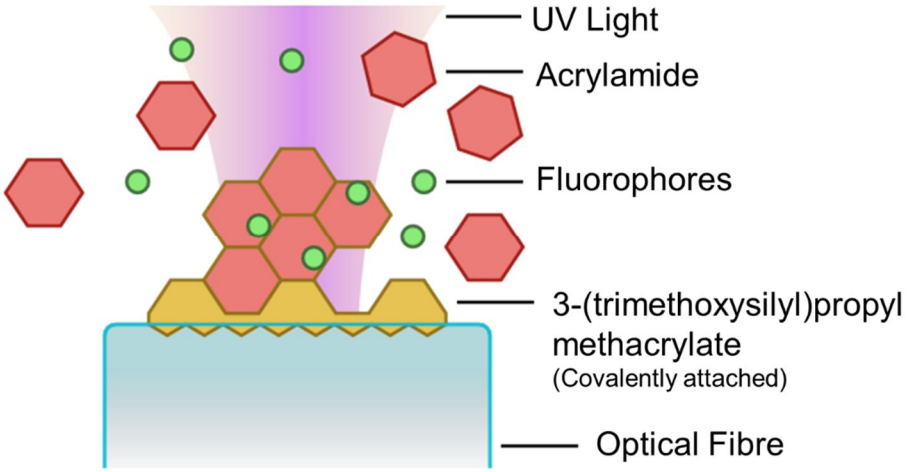

Figure 17. An example of a fluorescence tip-sensor. A fluorophore is immobilised to a fibre tip using a light-catalysed polymerisation of a fluorophore-doped acrylamide solution.[111,113]

1.4.2 Microstructured Fibres

Microstructured optical fibres (MOFs) are optical fibres with a structured lattice of air holes that run the length of the fibre.[115] For sensing purposes, the suspended core fibre is the ideal MOF,[116,117] which can be made relatively large, while the core which guides the light can be relatively small. This allows a significant proportion of the evanescent field to extend beyond the solid fibre core to enable its interaction with and sensing of analytes within the air holes (**Figure 18**). This sensing architecture allows for very low sample volumes and detection limits,[118,119] improved in recent years to detect single nanocrystals from a distance along the fibre.[44]

Although the detection limit of MOFs is in general extremely low, the sensing region (**Figure 16**) is within the fibre. Thus, for continued imaging of a biological sample that may change over time, there must be continuous flow of media through the sensing region (i.e. air holes). This may then require complicated fluidics to ensure the media within the fibre most accurately represents the environment near the cell. The required fluidics may introduce a complexity that outweighs the benefit of nL sensing volumes and hence reduce its effectiveness as a sensor. Preliminary results using microstructured fibres for H_2O_2 sensing also revealed difficulties in reproducibility and surface attachment.[120] This is primarily due to

the difficulty of functionalising interior glass surfaces within the MOFs. In order to functionalise these surfaces, liquid is forced through the MOF by external pressure from a nitrogen chamber. Slight variations in this pressure or concentration of the molecule for attachment thus cause non-uniform surface coatings.

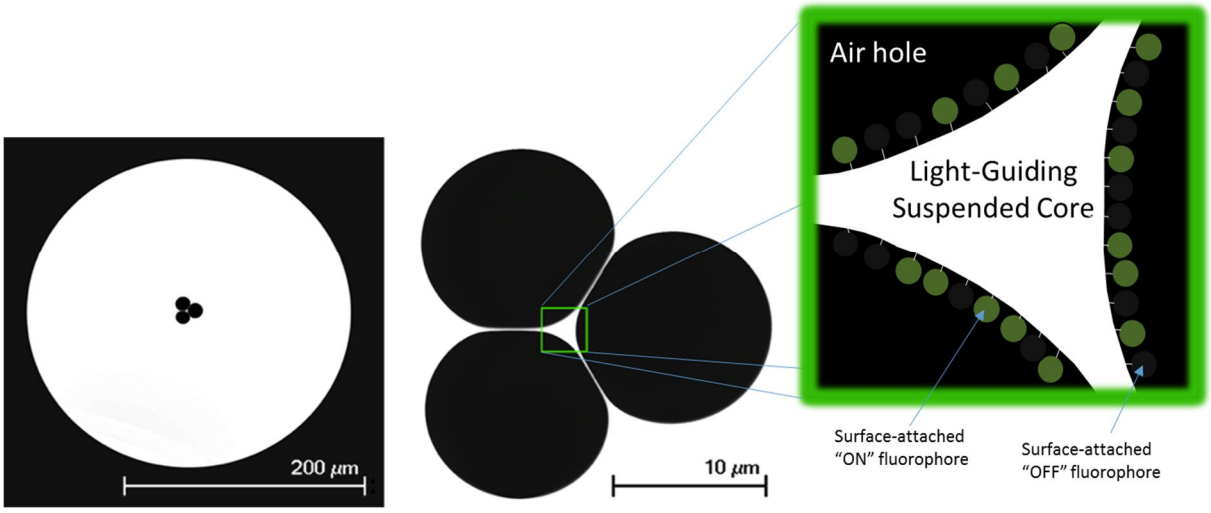

Figure 18. Cross-section of a suspended core MOF. The suspended core highlighted in green shows fluorophore molecules attached to the glass surface, such that the evanescent field from light guided through the core will excite the fluorophores.

1.5 PROJECT OUTLINE

The literature presented clearly details the necessity of detecting H_2O_2 in reproductive health. Furthermore, a clear gap exists between the current technologies for detecting H_2O_2 using organic fluorescent probes and the target biological application. Organic fluorophores cannot be used in developing human embryos during *in vitro* fertilisation (IVF) due to stringent regulations prohibiting addition of external reagents. A non-invasive approach is required to monitor H_2O_2 levels near embryos without introducing molecules of unknown toxicity into the solution. Optical fibre-based sensors were proposed for this purpose, by attaching the fluorescent probe for H_2O_2 to the surface. As the fluorophore is immobilised to the fibre surface, it will not pass into the embryo when immersed in solution. This would allow detection of H_2O_2 and hence monitoring of embryo health in IVF. Furthermore, this technology is not only desirable for clinical purposes, but for fundamental research into the role of H_2O_2 in male fertility and the development of embryos.

1.5.1 Commercial Motivation

This project was initiated in collaboration with Cook Medical Australia, through an Australian Research Council linkage grant (LP 110200736). The aims of this collaboration were to produce a H_2O_2 sensor that could be used in an embryo incubator to monitor the health of the embryo. In addition to this, concurrent research by Dr. Erik Schartner at the University of

Adelaide investigated non-invasive pH and temperature sensors. Detection of local pH and temperature of embryos are also desirable as markers of embryonic health. A significant goal of this linkage project was to combine these sensing capacities with detection of H_2O_2 to obtain a more complete picture of health of developing embryos. Ultimately, the sensors could be incorporated into a commercially available incubators, giving better information to IVF clinics and more successful outcomes for patients.

1.5.2 Research Objectives

This thesis is hence concerned with the following objectives:

1. Demonstrate detection of H_2O_2 in a reproductive biological context using a new aryl boronate-based fluorophore that is specific for H_2O_2, with the exclusion of other ROS.
2. Determine the most effective class of fluorescent probe for detection of H_2O_2 for this biological context.
3. Develop a functional non-invasive optical fibre-based probe for the detection of H_2O_2.
4. Integrate this H_2O_2 probe with other relevant sensors such as pH or temperature for use in reproductive biology.

1.5.3 Thesis Structure

Table 1. Overview of the objectives addressed in each chapter of this thesis.

	Objective 1	Objective 2	Objective 3	Objective 4	Extensions/Applications
Chapter 1	INTRODUCTION				
Chapter 2	✓	✓			
Chapter 3			✓		
Chapter 4			✓	✓	
Chapter 5	✓	✓			
Chapter 6		✓	✓		✓
Chapter 7	✓				✓

Chapter 1 has introduced the topics of H_2O_2, fluorescent sensors and optical fibres.

Chapter 2 focuses on the use of aryl boronates to detect H_2O_2 in human spermatozoa. Three synthesised aryl boronate probes are compared against commonly used fluorophores for ROS detection. The results show that aryl boronates, particularly the novel probe

(**EEPF1**) are extremely effective for detecting H_2O_2 in human spermatozoa and validate their use in reproductive biology.

Chapter 3 extends the use of aryl boronate probes to detect H_2O_2 while bound to glass surfaces. The aryl boronate probe carboxyPF1 (**CPF1**) was first functionalised to glass slides to characterise its interaction with H_2O_2 on a surface. **CPF1** was then immobilised to optical fibre tips to create a functional non-invasive probe specific for H_2O_2.

Chapter 4 incorporates the H_2O_2 probe created in Chapter 3 using **CPF1** with a pH sensor, seminapthorhodofluor-2 (**SNARF2**). This dual probe for H_2O_2 and pH is shown to be effective across the physiological pH range and improves upon the single H_2O_2 probe design.

Chapter 5 compares two novel BODIPY-based probes for H_2O_2, peroxyBODIPY-1 (**PB1**), and nitrobenzoylBODIPY (**NbzB**). The mechanism of sensing using aryl boronate and benzil moieties respectively are directly compared to give the strengths and weaknesses of each approach. **PB1** shows a greater fluorescent response to H_2O_2 than **NbzB**, however **NbzB** was shown to be more selective for H_2O_2 over other ROS.

Chapter 6 demonstrates efforts to improve the solution-based and fibre-based detection of H_2O_2. A red-emitting fluorescent probe, napthoperoxyfluor-1 (**NPF1**) was synthesised for use in solution with cells of high autofluorescence in the green region. A reversible probe for ROS, nicotinamide coumarin redox sensor 3 (**NCR3**) was attached to an optical fibre tip to create a reversible non-invasive probe for H_2O_2.

Chapter 7 discusses further applications of the work presented in **chapters 1-6** and summarises the conclusions of this thesis.

1.6 REFERENCES

1. Sanders, L. H.; McCoy, J.; Hu, X.; Mastroberardino, P. G.; Dickinson, B. C.; Chang, C. J.; Chu, C. T.; Van Houten, B.; Greenamyre, J. T. Mitochondrial DNA damage: Molecular marker of vulnerable nigral neurons in Parkinson's disease. *Neurobiology of Disease* **2014,** *70*, 214-223.
2. Jones, R.; Mann, T.; Sherins, R. Peroxidative breakdown of phospholipids in human spermatozoa, spermicidal properties of fatty acid peroxides, and protective action of seminal plasma. *Fertility and sterility* **1979,** *31* (5), 531-537.
3. Aitken, R. J.; Clarkson, J. S. Cellular basis of defective sperm function and its association with the genesis of reactive oxygen species by human spermatozoa. *Journal of Reproduction and Fertility* **1987,** *81* (2), 459-469.
4. Alvarez, J. G.; Touchstone, J. C.; Blasco, L.; Storey, B. T. Spontaneous Lipid Peroxidation and Production of Hydrogen Peroxide and Superoxide in Human Spermatozoa Superoxide Dismutase as Major Enzyme Protectant Against Oxygen Toxicity. *Journal of Andrology* **1987,** *8* (5), 338-348.

5. Aitken, R. J.; Curry, B. J. Redox regulation of human sperm function: from the physiological control of sperm capacitation to the etiology of infertility and DNA damage in the germ line. *Antioxid Redox Signal* **2011,** *14* (3), 367-81.
6. Gong, S.; Gabriel, M. C. S.; Zini, A.; Chan, P.; O'Flaherty, C. Low Amounts and High Thiol Oxidation of Peroxiredoxins in Spermatozoa From Infertile Men. *Journal of Andrology* **2012,** *33* (6), 1342-1351.
7. Morado, S.; Cetica, P.; Beconi, M.; Thompson, J. G.; Dalvit, G. Reactive oxygen species production and redox state in parthenogenetic and sperm-mediated bovine oocyte activation. *Reproduction* **2013,** *145* (5), 471-8.
8. Camello-Almaraz, C.; Gomez-Pinilla, P. J.; Pozo, M. J.; Camello, P. J. *Mitochondrial reactive oxygen species and Ca2+ signaling*. 2006; Vol. 291, p C1082-C1088.
9. Balaban, R. S.; Nemoto, S.; Finkel, T. Mitochondria, oxidants, and aging. *Cell (Cambridge, MA, United States)* **2005,** *120* (4), 483-495.
10. Winterbourn, C. C. Reconciling the chemistry and biology of reactive oxygen species. *Nature Chemical Biology* **2008,** *4* (5), 278-286.
11. Dröge, W. Free Radicals in the Physiological Control of Cell Function. *Physiological Reviews* **2002,** *82* (1), 47-95.
12. Aitken, R. J.; Wingate, J. K.; De Iuliis, G. N.; Koppers, A. J.; McLaughlin, E. A. Cis-unsaturated fatty acids stimulate reactive oxygen species generation and lipid peroxidation in human spermatozoa. *Journal of Clinical Endocrinology and Metabolism* **2006,** *91* (10), 4154-4163.
13. Camello-Almaraz, C.; Gomez-Pinilla, P. J.; Pozo, M. J.; Camello, P. J. Mitochondrial reactive oxygen species and Ca2+ signaling. *American Journal of Physiology - Cell Physiology* **2006,** *291* (5), C1082-C1088.
14. Maghzal, G. J.; Krause, K.-H.; Stocker, R.; Jaquet, V. Detection of reactive oxygen species derived from the family of NOX NADPH oxidases. *Free Radical Biology & Medicine* **2012,** *53* (10), 1903-1918.
15. Vandaele, L.; Thys, M.; Bijttebier, J.; Van Langendonckt, A.; Donnay, I.; Maes, D.; Meyer, E.; Van Soom, A. Short-term exposure to hydrogen peroxide during oocyte maturation improves bovine embryo development. *Reproduction (Bristol, United Kingdom)* **2010,** *139* (3), 505-511.
16. Rahman, M. B.; Vandaele, L.; Rijsselaere, T.; Zhandi, M.; Maes, D.; Shamsuddin, M.; Van Soom, A. Oocyte quality determines bovine embryo development after fertilisation with hydrogen peroxide-stressed spermatozoa. *Reproduction, fertility, and development* **2012,** *24* (4), 608-18.
17. Nasr-Esfahani, M. H.; Aitken, J. R.; Johnson, M. H. Hydrogen peroxide levels in mouse oocytes and early cleavage stage embryos developed in vitro or in vivo. *Development* **1990,** *109* (2), 501-507.
18. Pacher, P.; Beckman, J. S.; Liaudet, L. Nitric Oxide and Peroxynitrite in Health and Disease. *Physiological Reviews* **2007,** *87* (1), 315-424.
19. Groeger, G.; Quiney, C.; Cotter, T. G. Hydrogen peroxide as a cell-survival signaling molecule. *Antioxid Redox Signal* **2009,** *11* (11), 2655-71.
20. Miller, E. W.; Tulyanthan, O.; Isacoff, E. Y.; Chang, C. J. Molecular imaging of hydrogen peroxide produced for cell signaling. *Nature Chemical Biology* **2007,** *3* (5), 263-267.
21. Stone, J. R.; Yang, S. Hydrogen Peroxide: A Signaling Messenger. *Antioxidants & Redox Signaling* **2006,** *8* (3 & 4), 243-270.
22. Thannickal, V. J.; Fanburg, B. L. *Reactive oxygen species in cell signaling*. 2000; Vol. 279, p L1005-L1028.
23. Aitken, R. J.; Buckingham, D.; Harkiss, D. Use of a xanthine oxidase free radical generating system to investigate the cytotoxic effects of reactive oxygen species on human spermatozoa. *Journal of Reproduction and Fertility* **1993,** *97* (2), 441-450.
24. Armstrong, J. S.; Rajasekaran, M.; Chamulitrat, W.; Gatti, P.; Hellstrom, W. J.; Sikka, S. C. Characterization of reactive oxygen species induced effects on human spermatozoa movement and energy metabolism. *Free Radical Biology and Medicine* **1999,** *26* (7–8), 869-880.

25. Baumber, J.; Ball, B. A.; Gravance, C. G.; Medina, V.; Davies-Morel, M. C. G. The Effect of Reactive Oxygen Species on Equine Sperm Motility, Viability, Acrosomal Integrity, Mitochondrial Membrane Potential, and Membrane Lipid Peroxidation. *Journal of Andrology* **2000,** *21* (6), 895-902.
26. Chan, J.; Dodani, S. C.; Chang, C. J. Reaction-based small-molecule fluorescent probes for chemoselective bioimaging. *Nature Chemistry* **2012,** *4* (12), 973-984.
27. Shelfscientific. Micro Dissolved Oxygen Electrode. http://www.shelfscientific.com/cgi-bin/tame/newlaz/domicro.tam (accessed 18/10/2012).
28. Altura, D., Personal communication, 2012, Lazar Research Laboratories.
29. Yu, M.; Beyers, R. J.; Gorden, J. D.; Cross, J. N.; Goldsmith, C. R. A Magnetic Resonance Imaging Contrast Agent Capable of Detecting Hydrogen Peroxide. *Inorganic Chemistry* **2012,** *51* (17), 9153-9155.
30. Lippert, A. R.; Van de Bittner, G. C.; Chang, C. J. Boronate Oxidation as a Bioorthogonal Reaction Approach for Studying the Chemistry of Hydrogen Peroxide in Living Systems. *Accounts of Chemical Research* **2011,** *44* (9), 793-804.
31. Alexa Fluor® 488 dye. https://www.thermofisher.com/au/en/home/life-science/cell-analysis/fluorophores/alexa-fluor-488.html?icid=fr-af488-main (accessed 07/10/2015).
32. Lindhoud, S.; Westphal, A. H.; Visser, A. J. W. G.; Borst, J. W.; van Mierlo, C. P. M. Fluorescence of Alexa Fluor Dye Tracks Protein Folding. *PLoS ONE* **2012,** *7* (10), e46838.
33. Howarth, M.; Takao, K.; Hayashi, Y.; Ting, A. Y. Targeting quantum dots to surface proteins in living cells with biotin ligase. *Proc Natl Acad Sci U S A* **2005,** *102* (21), 7583-8.
34. Kuo, Y.; Hsu, T. Y.; Wu, Y. C.; Chang, H. C. Fluorescent nanodiamond as a probe for the intercellular transport of proteins in vivo. *Biomaterials* **2013,** *34* (33), 8352-60.
35. Misteli, T.; Spector, D. L. Applications of the green fluorescent protein in cell biology and biotechnology. *Nat Biotech* **1997,** *15* (10), 961-964.
36. Terai, T.; Nagano, T. Small-molecule fluorophores and fluorescent probes for bioimaging. *Pflugers Archiv : European journal of physiology* **2013,** *465* (3), 347-59.
37. Heng, S.; McDevitt, C. A.; Stubing, D. B.; Whittall, J. J.; Thompson, J. G.; Engler, T. K.; Abell, A. D.; Monro, T. M. Microstructured Optical Fibers and Live Cells: A Water-Soluble, Photochromic Zinc Sensor. *Biomacromolecules* **2013,** *14* (10), 3376-3379.
38. Heng, S.; Nguyen, M.-C.; Kostecki, R.; Monro, T. M.; Abell, A. D. Nanoliter-scale, regenerable ion sensor: sensing with a surface functionalized microstructured optical fibre. *RSC Advances* **2013,** *3* (22), 8308.
39. Heng, S.; Mak, A. M.; Stubing, D. B.; Monro, T. M.; Abell, A. D. Dual Sensor for Cd(II) and Ca(II): Selective Nanoliter-Scale Sensing of Metal Ions. *Analytical Chemistry* **2014,** *86* (7), 3268-3272.
40. Apfel, U.-P.; Buccella, D.; Wilson, J. J.; Lippard, S. J. Detection of Nitric Oxide and Nitroxyl with Benzoresorufin-Based Fluorescent Sensors. *Inorganic Chemistry* **2013,** *52* (6), 3285-3294.
41. Valeur, B. *Molecular Fluorescence Principles and Applications (2nd Edition)*. John Wiley & Sons, Incorporated: Somerset, NJ, USA, 2013.
42. Atkins, P.; de Paula, J. *Atkins' Physical Chemistry*. OUP Oxford: 2010.
43. Schartner, E. P.; Jin, D.; Ebendorff-Heidepriem, H.; Piper, J. A.; Lu, Z.; Monro, T. M. Lanthanide upconversion within microstructured optical fibers: improved detection limits for sensing and the demonstration of a new tool for nanocrystal characterization. *Nanoscale* **2012,** *4* (23), 7448-7451.
44. Zhao, J.; Jin, D.; Schartner, E. P.; Lu, Y.; Liu, Y.; Zvyagin, A. V.; Zhang, L.; Dawes, J. M.; Xi, P.; Piper, J. A.; Goldys, E. M.; Monro, T. M. Single-nanocrystal sensitivity achieved by enhanced upconversion luminescence. *Nat Nano* **2013,** *8* (10), 729-734.
45. Stanton, I. N. Synthesis, Characterization, and Spectroscopy of Lanthanide-Doped Inorganic Nanocrystals; Radiant Flux and Absolute Quantum Yield Measurements of Upconversion Nanocrystals, and Fabrication of a Fiber-Optic Radiation Detector Utilizing Synthetically Optimized, Linearly Responsive Nanoscintillators. 2013.

46. Kim, Y.; Ho, S. O.; Gassman, N. R.; Korlann, Y.; Landorf, E. V.; Collart, F. R.; Weiss, S. Efficient Site-Specific Labeling of Proteins via Cysteines. *Bioconjugate Chemistry* **2008,** *19* (3), 786-791.
47. Carter, K. P.; Young, A. M.; Palmer, A. E. Fluorescent Sensors for Measuring Metal Ions in Living Systems. *Chemical Reviews* **2014,** *114* (8), 4564-4601.
48. Loudet, A.; Burgess, K. BODIPY Dyes and Their Derivatives: Syntheses and Spectroscopic Properties. *Chemical Reviews* **2007,** *107* (11), 4891-4932.
49. Zheng, H.; Zhan, X.-Q.; Bian, Q.-N.; Zhang, X.-J. Advances in modifying fluorescein and rhodamine fluorophores as fluorescent chemosensors. *Chemical Communications (Cambridge, United Kingdom)* **2013,** *49* (5), 429-447.
50. Li, X.; Gao, X.; Shi, W.; Ma, H. Design strategies for water-soluble small molecular chromogenic and fluorogenic probes. *Chem Rev* **2014,** *114* (1), 590-659.
51. Robertson, T.; Bunel, F.; Roberts, M. Fluorescein Derivatives in Intravital Fluorescence Imaging. *Cells* **2013,** *2* (3), 591-606.
52. Beija, M.; Afonso, C. A.; Martinho, J. M. Synthesis and applications of Rhodamine derivatives as fluorescent probes. *Chem Soc Rev* **2009,** *38* (8), 2410-33.
53. Hitomi, Y.; Takeyasu, T.; Funabiki, T.; Kodera, M. Detection of Enzymatically Generated Hydrogen Peroxide by Metal-Based Fluorescent Probe. *Analytical Chemistry (Washington, DC, United States)* **2011,** *83* (24), 9213-9216.
54. Miller, E. W.; Albers, A. E.; Pralle, A.; Isacoff, E. Y.; Chang, C. J. Boronate-Based Fluorescent Probes for Imaging Cellular Hydrogen Peroxide. *Journal of the American Chemical Society* **2005,** *127* (47), 16652-16659.
55. Zhao, B.; Ranguelova, K.; Jiang, J.; Mason, R. P. Studies on the photosensitized reduction of resorufin and implications for the detection of oxidative stress with Amplex Red. *Free Radical Biology & Medicine* **2011,** *51* (1), 153-159.
56. Albers, A. E.; Okreglak, V. S.; Chang, C. J. A FRET-Based Approach to Ratiometric Fluorescence Detection of Hydrogen Peroxide. *Journal of the American Chemical Society* **2006,** *128* (30), 9640-9641.
57. Du, L.; Ni, N.; Li, M.; Wang, B. A fluorescent hydrogen peroxide probe based on a click' modified coumarin fluorophore. *Tetrahedron Letters* **2010,** *51* (8), 1152-1154.
58. Hanthorn, J. J.; Haidasz, E.; Gebhardt, P.; Pratt, D. A. A versatile fluorescence approach to kinetic studies of hydrocarbon autoxidations and their inhibition by radical-trapping antioxidants. *Chemical Communications (Cambridge, United Kingdom)* **2012,** *48* (81), 10141-10143.
59. Pramitha, P.; Bahulayan, D. Stereoselective synthesis of bio-hybrid amphiphiles of coumarin derivatives by Ugi-Mannich triazole randomization using copper catalyzed alkyne azide click chemistry. *Bioorganic & Medicinal Chemistry Letters* **2012,** *22* (7), 2598-2603.
60. Soh, N.; Sakawaki, O.; Makihara, K.; Odo, Y.; Fukaminato, T.; Kawai, T.; Irie, M.; Imato, T. Design and development of a fluorescent probe for monitoring hydrogen peroxide using photoinduced electron transfer. *Bioorganic & Medicinal Chemistry* **2005,** *13* (4), 1131-1139.
61. Kim, D.; Yamamoto, K.; Ahn, K. H. A BODIPY-based reactive probe for ratiometric fluorescence sensing of mercury ions. *Tetrahedron* **2012,** *68* (26), 5279-5282.
62. Komatsu, T.; Oushiki, D.; Takeda, A.; Miyamura, M.; Ueno, T.; Terai, T.; Hanaoka, K.; Urano, Y.; Mineno, T.; Nagano, T. Rational design of boron dipyrromethene (BODIPY)-based photobleaching-resistant fluorophores applicable to a protein dynamics study. *Chemical communications* **2011,** *47* (36), 10055-7.
63. Lai, Y.-C.; Chang, C.-C. Photostable BODIPY-based molecule with simultaneous type I and type II photosensitization for selective photodynamic cancer therapy. *Journal of Materials Chemistry B* **2014,** *2* (11), 1576.
64. Zhang, C.; Zhao, J.; Wu, S.; Wang, Z.; Wu, W.; Ma, J.; Guo, S.; Huang, L. Intramolecular RET enhanced visible light-absorbing bodipy organic triplet photosensitizers and application in photooxidation and triplet-triplet annihilation upconversion. *J Am Chem Soc* **2013,** *135* (28), 10566-78.

65. Ziessel, R.; Ulrich, G.; Haefele, A.; Harriman, A. An artificial light-harvesting array constructed from multiple Bodipy dyes. *J Am Chem Soc* **2013,** *135* (30), 11330-44.
66. Grecco, H. E.; Verveer, P. J. FRET in Cell Biology: Still Shining in the Age of Super-Resolution? *ChemPhysChem* **2011,** *12* (3), 484-490.
67. Yuan, L.; Lin, W.; Zheng, K.; Zhu, S. FRET-Based Small-Molecule Fluorescent Probes: Rational Design and Bioimaging Applications. *Accounts of Chemical Research* **2013,** *46* (7), 1462-1473.
68. Lakowicz, J. R. *Principles of Fluorescence Spectroscopy*. Springer US: 2013.
69. Lee, M. H.; Kim, H. J.; Yoon, S.; Park, N.; Kim, J. S. Metal Ion Induced FRET OFF−ON in Tren/Dansyl-Appended Rhodamine. *Organic Letters* **2008,** *10* (2), 213-216.
70. Yuan, L.; Lin, W.; Xie, Y.; Chen, B.; Song, J. Development of a ratiometric fluorescent sensor for ratiometric imaging of endogenously produced nitric oxide in macrophage cells. *Chemical communications* **2011,** *47* (33), 9372-4.
71. Englich, F. V.; Foo, T. C.; Richardson, A. C.; Ebendorff-Heidepriem, H.; Sumby, C. J.; Monro, T. M. Photoinduced electron transfer based ion sensing within an optical fiber. *Sensors* **2011,** *11*, 9560-9572.
72. Kobayashi, H.; Ogawa, M.; Alford, R.; Choyke, P. L.; Urano, Y. New Strategies for Fluorescent Probe Design in Medical Diagnostic Imaging. *Chemical Reviews* **2010,** *110* (5), 2620-2640.
73. Schaeferling, M.; Groegel, D. B. M.; Schreml, S. Luminescent probes for detection and imaging of hydrogen peroxide. *Microchimica Acta* **2011,** *174* (1-2), 1-18.
74. Owusu-Ansah, E.; Yavari, A.; Banerjee, U. A protocol for _in vivo_ detection of reactive oxygen species. **2008**.
75. Robinson, K. M.; Janes, M. S.; Pehar, M.; Monette, J. S.; Ross, M. F.; Hagen, T. M.; Murphy, M. P.; Beckman, J. S. Selective fluorescent imaging of superoxide in vivo using ethidium-based probes. *Proc Natl Acad Sci U S A* **2006,** *103* (41), 15038-43.
76. Robinson, K. M.; Janes, M. S.; Beckman, J. S. The selective detection of mitochondrial superoxide by live cell imaging. *Nature protocols* **2008,** *3* (6), 941-7.
77. Wardman, P. Fluorescent and luminescent probes for measurement of oxidative and nitrosative species in cells and tissues: Progress, pitfalls, and prospects. *Free Radical Biology and Medicine* **2007,** *43* (7), 995-1022.
78. Zielonka, J.; Kalyanaraman, B. Hydroethidine- and MitoSOX-derived red fluorescence is not a reliable indicator of intracellular superoxide formation: Another inconvenient truth. *Free Radical Biology and Medicine* **2010,** *48* (8), 983-1001.
79. Hempel, S. L.; Buettner, G. R.; O'Malley, Y. Q.; Wessels, D. A.; Flaherty, D. M. Dihydrofluorescein diacetate is superior for detecting intracellular oxidants: comparison with 2′,7′-dichlorodihydrofluorescein diacetate, 5(and 6)-carboxy-2′,7′-dichlorodihydrofluorescein diacetate, and dihydrorhodamine 123. *Free Radical Biology and Medicine* **1999,** *27* (1–2), 146-159.
80. Qin, Y.; Lu, M.; Gong, X. Dihydrorhodamine 123 is superior to 2,7-dichlorodihydrofluorescein diacetate and dihydrorhodamine 6G in detecting intracellular hydrogen peroxide in tumor cells. *Cell Biology International* **2008,** *32* (2), 224-228.
81. Kalyanaraman, B.; Darley-Usmar, V.; Davies, K. J. A.; Dennery, P. A.; Forman, H. J.; Grisham, M. B.; Mann, G. E.; Moore, K.; Roberts, L. J., II; Ischiropoulos, H. Measuring reactive oxygen and nitrogen species with fluorescent probes: challenges and limitations. *Free Radical Biology & Medicine* **2012,** *52* (1), 1-6.
82. Koide, Y.; Kawaguchi, M.; Urano, Y.; Hanaoka, K.; Komatsu, T.; Abo, M.; Terai, T.; Nagano, T. A reversible near-infrared fluorescence probe for reactive oxygen species based on Te-rhodamine. *Chemical communications* **2012,** *48* (25), 3091-3.
83. Yeow, J.; Kaur, A.; Anscomb, M. D.; New, E. J. A novel flavin derivative reveals the impact of glucose on oxidative stress in adipocytes. *Chemical communications* **2014,** *50* (60), 8181-8184.
84. Kaur, A.; Haghighatbin, M. A.; Hogan, C. F.; New, E. J. A FRET-based ratiometric redox probe for detecting oxidative stress by confocal microscopy, FLIM and flow cytometry. *Chemical communications* **2015,** *51* (52), 10510-10513.

85. Amplex® Red Hydrogen Peroxide/Peroxidase Assay Kit. https://www.thermofisher.com/order/catalog/product/A22188 (accessed 06/10/2015).
86. Maeda, H.; Fukuyasu, Y.; Yoshida, S.; Fukuda, M.; Saeki, K.; Matsuno, H.; Yamauchi, Y.; Yoshida, K.; Hirata, K.; Miyamoto, K. Fluorescent probes for hydrogen peroxide based on a non-oxidative mechanism. *Angewandte Chemie, International Edition* **2004,** *43* (18), 2389-2391.
87. Xu, K.; Tang, B.; Huang, H.; Yang, G.; Chen, Z.; Li, P.; An, L. Strong red fluorescent probes suitable for detecting hydrogen peroxide generated by mice peritoneal macrophages. *Chemical Communications (Cambridge, United Kingdom)* **2005,** (48), 5974-5976.
88. Mishin, V.; Gray, J. P.; Heck, D. E.; Laskin, D. L.; Laskin, J. D. Application of the Amplex red/horseradish peroxidase assay to measure hydrogen peroxide generation by recombinant microsomal enzymes. *Free Radical Biology & Medicine* **2010,** *48* (11), 1485-1491.
89. Schartner, E. P. Hydrogen Peroxide Sensing with Microstructured Optical Fibres. University of Adelaide, 2011.
90. Chen, X.; Tian, X.; Shin, I.; Yoon, J. Fluorescent and luminescent probes for detection of reactive oxygen and nitrogen species. *Chemical Society Reviews* **2011,** *40* (9), 4783-4804.
91. Belousov, V. V.; Fradkov, A. F.; Lukyanov, K. A.; Staroverov, D. B.; Shakhbazov, K. S.; Terskikh, A. V.; Lukyanov, S. Genetically encoded fluorescent indicator for intracellular hydrogen peroxide. *Nature Methods* **2006,** *3* (4), 281-286.
92. Bilan, D. S.; Pase, L.; Joosen, L.; Gorokhovatsky, A. Y.; Ermakova, Y. G.; Gadella, T. W. J.; Grabher, C.; Schultz, C.; Lukyanov, S.; Belousov, V. V. HyPer-3: A Genetically Encoded H2O2 Probe with Improved Performance for Ratiometric and Fluorescence Lifetime Imaging. *ACS Chemical Biology*, Ahead of Print.
93. Kuivila, H. G.; Armour, A. G. Electrophilic Displacement Reactions. IX. Effects of Substituents on Rates of Reactions between Hydrogen Peroxide and Benzeneboronic Acid. *Journal of the American Chemical Society* **1957,** *79* (21), 5659-5662.
94. Chang, M. C. Y.; Pralle, A.; Isacoff, E. Y.; Chang, C. J. A selective, cell-permeable optical probe for hydrogen peroxide in living cells. *Journal of the American Chemical Society* **2004,** *126* (47), 15392-15393.
95. Albers, A. E.; Dickinson, B. C.; Miller, E. W.; Chang, C. J. A red-emitting naphthofluorescein-based fluorescent probe for selective detection of hydrogen peroxide in living cells. *Bioorganic & Medicinal Chemistry Letters* **2008,** *18* (22), 5948-5950.
96. Dickinson, B. C.; Huynh, C.; Chang, C. J. A Palette of Fluorescent Probes with Varying Emission Colors for Imaging Hydrogen Peroxide Signaling in Living Cells. *Journal of the American Chemical Society* **2010,** *132* (16), 5906-5915.
97. Dickinson, B. C.; Lin, V. S.; Chang, C. J. Preparation and use of MitoPY1 for imaging hydrogen peroxide in mitochondria of live cells. *Nature protocols* **2013,** *8* (6), 1249-59.
98. Srikun, D.; Albers, A. E.; Nam, C. I.; Iavarone, A. T.; Chang, C. J. Organelle-Targetable Fluorescent Probes for Imaging Hydrogen Peroxide in Living Cells via SNAP-Tag Protein Labeling. *Journal of the American Chemical Society* **2010,** *132* (12), 4455-4465.
99. Dickinson, B. C.; Peltier, J.; Stone, D.; Schaffer, D. V.; Chang, C. J. Nox2 redox signaling maintains essential cell populations in the brain. *Nat Chem Biol* **2011,** *7* (2), 106-112.
100. Sikora, A.; Zielonka, J.; Lopez, M.; Joseph, J.; Kalyanaraman, B. Direct oxidation of boronates by peroxynitrite: Mechanism and implications in fluorescence imaging of peroxynitrite. *Free Radical Biology & Medicine* **2009,** *47* (10), 1401-1407.
101. Zielonka, J.; Sikora, A.; Joseph, J.; Kalyanaraman, B. Peroxynitrite Is the Major Species Formed from Different Flux Ratios of Co-generated Nitric Oxide and Superoxide: Direct Reaction with Boronate-based Fluorescent Probe. *Journal of Biological Chemistry* **2010,** *285* (19), 14210-14216.
102. Sawaki, Y.; Foote, C. S. Acyclic mechanism in the cleavage of benzils with alkaline hydrogen peroxide. *Journal of the American Chemical Society* **1979,** *101* (21), 6292-6296.

103. Abo, M.; Urano, Y.; Hanaoka, K.; Terai, T.; Komatsu, T.; Nagano, T. Development of a Highly Sensitive Fluorescence Probe for Hydrogen Peroxide. *Journal of the American Chemical Society* **2011,** *133* (27), 10629-10637.
104. Abo, M.; Minakami, R.; Miyano, K.; Kamiya, M.; Nagano, T.; Urano, Y.; Sumimoto, H. Visualization of phagosomal hydrogen peroxide production by a novel fluorescent probe that is localized via SNAP-tag labeling. *Anal Chem* **2014,** *86* (12), 5983-90.
105. Culshaw, B. Optical fiber sensor technologies: opportunities and-perhaps-pitfalls. *Lightwave Technology, Journal of* **2004,** *22* (1), 39-50.
106. Thompson, R. B.; Lakowicz, J. R. Fiber optic pH sensor based on phase fluorescence lifetimes. *Analytical Chemistry* **1993,** *65* (7), 853-856.
107. Kermis, H. R.; Kostov, Y.; Harms, P.; Rao, G. Dual Excitation Ratiometric Fluorescent pH Sensor for Noninvasive Bioprocess Monitoring: Development and Application. *Biotechnology Progress* **2002,** *18* (5), 1047-1053.
108. Leung, A.; Shankar, P. M.; Mutharasan, R. A review of fiber-optic biosensors. *Sensors and Actuators B: Chemical* **2007,** *125* (2), 688-703.
109. Tan, W.; Shi, Z. Y.; Smith, S.; Birnbaum, D.; Kopelman, R. Submicrometer intracellular chemical optical fiber sensors. *Science* **1992,** *258* (5083), 778-81.
110. Schartner, E.; Monro, T. Fibre Tip Sensors for Localised Temperature Sensing Based on Rare Earth-Doped Glass Coatings. *Sensors* **2014,** *14* (11), 21693.
111. Song, A.; Parus, S.; Kopelman, R. High-Performance Fiber-Optic pH Microsensors for Practical Physiological Measurements Using a Dual-Emission Sensitive Dye. *Analytical Chemistry* **1997,** *69* (5), 863-867.
112. Podrazký, O.; Mrázek, J.; Vytykáčová, S.; Proboštová, J.; Kašík, I. In *Fiber optic pH sensing system with microscopic spatial resolution*, 2015; pp 950612-950612-6.
113. Henderson, M. R.; Schartner, E. P.; Callen, D. F.; Gill, P. G.; Monro, T. M. In *Fibre tip pH sensor for tumor detection during surgery*, 2015; pp 950611-950611-8.
114. Botero-Cadavid, J. F.; Brolo, A. G.; Wild, P.; Djilali, N. Detection of hydrogen peroxide using an optical fiber-based sensing probe. *Sensors and Actuators B: Chemical* **2013,** *185*, 166-173.
115. Monro, T. M.; Belardi, W.; Furusawa, K.; Baggett, J. C.; Broderick, N. G. R.; Richardson, D. J. Sensing with microstructured optical fibres. *Measurement Science and Technology* **2001,** *12*, 854-858.
116. Frazão, O.; Silva, R. M.; Ferreira, M. S.; Santos, J. L.; Lobo Ribeiro, A. B. Suspended-core fibers for sensing applications. *Photonic Sensors* **2012,** *2* (2), 118-126.
117. Schartner, E. P.; Ebendorff-Heidepriem, H.; Monro, T. M. Sensitive fluorescence detection with microstructured optical fibers. *Proceedings of SPIE* **2011,** *8028* (Fiber Optic Sensors and Applications VIII), 802805/1-802805/8.
118. Schartner, E. P.; Ebendorff-Heidepriem, H.; Warren-Smith, S. C.; White, R. T.; Monro, T. M. Driving down the detection limit in microstructured fiber-based chemical dip sensors. *Sensors* **2011,** *11*, 2961-2971.
119. Schartner, E. P.; Ebendorff-Heidepriem, H.; Monro, T. M. Low concentration fluorescence sensing in suspended-core fibers. *Proceedings of SPIE* **2011,** *7753* (Pt. 1, 21st International Conference on Optical Fiber Sensors, 2011), 77534Q/1-77534Q/4.
120. Schartner, E. P.; Zvarec, O.; Francois, A.; Ebendorff-Heidepriem, H.; Abell, A. D.; Monro, T. M. A Low Volume Sensor for Hydrogen Peroxide Based on Surface Functionalised Microstructured Optical Fibres. University of Adelaide: 2012.

Chapter 2

BORONATE PROBES FOR THE DETECTION OF HYDROGEN PEROXIDE RELEASE FROM HUMAN SPERMATOZOA

There are no such things as applied sciences, only applications of science.

Louis Pasteur

STATEMENT OF AUTHORSHIP

Title of Paper	Boronate Probes for the Detection of Hydrogen Peroxide Release from Human Spermatozoa
Publication Status	☑ Published ☐ Accepted for Publication ☐ Submitted for Publication ☐ Publication Style
Publication Details	Purdey, M. S.; Connaughton, H. S.; Whiting, S.; Schartner, E. P.; Monro, T. M.; Thompson, J. G.; Aitken, R. J.; Abell, A. D., Boronate probes for the detection of hydrogen peroxide release from human spermatozoa. *Free Radical Biology and Medicine* **2015,** *81* (0), 69-76.

Principal Author

Name of Principal Author (Candidate)	Malcolm S. Purdey		
Contribution to the Paper	Synthesis of Fluorescent Probes, solution-based fluorescence studies, selectivity assays for various reactive oxygen species, assistance with biological assays, assistance with FACS data analysis, statistical analysis of data, assistance with photostability experiment, writing of manuscript.		
Overall percentage (%)	60 %		
Signature		Date	13/10/15

Co-Author Contributions

By signing the Statement of Authorship, each author certifies that:

i. the candidate's stated contribution to the publication is accurate (as detailed above);

ii. permission is granted for the candidate in include the publication in the thesis; and

iii. the sum of all co-author contributions is equal to 100% less the candidate's stated contribution.

Name of Co-Author	Haley S. Connaughton		
Contribution to the Paper	Biological assays in sperm, FACS data analysis.		
Signature		Date	13/10/2015

Name of Co-Author	Sara Whiting
Contribution to the Paper	Biological assays in sperm, FACS data analysis.

Signature		Date	13/10/2015

Name of Co-Author	Erik P. Schartner		
Contribution to the Paper	Photostability experiment and editing of manuscript.		
Signature		Date	27/10/15

Name of Co-Author	Tanya M. Monro		
Contribution to the Paper	Project direction and editing of manuscript.		
Signature		Date	4/12/15

Name of Co-Author	Jeremy G. Thompson		
Contribution to the Paper	Project direction and editing of manuscript.		
Signature		Date	28/10/2015

Name of Co-Author	R. John Aitken		
Contribution to the Paper	Supervision of biological experiments, project direction and editing of manuscript.		
Signature		Date	15/10/2015

Name of Co-Author	Andrew D. Abell		
Contribution to the Paper	Supervision of synthesis and solution-based fluorescence assays, project direction and editing of manuscript.		
Signature		Date	16/10/2015

Chapter 2: Boronate Probes for the Detection of Hydrogen Peroxide Release from Human Spermatozoa*

Malcolm S. Purdey[a], Haley S. Connaughton[b], Sara Whiting[b], Erik P. Schartner[a], Tanya M. Monro[a], Jeremy G. Thompson[c], R. John Aitken[b]* and Andrew D. Abell[a]*

[a] ARC Centre of Excellence for Nanoscale BioPhotonics, Institute of Photonics & Advanced Sensing and School of Chemistry & Physics, The University of Adelaide, South Australia, Australia 5005

[b] Discipline of Biological Sciences and Priority Research Centre in Reproductive Science, Faculty of Science and IT, University of Newcastle, Callaghan, NSW, Australia 2308

[c] ARC Centre of Excellence for Nanoscale BioPhotonics, The Robinson Research Institute and School of Paediatrics and Reproductive Health, The University of Adelaide, South Australia, Australia 5005

2.1 ABSTRACT

Human spermatozoa are compromised by production of reactive oxygen species (ROS) and detection of ROS in spermatozoa is important for the diagnosis of male infertility. Probes 2',7'-dichlorohydrofluorescein diacetate (**DCFH**), dihydroethidium (**DHE**) and MitoSOX red (**MSR**) are commonly used for detecting ROS by flow cytometry, however these probes lack sensitivity to hydrogen peroxide (H_2O_2), which is particularly damaging to mammalian sperm cells. This study reports the synthesis and use of three aryl boronate probes, peroxyfluor-1 (**PF1**), carboxy peroxyfluor-1 (**CPF1**) and a novel probe 2(2-ethoxyethoxy)ethoxy peroxyfluor-1 (**EEPF1**) in human spermatozoa. **PF1** and **EEPF1** were found to be effective in detecting H_2O_2 and peroxynitrite ($ONOO^-$) produced by spermatozoa when stimulated with menadione or 4-hydroxynonenal. **EEPF1** was more effective at detection of ROS in spermatozoa than **DCFH**, **DHE** and **MSR**; furthermore it distinguished poorly motile sperm as shown by greater ROS production. **EEPF1** should therefore have a significant role in diagnosis of oxidative stress in male infertility, cryopreservation, age, lifestyle and exposure to environmental toxicants.

* Purdey, M. S.; Connaughton, H. S.; Whiting, S.; Schartner, E. P.; Monro, T. M.; Thompson, J. G.; Aitken, R. J.; Abell, A. D. *Free Radical Biology and Medicine* **2015**, *81*, 69-76.

2.2 INTRODUCTION

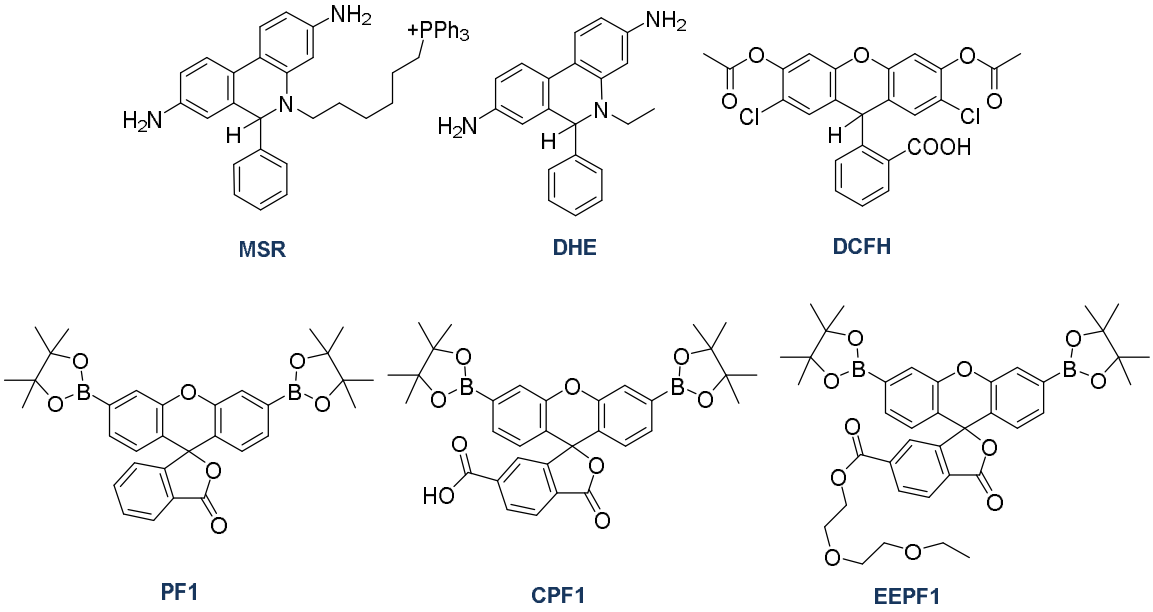

Figure 19. Chemical structures of the ROS sensors used in this study. **MSR**, **DHE** and **DCFH** are oxidised by removal of the indicated hydrogens to produce a fluorescent aromatic structure. **PF1**, **CPF1** and **EEPF1** are oxidised by the deprotection of the pinacolatoboron groups to produce highly fluorescent structures.

Reactive oxygen species (ROS) produced by human spermatozoa compromise sperm function[2-6] and as such their detection is important for the diagnosis of male infertility.[121] ROS are typically detected in human spermatozoa using fluorescent probes such as dihydroethidium (**DHE**), MitoSOX Red (**MSR**) and 2',7'-dichlorohydrofluorescein diacetate (**DCFH**) (**Figure 19**).[122] **DHE** is an intracellular ROS probe that fluoresces within both the head and the mitochondrial midsection of the spermatozoa upon oxidation. It is most commonly used for detection of superoxide ($O_2^{\bullet-}$), although it also reacts with hydrogen peroxide (H_2O_2) in the presence of peroxidases, and with oxidases and cytochromes.[75] **MSR** is a charged variant of **DHE** that localises in the mitochondrial matrix to predominantly respond to and measure the generation of $O_2^{\bullet-}$. **DCFH** is a fluorescein-based nonspecific probe that reportedly reacts with H_2O_2[123] and other ROS, particularly hydroxyl radicals ($^{\bullet}OH$) and peroxynitrite ($ONOO^-$).[124] This probe has some disadvantages, since it requires the concomitant presence of peroxidases to react with H_2O_2,[125] can undergo autoxidation and is known to catalyse $O_2^{\bullet-}$ production.[123] An aryl boronate probe reported by Chang et al.,[94] peroxyfluor-1 (**PF1**, **9**), reacts with both H_2O_2 and $ONOO^-$; but not $^{\bullet}OH$, $O_2^{\bullet-}$, nitrous oxide (NO) or hypochlorite (^-OCl).[94,100] This class of probe has found wide use for the *in vivo* detection of H_2O_2,[30] including research into ROS production in cryopreserved mouse spermatozoa.[126] The ability of aryl boronates to detect the low levels of ROS generated by mammalian spermatozoa suggests this class of probe as a potential diagnostic tool for the selective detection of ROS, particularly H_2O_2 in sperm cells. This would be of clinical

significant as several independent studies have indicated that H_2O_2 is particularly damaging to mammalian sperm function.[23-25]

A number of aryl boronates have been developed for use in a range biological applications.[30] We chose to use **PF1**, carboxyPF1 (**CPF1**) and a new probe 2(2-ethoxyethoxy)ethoxy-PF1 (**EEPF1**) for the study as they are structurally similar to allow for direct and meaningful comparison, while being relatively easy to prepare on both small and larger scale. This is an important consideration for future work in this area. **CPF1** is a variant of **PF1** originally synthesised for attachment to other functional groups.[127,128] **EEPF1** contains a truncated polyethylene glycol (PEG) group with increased hydrogen bond acceptors to enhance the aqueous solubility relative to **PF1**. A series of comparative studies were performed to define the relative ability of all three probes to detect ROS generation by human spermatozoa in a sensitive and selective manner. This study examines the relative capacities of these probes to detect H_2O_2 and $ONOO^-$ spontaneously generated by human spermatozoa exhibiting impaired motility. The results have important diagnostic implications for the facilitated detection of oxidative stress in mammalian spermatozoa exhibiting signs of impaired functionality.

2.3 RESULTS AND DISCUSSION

2.3.1 ROS Characterisation of Probes

The sensitivity of **EEPF1** to H_2O_2 was defined by incubating separate samples with 0-100 μM H_2O_2 and monitoring the resultant fluorescence, see **Figure 20A**. A clear, dose dependant response is evident, with an emission maximum at 525 nm. **EEPF1** was also incubated with 100 μM of each individual ROS to determine the selectivity of **EEPF1** for various ROS and the reactivity profiles are summarised in **Figure 20B**. For comparison, the reaction of **DCFH** with each ROS was also characterised and the results are shown in **Figure 20C**. Similar reactivity profiles for **PF1** and **CPF1** are reported in the supplementary data. **EEPF1** showed good reactivity with H_2O_2, and although there is a significant initial fluorescence response from $ONOO^-$, a greater overall fluorescence was observed for H_2O_2 over 40 min. This is likely due to the more transient nature of $ONOO^-$ compared with H_2O_2. Limited fluorescence was observed for the reaction of **EEPF1** with all other ROS studied, with a similar result for the other aryl boronates (section **2.7**, **Figure 25**). By contrast, **DCFH** reacts best with both $ONOO^-$ and $^{\bullet}OH$ (**Figure 20C**) and to a lesser extent with ^-OCl and $O_2^{\bullet-}$, but not H_2O_2, as shown in **Figure 20C**. This lack of reactivity to H_2O_2 is consistent with some literature,[124] but contrasts other reports that infer the detection of H_2O_2 using this probe.[123] However, **DCFH** is able to detect other ROS such as $^{\bullet}OH$ produced from H_2O_2 *in* vivo, and also H_2O_2 in the

presence of peroxidases.[125] Thus, the aryl boronates have a clear advantage over **DCFH** for the detection of H_2O_2 in the absence of any external catalyst.

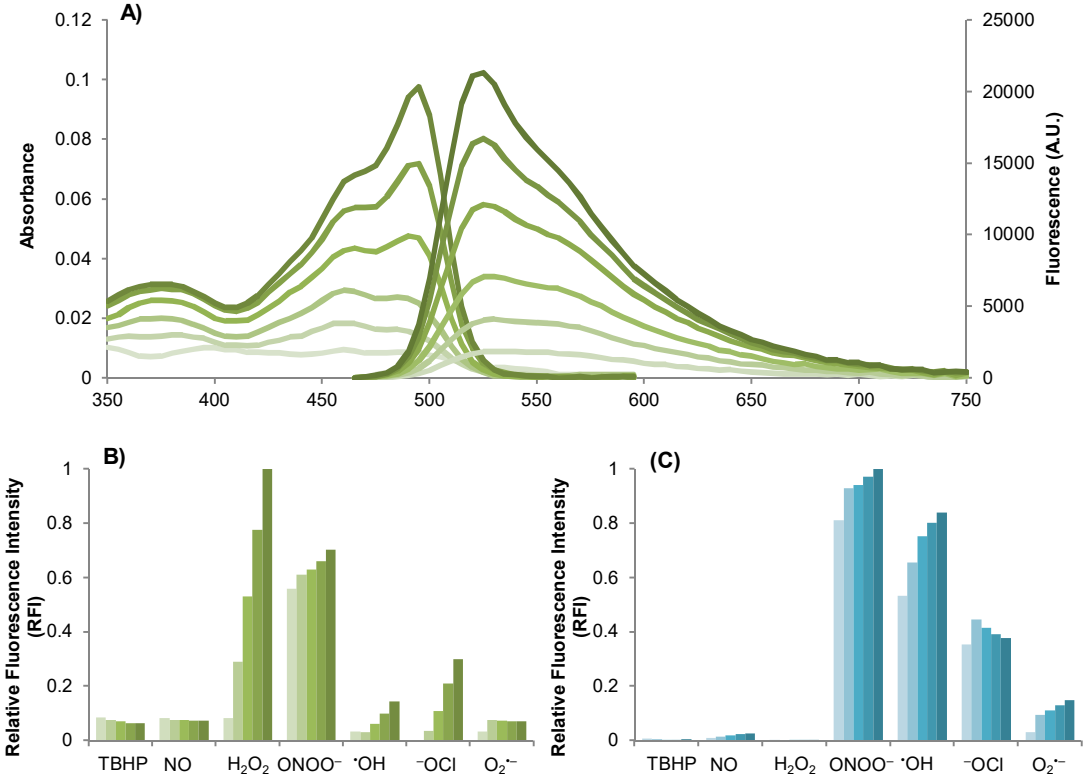

Figure 20. Fluorescence characterisation of **EEPF1** and comparison with **DCFH** for selectivity to ROS. A) Absorption and emission spectra of **EEPF1** when treated with 0, 10, 25, 50, 75 and 100 µM H_2O_2 and incubated at 37 °C for 40 min in 20 mM HEPES buffer. (Excitation at 450 nm). B) **EEPF1** and C) **DCFH** selectivity data, each incubated at 37 °C with 100 µM ROS and measured at 0, 10, 20, 30 and 40 min. (Excitation 450 nm, emission 520 nm).

2.3.2 Comparative Study on ROS Production in Human Spermatozoa

The ability of the aryl boronates **PF1**, **CPF1**, **EEPF1** and other probes described in the literature (the dihydrofluorescein **DCFH** and the hydroethidiums **DHE** and **MSR**) to detect ROS in spermatozoa was then studied in populations of human spermatozoa, with a view to defining their relative abilities to detect cellular ROS generation. ROS production in human spermatozoa was induced by treating samples with three different compounds, menadione, arachidonic acid (AA) and 4-hydroxynonenal (4HNE).[122] Menadione is a redox cycling quinone known to produce significant oxidative stress due to quinone oxidoreductase activity.[129,130] AA is a cis-unsaturated fatty acid associated with the production of $O_2^{\bullet-}$ by sperm mitochondria,[12,131] while 4HNE is a lipid-derived aldehyde responsible for the induction of mitochondrial ROS generation in senescent spermatozoa.[132] Further samples were also treated with 4mM H_2O_2 as a positive control for probes sensitive to H_2O_2 (**DCFH**, **PF1**, **CPF1**, **EEPF1**). The ROS-producing compounds were incubated separately with each

probe (**DCFH**, **DHE**, **MSR**, **PF1**, **CPF1** and **EEPF1**) and the resulting fluorescence response was measured by flow cytometry.

Figure 21 shows the percentage of fluorescent spermatozoa, indicating the percentage of spermatozoa that generated ROS as measured by each probe. **MSR** showed the largest background fluorescence in the negative control samples (**Figure 21A**), with significantly higher fluorescent populations ($P < 0.05$) than aryl boronates **PF1** and **CPF1**, presumably reflecting the active generation of mitochondrial ROS by populations of human spermatozoa, as previously described.[133] For the treated sperm samples, those incubated with **DHE** exhibited the smallest fluorescent populations for all stimuli (**Figure 21B-D**). Conversely, those stained with **EEPF1** consistently showed the largest fluorescent populations, with over 90% responding positively following treatment with the ROS-generating reagents (**Figure 21B-D**). **PF1** also showed readily measurable fluorescent responses to the stimuli, with comparable or larger fluorescent populations than **DCFH**, **DHE** and **MSR** (**Figure 21B-D**). Staining spermatozoa with **CPF1** gave the lowest fluorescent populations of all three aryl boronates. Nevertheless, treated sperm were more fluorescent with **CPF1** than with **DHE** and **DCFH** within the sperm treated with AA (**Figure 21C**) and 4HNE (**Figure 21D**) treatment groups.

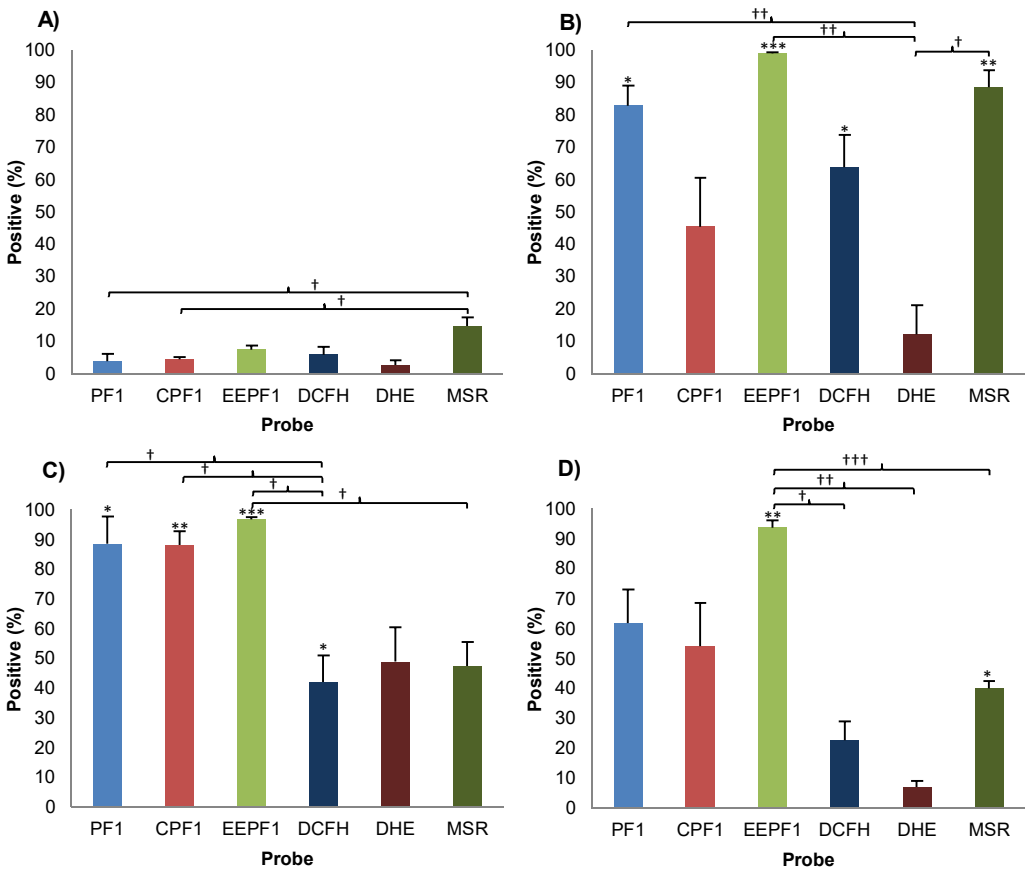

Figure 21. Analysis of flow cytometry results, showing the percentage of human sperm populations which indicated a fluorescent response. A) Negative control sample with no external stimulus. Samples exposed to stimuli: B) 50 µM menadione for 15 min, C) 50 µM AA for 15 min or D) 200 µM 4HNE for 30 min. Significance levels: *P < 0.05, **P < 0.01, ***P < 0.001 compared with untreated sample. †P < 0.05, ††P < 0.01, †††P < 0.001 as compared on graphs.

Thus the aryl boronates **PF1** and **EEPF1** were the most broadly sensitive of the probes to ROS produced by spermatozoa on stimulation with menadione, AA and 4HNE (**Figure 21B-D**) with the latter clearly being the most sensitive. The third aryl boronate (**CPF1**), while sensitive, gave less consistent results. Of the other probes, **MSR** gave the greatest response to each stimuli (**Figure 21B-D**), while **DHE** was the least sensitive.

The fluorescent populations shown in **Figure 21** also provide some insights into which ROS are produced by spermatozoa on treatment with menadione and 4HNE (results for AA are discussed separately, see **Figure 22**). Thus for samples stained with **MSR**, a smaller proportion of fluorescent cells was apparent for 4HNE treatments (**Figure 21D**) compared to menadione (**Figure 21B**), suggesting that the latter is the more efficient stimulator of $O_2^{\bullet-}$ production. In contrast, fluorescence of the aryl boronates **PF1**, **CPF1** and **EEPF1** were similar between menadione and 4HNE treatments (**Figure 21B & D**), indicating similar levels of H_2O_2/$ONOO^-$ production. This suggests an efficient conversion of $O_2^{\bullet-}$ (detected by **MSR**) to H_2O_2 or $ONOO^-$ (detected by the aryl boronates) in those samples treated with 4HNE.

However, similar to **MSR**, **DCFH** showed a lack of sensitivity for the ROS produced in response to 4HNE (**Figure 21D**) compared with the menadione (**Figure 21B**) treatments. Yet **DCFH** is also known to react with H_2O_2 and $ONOO^-$, as do the aryl boronates, suggesting that **DCFH** should have similar sensitivity to the 4HNE treatment as to menadione. This incongruity could be due to the production of $^{\bullet}OH$ in samples treated with menadione and not those treated with 4HNE. The $^{\bullet}OH$ radical reacts with **DCFH** but not with the aryl boronates, which would result in the greater positive populations observed for **DCFH** in samples treated with menadione than 4HNE (**Figure 21B & D**). Another likely explanation is the need for oxidation of **DCFH** to be facilitated by peroxidase which may not be trivial due to the highly compartmentalised nature of the spermatozoon, limiting the distribution and hence catalytic availability of the peroxidase. This again highlights the significant advantage of the aryl boronates over **DCFH** in this regard, as no external catalysis is required to produce a fluorescent response.

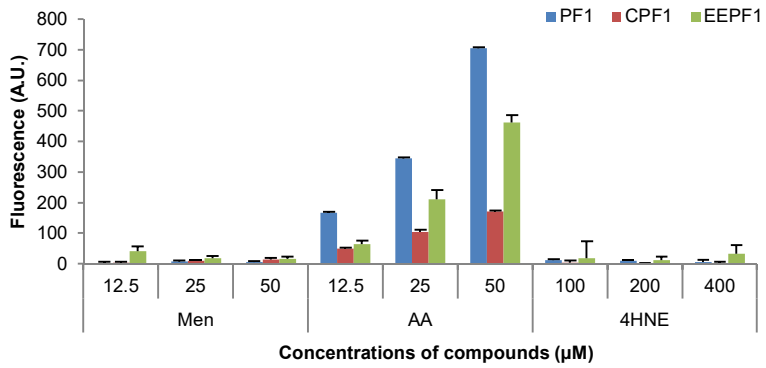

Figure 22. Fluorescence response of **PF1**, **CPF1** and **EEPF1** to menadione, AA and 4HNE in the absence of spermatozoa. Fluorescence readings were recorded in BWW solution after 30 min of incubation at 37 °C by a microplate reader. Excitation wavelength was 485 nm, emission recorded at 520 nm. Each probe gave a dose-dependent response upon exposure to AA, however no significant response was recorded when incubated with either menadione or 4HNE.

We next investigated the fluorescence of **PF1**, **CPF1** and **EEPF1** on incubation with menadione, AA and 4HNE in absence of spermatozoa, to directly assess the reactivity of the probes to these compounds. Menadione (12.5, 25, 50µM), AA (12.5, 25, 50µM) and 4HNE (100, 200, 400µM) were separately incubated with **PF1**, **CPF1** and **EEPF1** and the resulting fluorescence measured. A fluorescent response was not observed when **PF1**, **CPF1** or **EEPF1** were incubated with menadione or 4HNE (see **Figure 22**). However, AA did cause a dose-dependent response with **PF1** (r = 0.9999), **CPF1** (r = 0.9898) and **EEPF1** (0.9994) as shown in **Figure 22**. This is possibly due to auto-oxidation of AA, generating a hydroperoxide[134] capable of deprotecting the aryl boronates of the probes, thus leading to a fluorescent response. This may explain the observed increase in fluorescent population for

PF1, **CPF1** and **EEPF1** in the presence of AA compared to those populations stained with **DCFH**, **DHE** and **MSR**. AA was not used to induce ROS production in further experiments using spermatozoa with **PF1**, **CPF1** and **EEPF1**.

2.3.3 Sensitivity of Aryl Boronates to ROS Production in Human Spermatozoa

Dose-dependent studies were subsequently carried out to further define the sensitivity of the three new aryl boronates **PF1**, **CPF1** and **EEPF1** in spermatozoa stimulated with menadione, 4HNE and H_2O_2. Diphenylene iodonium (DPI), an inhibitor of NO and $O_2^{\bullet-}$ production by flavoproteins, was used to further test the sensitivity of the probes for ROS generation.

2.3.3.1 Menadione

Populations of spermatozoa treated with menadione and incubated with **EEPF1** show the largest fluorescent populations, see **Figure 23A**. This result is consistent with the earlier study comparing the aryl boronates to previously studied probes, where **EEPF1** gave the greatest fluorescent response of the six probes as shown in **Figure 21**. However, the populations stained with **EEPF1** (**Figure 23A**) were over 90 % positive at even the lowest concentration of menadione (12.5 μM), significantly larger than **PF1** ($P < 0.05$). Populations stained with **PF1** also revealed a dose-dependent increase in activity when treated with 12.5-50 μM menadione (**Figure 23A**, $r = 0.937$). In contrast, the fluorescent responses of populations stained with **CPF1** were not statistically significant even at 50 μM menadione (**Figure 23A**). Thus it appears that the new probe **EEPF1** is the most effective of the probes for ROS production in spermatozoa on stimulation with menadione. The existing aryl boronate **PF1** is significantly less effective, while **CPF1** is the least effective of all three. Microscope images of spermatozoa stained with **CPF1** and **EEPF1** were obtained (see supplementary data, **2.7**). ROS produced by both the head and the mitochondria-rich midpiece can be seen, indicating that neither **CPF1** nor **EEPF1** stained specifically for a location inside the cell.

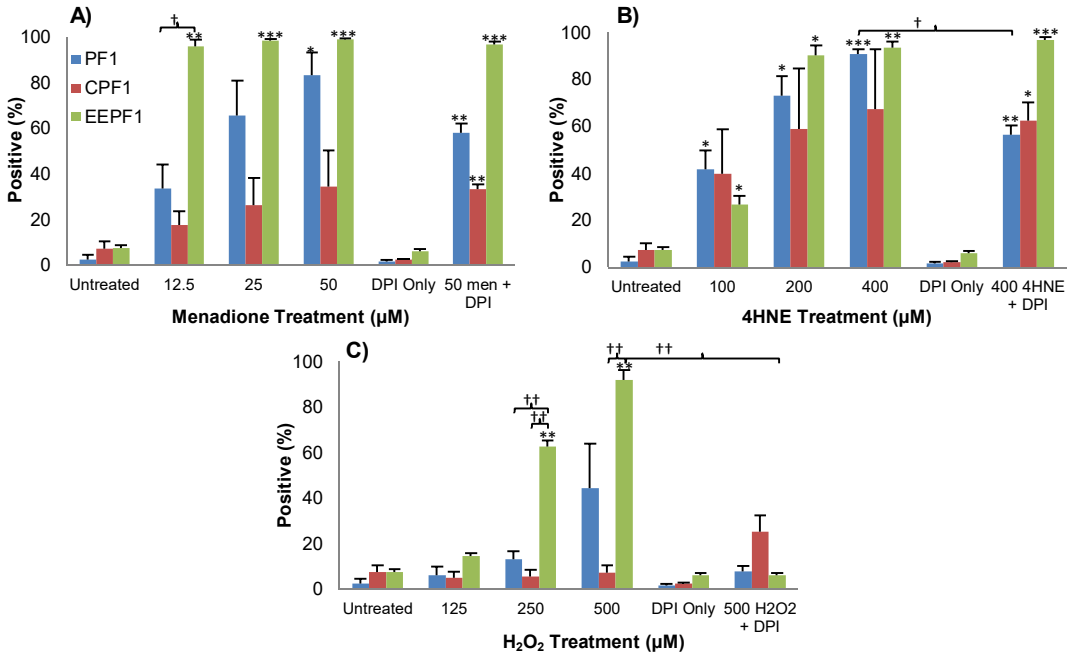

Figure 23. Analysis of flow cytometry results for menadione, 4HNE and H_2O_2 treated spermatozoa. A) Menadione treated spermatozoa exhibit dose-response correlation with **PF1** and **CPF1**; however **EEPF1** show large positive populations to 12.5, 25 and 50 µM treatments. B) **PF1**, **CPF1** and **EEPF1** all exhibit dose-response correlations to sperm stimulated with 4HNE. C) **EEPF1** show a dose-response correlating to spermatozoa treated with H_2O_2 concentrations 0-500 µM. Significance levels: *P < 0.05, **P < 0.01, ***P < 0.001 compared with untreated sample. †P < 0.05, ††P < 0.01 as compared on graph.

Co-incubation of DPI with 50 µM menadione did not significantly decrease the positive population for **EEPF1** and although suggested, no statistically significant reduction in signal was recorded in the presence of **PF1** and **CPF1** (**Figure 23A**) when treated with DPI. Overall, incubation with menadione indicated greater sensitivity of **EEPF1** over **PF1** and **CPF1**, suggesting that it may be a particularly useful probe for the detection of intracellular ROS.

2.3.3.2 4HNE

Figure 23B shows the fluorescent responses for spermatozoa treated with 4HNE. Samples stained with **PF1** or **EEPF1** revealed significant fluorescent populations at 100, 200 and 400 µM treatments of 4HNE. However those samples incubated with **CPF1** did not produce a significant fluorescent response as a consequence of the large variation associated with these measurements. The signal generated in the presence of **PF1** was significantly reduced ($P < 0.05$) in the presence of DPI. However, incubating with DPI did not reduce the fluorescent response for samples treated with **EEPF1**, again suggesting an increased efficacy over **PF1**. From these results it is clear that both **PF1** and **EEPF1** were capable of detecting significant H_2O_2 or $ONOO^-$ production by 4HNE-stimulated spermatozoa.

2.3.3.3 H_2O_2

EEPF1 gave the greatest fluorescent response to ROS in populations of spermatozoa treated with H_2O_2, see **Figure 23C**. These fluorescent populations correlated with the concentration of H_2O_2 added ($r = 0.946$, $P < 0.01$). **Figure 23C** also shows that in contrast, samples stained with **PF1** only gave a limited increase in positivity at 250 µM and 500 µM of H_2O_2 while **CPF1** generated a negligible fluorescence response, even for samples treated with up to 500 µM of H_2O_2. These results again indicate greater efficacy of **EEPF1** over **PF1** and **CPF1** for the detection of ROS produced by human spermatozoa stimulated with H_2O_2.

The mechanism by which H_2O_2 stimulates enhanced ROS generation by human spermatozoa is thought to involve the induction of lipid peroxidation followed by the covalent binding of lipid aldehydes such as 4HNE to proteins in the mitochondrial electron transport chain (ETC), particularly, succinic acid dehydrogenase.[12] The adduction of proteins within the ETC is, in turn, thought to lead to electron leakage and sustained ROS generation. The fact that DPI, an inhibitor of flavoproteins involved in mitochondrial electron transport such as succinic acid dehydrogenase, could significantly impair the ROS response to H_2O_2 as detected by **EEPF1** is in good agreement with this model.

In light of these results, **EEPF1** is clearly able to sense ROS produced by human spermatozoa more effectively than **PF1**, **CPF1**, **DCFH**, **DHE** or **MSR**. Hence, we suggest that **EEPF1** should be used in preference to **DCFH**, **DHE** or **PF1**, particularly for detection of low concentrations (0-100 µM) of H_2O_2 or $ONOO^-$ in human spermatozoa.

The different fluorescent responses of **PF1**, **CPF1** and **EEPF1** to ROS produced by spermatozoa (**Figure 21** and **Figure 23**) also provide some preliminary insights into structure-activity relationships for the aryl boronate class of probe. **CPF1** consistently detected lower numbers of reactive spermatozoa than **PF1** and **EEPF1**. As fluorescein-based probes are susceptible to photobleaching, 10 µM solutions of **CPF1** and **PF1** were irradiated with a 100 mW 488 nm argon laser to ensure the cause for differing fluorescent responses was not a photobleaching effect. **CPF1** and **PF1** showed comparable rates of photobleaching, as such, the reduced **CPF1** positive populations observed in **Figure 23** are not the results of differences in rates of photobleaching. However, for spermatozoa to be analysed by flow cytometry, the probe must be able to cross the plasma membrane in order to react with intracellular ROS and generate a fluorescent signal. It is therefore likely that the impaired cellular uptake of **CPF1** is responsible for its lack of activity. Any localised fluctuation in pH would affect the ionisation of the carboxyl group of **CPF1**, which would, in turn, be expected to influence cell permeability and hence the intracellular concentration of this probe. By contrast, **EEPF1** is esterified with a truncated PEG (see **Scheme 4**) so would

be expected to possess a higher capacity for intracellular penetration. Furthermore, hydrolysis of the PEG ester by intracellular esterases may enhance cellular retention of the active species, as reported for a similar aryl boronate probe, **PF6-AM**.[99]

2.3.3.4 Spontaneous ROS Generation by Human Spermatozoa

Finally, the use of **PF1**, **CPF1** and **EEPF1** to detect spontaneous ROS generation by human spermatozoa was investigated to validate the use of these probes for detecting the increased ROS production associated with poorly motile sperm. To this end, the spermatozoa were separated on discontinuous Percoll gradients into subpopulations exhibiting high and low levels of motility respectively[122] (see methods, **2.6**, for detail). These sperm populations were then separately incubated with either **PF1**, **CPF1** or **EEPF1**. **Figure 24** clearly demonstrates the increased generation of ROS by poorly motile spermatozoa compared with their more motile counterparts. A relative increase in the proportion of ROS–generating cells was detected in the poorly motile cells with **PF1**, **CPF1** and **EEPF1**. The largest increase was seen with **EEPF1**, which detected ROS generation in around 40% of the poorly motile cells compared with < 15% with **PF1** and **CPF1**. These results confirm **EEPF1** as the most effective of these probes for the detection of released ROS in human spermatozoa. As such, **EEPF1** is recommended for use as an intracellular probe for detection of ROS in human spermatozoa.

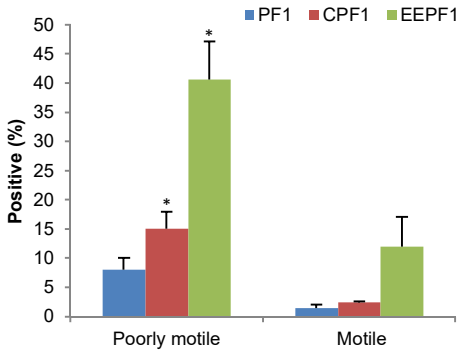

Figure 24. Analysis of flow cytometry results showing the percentage of poorly motile and motile samples of human spermatozoa populations indicating a fluorescent response. **EEPF1** provides a greater fluorescent response to the ROS produced in poorly motile sperm. Significance level relative to motile sample: *P < 0.05

2.4 CONCLUSION

The aryl boronate probes discussed here react directly with H_2O_2 and therefore present a distinct advantage over **DCFH**, which we show to be insensitive to H_2O_2. **PF1** and **EEPF1** were also shown to be effective fluorescent probes for the detection of both H_2O_2 and $ONOO^-$ in human spermatozoa. Both **PF1** and **EEPF1** were significantly more effective at detection of ROS by flow cytometry compared to **DCFH** and **DHE** when stimulated using menadione and 4HNE. In particular, **EEPF1** was the most effective of the studied probes for

externally stimulated and spontaneously generated ROS produced by human spermatozoa. This particular probe should therefore have a significant role to play in the diagnosis of oxidative stress in spermatozoa in the context of a variety of circumstances including spontaneous male infertility, cryopreservation, age, lifestyle and exposure to environmental toxicants.

2.5 Acknowledgements

This research was supported in part by Cook Medical Pty Ltd and Australian Research Council linkage grant LP 110200736 and the ARC Centre of Excellence in Nanoscale BioPhotonics (CNBP) for the Adelaide laboratory and DP 110103951 in the case of Newcastle. T.M. acknowledges the support of an ARC Georgina Sweet Laureate Fellowship FL130100044.

2.6 MATERIALS AND METHODS

2.6.1 Materials:

Unless otherwise stated all chemicals were purchased from Sigma Aldrich. N-(3-Dimethylaminopropyl)-N′-ethylcarbodiimide hydrochloride (EDC-HCl) was obtained from GL Biochem (Shanghai). 4HNE was from Sapphire Biosciences; MitoSox Red, dihydroethidium and Live/dead fixable FAR red stain were from Life Technologies. 2',7'-Dichlorofluorescein diacetate was from molecular probes. Freshly prepared Biggers, Whitten and Whittingham (BWW) medium was used for all experiments, supplemented with 1 mg/ml polyvinyl alcohol, 5 units/ml penicillin and 5 mg/ml streptomycin, and the osmolarity was kept between 290 and 310 mOsm/kg.[135]

2.6.2 Semen Samples:

The University of Newcastle human ethics committee and the NSW state Minister for Health approved the use of semen samples for research. A cohort of unselected, normozoospermic donors, mainly university students of unknown fertility status, supplied semen samples for this study. Semen samples were produced into a sterile container and delivered to the laboratory within 1 hour of ejaculation.

2.6.3 Sample Preparation:

Spermatozoa were isolated by discontinuous Percoll gradient centrifugation using a simple 2-step design incorporating 44% and 88% Percoll as described previously.[136] Purified spermatozoa were recovered and washed with HEPES-buffered BWW supplemented with 1 mg/ml PVA,[135] centrifuged at 500 ***g*** for 5 minutes, and resuspended at a concentration of 2×10^7 cells/ml.

2.6.4 Leukocyte Removal:

Where indicated, all residual traces of leukocyte contamination in the sperm suspensions were removed using magnetic beads (Dynabeads, Dynal, Oslo, Norway) coated with a monoclonal antibody against the common leukocyte antigen, CD45 (Invitrogen, Carlsbad, C). Following Percoll isolation, 5 × 10^6 cells in 100 µl BWW were added to pre-washed antibody-bound Dynabeads and then placed on a rotor for 30 min. Following incubation, each sample was placed in a magnetic holder to separate leukocyte-bound Dynabeads from purified sperm cells in BWW. Luminol-peroxidase mediated chemiluminescence was then used in order to confirm the removal of leukocytes from each sperm suspension; for this purpose 20 µl of zymosan opsonized with autologous serum was added to each 400 µl sample, 5 min from the beginning of the luminometry run.[122]

2.6.5 Treatments:

Spermatozoa were treated with menadione (0-50 µM), AA (0-50 µM) and H_2O_2 (0-4 mM) for 15 min at 37 °C. Treatments with 4HNE (0-400 µM) were for 30 min at 37 °C. Stock solutions of menadione were made up fresh daily in dimethyl sulfoxide (DMSO), with a minimum dilution of 1/100 in BWW before being added to spermatozoa.

2.6.6 Staining:

After spermatozoa were treated they were incubated with **PF1**, **CPF1** and **EEPF1** for 30 mins @ 37°C at a final concentration of 10 µM. Stock solutions were made up using (DMSO) at a concentration of 10 mM.

2.6.7 Flow Cytometry:

A FACS-Canto Flow Cytometer (Becton Dickinson) was employed using a 488 nm argon laser coupled with emission measurements using the 530/30 band pass (green) FITC channel. Ten thousand sperm events were recorded after non-sperm events were gated out. Data were analysed using BD Diva Software (Becton Dickinson).

2.6.8 Statistical Analysis:

All graphed results are expressed as the mean ± standard error of the mean (SE). Experiments were replicated at least three times with independent samples. Data was then analysed by one-way analysis of variance (ANOVA) using Graphpad Prism 6, followed by post-hoc comparison by Fisher's LSD (Least Significant Difference).

2.6.9 ROS Selectivity Study:

Solutions of **PF1**, **CPF1**, **EEPF1** and **DCFH** in 20 mM HEPES buffer at pH 7.4 were treated with 100 µM of ROS: H_2O_2, $ONOO^-$, ^-OCl, $^{\bullet}OH$, $O_2^{\bullet-}$, NO, and *tert*-butyl hydroperoxide

(TBHP). A stock solution of approximately 100 mM H_2O_2 in Milli-Q water was prepared from a 30% H_2O_2 solution in water and the exact concentration was determined by UV absorption at 240 nm (ε_{240} = 43.6 $M^{-1}cm^{-1}$) using a Cary UV-Vis-NIR 5000 Spectrophotometer. A stock solution of NaOCl was similarly prepared and the ^{-}OCl concentration determined by UV absorption at 292 nm (ε_{292} = 350 $M^{-1}cm^{-1}$). A solution of $ONOO^{-}$ was prepared by a known method,[79] and its concentration determined using UV absorption at 302 nm (ε_{302} = 1670 $M^{-1}cm^{-1}$). $^{\bullet}OH$ was produced by the Fenton reaction of 100 µM H_2O_2 with 1 mM $FeClO_4$. $O_2^{\bullet-}$ was also produced by a known method,[95] using a xanthine/xanthine oxidase system for production of $O_2^{\bullet-}$ and catalase as a scavenger for any H_2O_2 produced. NO was generated from S-nitrosoglutathione, and TBHP was diluted from a stock solution. The ROS were added to each probe and the fluorescence was monitored using a Biotek Synergy H4 fluorescence plate reader (excitation 450 nm, emission 520 nm) over 40 min.

2.6.10 Fluorescence Controls for Menadione, AA and 4HNE

Solutions of **PF1**, **CPF1**, **EEPF1** in BWW were treated with menadione (0-50 µM), AA (0-50 µM) or 4HNE (0-400 µM) to give a final probe concentration of 10 µM. Samples were incubated for 15 min (30 min for 4HNE) at 37°C, then fluorescence emission quantified using a Fluostar Optima (BMG Labtech),with settings of excitation filter 485 ± 10 nm, and emission filter at 520 nm.

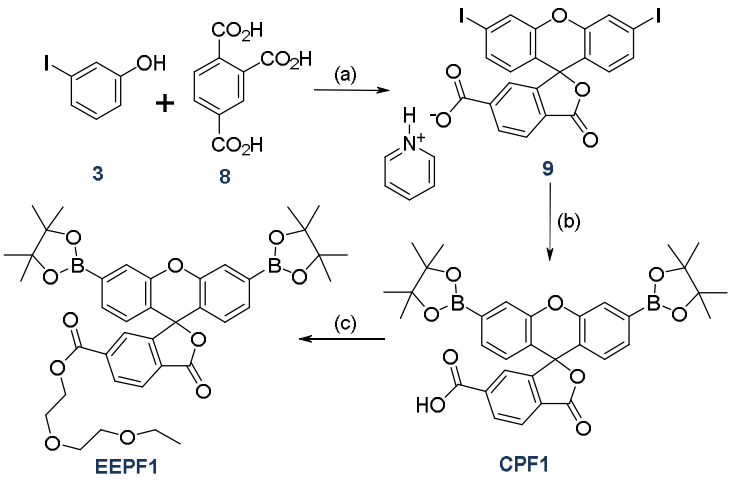

Scheme 4. Synthesis of **CPF1** and **EEPF1**. (a) 1. $MeSO_3H$, 140 °C, 72 h 2. Recrystallisation 2:1 acetic anhydride: pyridine[56] (b) Bis(pinacolato)diboron, $Pd(dppf)Cl_2$, KOAc, DMF, mic. synth., 100 °C, 3 h (c) 1. N-Hydroxysuccinimide, EDC-HCl, DMF, 1 h. 2. 2-(2-ethoxyethoxy)ethanol, 2 h.

2.6.11 Synthesis

Peroxyfluor-1 (**PF1**) was prepared as described[94] using microwave irradiation in place of conventional heating: 3',6'-diiodofluoran[94] (89 mg, 0.16 mmol), bis(pinacolato)diboron (160 mg, 0.63 mmol), potassium acetate (141 mg, 0.63 mmol) and $Pd(dppf)Cl_2$ (14 mg, 0.02

mmol) pre-dried *in vacuo,* were dissolved in DMF (4 mL) under N_2 atmosphere in a sealed microwave vial fitted with a Teflon cap. The light brown mixture was reacted in a CEM Discover microwave synthesiser (Matthews, NC) at 80 °C for 2 h. The solvent was removed under reduced pressure to give a dark brown powder which was purified by column chromatography eluting with 4:1 hexane:ethyl acetate to give **PF1** as a white solid. (40 mg, 45%) The sample was characterised by 300 MHz proton nuclear magnetic resonance spectroscopy (^{1}HNMR) in deuterated chloroform. ^{1}HNMR data: δ 8.03 (1H, m), 7.74 (2H, s), 7.60 (2H, m), 7.43 (2H, dd, J_1=7.8Hz, J_2=1.1Hz), 7.06 (1H, m), 6.86 (2H, d, J=7.8Hz), 1.35 (24H, s).

CarboxyPeroxyfluor-1 (**CPF1**)[127] was similarly prepared: 3',6'-Diiodo-6-carboxyfluoran pyridinium salt (**9**)[56] (109 mg, 0.16 mmol), bis(pinacolato)diboron (160 mg, 0.63 mmol), potassium acetate (142 mg, 0.63 mmol) and Pd(dppf)Cl_2 (13.9 mg, 0.017 mmol) were dissolved in dry DMF (4 mL) in an anhydrous N_2 atmosphere. The resultant solution was reacted in a sealed microwave vial sealed with a Teflon cap at 100 °C for 3 h in a CEM Discover microwave synthesiser (Matthews, NC). The solution was evaporated under reduced pressure to give a dark brown powder, which was purified by flash column chromatography eluting with neat ethyl acetate to give **CPF1** as a light brown solid. (55 mg, 58%) The sample was similarly characterised: ^{1}HNMR ($CDCl_3$, 300MHz): δ 8.29 (dd, 1H, J_1=7.8Hz, J_2=1.4Hz), 8.11 (d, 1H, J=7.8Hz), 7.79-7.73 (m, 3H), 7.43 (dd, 2H, J_1=7.8Hz, J_2=1.1Hz), 6.81 (d, 2H, J=7.8Hz), 1.35 (s, 24H).

2-(2-Ethoxyethoxy)ethoxy Peroxyfluor-1 (**EEPF1**): **CPF1** (50 mg, 0.08 mmol), N-hydroxysuccinimide (11 mg, 0.08 mmol) and EDC-HCl (26 mg, 0.13 mmol) were added to DMF (1 mL) in a dry N_2 glovebox and stirred for 1 h. 2-(2-Ethoxyethoxy)ethanol (23 µL, 0.17 mmol) in dry DMF (0.5mL) was added and the solution stirred for a further 2 h. The solvent was removed under reduced pressure, and the resultant solid was purified by column chromatography eluting with ethyl acetate to give **EEPF1** as a white powder. (28 mg, 47%) The sample was similarly characterised by ^{1}HNMR ($CDCl_3$, 500MHz): δ 8.28 (1H, dd, J_1=8.0Hz, J_2=1.0Hz), 8.09 (1H, d, J_1=8.0Hz), 7.76 (2H, s), 7.71 (1H, s), 7.44 (2H, d, J_1=8.0Hz), 6.82 (2H, d, J=7.5Hz), 4.42 (2H, t, J=4.5Hz), 3.76 (2H, t, J=4Hz), 3.61 (2H, t, J=2.75), 3.52 (2H, t, J=4.5Hz), 3.45 (2H, q, J=7Hz), 1.35 (24H, s), 1.14 (3H, t, J=7Hz). This new boronate probe was also characterised by 500MHz carbon 13 nuclear magnetic resonance spectroscopy (^{13}CNMR) and high resolution mass spectrometry (HRMS).^{13}CNMR ($CDCl_3$, 125MHz): δ 168.6, 164.9, 154.0, 150.5, 136.5, 131.2, 130.0, 129.7, 129.4, 129.0, 128.8, 126.9, 125.3, 125.1, 123.8, 120.5, 84.2, 70.6, 69.8, 68.9, 64.8, 24.9, 15.1. HRMS: calculated 712.3226, found 712.3237.

2.7 SUPPLEMENTARY DATA

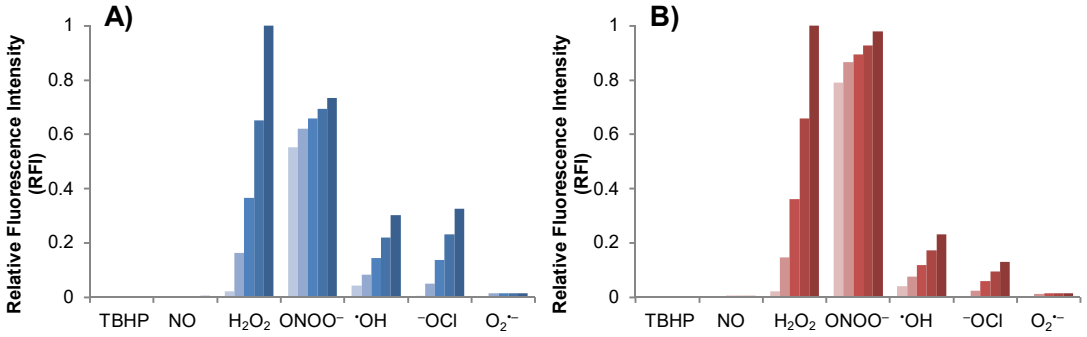

Figure 25. A) **PF1** and B) **CPF1** selectivity data, each incubated at 37 °C with 100 µM ROS for 0, 10, 20, 30 and 40 min. Excitation 450 nm, emission 520 nm, see methods for further details on production of ROS.

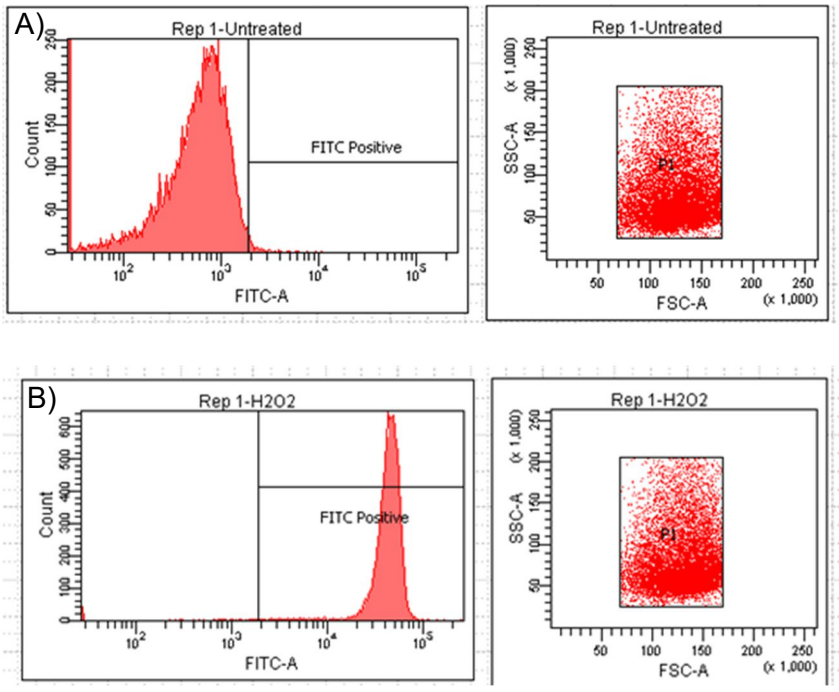

Figure 26. Representative flow cytometry histograms, indicating the level of fluorescence for each of the 10,000 spermatozoa measured per sample. The indicated region in each graph marked as “FITC positive” denotes spermatozoa that are counted as positive for ROS production. The samples shown above are sperm samples incubated with **PF1**: A) Untreated spermatozoa (negative control). B) Spermatozoa treated with a 4mM H_2O_2 (positive control).

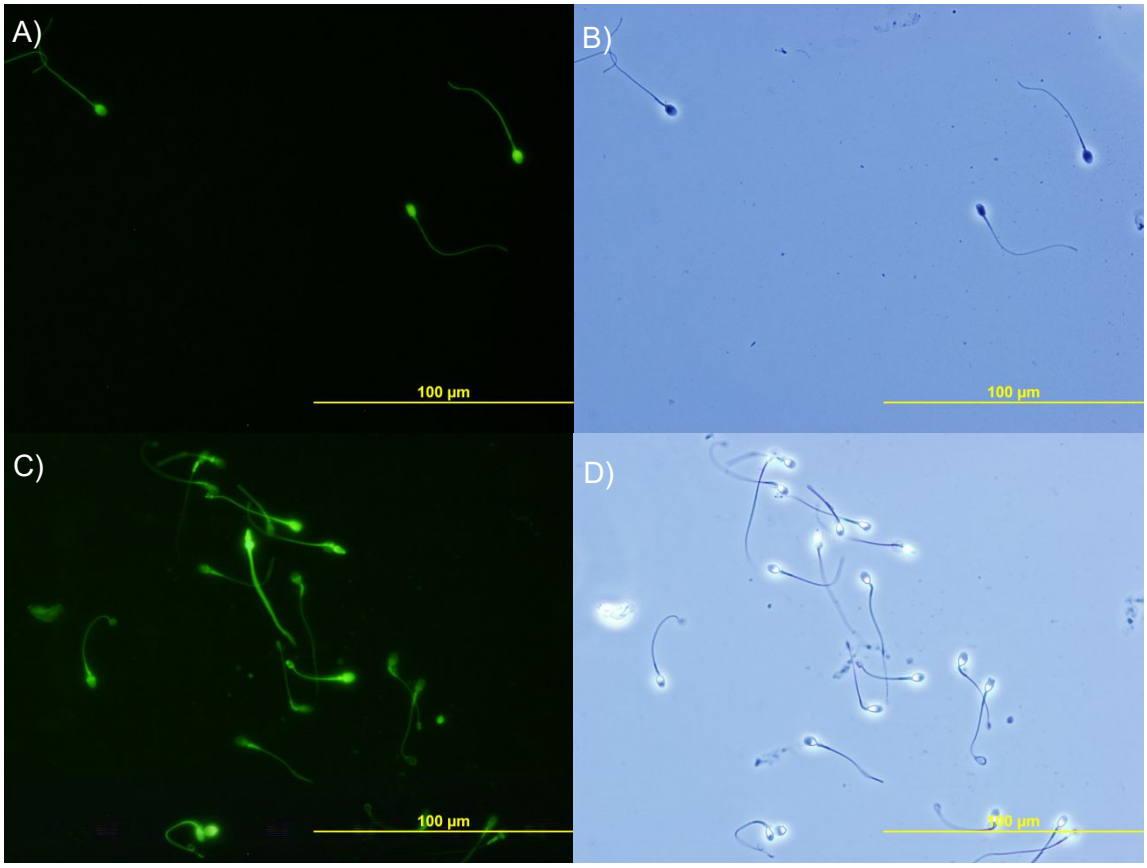

Figure 27. Microscope images at 40x magnification. Fluorescence response of sperm cells of menadione treatments stained with: A) **CPF1**, B) backlight image of A); C) **EEPF1** with D) backlight image of C).

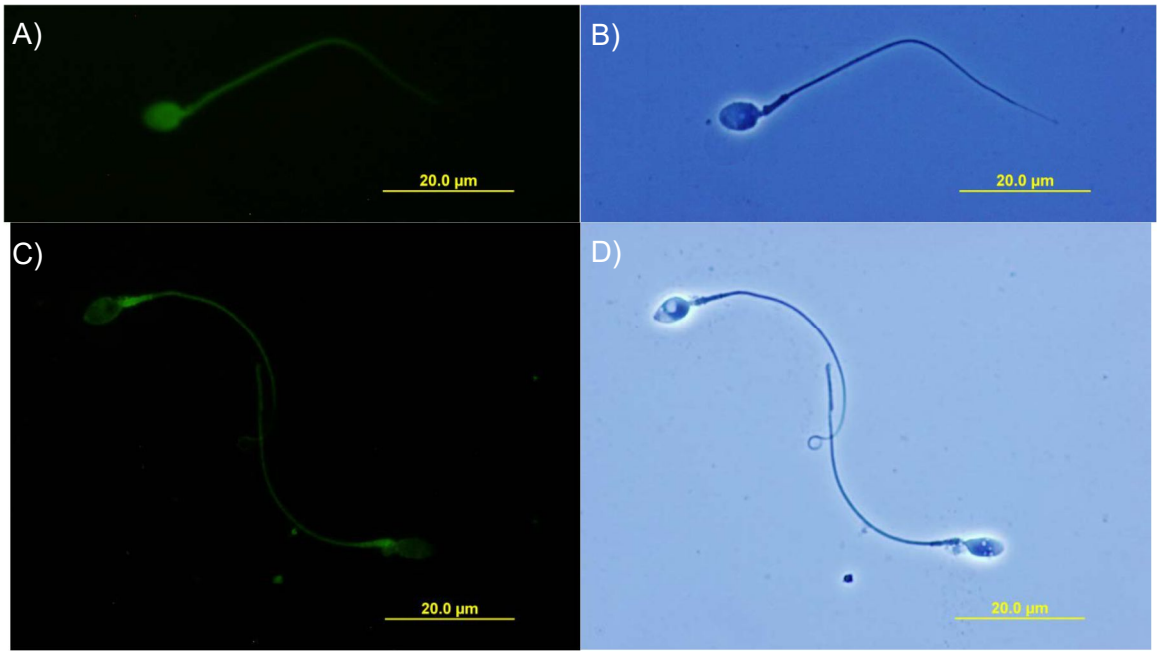

Figure 28. Microscope images at 100x magnification: Fluorescence response of spermatozoa cells treated with: A) Menadione, stained with **CPF1**. B) Backlight images of A). C) H_2O_2, stained with **EEPF1**, showing only staining in mitochondria. D) Backlight images of C).

Images of **CPF1**- or **EEPF1**-stained spermatozoa treated with menadione or H_2O_2 showed fluorescence in both the head and midsection (**Figure 27** and **Figure 28**). However, some spermatozoa (**Figure 27**) only showed a fluorescent response in the mitochondrial midsect.

2.8 REFERENCES

2. Jones, R.; Mann, T.; Sherins, R. Peroxidative breakdown of phospholipids in human spermatozoa, spermicidal properties of fatty acid peroxides, and protective action of seminal plasma. *Fertility and sterility* **1979,** *31* (5), 531-537.
3. Aitken, R. J.; Clarkson, J. S. Cellular basis of defective sperm function and its association with the genesis of reactive oxygen species by human spermatozoa. *Journal of Reproduction and Fertility* **1987,** *81* (2), 459-469.
4. Alvarez, J. G.; Touchstone, J. C.; Blasco, L.; Storey, B. T. Spontaneous Lipid Peroxidation and Production of Hydrogen Peroxide and Superoxide in Human Spermatozoa Superoxide Dismutase as Major Enzyme Protectant Against Oxygen Toxicity. *Journal of Andrology* **1987,** *8* (5), 338-348.
5. Aitken, R. J.; Curry, B. J. Redox regulation of human sperm function: from the physiological control of sperm capacitation to the etiology of infertility and DNA damage in the germ line. *Antioxid Redox Signal* **2011,** *14* (3), 367-81.
6. Gong, S.; Gabriel, M. C. S.; Zini, A.; Chan, P.; O'Flaherty, C. Low Amounts and High Thiol Oxidation of Peroxiredoxins in Spermatozoa From Infertile Men. *Journal of Andrology* **2012,** *33* (6), 1342-1351.
12. Aitken, R. J.; Wingate, J. K.; De Iuliis, G. N.; Koppers, A. J.; McLaughlin, E. A. Cis-unsaturated fatty acids stimulate reactive oxygen species generation and lipid peroxidation in human spermatozoa. *Journal of Clinical Endocrinology and Metabolism* **2006,** *91* (10), 4154-4163.
23. Aitken, R. J.; Buckingham, D.; Harkiss, D. Use of a xanthine oxidase free radical generating system to investigate the cytotoxic effects of reactive oxygen species on human spermatozoa. *Journal of Reproduction and Fertility* **1993,** *97* (2), 441-450.
24. Armstrong, J. S.; Rajasekaran, M.; Chamulitrat, W.; Gatti, P.; Hellstrom, W. J.; Sikka, S. C. Characterization of reactive oxygen species induced effects on human spermatozoa movement and energy metabolism. *Free Radical Biology and Medicine* **1999,** *26* (7–8), 869-880.
25. Baumber, J.; Ball, B. A.; Gravance, C. G.; Medina, V.; Davies-Morel, M. C. G. The Effect of Reactive Oxygen Species on Equine Sperm Motility, Viability, Acrosomal Integrity, Mitochondrial Membrane Potential, and Membrane Lipid Peroxidation. *Journal of Andrology* **2000,** *21* (6), 895-902.
30. Lippert, A. R.; Van de Bittner, G. C.; Chang, C. J. Boronate Oxidation as a Bioorthogonal Reaction Approach for Studying the Chemistry of Hydrogen Peroxide in Living Systems. *Accounts of Chemical Research* **2011,** *44* (9), 793-804.
56. Albers, A. E.; Okreglak, V. S.; Chang, C. J. A FRET-Based Approach to Ratiometric Fluorescence Detection of Hydrogen Peroxide. *Journal of the American Chemical Society* **2006,** *128* (30), 9640-9641.
75. Robinson, K. M.; Janes, M. S.; Pehar, M.; Monette, J. S.; Ross, M. F.; Hagen, T. M.; Murphy, M. P.; Beckman, J. S. Selective fluorescent imaging of superoxide in vivo using ethidium-based probes. *Proc Natl Acad Sci U S A* **2006,** *103* (41), 15038-43.
79. Hempel, S. L.; Buettner, G. R.; O'Malley, Y. Q.; Wessels, D. A.; Flaherty, D. M. Dihydrofluorescein diacetate is superior for detecting intracellular oxidants: comparison with 2',7'-dichlorodihydrofluorescein diacetate, 5(and 6)-carboxy-2',7'-dichlorodihydrofluorescein diacetate, and dihydrorhodamine 123. *Free Radical Biology and Medicine* **1999,** *27* (1–2), 146-159.
94. Chang, M. C. Y.; Pralle, A.; Isacoff, E. Y.; Chang, C. J. A selective, cell-permeable optical probe for hydrogen peroxide in living cells. *Journal of the American Chemical Society* **2004,** *126* (47), 15392-15393.

95. Albers, A. E.; Dickinson, B. C.; Miller, E. W.; Chang, C. J. A red-emitting naphthofluorescein-based fluorescent probe for selective detection of hydrogen peroxide in living cells. *Bioorganic & Medicinal Chemistry Letters* **2008,** *18* (22), 5948-5950.
99. Dickinson, B. C.; Peltier, J.; Stone, D.; Schaffer, D. V.; Chang, C. J. Nox2 redox signaling maintains essential cell populations in the brain. *Nat Chem Biol* **2011,** *7* (2), 106-112.
100. Sikora, A.; Zielonka, J.; Lopez, M.; Joseph, J.; Kalyanaraman, B. Direct oxidation of boronates by peroxynitrite: Mechanism and implications in fluorescence imaging of peroxynitrite. *Free Radical Biology & Medicine* **2009,** *47* (10), 1401-1407.
121. Aitken, R. J.; Iuliis, G.; Baker, M. Direct Methods for the Detection of Reactive Oxygen Species in Human Semen Samples. In *Studies on Men's Health and Fertility*, Agarwal, A.; Aitken, R. J.; Alvarez, J. G., Eds. Humana Press: 2012; pp 275-299.
122. Aitken, R. J.; Smith, T. B.; Lord, T.; Kuczera, L.; Koppers, A. J.; Naumovski, N.; Connaughton, H.; Baker, M. A.; De Iuliis, G. N. On methods for the detection of reactive oxygen species generation by human spermatozoa: analysis of the cellular responses to catechol oestrogen, lipid aldehyde, menadione and arachidonic acid. *Andrology* **2013,** *1* (2), 192-205.
123. Murphy, M. P.; Holmgren, A.; Larsson, N.-G.; Halliwell, B.; Chang, C. J.; Kalyanaraman, B.; Rhee, S. G.; Thornalley, P. J.; Partridge, L.; Gems, D.; Nystroem, T.; Belousov, V.; Schumacker, P. T.; Winterbourn, C. C. Unraveling the Biological Roles of Reactive Oxygen Species. *Cell Metabolism* **2011,** *13* (4), 361-366.
124. Setsukinai, K.; Urano, Y.; Kakinuma, K.; Majima, H. J.; Nagano, T. Development of novel fluorescence probes that can reliably detect reactive oxygen species and distinguish specific species. *The Journal of biological chemistry* **2003,** *278* (5), 3170-5.
125. Myhre, O.; Andersen, J. M.; Aarnes, H.; Fonnum, F. Evaluation of the probes 2',7'-dichlorofluorescin diacetate, luminol, and lucigenin as indicators of reactive species formation. *Biochemical Pharmacology* **2003,** *65* (10), 1575-1582.
126. Gray, J. E.; Starmer, J.; Lin, V. S.; Dickinson, B. C.; Magnuson, T. Mitochondrial hydrogen peroxide and defective cholesterol efflux prevent in vitro fertilization by cryopreserved inbred mouse sperm. *Biology of reproduction* **2013,** *89* (1), 17.
127. Srikun, D.; Albers, A. E.; Chang, C. J. A dendrimer-based platform for simultaneous dual fluorescence imaging of hydrogen peroxide and pH gradients produced in living cells. *Chemical Science* **2011,** *2* (6), 1156-1165.
128. He, F.; Tang, Y.; Yu, M.; Wang, S.; Li, Y.; Zhu, D. Fluorescence-amplifying detection of hydrogen peroxide with cationic conjugated polymers, and its application to glucose sensing. *Advanced Functional Materials* **2006,** *16* (1), 91-94.
129. Hughes, L. M.; Griffith, R.; Carey, A.; Butler, T.; Donne, S. W.; Beagley, K. W.; Aitken, R. J. The spermostatic and microbicidal actions of quinones and maleimides: toward a dual-purpose contraceptive agent. *Molecular Pharmacology* **2009,** *76* (1), 113-124.
130. Mitchell, L. A.; De Iuliis, G. N.; Aitken, R. J. The TUNEL assay consistently underestimating DNA damage in human spermatozoa and is influenced by DNA compaction and cell vitality: development of an improved methodology. *International Journal of Andrology* **2011,** *34* (1), 2-13.
131. Koppers, A. J.; Garg, M. L.; Aitken, R. J. Stimulation of mitochondrial reactive oxygen species production by unesterified, unsaturated fatty acids in defective human spermatozoa. *Free Radical Biology & Medicine* **2010,** *48* (1), 112-119.
132. Aitken, R. J.; Whiting, S.; De Iuliis, G. N.; McClymont, S.; Mitchell, L. A.; Baker, M. A. Electrophilic aldehydes generated by sperm metabolism activate mitochondrial reactive oxygen species generation and apoptosis by targeting succinate dehydrogenase. *The Journal of biological chemistry* **2012,** *287* (39), 33048-60.
133. Koppers, A. J.; De Iuliis, G. N.; Finnie, J. M.; McLaughlin, E. A.; Aitken, R. J. Significance of mitochondrial reactive oxygen species in the generation of oxidative stress in spermatozoa. *Journal of Clinical Endocrinology and Metabolism* **2008,** *93* (8), 3199-3207.

134. Porter, N. A.; Wolf, R. A.; Yarbro, E. M.; Weenen, H. The autoxidation of arachidonic acid: Formation of the proposed SRS-A intermediate. *Biochemical and Biophysical Research Communications* **1979,** *89* (4), 1058-1064.
135. Biggers, J., Whitten, WK and Whittingham, DG. The culture of mouse embryos in vitro. In *Methods of Mammalian Embryology*, Daniel, J., Ed. WH Freeman: San Fransisco, 1971; pp 86-118.
136. Aitken, R. J.; Harkiss, D.; Knox, W.; Paterson, M.; Irvine, D. S. A novel signal transduction cascade in capacitating human spermatozoa characterised by a redox-regulated, cAMP-mediated induction of tyrosine phosphorylation. *Journal of Cell Science* **1998,** *111* (5), 645-656.

Chapter 3

LOCALISED HYDROGEN PEROXIDE SENSING WITH SURFACE FUNCTIONALISED FLUOROPHORES

I have made this longer than usual because I lack the time to make it shorter.

Blaise Pascal

Chapter 3: Localised Hydrogen Peroxide Sensing with Surface Functionalised Fluorophores†

3.1 INTRODUCTION

H_2O_2 is typically detected in cells using soluble fluorescent probes,[26,30] examples of this are discussed in **Chapter 2**. However, the use of such fluorophores to study the local release of H_2O_2 during *in vitro* fertilisation (IVF) poses significant scientific and ethical problems. The effect that these probes may have on embryonic development is unknown and as such direct contact with the embryo is not advisable. Hence, non-invasive and non-toxic diagnostic sensors for H_2O_2 are highly sought after by clinical IVF laboratories.

A non-invasive alternative to solution-based measurements is to chemically attach the fluorescent probe to a functional surface.[38,39,137] Immobilising a suitable fluorophore to a surface allows the detection of H_2O_2 in a way that avoids exposure to the embryo. Optical fibres are a unique platform that provide an opportunity for surface attachment of the fluorophore to the fibre tip.[109] The fibre guides the excitation light to the fluorophore on the tip and the reflected emission light back to the spectrometer. This allows the sensing domain of the fibre tip to be localised at a desired location within a sample, providing an opportunity for temporal or spatial mapping.

Immobilisation of the fluorophore onto a glass surface can be achieved covalently using a suitable linker or by embedding it within a material attached to the surface. The fluorophore must therefore have a functional group compatible with attachment to the linker, e.g. a carboxylic acid for attachment to an amine-functionalised surface. The selected surface attachment method should also involve simple, reproducible chemistry. This is necessary to control the deposition of fluorophore on the surface and hence provide the required sensitivity of the fibre probe to H_2O_2. Additionally, the layer must not absorb significant amounts of light as this would affect the performance of the device, and a uniform layer is necessary to avoid scattering of light. Therefore, it is important that multiple surface attachment methods be trialled in order to obtain the most effective H_2O_2 probe.

† This work was in part presented as a conference paper accepted for publication at SPIE Optics and Optoelectronics, Prague, Czech Republic:
Purdey, M. S.; Schartner, E. P.; Sutton-McDowall, M. L.; Ritter, L. J.; Thompson, J. G.; Monro, T. M.; Abell, A. D., Localised hydrogen peroxide sensing for reproductive health. *Proceedings of SPIE* **2015,** *9506*, 950614.

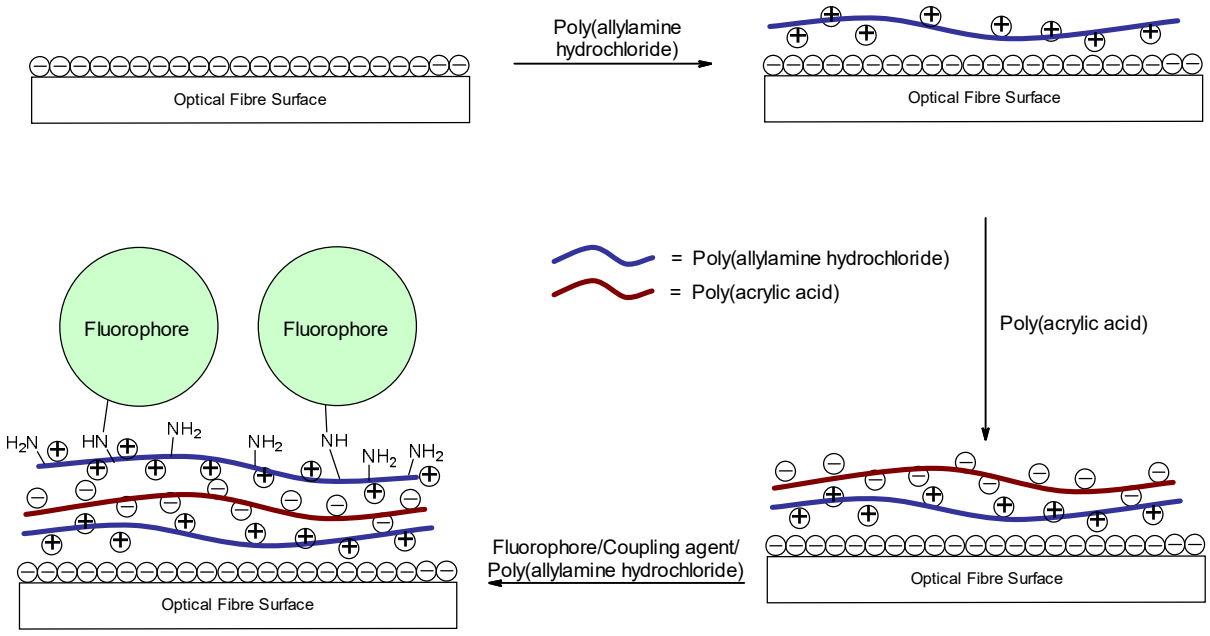

Scheme 5. Representative diagram of the deposition of poly electrolyte layers poly(allylamine hydrochloride) and poly(acrylic acid) to a glass surface. The fluorophore is attached to the amines on the final layer of poly(allylamine hydrochloride).

Polyelectrolyte deposition (**Scheme 5**) is a surface functionalisation technique where layers of positively and negatively charged polymers are deposited alternately on the glass surface.[138,139] Glass has a negative surface charge, so positively charged polymers such as poly(allylamine hydrochloride) display strong ionic interactions that immobilise the polymer to the surface. By alternating deposition of poly(allylamine hydrochloride) with negatively charged poly(acrylic acid), layers of positively/negatively charged polymers are built up to evenly coat the glass. Poly(allylamine hydrochloride) also contains amine functional groups to which a fluorophore is covalently linked, hence immobilising it on the surface. The rapid nature of layer-by-layer deposition is an important advantage of polyelectrolytes over other surface functionalisation techniques. Furthermore, polyelectrolytes are deposited on the surface in an aqueous solution. This requires less complicated washing steps and does not involve organic solvents that may be harmful in a biological environment.[139]

3-Aminopropyl triethoxysilane (APTES) is commonly used for fluorophore attachment to a surface, e.g. attachment of metal ion sensors to microstructured optical fibres.[137,140] This silane can be functionalised to a glass surface to create an amino monolayer (**Scheme 6**). It is generally deposited on a glass surface in the absence of water to prevent self-polymerisation.[141,142] However, self-polymerisation of APTES on glass often occurs and forms uneven coatings, despite the widespread assumption that a single monolayer is formed.[140,143] The amine of APTES can then be attached to a carboxy-terminal fluorophore using traditional amide coupling agents.

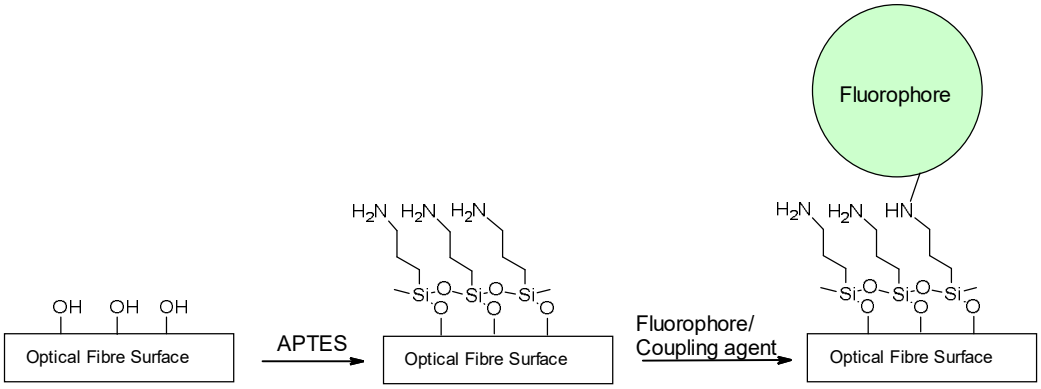

Scheme 6. Surface functionalisation of a fluorophore using APTES. Deposition of APTES to the fibre surface is performed in anhydrous conditions to avoid polymerisation and create an even monolayer.

A fluorophore can also be immobilised to a surface within a polyacrylamide matrix (**Scheme 7**; see also **Chapter 1**, **Figure 17**).[111] Specifically, 3-(trimethoxysilyl)propyl acrylate is deposited on the glass surface, then immersed in a solution containing the fluorophore and monomers acrylamide and bisacrylamide. Under light-catalysis, the monomers polymerise to form a cross-linked polyacrylamide matrix. The fluorophore is thus trapped within the matrix and hence physically immobilised to the surface. This is a non-covalent method for linking the fluorophore to the surface and it has been employed for pH sensing on an optical fibre tip in biological systems.[111,144-146]

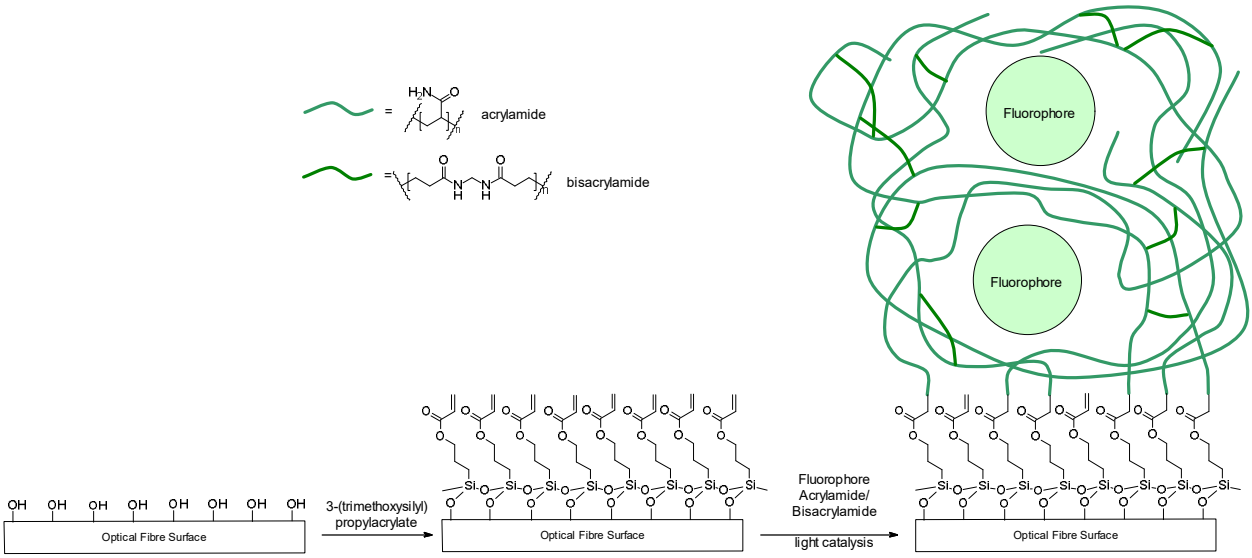

Scheme 7. Formation of a polyacrylamide matrix containing a fluorophore. A silane layer is deposited with propylacrylate functionality. The polymer is then formed on the tip by immersing the fibre tip in an aqueous solution of acrylamide/bisacrylamide with the fluorophore and irradiating with a light source.

However, the characterisation of optical fibre surfaces functionalised with a fluorophore is notoriously difficult using standard surface analysis techniques.[143] Optical fibres are extremely small with curved surfaces or even internal surfaces and fluid flow considerations

in the case of microstructured fibres (MOFs). For example, typhoon imaging scans a larger surface area and cannot precisely measure fluorescence on a fibre tip only 200 μm in diameter. Likewise, the curved internal surfaces of MOFs cannot be characterised in this manner. Conversely, a flat macroscopic glass surface made from the same glass composition as the fibre to be used in the sensor provides a good model for the fibre tip and allows the use of techniques such as typhoon imaging.[137] Glass slides are useful for this purpose and provides an opportunity to compare surface-attached and solution-based detection using a fluorophore.

This chapter reports the rationale for selection of the aryl boronate **CPF1** and its immobilisation to glass slides and optical fibre tips for the non-invasive detection of H_2O_2.

3.2 FLUOROPHORE DESIGN

Derivatives of **PF1** (**Figure 29**) were selected for immobilisation to glass surfaces in this study since aryl boronates react selectively with H_2O_2 over other ROS.[56,94,127] Furthermore, this class of fluorophore effectively detected H_2O_2 in a reproductive context as demonstrated in **Chapter 2**. **PF1** (**Figure 29**) is simple and easily synthesised, however it does not contain a suitable functional group to allow attachment to a surface. Conversely, the carboxylic acid on **CPF1** (**Figure 29**) can be attached to an amine-functional surface by a simple amidation. A linker with a terminal amine could be coupled to the carboxyl group to allow different surface attachment protocols. For example, attachment to an amine-functionalised surface can be performed in the absence of external coupling reagents by converting the carboxyl group of **CPF1** to an N-hydroxysuccinimide (**CPF1-NHS**, **Figure 29**). **CPF1** was therefore synthesised to compare to other **PF1** derivatives shown in **Figure 29**.

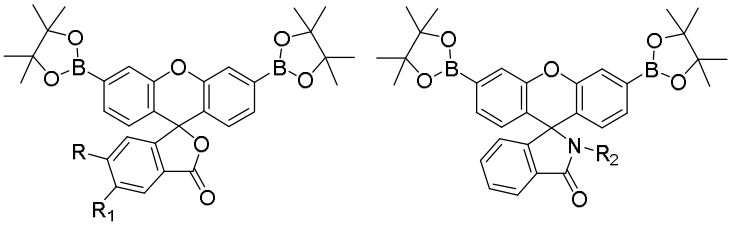

Figure 29. **PF1** can be modified to give any of the possible structures: A carboxy functional group (**CPF1**), brominated variant (**10**) can be synthesised for alternate attaching strategies. **CPF1-NHS** is a carboxy-activated derivative of **CPF1**. Right (**11**): The lactone ring has been converted to a lactam with a functional side chain at R_2 for surface attachment.

Bromo-PF1 (**10**, **Figure 29**) provides another option for surface attachment to glass. The component bromo substituent could be coupled with an alkene-functionalised surface via a

Heck reaction.[147] Compound **10** was prepared by Tim Engler‡,[148] and is here compared with **CPF1** for potential attachment to a surface.

The relative sensitivity of **10** and **CPF1** to H_2O_2 were compared in solution. Specifically, 2 mM stock solutions of **10** and **CPF1** were prepared in DMSO. These were then diluted to 10 μM in α-MEM buffer solution with H_2O_2 of concentration 0, 20, 40 or 60 μM. The fluorescent response of each solution was recorded using a Cary Eclipse Fluorescence Spectrometer at 37 °C with the results shown in **Figure 30**. **10** showed no fluorescent response to H_2O_2, even after 5 h incubation. Conversely, **CPF1** showed a significant fluorescent response within 1 h. This suggests that fluorescence of bromo-substituted **10** is quenched even after reaction with H_2O_2, due to the presence of the 6-bromo group. The ultimate derivative of **10** attached to the surface may not experience this quenching, however this could not be compared to the fluorescent response of **10** in solution, whereas a solution comparison is possible for **CPF1**. This result therefore suggests **CPF1** is a better candidate than **10** for surface attachment. Thus, **CPF1** presents an opportunity to directly compare the reaction of a fluorophore with H_2O_2 in solution and on a glass surface.

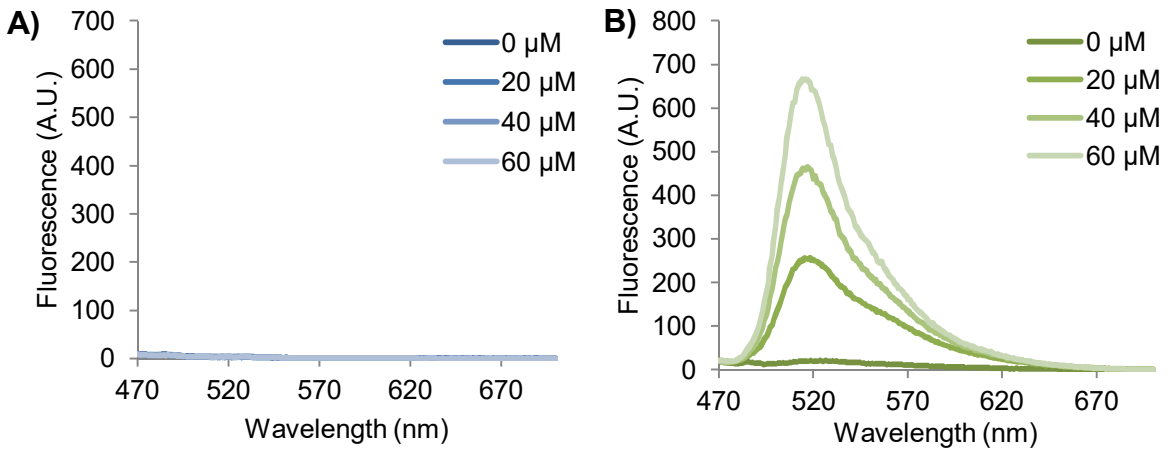

Figure 30. Fluorescent response of A) **10** to 0, 20, 40 and 60 μM H_2O_2 over 5 h. B) **CPF1** to 0, 20, 40 and 60 μM H_2O_2 over 1 h.

Moreover, the precursor of **10** (**Scheme 8**) proved extremely difficult to separate from an isomeric mixture. Multiple purifications by column chromatography gave only 5 % of the isomerically pure 5',6'-iodo-6-bromofluoran.[148] Conversely, 5',6'-iodo-5-carboxyfluoran (see **Scheme 8**) was obtained as a single isomer by recrystallization, giving a much higher yield of 36 %.[149,150]

‡ Timothy Engler was an Honours student at the University of Adelaide in 2012.

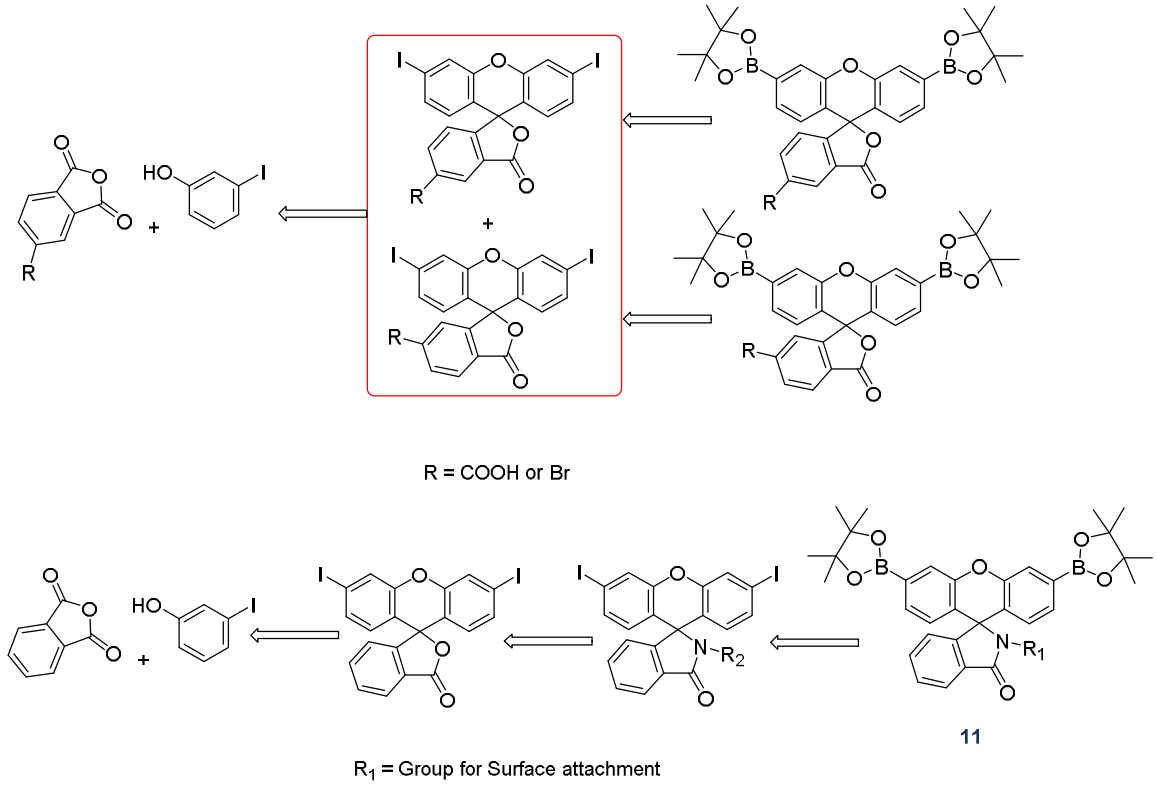

Scheme 8. Retrosynthesis of **PF1** derivatives. The red box highlights the 5- and 6- isomers of bromo/carboxy diiodofluoran.

An alternative fluorophore for surface attachment is suggested in **Figure 29** where the lactone of **PF1** is replaced with a lactam that provides an R_2 group for surface attachment. The synthesis of lactam **11** as outlined in **Scheme 8** would also avoid problems associated with isomeric separation of the precursors of both **CPF1** and **10**. A model system (**12**, **Scheme 9**) for the lactam **11** was explored using a similar fluorophore, **Rhodamine B**. **Rhodamine B** was amidated with propargyl amine (**Scheme 9**) to give a Rhodamine B alkyne (**12**). This compound was isolated as a light pink solid that, unlike **Rhodamine B**, did not fluoresce. This lack of fluorescence is thought to arise from formation of the non-fluorescent lactam **13** shown in **Scheme 9**. Other rhodamines and fluoresceins are also known to be quenched when this corresponding carboxyl group is amidated.[151,152] The lactam **11** (**Scheme 8**) would react with H_2O_2 to form a fluorescein analogous to **13**, which would similarly be expected to have quenched fluorescence. Therefore, given the anticipated shortfalls of both **10** and **11**, **CPF1** was selected for functionalisation to glass surfaces in this study.

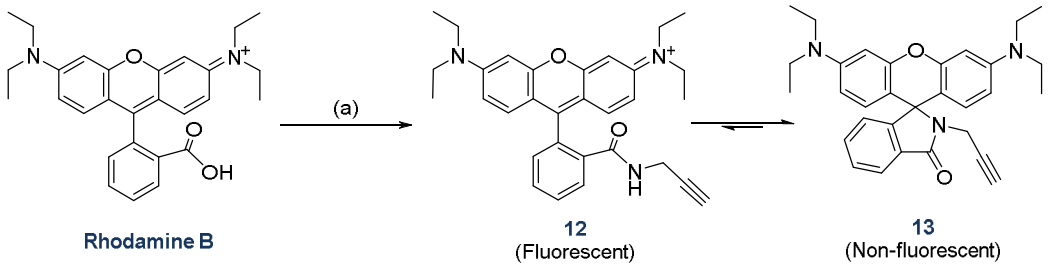

Scheme 9. Synthesis of a Rhodamine B alkyne **13**. The favoured and more stable form is the cyclised lactam (**13**), which does not fluoresce. (a) 1. Oxalyl chloride, DCM, DMF, 1 h; 2. Propargyl amine, Na_2CO_3, DCM, 16 h, 52 % yield.

The change in absorption and fluorescence spectra of **CPF1** was then measured in H_2O_2 of concentration 10-100 µM, to more accurately characterise its response to H_2O_2. Samples of **CPF1** were incubated at 37 °C with 0, 10, 25, 50, 75 and 100 µM of H_2O_2 and the resultant fluorescence was recorded with a microplate reader over 40 min (**Figure 31A**). A significant increase in absorption and fluorescence was observed after 40 min exposure of **CPF1** to as little as 10 µM of H_2O_2. Furthermore, higher concentrations of H_2O_2 gave rise to a greater fluorescent response from **CPF1**. The emission peak from the product of **CPF1** with 100 µM H_2O_2 was monitored during this 40 min period. A clear, linear increase is evident in **Figure 31B**. Therefore **CPF1** effectively detects 10 µM H_2O_2 in buffer, and a linear increase in fluorescence is observed from samples over a 40 min period in 100 µM H_2O_2.

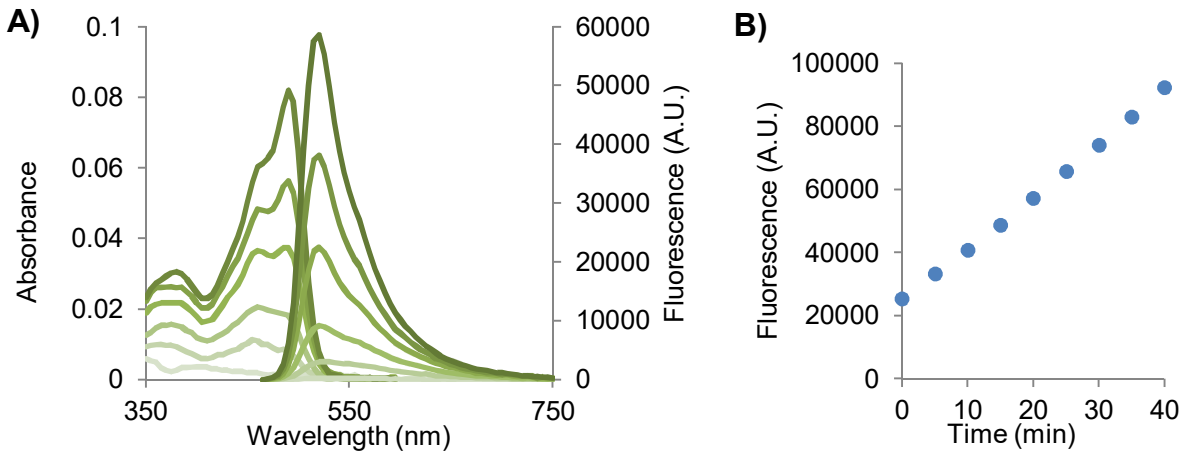

Figure 31. A) Absorption and emission spectra of **CPF1** in 20 mM HEPES at pH 7.4 when treated with 0, 10, 25, 50, 75 and 100 µM H_2O_2. B) Fluorescence over 40 min of **CPF1** treated with 100 µM H_2O_2. Excitation was at 450 nm and emission at 520 nm with a band pass of 20 nm.

3.3 CHARACTERISATION OF CPF1 ATTACHED TO GLASS SLIDES

CPF1 was initially functionalised by polyelectrolyte deposition to glass confocal microscope dishes, rather than optical fibre tips, as discussed in section **3.1**. Each microscope dish was immersed in a solution of poly(allylamine hydrochloride), depositing a layer of positively charged polymer onto the negatively charged glass surface. The dishes were washed with

Milli-Q water, then immersed in a solution containing poly(acrylic acid) in order to deposit this negatively charged polymer layer on top of the initial positive layer. Another layer of poly(allylamine hydrochloride) was then deposited, and **CPF1** was finally coupled to this layer using N-(3-Dimethylaminopropyl)-N′-ethylcarbodiimide hydrochloride (EDC-HCl) and N-hydroxysuccinimide (NHS) (see **3.7.5.1**). These functionalised dishes were then immersed in a solution of H_2O_2 to oxidise the **CPF1** on the surface to increase the fluorescence. The typhoon imager was then used to measure the resulting surface fluorescence, see **Figure 32**. A control was also established by functionalising only with polyelectrolyte layers, not **CPF1**. An increase in fluorescence intensity is shown from this control to the samples with **CPF1** attached (**Figure 32).** This increase in fluorescence confirms that **CPF1** was deposited on the surface. The dishes functionalised with **CPF1** and treated with H_2O_2 showed a further increase in fluorescence (**Figure 32**). This observed fluorescent response indicates that **CPF1** reacted with H_2O_2 on the glass surface in a similar manner to the solution-based studies.

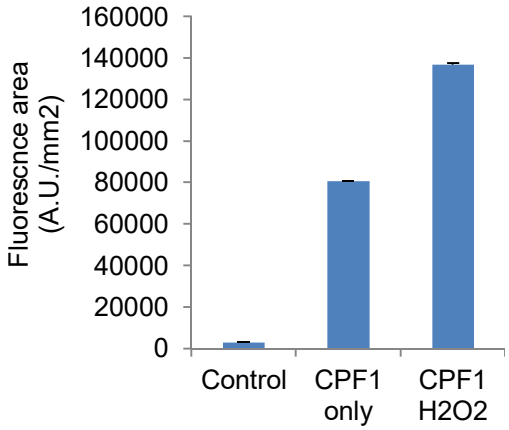

Figure 32. Characterisation of glass dish functionalised with **CPF1** on polyelectrolytes. The above data is an analysis of the fluorescence measured by typhoon imaging. Error bars represent the standard error of the mean (SE). The control sample was functionalised only with polyelectrolytes.

Functionalised microscope dishes were then treated with lower concentrations of H_2O_2 in order to examine its sensitivity to H_2O_2. These dishes were functionalised with **CPF1** as above, and 5 µL drops of bovine IVF media containing 0, 10, 50 and 100 µM of H_2O_2 were added. The droplets were overlaid with paraffin oil to avoid evaporation in accordance with standard IVF experiments. These dishes were then imaged with a typhoon imager (**Figure 33A**) and a confocal microscope (**Figure 33B-E**). The results clearly show that higher concentrations of H_2O_2 (i.e. **Figure 33E**) lead to a greater fluorescence than lower concentrations (c.f. **Figure 33B-C**). A clear increase in fluorescence is visible for droplets containing 10 µM H_2O_2 (**Figure 33A,C**) compared to the control in the absence of H_2O_2 (**Figure 33A-B**). Therefore, while bound to a surface, **CPF1** effectively detects H_2O_2 as it

does in solution-based experiments. This also demonstrates the compatibility of surface-bound **CPF1** with experimental conditions associated with IVF.

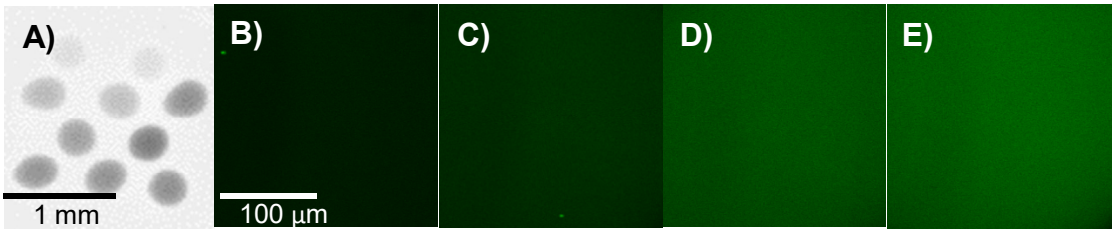

Figure 33. A glass slide functionalised with **CPF1** has several droplets with differing concentrations of H_2O_2. A) Typhoon image with concentrations increasing from left to right, top to bottom. Confocal microscope images corresponding to these droplets show increasingly bright green fluorescence for increased concentration of H_2O_2: B) 0 µM C) 10 µM D) 50 µM E) 100 µM**.**

3.4 ATTACHMENT METHODS OF CPF1 TO OPTICAL FIBRE TIPS

CPF1 was then functionalised to silica optical fibre tips in order to create a tip-probe for H_2O_2. Three methods of functionalisation were compared in order to produce the most effective probe. Silica fibres (FG200UCC, Thorlabs) were selected for durability and attenuation properties.

3.4.1 Polyelectrolyte deposition

Polyelectrolyte deposition (**Scheme 5**) was the first method of functionalisation investigated on optical fibre tips. This allowed a direct comparison between the tip-probe and confocal microscope slides functionalised in section **3.3**. The fibre tips were dipped in a solution of positively charged polymer poly(allylamine hydrochloride), then washed in Milli-Q water. The tips were then dipped into negatively charged poly(acrylic acid) and washed in Milli-Q again. Fifteen alternate layers of positive and negative polymers were deposited on the fibre tip. The final three layers of the positively charged poly(allylamine hydrochloride) also contained **CPF1-NHS**. This ensured a denser surface coverage of **CPF1** to increase the fluorescent signal. The distal end of these functionalised fibres were then coupled into a 473 nm light source to detect any increase in fluorescence from the tip (see experimental section **6.5.4**). The functionalised tip of the fibre was dipped into 1 mM H_2O_2 and the fluorescence monitored over 20 min (**Figure 34**). No significant increase in fluorescence was apparent, despite the high 1 mM concentration of H_2O_2. The observed unchanging signal at 515 nm (**Figure 34**) corresponds to background fluorescence from the glass fibre.

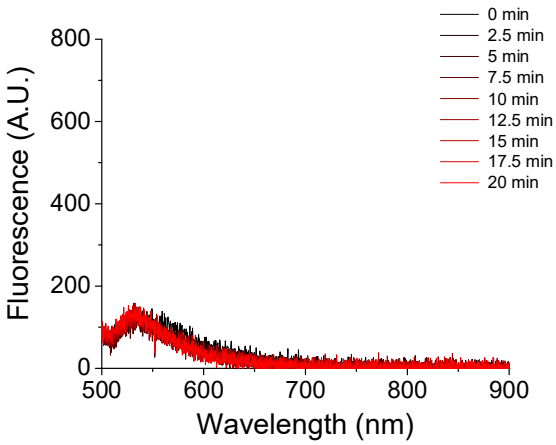

Figure 34. Poly electrolyte coating with **CPF1** attached, in 1 mM H_2O_2 for 20 min. The lack of increase in fluorescence indicates the poor signal on the fibre tip.

By comparison, the use of polyelectrolytes on glass slides (section **3.3**) had been effective at detecting an increase in H_2O_2. This difference could be due to the higher sensitivity of the confocal microscope and typhoon imager used in section **3.3**, compared with the lower laser power used in this experiment that was required to minimise photobleaching on the fibre tip. It is clear that while polyelectrolyte deposition affords an acceptable fluorescent response from **CPF1** on glass confocal microscope dishes, there is insufficient **CPF1** deposited on a fibre tip for H_2O_2 detection.

3.4.2 Silane Monolayer Formation

The next method of functionalisation formed an amine-functional silane layer on the fibre tip (**Scheme 6**). The tips were dipped into a mixture of 5 % APTES in toluene under anhydrous conditions. The tips were washed in toluene then acetonitrile, before immersing in a solution of **CPF1-NHS** in acetonitrile and washed in acetonitrile, then Milli-Q water. The distal end of the fibre was coupled to a 473 nm laser and the functionalised tip dipped into a 1 mM solution of H_2O_2 in bovine IVF media. The resultant fluorescence over 20 min is recorded in **Figure 35**. A slight increase was observed in the fluorescence maximum at 520 nm, showing **CPF1** immobilised to the fibre tip was reacting with H_2O_2. However, the increase in fluorescence that was expected should be much higher than the observed fluorescence. In solution, **CPF1** showed an increase in fluorescence upon reaction with as little as 10 µM H_2O_2 (**Figure 31**). By comparison, this surface gives a relatively poor fluorescent response to a 100-fold greater concentration of H_2O_2. This suggests that while the APTES coating method was superior to using polyelectrolytes, it is not sensitive enough to be an effective tip-probe for H_2O_2.

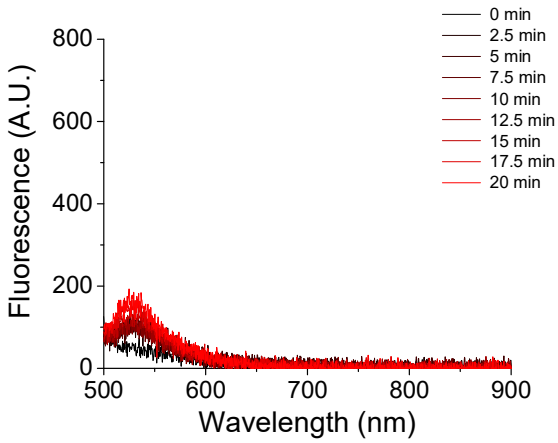

Figure 35. APTES-coated fibre tip shows a poor increase in fluorescence to 1 mM H_2O_2.

3.4.3 Light-Catalysed Polymerisation of Acrylamide/Bisacrylamide Matrix

The third functionalisation method trialled was the light-catalysed formation of a polyacrylamide matrix on the fibre tip (**Scheme 7**). Fibre tips were immersed in an aqueous solution of 3-(trimethoxysilyl)propyl acrylate to form an acrylate monolayer on the tips. Each tip was then dipped into a solution of **CPF1-NHS** in acrylamide/bisacrylamide. 405 nm light was coupled into the fibre catalysing polymerisation to the silane acrylate on the surface. The thus formed cross-linked polyacrylamide effectively traps **CPF1-NHS** in the polymer matrix, while allowing small molecules such as H_2O_2 to diffuse through it. The fibre tip was then washed in pH 7.4 buffer and 473 nm light was coupled into the distal end of the fibre. The functionalised tip was dipped into 1 mM H_2O_2 and the fluorescence of **CPF1-NHS** was recorded over 20 min (**Figure 36**).

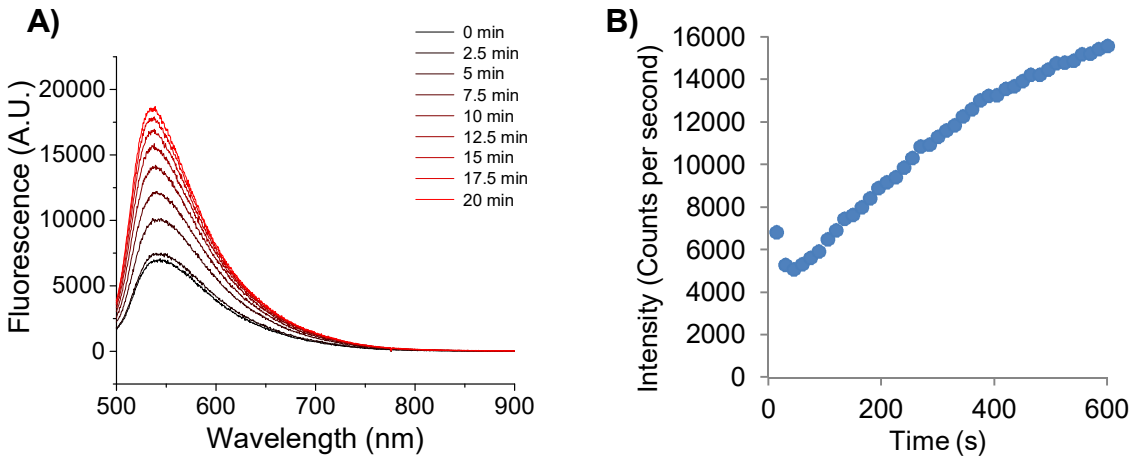

Figure 36. The response of **CPF1-NHS** in polyacrylamide to 1 mM H_2O_2 (ex. 473 nm laser): A) Overlaid spectra over 20 min of exposure to H_2O_2. B) Intensity change over time at emission peak 520 nm. The initial drop in fluorescence at 0 s represents the fibre tip being dipped into solution; the fluorescence is quenched slightly in water compared with air.

A near linear increase can be seen in the fluorescence maximum over 20 min (**Figure 36B**), indicating a kinetic response of **CPF1-NHS** to H_2O_2; similar to the initial solution-based studies (**Figure 31B**). The fluorescent response of this probe using the polyacrylamide method was roughly 100-fold greater than the probe functionalised with APTES (**Figure 35**). Hence, the polyacrylamide method gives a higher surface density of fluorophore than either APTES or polyelectrolyte functionalisation. The probe produced using the polyacrylamide method is the most effective at detecting H_2O_2 and produces a functional tip-probe for H_2O_2.

3.5 USE OF OPTICAL FIBRE PROBES WITH MICROMANIPULATORS

The fibre tips functionalised with **CPF1-NHS** using polyacrylamide were then trialled with a microscope setup. This aimed to validate the combination of the fibre tip-probe with the equipment used in biological experiments. Fibres were functionalised with **CPF1-NHS** in polyacrylamide as above and mounted to a micromanipulator (see experimental section **3.7.7**). A sample was prepared by adding a 1 µL drop of 100 mM H_2O_2 embryo culture media into a confocal microscope dish. Using the micromanipulators (with assistance from Ms. Leslie Ritter, Dr. Erik Schartner and Dr. Melanie Sutton-McDowall[§]), the fibre tip was inserted into the droplet containing H_2O_2 while under a microscope. The 473 nm laser source was coupled into the distal end of the fibre and the fluorescence was recorded over 6.5 min (**Figure 37**). A rapid increase in the integrated fluorescent signal was observed due to the high concentration of H_2O_2. This result confirmed that micromanipulators can precisely guide the optical fibres into a single droplet of media.

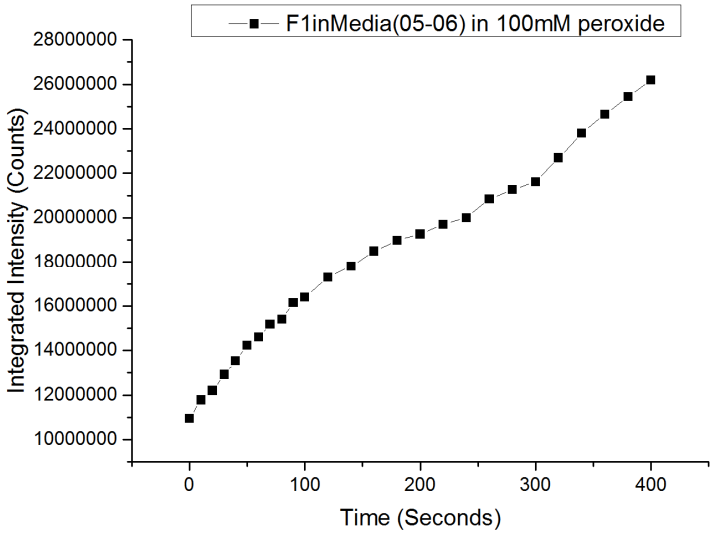

Figure 37. Fibre tip functionalised with **CPF1-NHS** and dipped into 100mM H_2O_2 using micromanipulators. A high concentration of H_2O_2 was used in these trials to ensure a large fluorescent response.

[§] Dr. Erik Schartner is an ARC postdoctoral fellow at the Institute for Photonics and Advanced Sensing, University of Adelaide, SA, Australia. Ms. Leslie Ritter is a research assistant in the Robinson Research Institute, University of Adelaide, SA, Australia. Dr. Melanie Sutton-McDowall is an ARC postdoctoral fellow in the Robinson Research Institute, University of Adelaide, SA, Australia.

The same microscope and micromanipulator setup was then used to sense H_2O_2 by mimicking the release of H_2O_2 into media from a cell. A fibre, functionalised as before, was placed in the micromanipulator and the tip inserted into a drop of embryo culture media, under the microscope. A second micromanipulator was used to manoeuvre the tip of a controlled liquid dispenser into the droplet, within 100 µm of the fibre tip. A concentrated solution of 100 mM H_2O_2 in the dispenser was released slowly over 5 min. Fluorescence was monitored during this period and after the addition of the H_2O_2 for 45 min (**Figure 38**). This graph indicates that the initial addition of H_2O_2 actually caused a rapid decrease in integrated fluorescence within a couple of minutes. This spatially corresponded to H_2O_2 solution flowing directly over the fibre tip. The flow rate was clearly too high over the tip, as turbulence of the solution caused disruption of the polymer layers on the tip, leading to a decrease in fluorescence.

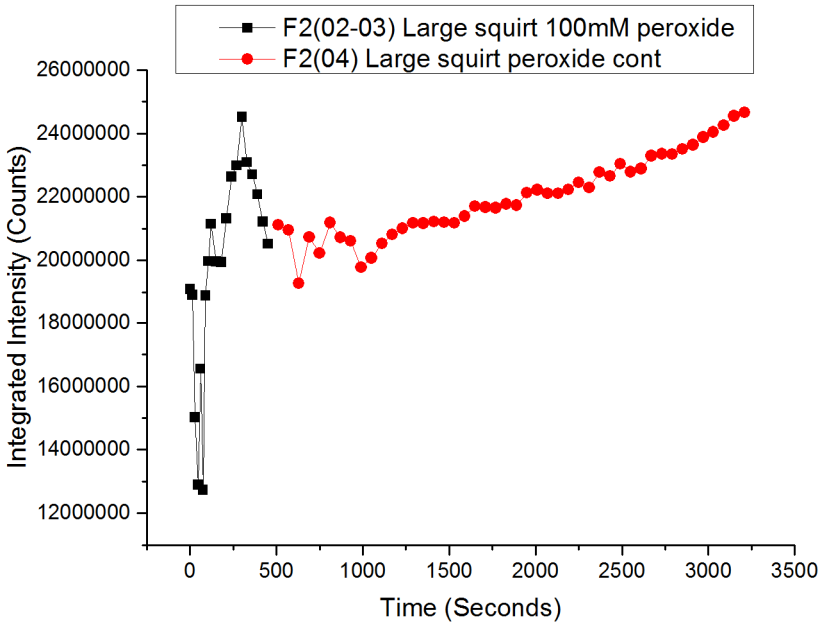

Figure 38. Fluorescent response from **CPF1-NHS** on a fibre tip after dispensing 100mM H_2O_2 into the drop over 5 min.

The spatial direction of flow was then altered several times, then a gentler flow rate of H_2O_2 again over the tip gave rise to the large spike at 250 s (**Figure 38**). However, increasing the flow rate again led to a sharp decrease in fluorescence intensity, indicating that the flow negatively affected the polymer layers. At 500 s, the flow was ceased in order to observe the fluorescent response from diffusion of the H_2O_2 throughout the droplet. A more stable fluorescence intensity signal was observed after 500 s (**Figure 38,** shown in red). At 1000 s, the fluorescent intensity then began to increase. This was likely due to the dispersion of the H_2O_2 throughout the drop of media and the fibre tip was exposed to the now diluted H_2O_2. This suggests that a precise release of H_2O_2 into a droplet of media, even if not directed at

the fibre tip, will cause a fluorescent response within 10 min. The flow of H_2O_2 directly over the tip also gave a valuable insight into the effect of turbulence on the fluorescence from **CPF1-NHS** in the polymer layers. By contrast, a gradual increase in fluorescent intensity was observed due to passive diffusion which is more similar to the release expected from a cell.

3.6 CONCLUSION

CPF1 and carboxy-activated **CPF1-NHS** were selected from similar aryl boronate probes and functionalised to glass surfaces for non-invasive detection of H_2O_2. **CPF1** effectively detected H_2O_2 when bound to a surface by polyelectrolyte deposition onto glass confocal microscope dishes. Furthermore, a working optical fibre tip-probe for H_2O_2 was demonstrated by light-catalysed polymerisation of polyacrylamide with **CPF1-NHS** to the fibre tip. The use of the polyacrylamide coating method produced a high surface density of **CPF1** on the tip, giving a greater fluorescent response to H_2O_2 compared with polyelectrolytes or APTES deposition techniques. This probe detected H_2O_2 both in stock solutions, and by passive diffusion in droplets of bovine IVF media when guided with micromanipulators and a microscope. This shows that the fibre tip-probe effectively detects H_2O_2, and demonstrates its compatibility with equipment commonly used to image embryos.

3.7 EXPERIMENTAL

3.7.1 Materials

All chemicals were purchased from Sigma-Aldrich unless otherwise stated. Bovine IVF medium was prepared using VitroFert from IVF Vet Solutions (Adelaide, Australia); 4 mg/ml fatty acid free BSA (ICPBio Ltd; Auckland, New Zealand); 10 IU/ml heparin, 25 µM penicillamine, 12.5 µM hypotaurine and 1.25 µM epinephrine. Bis(acrylamide) was purchased from Polysciences (Warrington, PA). HPLC grade toluene was purchased from Southern Cross Science (Adelaide, AUS), and dried using a Puresolv solvent purifier from Innovative Technology (Amesbury, MA). HPLC grade methanol and acetonitrile was purchased from Scharlau. 200 µm core diameter multimode fibre was purchased from Thorlabs (USA). **CPF1** was prepared as described in Chapter 2.[153] Milli-Q water was purified by a Millipore purification system (Billerica, MA). Glass bottom, confocal microscope dishes were purchased from Cell E&G (Houston TX).

3.7.2 Synthesis

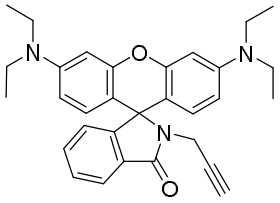

Rhodamine B Alkyne (**13**): Modified from a literature procedure of a similar compound.[154] **Rhodamine B** (958 mg, 2 mmol), oxalyl chloride (5 mL, 60 mmol) and a catalytic amount of dry DMF (3 drops) were stirred in dry DCM (60 mL) for 1 h. Solvent removed by vacuum, then resultant solid redissolved in dry DCM (100 mL) and anhydrous sodium carbonate (1.06 g) added. Propargyl amine (0.64 mL, 10.0 mmol) was added dropwise over 5 min and stirred for 20 h. $NaCO_3$ removed by filtration, then solvent and residual propargyl amine removed by vacuum to give a crude pink solid. This was eluted through a silica column using 1 % methanol in DCM as eluent, to give a light pink solid **22** (540 mg, 52 %) ^{1}HNMR (DMSO-d_6, 600MHz): δ(ppm) 7.80 (dd, 1H, J_1 = 6.0 Hz J_2 = 1.2 Hz), 7.50 (m, 2H), 7.02 (dd, 1H, J_1 = 6.6 Hz, J_2 = 1.2 Hz), 6.37 (d, 2H, J = 1.8 Hz), 6.35-6.31 (m, 4H), 3.77 (d, 2H, J = 2.4 Hz), 3.31 (q, 8H, J = 7.0 Hz), 2.64 (t, 1H, J = 2.4 Hz), 1.08 (t, 12H, J = 7.2 Hz) ^{13}CNMR (DMSO-d_6, 600MHz): δ(ppm) 166.3, 153.6, 152.7, 148.4, 132.9, 129.5, 128.4, 128.3, 123.6, 122.4, 108.0, 104.3, 97.2, 78.6, 72.6, 64.0, 43.6, 28.1, 12.4. LC-MS [$C_{31}H_{34}N_3O_2$] Calculated 480.3, found 480.2.

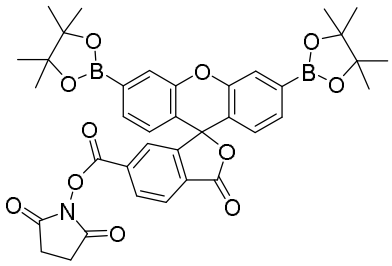

CPF1-NHS:[127] **CPF1**[153] (276 mg, 0.46 mmol), EDC•HCl (157 mg, 0.77 mmol) and N-hydroxysuccinimide (67 mg, 0.50 mmol) were dissolved in anhydrous dimethylformamide (7 mL) under nitrogen and stirred for 1 h. The reaction mixture was poured into diethyl ether (100 mL) and washed with water (100 mL). The aqueous phase was washed with diethyl ether (2x100 mL), the organic layers combined and dried over $MgSO_4$. The resultant solution was filtered, evaporated onto celite and eluted through a silica column using 1% methanol in dichloromethane to afford an off-white solid **CPF1-NHS** (165 mg, 53%) ^{1}HNMR ($CDCl_3$, 500 MHz): δ(ppm) 8.32 (d, 1H, J = 8.1 Hz), 8.15 (dd, 1H, J_1 = 8.0 Hz, J_2 = 1 Hz), 7.78 (s, 1H), 7.74 (s, 2H), 7.45 (d, 2H, J = 7.8 Hz), 6.81 (dd, 2H, J_1 = 7.8 Hz), 2.82 (br. s, 4H), 1.32 (s, 24H)

3.7.3 Fluorescence Assay in Fluorimeter

The response of **CPF1** and **10** to H_2O_2 was compared using a Cary Eclipse Fluorescence Spectrometer. **CPF1** and **10** were dissolved in DMSO to 2 mM and then diluted to a final concentration of 10 μM in separate α-MEM buffer solutions. H_2O_2 was added to give final concentrations of 0, 20, 40 and 60 μM. Fluorescence spectra were measured after 40 min of incubation at 37°C.

3.7.4 Fluorescence Assay in Plate Reader

The response of **CPF1** to H_2O_2 was measured using a Biotek Synergy H4 plate reader. **CPF1** was dissolved in DMSO to 2 mM, then diluted to a final concentration of 10 μM in 20 mM HEPES buffer at pH 7.4. H_2O_2 was added to give final concentrations of 0, 10, 25, 50, 75 and 100 μM. Absorption and fluorescence spectra were measured after 40 min of incubation at 37°C.

3.7.5 Surface Attachment Protocols

3.7.5.1 Preparation of Confocal Microscope Dishes

Confocal microscope dishes were washed with Milli-Q water before being sonicated in HPLC grade methanol for 20 min and dried under vacuum for 1 h. Stock solutions of poly(allylamine hydrochloride) and poly(acrylic acid) were made up to 1 mg/mL in a 1 M sodium chloride solution. 1 mL of poly(allylamine hydrochloride) stock was carefully pipetted onto the exposed glass surface of the cleaned confocal dish and left for 15 min. The poly(allylamine hydrochloride) solution was decanted, and the surface carefully rinsed 4x with 2.5 mL of Milli-Q water. 1 mL of poly(acrylic acid) stock was then pipetted onto the glass surface and left for 15 min. After decanting, the glass was rinsed with a further 4x 2.5 mL of Milli-Q water. A further layer of poly(allylamine hydrochloride) was deposited and rinsed as previously described. 1 mL of an aqueous solution of EDC•HCl (1 mM), NHS (1 mM) and **CPF1** (10 μM) was pipetted onto the glass and left for 1 h. The excess was decanted and the dish washed with 4x 2.5 mL of Milli-Q water and placed under vacuum for 12 h to remove excess water.

5 μL droplets of Bovine IVF medium with increasing concentrations of H_2O_2 (0-500 μM) were added to the plates and covered with paraffin oil (Merck; Darmstadt, Germany) to eliminate evaporation, then incubated at 38.5 °C for 1 h. The fluorescence of individual media drops on the plates was captured using an Olympus (Tokyo) Fluoview FV10i (ex = 470 nm and em = 500-600 nm), before being imaged on the Amersham Typhoon imager as per below.

The fluorescence generated on the glass slides before and on reaction with H_2O_2 was measured using a Typhoon TM 8600 variable mode imager from Amersham Bioscience. Excitation was performed using a 488 nm laser, and the emission measured through a 520 nm filter with a 40 nm bandwidth. Sensitivity was set to 100 μm per pixel, and photomultiplier tube voltage was 500 V. Average fluorescence intensity per mm^2 was collected from 100 data points and the error was calculated to give the standard error of the mean (SE).

3.7.5.2 Polyelectrolyte Deposition on Optical Fibre Tips

Stock solutions of poly(allylamine hydrochloride), poly(acrylic acid) (1 mg/mL in a 1 M sodium chloride) and a 100 μM **CPF1-NHS** solution with 1 mg/mL poly(allylamine hydrochloride) in 1M sodium chloride were prepared. The freshly cleaved tip of a length of multi-mode fibre (200μm) was immersed in the poly(allylamine hydrochloride) solution for 5 min, rinsed in Milli-Q water and then re-immersed in poly(acrylic acid) for 5 min (**Scheme 10**). This process was repeated 11 times to give alternating layers of poly(allylamine hydrochloride) and poly(acrylic acid). The fibre tip was finally immersed in the poly(allylamine hydrochloride) solution containing **CPF1-NHS** for 5 min and then washed and immersed in poly(acrylic acid) for 5 min. This process was repeated to give 3 layers of poly(allylamine hydrochloride) containing **CPF1-NHS** on the fibre tip, with 15 layers of poly(allylamine hydrochloride) in total.

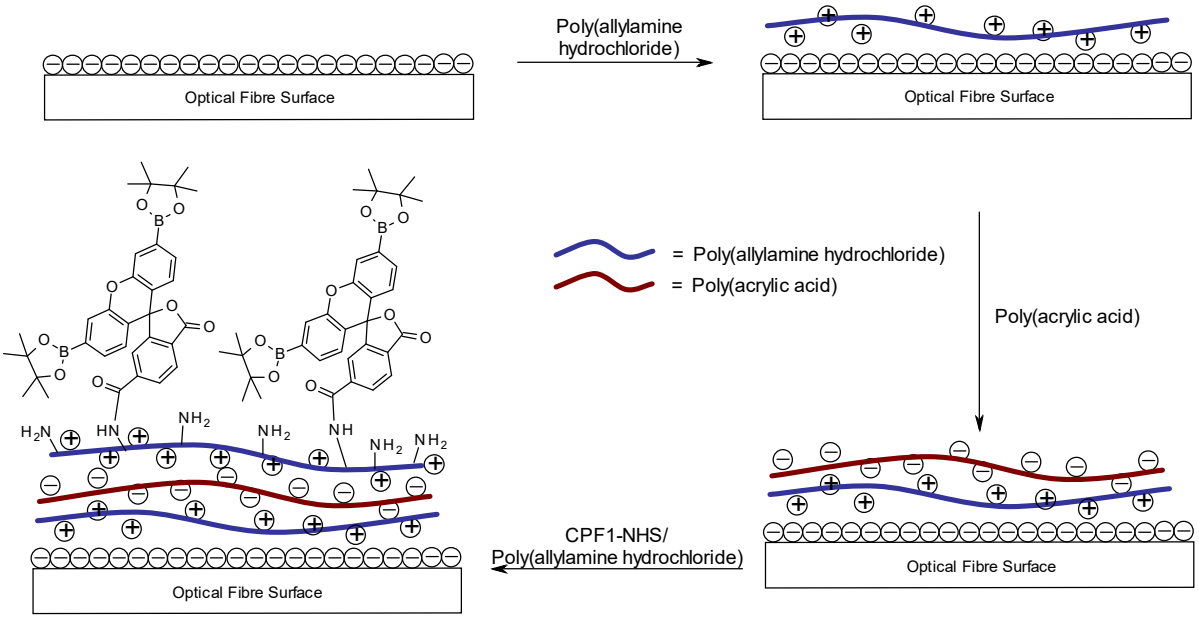

Scheme 10. Representative diagram of the deposition of poly electrolyte layers poly(allylamine hydrochloride) and poly(acrylic acid) to a glass surface. Although this schematic depicts 3 layers, 15 alternate layers of each polymer were actually deposited on the fibre tip. The final three deposited layers of poly(allylamine hydrochloride) contained **CPF1-NHS**.

3.7.5.3 Silane Functionalisation on Optical Fibre Tips

Multi-mode fibre (200 μm diameter) was cut to length and the end face was cleaved in order to provide a clean surface. Under a dry nitrogen atmosphere, the fibre tips were washed with ethanol followed by dry toluene for 30 min. The fibre tips were then functionalised by placing them in a 5% mixture of (3-aminopropyl)triethoxysilane (APTES) in toluene before a further wash with dry toluene (**Scheme 11**). The fibre was removed from nitrogenous atmosphere and washed with HPLC grade acetonitrile. The tip was immersed in a mixture of EDC•HCl (1 mM), NHS (1 mM) and **CPF1** (100 μM) in HPLC grade acetonitrile. The fibre tip was then removed, washed with further acetonitrile and Milli-Q water for use on an optical fibre setup.

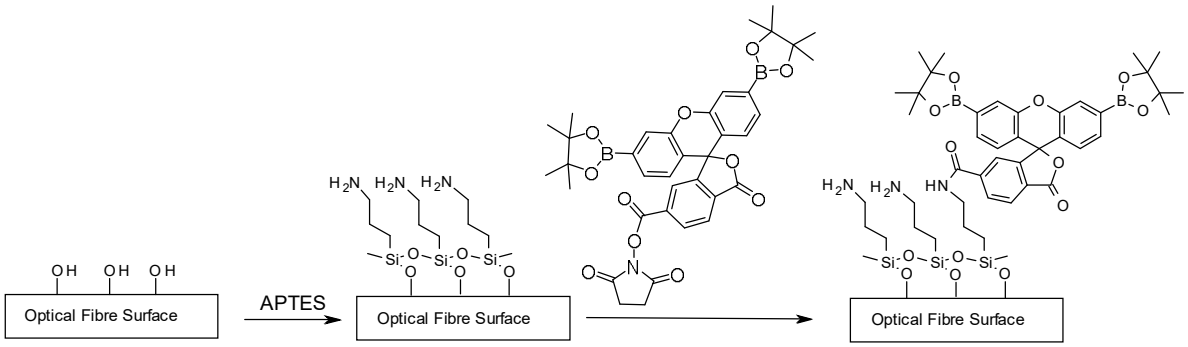

Scheme 11. Surface functionalisation of **CPF1-NHS** with APTES. Deposition of APTES to the fibre surface is performed in anhydrous conditions to avoid polymerisation and create an even monolayer.

3.7.5.4 Polyacrylamide Photopolymerisation on Optical Fibre Tips

A solution of 3-(trimethoxysilyl)propyl methacrylate in pH 3.5 adjusted Milli-Q water was mixed and sonicated until clear. Multi-mode fibre (200 μm diameter) was cut to length and the end face was cleaved in order to provide a clean surface, then immersed in the methacrylate solution for 1 h (**Scheme 12**). The fibre tip was then dried under N_2, rinsed with Milli-Q water and dried under N_2 again. The distal end of the fibre was then coupled into the fibre setup shown in **Figure 61** below. A monomeric stock solution comprising of 3% bisacrylamide, 27% acrylamide and 70% pH 6.5 phosphate buffer solution was dissolved under sonication. **CPF1-NHS** (0.2 mg) was dissolved in the monomeric solution (400 μL) with triethylamine (10 μL) and 200 μL of this was pipetted into a small Eppendorf tube. The functionalised fibre tip was immediately immersed in this solution, and irradiated under 405 nm light for 2s to form a polymeric coating on the fibre tip (**Scheme 12**).

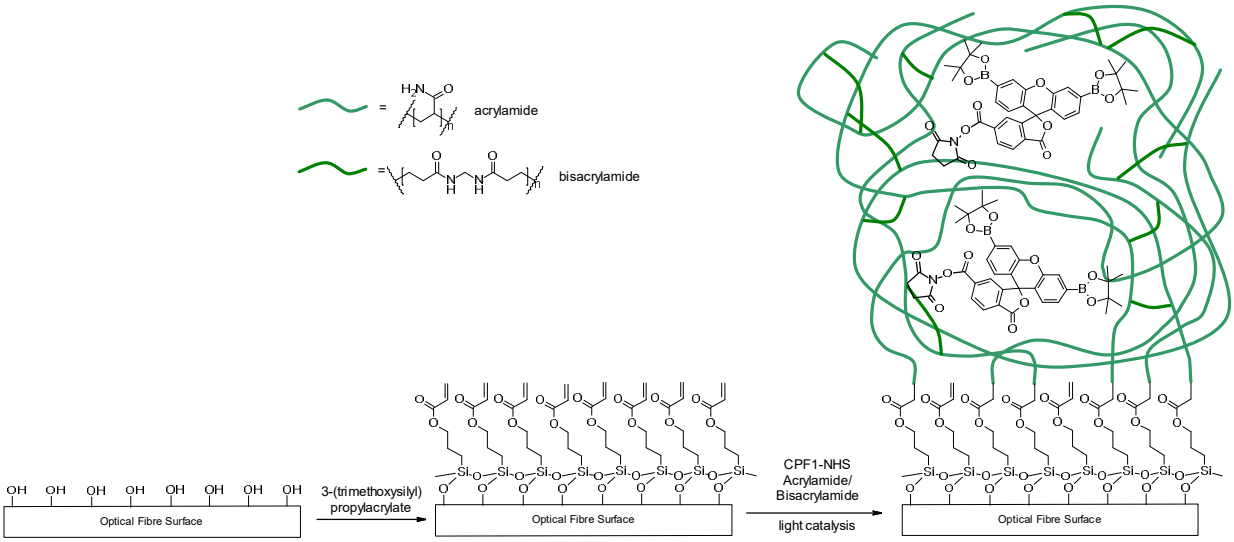

Scheme 12. Formation of a polyacrylamide matrix containing **CPF1-NHS**. A silane layer is deposited with propylacrylate functionality. The polymer is then formed on the tip by immersing the fibre tip in an aqueous solution of **CPF1-NHS** in acrylamide/bisacrylamide and irradiating through the fibre with a 405 nm laser source.

3.7.6 Fibre Setup

A schematic of the optical setup is shown in **Figure 61**, for both photopolymerisation of the polymer using the 405 nm source, and optical measurements using the 473 nm source.

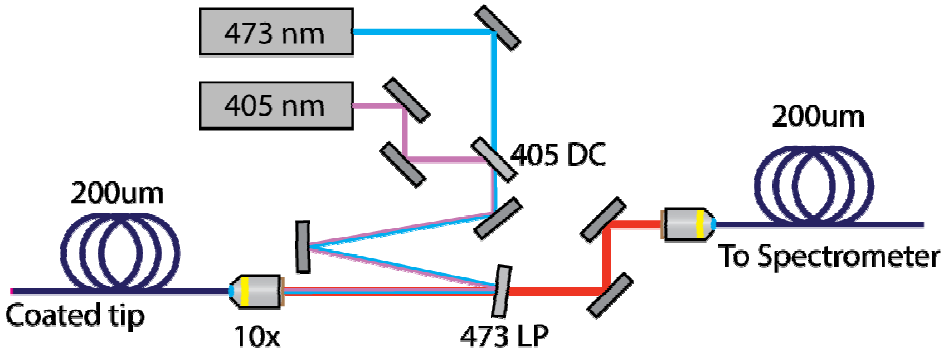

Figure 39. Experimental configuration for photopolymerisation, and optical measurements.

For excitation of the fluorophore for both direct attached and polymer embedded methods, the 473 nm laser (Toptica iBeam Smart) was coupled into the distal end of the probe fibre, with the 405 nm arm blocked. The coupled laser light then excites the fluorophore-doped probe tip, and a portion of this fluorescent light is then captured into a back-propagating mode in the fibre. This then passes through a 473 nm long-pass filter (Semrock EdgeBasic) to remove excess pump light, before being coupled into a spectrometer (Horiba iHR320) via a 200 µm optical fibre patch cable.

The same experimental configuration was used to induce photopolymerisation on the fibre tips, with the 473 nm path blocked, and a timed shutter used on the 405 nm source to control the deposition time of the polymer.

3.7.7 Micromanipulator Trials

Fibres functionalised as in **6.5.3.1** were attached to an Eppendorf TransferMan NK2 micromanipulator for use with a Nikon Eclipse TE2000-E microscope. 473 nm laser light (Toptica iBeam Smart) was coupled into the fibre and the fluorescence recorded as in section **6.5.4** with a Horiba iHR320 spectrometer.

Droplets of Bovine IVF media (1 mL) were prepared in a confocal microscope dish with or without 100 mM H_2O_2. The optical fibre tip was gently inserted into the droplet of media by use of the controls on the micromanipulator. A second micromanipulator was used to move the tip of an Eppendorf AG oil Cell Tram dispenser into the droplet of media for controlled addition of low volumes of 100 mM H_2O_2.

3.8 REFERENCES

26. Chan, J.; Dodani, S. C.; Chang, C. J. Reaction-based small-molecule fluorescent probes for chemoselective bioimaging. *Nature Chemistry* **2012,** *4* (12), 973-984.
30. Lippert, A. R.; Van de Bittner, G. C.; Chang, C. J. Boronate Oxidation as a Bioorthogonal Reaction Approach for Studying the Chemistry of Hydrogen Peroxide in Living Systems. *Accounts of Chemical Research* **2011,** *44* (9), 793-804.
38. Heng, S.; Nguyen, M.-C.; Kostecki, R.; Monro, T. M.; Abell, A. D. Nanoliter-scale, regenerable ion sensor: sensing with a surface functionalized microstructured optical fibre. *RSC Advances* **2013,** *3* (22), 8308.
39. Heng, S.; Mak, A. M.; Stubing, D. B.; Monro, T. M.; Abell, A. D. Dual Sensor for Cd(II) and Ca(II): Selective Nanoliter-Scale Sensing of Metal Ions. *Analytical Chemistry* **2014,** *86* (7), 3268-3272.
56. Albers, A. E.; Okreglak, V. S.; Chang, C. J. A FRET-Based Approach to Ratiometric Fluorescence Detection of Hydrogen Peroxide. *Journal of the American Chemical Society* **2006,** *128* (30), 9640-9641.
94. Chang, M. C. Y.; Pralle, A.; Isacoff, E. Y.; Chang, C. J. A selective, cell-permeable optical probe for hydrogen peroxide in living cells. *Journal of the American Chemical Society* **2004,** *126* (47), 15392-15393.
109. Tan, W.; Shi, Z. Y.; Smith, S.; Birnbaum, D.; Kopelman, R. Submicrometer intracellular chemical optical fiber sensors. *Science* **1992,** *258* (5083), 778-81.
111. Song, A.; Parus, S.; Kopelman, R. High-Performance Fiber-Optic pH Microsensors for Practical Physiological Measurements Using a Dual-Emission Sensitive Dye. *Analytical Chemistry* **1997,** *69* (5), 863-867.
127. Srikun, D.; Albers, A. E.; Chang, C. J. A dendrimer-based platform for simultaneous dual fluorescence imaging of hydrogen peroxide and pH gradients produced in living cells. *Chemical Science* **2011,** *2* (6), 1156-1165.
137. Foo, H. T. C.; Ebendorff-Heidepriem, H.; Sumby, C. J.; Monro, T. M. Towards microstructured optical fibre sensors: surface analysis of silanised lead silicate glass. *Journal of Materials Chemistry C* **2013,** *1* (41), 6782-6789.

138. Hong, J.-D.; Park, E.-S.; Park, A.-L. Effects of Added Salt on Photochemical Isomerization of Azobenzene in Alternate Multilayer Assemblies: Bipolar Amphiphile-Polyelectrolyte. *Langmuir* **1999,** *15* (19), 6515-6521.
139. Francois, A.; Cheung Foo, H. T.; Monro, T. In *Polyelectrolyte Multilayers for Surface Functionalization: Advantages and Challenges*, Advanced Photonics, Barcelona, 2014/07/27; Optical Society of America: Barcelona, 2014; p JTu4C.1.
140. Vashist, S. K.; Lam, E.; Hrapovic, S.; Male, K. B.; Luong, J. H. T. Immobilization of Antibodies and Enzymes on 3-Aminopropyltriethoxysilane-Functionalized Bioanalytical Platforms for Biosensors and Diagnostics. *Chemical Reviews* **2014,** *114* (21), 11083-11130.
141. Ulman, A. Formation and Structure of Self-Assembled Monolayers. *Chemical Reviews (Washington, D. C.)* **1996,** *96* (4), 1533-1554.
142. Haensch, C.; Hoeppener, S.; Schubert, U. S. Chemical modification of self-assembled silane based monolayers by surface reactions. *Chemical Society Reviews* **2010,** *39* (6), 2323-2334.
143. Foo, H. T. C. Optical Fibre Sensors with Surface-immobilised Fluoroionophores. University of Adelaide, 2013.
144. Chauhan, V. M.; Burnett, G. R.; Aylott, J. W. Dual-fluorophore ratiometric pH nanosensor with tuneable pKa and extended dynamic range. *Analyst (Cambridge, United Kingdom)* **2011,** *136* (9), 1799-1801.
145. Chen-Esterlit, Z.; Peteu, S. F.; Clark, H. A.; McDonald, W.; Kopelman, R. Comparative study of optical fluorescent nanosensors (PEBBLEs) and fiber optic microsensors for oxygen sensing. *Proc. SPIE-Int. Soc. Opt. Eng.* **1999,** *3602* (Advances in Fluorescence Sensing Technology IV), 156-163.
146. Jorge, P.; Caldas, P.; Da Silva, J. C. G.; Rosa, C.; Oliva, A.; Santos, J.; Farahi, F. Luminescence-Based Optical Fiber Chemical Sensors. *Fiber Integr. Opt.* **2005,** *24* (3-4), 201-225.
147. O'Leary, L. E.; Rose, M. J.; Ding, T. X.; Johansson, E.; Brunschwig, B. S.; Lewis, N. S. Heck Coupling of Olefins to Mixed Methyl/Thienyl Monolayers on Si(111) Surfaces. *Journal of the American Chemical Society* **2013,** *135* (27), 10081-10090.
148. Engler, T. K. Synthesis and Modification of Peroxyfluor-1. University of Adelaide, Adelaide, Australia, 2012.
149. Woodroofe, C. C.; Lim, M. H.; Bu, W.; Lippard, S. J. Synthesis of isomerically pure carboxylate- and sulfonate-substituted xanthene fluorophores. *Tetrahedron* **2005,** *61* (12), 3097-3105.
150. He, F.; Feng, F.; Wang, S.; Li, Y.; Zhu, D. Fluorescence ratiometric assays of hydrogen peroxide and glucose in serum using conjugated polyelectrolytes. *Journal of Materials Chemistry* **2007,** *17* (35), 3702-3707.
151. Brauch, S.; Henze, M.; Osswald, B.; Naumann, K.; Wessjohann, L. A.; van Berkel, S. S.; Westermann, B. Fast and efficient MCR-based synthesis of clickable rhodamine tags for protein profiling. *Organic & Biomolecular Chemistry* **2012,** *10* (5), 958-965.
152. Adamczyk, M.; Grote, J. Synthesis of novel spirolactams by reaction of fluorescein methyl ester with amines. *Tetrahedron Letters* **2000,** *41* (6), 807-809.
153. Purdey, M. S.; Connaughton, H. S.; Whiting, S.; Schartner, E. P.; Monro, T. M.; Thompson, J. G.; Aitken, R. J.; Abell, A. D. Boronate probes for the detection of hydrogen peroxide release from human spermatozoa. *Free Radical Biology and Medicine* **2015,** *81* (0), 69-76.
154. Yan, R.; El-Emir, E.; Rajkumar, V.; Robson, M.; Jathoul, A. P.; Pedley, R. B.; Arstad, E. One-Pot Synthesis of an 125I-Labeled Trifunctional Reagent for Multiscale Imaging with Optical and Nuclear Techniques. *Angewandte Chemie, International Edition* **2011,** *50* (30), 6793-6795, S6793/1-S6793/15.

Chapter 4

A DUAL SENSOR FOR PH AND HYDROGEN PEROXIDE USING POLYMER-COATED OPTICAL FIBRE TIPS

The difference between stupidity and genius is that genius has its limits.

Albert Einstein

STATEMENT OF AUTHORSHIP

Title of Paper	A dual sensor for pH and hydrogen peroxide using polymer-coated optical fibre tips.
Publication Status	☐ Published ☐ Accepted for Publication ☑ Submitted for Publication ☐ Publication Style
Publication Details	Purdey, M. S.; Thompson, J. G.; Monro, T. M.; Abell, A. D.; Schartner, E. P., A dual sensor for pH and hydrogen peroxide using polymer-coated optical fibre tips. *Sensors* **2015**, *Submitted for publication*

Principal Author

Name of Principal Author (Candidate)	Malcolm S. Purdey		
Contribution to the Paper	Synthesis of fluorescent probes, preparation and polymerisation on fibre tips, measurements in pH and hydrogen peroxide solutions, data analysis and writing of manuscript.		
Overall percentage (%)	65%		
Signature		Date	27/10/2015

Co-Author Contributions

By signing the Statement of Authorship, each author certifies that:

i. the candidate's stated contribution to the publication is accurate (as detailed above);

ii. permission is granted for the candidate in include the publication in the thesis; and

iii. the sum of all co-author contributions is equal to 100% less the candidate's stated contribution.

Name of Co-Author	Jeremy G. Thompson		
Contribution to the Paper	Project direction and manuscript editing.		
Signature		Date	28/10/2015

Name of Co-Author	Tanya M. Monro		
Contribution to the Paper	Project direction and manuscript editing.		
Signature		Date	4/12/15

Name of Co-Author	Andrew D. Abell		
Contribution to the Paper	Project direction, principal supervision of candidate and manuscript editing.		
Signature		Date	27/10/2015

Name of Co-Author	Erik P. Schartner		
Contribution to the Paper	Assistance with optical setup and polymerisation techniques, manuscript editing.		
Signature		Date	27/10/15

Chapter 4: A dual sensor for pH and hydrogen peroxide using polymer-coated optical fibre tips**

Malcolm S Purdey[a-c]*, Jeremy G Thompson[a,b,d], Tanya M Monro[a,b,e], Andrew D Abell[a-c], Erik P Schartner[a,b]

[a] ARC Centre of Excellence for Nanoscale BioPhotonics, Adelaide, SA, Australia

[b] Institute for Photonics and Advanced Sensing (IPAS), The University of Adelaide, North Terrace, Adelaide 5005, SA, Australia

[c] Discipline of Chemistry, School of Physical Sciences, The University of Adelaide, North Terrace, Adelaide 5005, SA, Australia

[d] Robinson Research Institute, School of Medicine, The University of Adelaide, North Terrace, Adelaide 5005, SA, Australia

[e] University of South Australia, North Terrace, Adelaide 5001, SA, Australia

* Corresponding author: malcolm.purdey@adelaide.edu.au

4.1 ABSTRACT

This paper demonstrates the first single optical fibre tip probe for concurrent detection of both hydrogen peroxide (H_2O_2) concentration and pH of a solution. The sensor is constructed by embedding two fluorophores [carboxyperoxyfluor-1 (**CPF1**) and seminaphtharhodafluor-2 (**SNARF2**)] within a polymer matrix located on the tip of the optical fibre. The functionalised fibre probe reproducibly measures pH, and is able to accurately detect H_2O_2 over a biologically relevant concentration range. This sensor offers potential for non-invasive detection of pH and H_2O_2 in biological environments using a single optical fibre.

** Purdey, M. S.; Thompson, J. G.; Monro, T. M.; Abell, A. D.; Schartner, E. P. , A dual sensor for pH and hydrogen peroxide using polymer-coated optical fibre tips. *Sensors* **2015**, *15* (12), 31904-31913.

4.2 INTRODUCTION

Hydrogen peroxide (H_2O_2) and pH play vital combined roles in cellular signalling,[22,155,156] tumour development[157-160] and reproductive health science.[17,24,25,161] For example, the unregulated production of H_2O_2 by an embryo is a hallmark of embryonic stress,[7] while pH fluctuations during embryo culture can negatively affect embryonic development.[162] The simultaneous detection of pH and H_2O_2 would therefore provide significant benefit in monitoring the associated cellular processes. H_2O_2 and pH can be detected in cells by specific fluorophores, measuring either an increase in fluorescence intensity,[26,30] or a change in emission spectra respectively.[163,164] However the use of these fluorescent probes in applications such as *in vitro* fertilisation (IVF) poses significant scientific and ethical questions, as their effect on the development of embryos is unknown. As such, direct contact of fluorophores with an embryo is ethically unsound and not allowable in most regulatory jurisdictions.

Optical fibre-based probes offer an attractive and non-invasive approach. Here a fluorophore of interest can be attached to the fibre surface for localised measurement without being released into the solution.[38,39,137] Various configurations of optical fibres have been examined for development of such fluorescent sensors, specifically; functionalized end-faces (tip sensors),[109,110] exposed core[165] and microstructured fibres.[166,167] Although microstructured fibre based sensors can be more sensitive than tip sensors,[168] filling of the air holes with analyte is required in order to perform a measurement. This typically restricts microstructured fibres to single temporal measurements, unless microfluidics or external flushing systems are employed, and these may impede on the cell culture environment. Exposed-core fibre sensors are ideal for environmental sensing and do not require microfluidics or external flushing and offer advantages in distributed sensing. However, tip-based sensors offer potential for temporal measurements in a single location rather than distributed along the length, or can be repositioned to obtain a spatial map of the sample as desired. Tip sensors often have reduced sensitivity compared to microstructured fibres,[168] especially as conventional attachment of a single layer of fluorophore to a fibre tip results in a low signal intensity.[169] However, the signal intensity can be improved by increasing the density of fluorophore on the fibre tip.

H_2O_2 can be detected by aryl boronate-based fluorophores such as peroxyfluor-1 (**PF1**)[94] and carboxyPF1 (**CPF1**, **Figure 40**).[153] These aryl boronates have been shown as particularly effective fluorescent probes for detection of H_2O_2 in human spermatozoa and bovine oocytes.[153,170] pH can be detected using a range of fluorophores, with seminaphthorhodofluor-2 (**SNARF2**, **Figure 40**) offering some advantages over alternative

probes, as the ratiometric emission from this probes changes its spectral features over the physiological pH range, with a pK_a of 7.5.[171] This minimises potential errors which could arise from using a solely intensity-based probe. Additionally, its emission spectrum overlaps minimally with the emission of **CPF1**,[127] allowing the separate interrogation of each fluorophore.

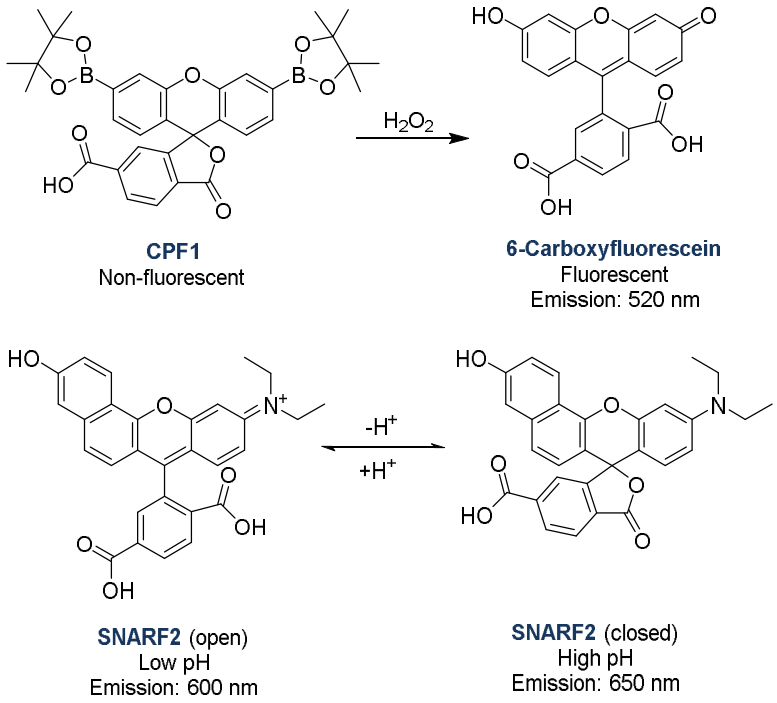

Figure 40. Chemical structures of fluorescent probes used in this study. Carboxyperoxyfluor-1 (**CPF1**) reacts with H_2O_2 to form the fluorescent 6-carboxyfluorescein. Seminaphthorhodofluor-2 (**SNARF2**) is found in the protonated (open) form and lactone (closed) at low and high pH respectively.

This paper reports the first dual probe for sensing pH and the detection of H_2O_2 by immobilising two separate fluorophores (**CPF1** and **SNARF2**) onto a single optical fibre tip in a polyacrylamide matrix. The two fluorophores are attached to a multi-mode fibre tip by a light-catalysed polymer coating,[111] to allow for greater control of fluorophore surface density and thus subsequent signal intensity. This then allows detection of both H_2O_2 and pH within a single system.

4.3 RESULTS AND DISCUSSION

4.3.1 Hydrogen Peroxide Detection

4.3.1.1 Detection of Biologically Relevant Hydrogen Peroxide Concentrations

CPF1 and **SNARF2** immobilised on fibre tips were tested in solutions containing H_2O_2 to establish the sensitivity of this surface configuration. Fibre tips were first functionalised with 3-(trimethoxysilyl)propyl methacrylate, then dipped into a solution of acrylamide/bisacrylamide with N-hydroxysuccinimide esters of **CPF1** and **SNARF2**. The N-succinimide esters of **CPF1** and **SNARF2** increase solubility in the acrylamide solution to provide a more reproducible density of fluorophores embedded in the polymer matrix. Excitation light (405 nm) was coupled into the distal end of the fibre and the tip irradiated for 10 s to form a polymer layer on the tip containing the fluorophores. The functionalised fibres were dipped into a range of concentrations of H_2O_2 (0, 50, 75 and 100 μM) in pH 7.5 phosphate buffer, and the emission peaks from **CPF1** at 520 nm and SNARF at 600 and 660 nm were observed under 473 nm excitation. A low excitation power was used (27 μW) for these trials to minimise any potential effects of photobleaching. The entire spectrum was then integrated and normalised to the initial peak of **CPF1** at 520 nm. This was necessary because each probe has slightly different initial fluorescence values and hence raw intensity values cannot be directly compared. Furthermore, each fibre probe was only used once for detection of H_2O_2 to ensure maximum consistency between trials. **Figure 41** shows an increase in normalised integrated fluorescence due to **CPF1** over a 20 min exposure to H_2O_2. This time interval was dictated by the reaction rate of aryl boronates such as **CPF1** with H_2O_2.[100]

Normalised fluorescence of **CPF1** in the presence of 100 μM H_2O_2 is greater than for the control, which lacked H_2O_2 (**Figure 41A**). This increase in fluorescence is consistent with **CPF1** reacting with H_2O_2 on the fibre tip. Furthermore, a plot of the rate of increase in fluorescence vs concentration of H_2O_2 (**Figure 41B**) clearly shows this rate increasing as the concentration of H_2O_2 increases from 0 μM to 50 μM, 75 μM and 100 μM of H_2O_2. A similar increase was observed in our previous studies on the detection of H_2O_2 with **CPF1** in solution,[169] and we have also shown that **CPF1** is able to detect relevant H_2O_2 concentrations in reproductive biology.[153] Hence this probe exhibits sufficient sensitivity for this biological environment.

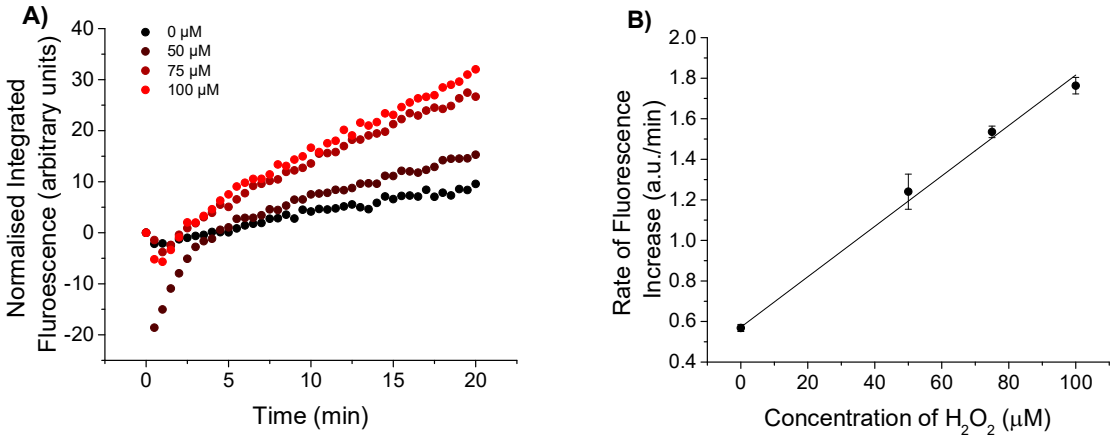

Figure 41. A) Integrated fluorescence intensity from **CPF1** using blue excitation with varied peroxide concentration in pH 7.5 buffer. 100 µM H_2O_2 shows an increased fluorescent response from the fibre without H_2O_2. B) Slope of integrated fluorescence for increasing concentrations of H_2O_2 (0, 50, 75 and 100 µM). Error bars indicate the standard error of the calculated slope.

An initial drop in fluorescence was observed for some probes (see **Figure 41A**), particularly the probe immersed in a 50 µM H_2O_2 solution. This is likely due to a change in emission properties of the fluorophores as the probe is moved from air into the solution. A more rapid increase in fluorescence was observed in the first 5 min, suggesting the probe is equilibrating in the new medium. After 5 min the probes show a near linear increase in fluorescence intensity. Thus, an incubation time of greater than 5 min is required to give an accurate indication of the rate of increase in fluorescence due to H_2O_2. A plateau was not observed over the time course of the experiment, suggesting quantitative data should be obtained from the rate of increase in fluorescence rather than the overall increase in fluorescence.

It is also important to note that an increase in the integrated fluorescent signal was evident, even in the absence of H_2O_2 (**Figure 41A**). A decrease in fluorescence would be expected if photobleaching or leaching of the fluorophore from the polymer occurred over the course of the experiment. The effect of photobleaching on **CPF1** was of particular interest, since **CPF1** is oxidised by H_2O_2 to give 5-carboxyfluorescein. 5-carboxyfluorescein is known to photobleach,[172] a process which occurs more rapidly in the presence of reactive oxygen species such as H_2O_2.[173] In order to accurately sense H_2O_2 with **CPF1**, low rates of photobleaching must be achieved. An increase in fluorescence in the absence of H_2O_2 suggests that photobleaching was not occurring on the fibre during the experiment. This is an important observation for the practical use of the probe since the fibre's ability to sense accurately would be reduced by photobleaching of the fluorophores on the fibre tip.

4.3.1.2 Effect of Change in pH on Detection of Hydrogen Peroxide

The effect of pH on the detection of H_2O_2 in fibre was next investigated by immersing functionalised fibre tips in solutions of H_2O_2 of differing pH. Fibre tips were functionalised with **CPF1** and **SNARF2** as before and separately immersed in 100 µM separate solutions of H_2O_2 at a pH of 7.05, 7.55 or 8.05. A 470 nm light source was coupled into the fibre for excitation and the increase in fluorescence was recorded over 20 min. All spectra were integrated and normalised as before, with the results shown in **Figure 42A**. The rate of increase in fluorescence was calculated as depicted in **Figure 42B**. The observed rate at pH 8.05 was 1.5 times greater than the rate observed at pH 7.05 (**Figure 42B**).

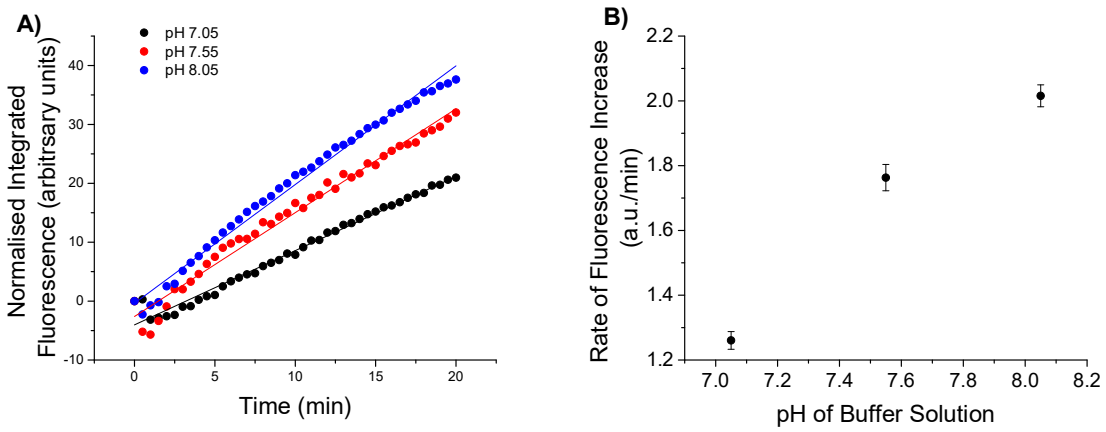

Figure 42. Response of **CPF1** to 100 µM H_2O_2 in solutions that varied in pH. A) Integrated fluorescent responses of probes to 100 µM H_2O_2 in pH 7.05, 7.55 and 8.05 over 20 min using blue excitation. B) Rate of increase in fluorescence of each probe with H_2O_2 in each of the 3 pH solutions. Error bars indicate the standard error of the calculated slope.

The reaction rate of aryl boronates (such as **CPF1**) with H_2O_2 is higher in more basic solutions.[174] **CPF1** reacts with the conjugate base of H_2O_2 (hydroperoxide ion HOO^-)[30] to give fluorescent 5-carboxyfluorescein. As the pH increases, more H_2O_2 dissociates into its conjugate base, HOO^-. The concentration of HOO^- available to react with **CPF1** will therefore be higher in more basic solutions, accounting for the observed upward trend in rates due to increasing pH (**Figure 42B**). Furthermore, the product of **CPF1** with H_2O_2 is a carboxyfluorescein, and fluorescein exhibits different quantum yields of fluorescence at differing pH.[175] Thus, the pH of the solution is highly pertinent to the accurate detection of H_2O_2. This is further highlighted by a comparison of rates of increase in fluorescence at different pH and H_2O_2 concentration, shown in **Figure 41B** and **Figure 42B**. A rate of approximately 1.2 a.u./min was calculated for a 100 µM solution of H_2O_2 in pH 7.05 (**Figure 42B**). However, a similar rate was calculated for a 50 µM solution of H_2O_2 at a pH of 7.55 (**Figure 41B**). The observed rate in these experiments is clearly dependent on the pH, in addition to the concentration of H_2O_2. It is hence necessary that the pH of a solution must be

known in order to calculate an unknown concentration of H_2O_2 resulting from an increase in fluorescence. Therefore it is critical that the probe also incorporates a pH sensitive component to accurately determine the H_2O_2 concentration. This improves upon many systems for detection of H_2O_2 that do not simultaneously measure pH, despite the reported effect on H_2O_2 detection.[30]

4.3.2 pH Sensing

4.3.2.1 Initial pH Sensing

The sensitivity of these functionalised fibre tips was defined across a series of solutions of differing pH, ranging from 6.5 to 8.5. Fibres functionalised with **CPF1** and **SNARF2** as before were dipped into phosphate buffer solutions of each pH. 532nm light attenuated to 13 μW was coupled into the fibre for excitation, and the fluorescent signal from immobilised **SNARF2** was collected after 1 min equilibration time. The fibre was removed from solution, dried, and immersed in a subsequent buffer solution. Two fibre probes were calibrated in this way using sixteen buffer solutions ranging from pH 6.5 to 8.5 as shown in **Figure 43**. This broad pH range (6.4-8.5) was chosen in order to demonstrate the potential of the probe in biological applications beyond the narrower constraints of an embryo. Five additional probes were then calibrated in selected solutions across this range (see fibres 3-7 in **Figure 43B**). The fluorescence spectra were recorded as shown in **Figure 43A**. The probe exhibits a decrease in intensity of fluorescence at 600 nm as the pH increases, with an increase in intensity at 660 nm.

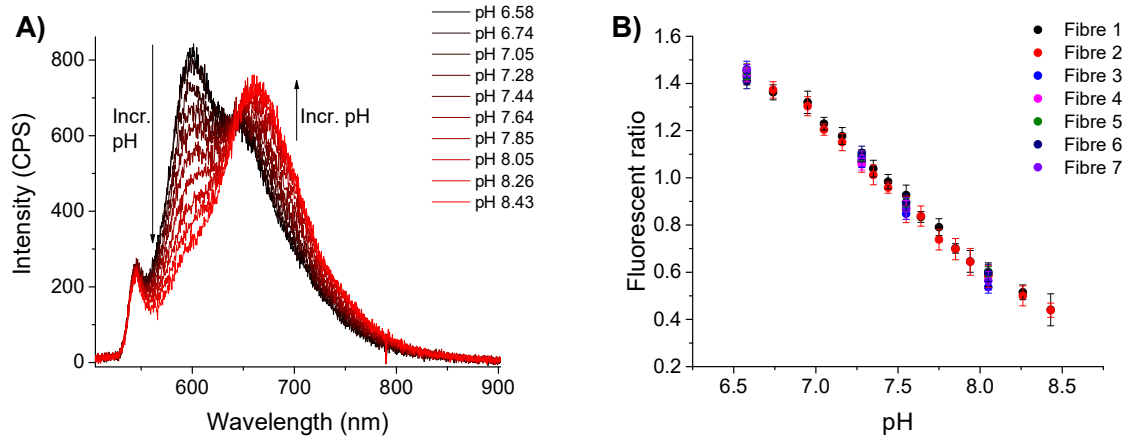

Figure 43. pH response of **SNARF2** embedded in polyacrylamide on fibre tip to varied pH. A) Emission spectra of **SNARF2** in various pH buffers. B) Ratio of emission peak intensities 600/660nm shown with over multiple trials. The effect of noise was reduced by taking the mean of eight values between 598-602 nm and 558-662 nm. Error bars represent the standard deviation of these values.

The pH of the buffer was correlated with the observed fluorescent signal by calculating the ratio of intensities at 600 nm and 660 nm for each spectrum (**Figure 43B**). This analysis

revealed an inverse correlation between this fluorescent ratio and pH of the solution. The plot also shows a linear trend over the pH range 7.0 to 8.0 and indicates that the sensor should be of use for determining the pH of a biological sample near physiological pH. Moreover, multiple fibre trials produced similar pH calibration curves (**Figure 43B**) showing good reproducibility between fibres. This data also indicates that **SNARF2** bound to a fibre tip behaves as in solution.[127] Therefore, **SNARF2** effectively senses the pH of a buffer solution when embedded in polyacrylamide on a fibre tip.

4.3.2.2 pH Sensing Before and After Detection of Hydrogen Peroxide

The functionalised fibre probes were used to sense pH before and after immersion in H_2O_2, in order to determine if this affected the pH sensing capability. Each fibre was functionalised with **CPF1** and **SNARF2** and calibrated in phosphate buffer solutions of known pH as described in section 3.2.1. The fibre tips were then immersed for 20 min in one of three H_2O_2 solutions: 100 µM solution of H_2O_2 in pH 7.55 buffer, 50 µM H_2O_2 in pH 7.55 buffer or 100 µM H_2O_2 in pH 7.05 buffer. These conditions represent the range of conditions that the probe may experience in unknown samples. Each probe was calibrated again in phosphate buffer solutions as above. The resulting pH calibration curves were plotted for each probe both before and after immersion in H_2O_2 (**Figure 44**).

The fluorescent ratios shown in **Figure 44A** show minimal changes before and after immersion in 100 µM H_2O_2 in pH 7.55. This indicates that reaction of H_2O_2 with **CPF1** does not affect the sensing of pH by **SNARF2**. **Figure 44B** reveals similar fluorescent ratios before and after immersion in 50 µM H_2O_2 in pH 7.55 buffer. H_2O_2 again does not affect the sensing of pH over the tested concentration range, 50 µM to 100 µM H_2O_2. **Figure 44C** shows the fluorescent ratios of **SNARF2** on fibre tips before and after immersing in 100 µM H_2O_2 in pH 7.05 buffer. As per the previous results, the fluorescent ratio curves did not change significantly after immersion in H_2O_2. Importantly, immersing the probe into a solution containing H_2O_2 does not affect the pH sensing capability of the probe. This demonstrates that **SNARF2** can be used on optical fibre tips for sensing pH independent of the detection of H_2O_2 by **CPF1**.

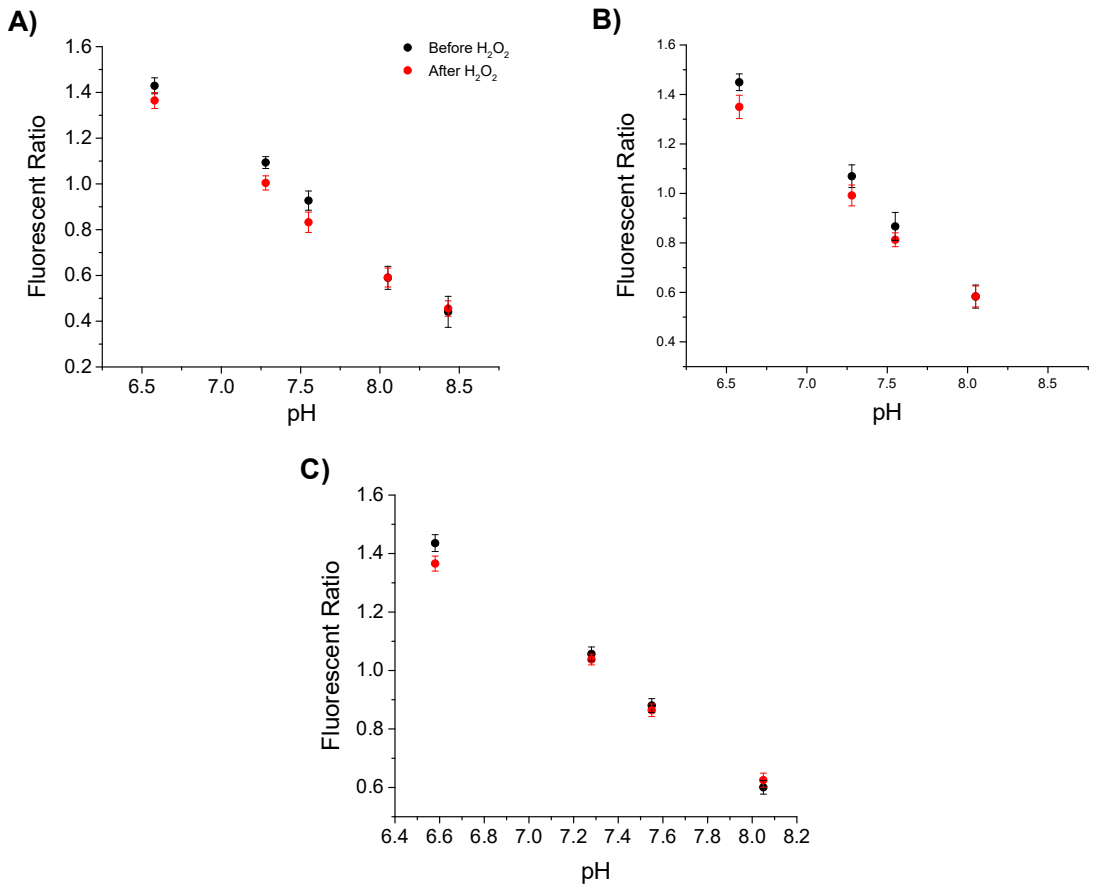

Figure 44. Sensing of pH before and after immersion in H_2O_2. Each graph plots the ratio of emission peaks of **SNARF2** at 600/660 nm with the pH of the buffer solution tested, before and after solutions: A) 100 µM solution of H_2O_2 in pH 7.55 buffer; B) 50 µM H_2O_2 in pH 7.55 buffer; C) 100 µM H_2O_2 in pH 7.05 buffer. Three different samples were trialled before and after H_2O_2 solutions to demonstrate the independence of the result to concentration of H_2O_2 or the pH of the H_2O_2 solution. The mean of eight values between 598-602 nm and 558-662 nm to reduce any effect of noise. Error bars represent the standard deviation of these values.

4.4 CONCLUSION

The tip of an optical fibre has been functionalised with two separate fluorophores, **CPF1** and **SNARF2** embedded in polyacrylamide, in order to allow measurement of the H_2O_2 concentration and pH simultaneously. The probe is demonstrated to effectively detect H_2O_2 over a physiological pH range. The probe shows a minimum detectable concentration of 50 µM H_2O_2 at pH 7.5, and pH was measured repeatedly over the range 6.5-8.5 with resolution of 0.1 pH units. Each fluorophore was used in tandem by alternating excitation sources, i.e. blue excitation to interrogate **CPF1** for H_2O_2 detection, and green excitation for **SNARF2** to sense pH, with minimal cross-talk. The combination of pH and H_2O_2 detection also addressed the crucial issue of accurate measurement of H_2O_2 in solutions with varying or unknown pH, where the pH of the solution alters the apparent H_2O_2 concentration. This is the first example of a dual pH and H_2O_2 probe and is an important proof of concept for the detection of pH and H_2O_2 in ethically complex biological environments such as found in an IVF laboratory.

This probe could find potential application if placed near the cumulus cells of an oocyte for monitoring of extracellular pH and H_2O_2 fluxes during fertilisation and during early embryonic development. Tapering of the fibre tip could also increase the resolution from 200 µm to a few micron if required.[108] This fibre probe may offer potential not only in embryology, but a range of biological applications whereby the system must remain isolated from any external agents such as organic fluorophores.

4.5 ACKNOWLEDGEMENTS

This research was supported in part by Cook Medical Pty Ltd and Australian Research Council linkage grant LP 110200736 and the ARC Centre of Excellence for Nanoscale BioPhotonics (CNBP). This work was performed in part at the OptoFab node of the Australian National Fabrication Facility (ANFF) utilising Commonwealth and SA State Government funding. T.M. acknowledges the support of an ARC Georgina Sweet Laureate Fellowship FL130100044.

4.6 CONFLICTS OF INTEREST

The authors declare no conflict of interest.

4.7 METHODS

4.7.1 Materials

All chemicals were purchased from Sigma-Aldrich unless otherwise stated. Bis(acrylamide) was purchased from Polysciences (Warrington, PA). HPLC grade acetonitrile was purchased from Scharlau. 100 mM Phosphate buffer solutions were prepared from monosodium phosphate and disodium phosphate in Milli-Q water. Multimode fibre (200 µm core diameter, FG200UCC) was purchased from Thorlabs (USA), with one end connectorised for attachment to the optical setup.

4.7.2 Polyacrylamide Photo-polymerisation on Optical Fibre Tips

A solution of 3-(trimethoxysilyl)propyl methacrylate (5 µL) in 10 % acetic acid solution (30 µL) and ethanol (1 mL) was mixed and sonicated until clear. Multi-mode fibre was cleaved and each segment immersed in the methacrylate solution for 1 h. The fibre tip was then dried under N_2, rinsed with Milli-Q water and re-dried under N_2. The distal end of the fibre was coupled into a 405 nm source (Crystalaser 405 nm) using a 10x microscope objective. A monomeric stock solution comprising of 3 % bisacrylamide, 27 % acrylamide and 70 % pH 6.5 phosphate buffer solution was dissolved under sonication. **CPF1-NHS** (0.2 mg), and **SNARF2-NHS** (0.2 mg) were added to this solution (400 µL) and 200 µL of the resulting solution was pipetted into a small Eppendorf tube. Triethylamine (10 µL/mL) was added to

the mixture, and the fibre tip was immersed in this solution exactly 60 s after addition of the triethylamine and immediately irradiated under 405nm light for 10 s at 13.4 mW, to form a polymeric coating on the fibre tip.

4.7.3 Optical Measurements

The experimental configuration used for optical measurements is shown in **Figure 45**.

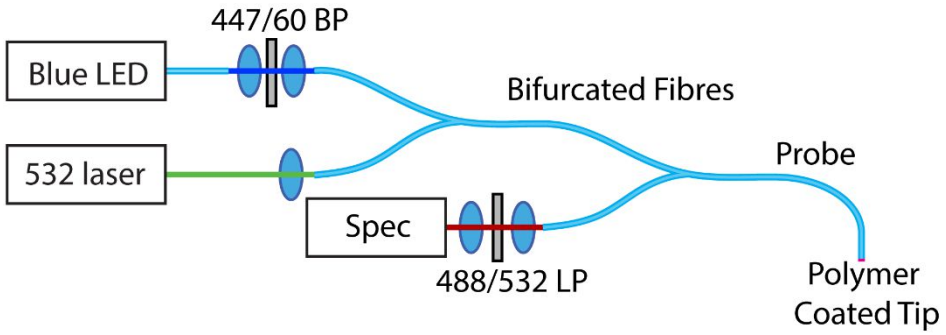

Figure 45. Experimental configuration for optical measurements of the combined pH/peroxide sensor. The blue LED source was used to illuminate the peroxide sensitive **CPF1** fluorophore, while the green excites the pH sensitive **SNARF2**.

A 470 nm blue LED source (Thorlabs M470F1) with an appropriate bandpass filter (Semrock Brightline 447/60) was coupled into one input of a bifurcated fibre (Ocean Optics 200 µm, UV/VIS). Attached **CPF1** was then excited with light from a 532 nm green laser (Crystalaser 25 mW) coupled into the other input for excitation of the **SNARF2**. An additional bifurcated fibre was used to connect the excitation sources to the sensing fibre, with the remaining input connected to the input of the spectrometer (Horiba iHR550, Synapse detector). Long-pass filters were inserted directly into the spectrometer input cage, with 488 nm (Semrock 488 nm Edgebasic) and 532 nm (Semrock 532 nm Razoredge) used for peroxide and pH respectively.

The two excitation channels were controlled independently, with only one excitation wavelength used at any particular time to excite either the peroxide or pH channel. The corresponding emission filter was used with each excitation source to attenuate residual pump light from the fibres. The use of connectorised fibres and multi-mode fibres greatly simplifies the measurement procedure, as no adjustments or realignment are required when swapping between pH and peroxide measurements.

4.8 SUPPLEMENTARY INFORMATION

4.8.1 Synthesis of CPF1 and SNARF2

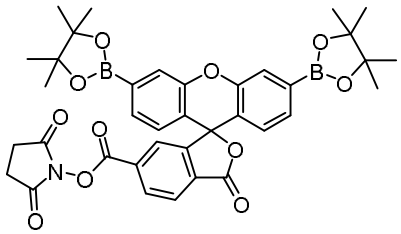

CPF1 N-hydroxysuccinimide ester (**CPF1-NHS**) was prepared using a modification of a literature procedure:[127] **CPF1**[153] (276 mg, 0.46 mmol), EDC•HCl (157 mg, 0.77 mmol) and N-hydroxysuccinimide (67 mg, 0.50 mmol) were dissolved in anhydrous dimethylformamide (7 mL) under nitrogen and stirred for 1 h. The reaction mixture was poured into diethyl ether (100 mL) and washed with water (100 mL). The aqueous phase was washed with diethyl ether (2x100 mL), the organic layers combined and dried over $MgSO_4$. The resultant solution was filtered, evaporated onto celite and eluted through a silica column using 1 % methanol in dichloromethane to afford an off-white solid **CPF1-NHS** (165 mg, 53 %) The product was then characterised by 500 MHz ^{1}HNMR in $CDCl_3$ for comparison to literature [1]: δ(ppm) 8.32 (d, 1H, J = 8.1 Hz), 8.15 (dd, 1H, J_1 = 8.0 Hz, J_2 = 1 Hz), 7.78 (s, 1H), 7.74 (s, 2H), 7.45 (d, 2H, J = 7.8 Hz), 6.81 (dd, 2H, J_1 = 7.8 Hz), 2.82 (br. s, 4H), 1.32 (s, 24H)

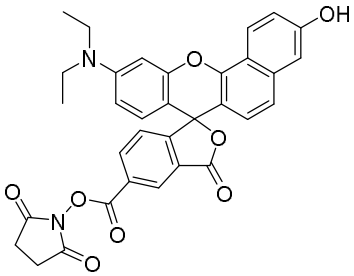

SNARF2 N-hydroxysuccinimide ester (**SNARF2-NHS**) was prepared according to literature.[127] The solid product was characterised by 500 MHz ^{1}HNMR in d_6-acetone for comparison to literature: δ(ppm) 8.65 (s, 1H), 8.50 (d, 1H, J = 9.1 Hz), 8.48 (d, 1H, J = 8.1 Hz), 7.59 (d, 1H, J = 7.9 Hz), 7.38 (d, 1H, J = 8.7 Hz), 7.32 (dd, 1H, J_1 = 9.0 Hz, J_2 = 2.3 Hz), 7.25 (d, 1H, J = 2.2 Hz), 6.84-6.81 (m, 2H), 6.78 (d, 1H, J = 9 Hz), 6.58 (dd, 1H, J_1 = 9 Hz, J_2 = 2.5 Hz), 3.74 (br. s, 4H), 3.49 (q, 4H, J = 5.3 Hz), 1.21 (t, 6H, J = 4.9 Hz)

4.8.2 Fluorescence Spectra of Functionalised Fibre Tips

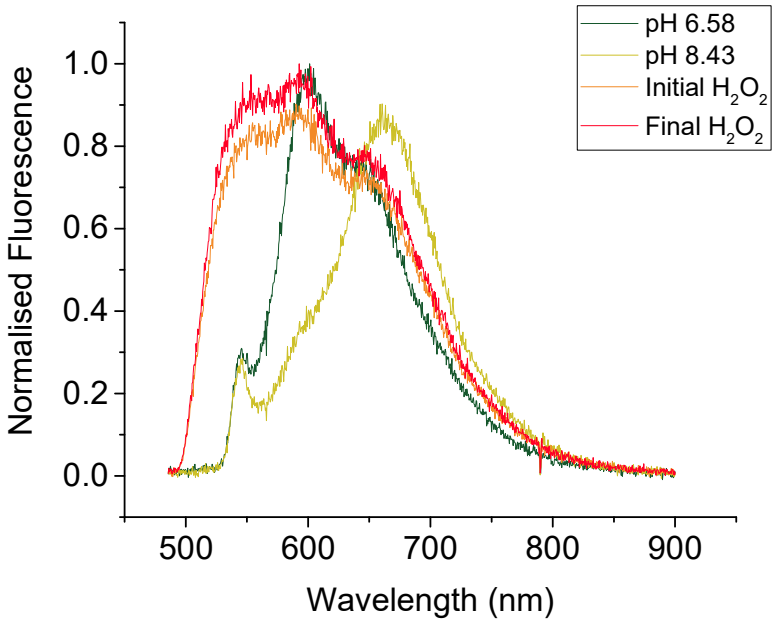

Figure 46. Fluorescence spectra of functionalised optical fibre dipped into various solutions: pH 6.5 and 8.4 in the absence of H_2O_2, excitation 532 nm. Initial (0 min) and final (20 min) when in 100 µM H_2O_2 at pH 7.4, excitation 488nm. The spectra were normalised at the fluorescent peak of 600 nm for visual comparison.

Figure 46 shows the normalised fluorescent spectra of the fibre probe when excited with either 488 or 532 nm. It clearly shows the ability of the probe to distinguish the **SNARF2** signal (532 nm excitation) from the increase in fluorescence from **CPF1** (473 nm excitation).

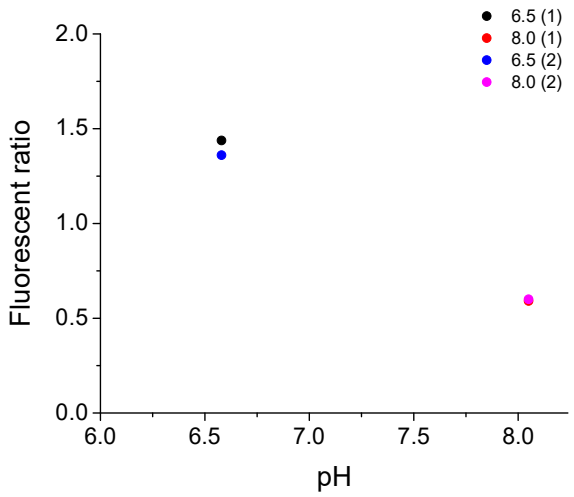

Figure 47. Fluorescent ratio of probes dipped into solutions of varying pH multiple times to determine if any hysteresis is shown.

Figure 47 shows the fluorescent ratio of functionalised probes dipped first into a solution pH 6.5, then into a pH 8.0 buffer. After the basic solution, probes were then inserted into the pH

6.5 solution a second time and finally into the pH 8.0 buffer. The graph exhibits a good correlation between each on both ascending in basicity and descending, suggesting the probes suffer from minimal hysteresis.

4.9 REFERENCES

7. Morado, S.; Cetica, P.; Beconi, M.; Thompson, J. G.; Dalvit, G. Reactive oxygen species production and redox state in parthenogenetic and sperm-mediated bovine oocyte activation. *Reproduction* **2013,** *145* (5), 471-8.

17. Nasr-Esfahani, M. H.; Aitken, J. R.; Johnson, M. H. Hydrogen peroxide levels in mouse oocytes and early cleavage stage embryos developed in vitro or in vivo. *Development* **1990,** *109* (2), 501-507.

22. Thannickal, V. J.; Fanburg, B. L. *Reactive oxygen species in cell signaling*. 2000; Vol. 279, p L1005-L1028.

24. Armstrong, J. S.; Rajasekaran, M.; Chamulitrat, W.; Gatti, P.; Hellstrom, W. J.; Sikka, S. C. Characterization of reactive oxygen species induced effects on human spermatozoa movement and energy metabolism. *Free Radical Biology and Medicine* **1999,** *26* (7–8), 869-880.

25. Baumber, J.; Ball, B. A.; Gravance, C. G.; Medina, V.; Davies-Morel, M. C. G. The Effect of Reactive Oxygen Species on Equine Sperm Motility, Viability, Acrosomal Integrity, Mitochondrial Membrane Potential, and Membrane Lipid Peroxidation. *Journal of Andrology* **2000,** *21* (6), 895-902.

26. Chan, J.; Dodani, S. C.; Chang, C. J. Reaction-based small-molecule fluorescent probes for chemoselective bioimaging. *Nature Chemistry* **2012,** *4* (12), 973-984.

30. Lippert, A. R.; Van de Bittner, G. C.; Chang, C. J. Boronate Oxidation as a Bioorthogonal Reaction Approach for Studying the Chemistry of Hydrogen Peroxide in Living Systems. *Accounts of Chemical Research* **2011,** *44* (9), 793-804.

38. Heng, S.; Nguyen, M.-C.; Kostecki, R.; Monro, T. M.; Abell, A. D. Nanoliter-scale, regenerable ion sensor: sensing with a surface functionalized microstructured optical fibre. *RSC Advances* **2013,** *3* (22), 8308.

39. Heng, S.; Mak, A. M.; Stubing, D. B.; Monro, T. M.; Abell, A. D. Dual Sensor for Cd(II) and Ca(II): Selective Nanoliter-Scale Sensing of Metal Ions. *Analytical Chemistry* **2014,** *86* (7), 3268-3272.

94. Chang, M. C. Y.; Pralle, A.; Isacoff, E. Y.; Chang, C. J. A selective, cell-permeable optical probe for hydrogen peroxide in living cells. *Journal of the American Chemical Society* **2004,** *126* (47), 15392-15393.

100. Sikora, A.; Zielonka, J.; Lopez, M.; Joseph, J.; Kalyanaraman, B. Direct oxidation of boronates by peroxynitrite: Mechanism and implications in fluorescence imaging of peroxynitrite. *Free Radical Biology & Medicine* **2009,** *47* (10), 1401-1407.

103. Abo, M.; Urano, Y.; Hanaoka, K.; Terai, T.; Komatsu, T.; Nagano, T. Development of a Highly Sensitive Fluorescence Probe for Hydrogen Peroxide. *Journal of the American Chemical Society* **2011,** *133* (27), 10629-10637.

108. Leung, A.; Shankar, P. M.; Mutharasan, R. A review of fiber-optic biosensors. *Sensors and Actuators B: Chemical* **2007,** *125* (2), 688-703.

109. Tan, W.; Shi, Z. Y.; Smith, S.; Birnbaum, D.; Kopelman, R. Submicrometer intracellular chemical optical fiber sensors. *Science* **1992,** *258* (5083), 778-81.

110. Schartner, E.; Monro, T. Fibre Tip Sensors for Localised Temperature Sensing Based on Rare Earth-Doped Glass Coatings. *Sensors* **2014,** *14* (11), 21693.

111. Song, A.; Parus, S.; Kopelman, R. High-Performance Fiber-Optic pH Microsensors for Practical Physiological Measurements Using a Dual-Emission Sensitive Dye. *Analytical Chemistry* **1997,** *69* (5), 863-867.

127. Srikun, D.; Albers, A. E.; Chang, C. J. A dendrimer-based platform for simultaneous dual fluorescence imaging of hydrogen peroxide and pH gradients produced in living cells. *Chemical Science* **2011,** *2* (6), 1156-1165.

137. Foo, H. T. C.; Ebendorff-Heidepriem, H.; Sumby, C. J.; Monro, T. M. Towards microstructured optical fibre sensors: surface analysis of silanised lead silicate glass. *Journal of Materials Chemistry C* **2013,** *1* (41), 6782-6789.
153. Purdey, M. S.; Connaughton, H. S.; Whiting, S.; Schartner, E. P.; Monro, T. M.; Thompson, J. G.; Aitken, R. J.; Abell, A. D. Boronate probes for the detection of hydrogen peroxide release from human spermatozoa. *Free Radical Biology and Medicine* **2015,** *81* (0), 69-76.
155. Gough, D. R.; Cotter, T. G. Hydrogen peroxide: a Jekyll and Hyde signalling molecule. *Cell death & disease* **2011,** *2*, e213.
156. Neill, S. J.; Desikan, R.; Clarke, A.; Hurst, R. D.; Hancock, J. T. Hydrogen peroxide and nitric oxide as signalling molecules in plants. *Journal of Experimental Botany* **2002,** *53* (372), 1237-1247.
157. Szatrowski, T. P.; Nathan, C. F. Production of large amounts of hydrogen peroxide by human tumor cells. *Cancer research* **1991,** *51* (3), 794-8.
158. Burdon, R. H. Superoxide and hydrogen peroxide in relation to mammalian cell proliferation. *Free Radic Biol Med* **1995,** *18* (4), 775-94.
159. Gerweck, L. E.; Seetharaman, K. Cellular pH gradient in tumor versus normal tissue: potential exploitation for the treatment of cancer. *Cancer research* **1996,** *56* (6), 1194-8.
160. Engin, K.; Leeper, D. B.; Cater, J. R.; Thistlethwaite, A. J.; Tupchong, L.; McFarlane, J. D. Extracellular pH distribution in human tumours. *International journal of hyperthermia : the official journal of European Society for Hyperthermic Oncology, North American Hyperthermia Group* **1995,** *11* (2), 211-6.
161. Bize, I.; Santander, G.; Cabello, P.; Driscoll, D.; Sharpe, C. Hydrogen peroxide is involved in hamster sperm capacitation in vitro. *Biology of reproduction* **1991,** *44* (3), 398-403.
162. Ocon, O. M.; Hansen, P. J. Disruption of Bovine Oocytes and Preimplantation Embryos by Urea and Acidic pH1. *Journal of Dairy Science* **2003,** *86* (4), 1194-1200.
163. Lin, J. Recent development and applications of optical and fiber-optic pH sensors. *TrAC Trends in Analytical Chemistry* **2000,** *19* (9), 541-552.
164. Han, J.; Burgess, K. Fluorescent Indicators for Intracellular pH. *Chemical Reviews* **2009,** *110* (5), 2709-2728.
165. Palmisano, T.; Prudenzano, F.; Warren-Smith, S. C.; Monro, T. M. Design of exposed-core fiber for methadone monitoring in biological fluids. *Journal of Non-Crystalline Solids* **2011,** *357* (8-9), 2000-2004.
166. Smolka, S.; Barth, M.; Benson, O. Highly efficient fluorescence sensing with hollow core photonic crystal fibers. *Optics Express* **2007,** *15* (20), 12783-12791.
167. Wolfbeis, O. S. Fiber-optic chemical sensors and biosensors. *Anal Chem* **2008,** *80* (12), 4269-83.
168. Schartner, E. P.; Tsiminis, G. T.; Henderson, M. R.; Monro, T. M. In *A Comparison Between Multimode Tip And Suspended Core Fluorescence Optical Fibre Sensors*, CLEO: 2015, Munich, Germany, Optical Society of America: Munich, Germany, 2015.
169. Purdey, M. S.; Schartner, E. P.; Sutton-McDowall, M. L.; Ritter, L. J.; Thompson, J. G.; Monro, T. M.; Abell, A. D. Localised hydrogen peroxide sensing for reproductive health. *Proceedings of SPIE* **2015,** *9506*, 950614.
170. Sutton-McDowall, M. L.; Purdey, M.; Brown, H. M.; Abell, A. D.; Mottershead, D. G.; Cetica, P. D.; Dalvit, G. C.; Goldys, E. M.; Gilchrist, R. B.; Gardner, D. K.; Thompson, J. G. Redox and anti-oxidant state within cattle oocytes following in vitro maturation with bone morphogenetic protein 15 and follicle stimulating hormone. *Molecular Reproduction and Development* **2015,** *82* (4), 281-294.
171. Whitaker, J. E.; Haugland, R. P.; Prendergast, F. G. Spectral and photophysical studies of benzo[c]xanthene dyes: Dual emission pH sensors. *Analytical Biochemistry* **1991,** *194* (2), 330-344.
172. Song, L.; Hennink, E. J.; Young, I. T.; Tanke, H. J. Photobleaching kinetics of fluorescein in quantitative fluorescence microscopy. *Biophysical Journal* **1995,** *68* (6), 2588-600.

173. Platkov, M.; Tirosh, R.; Kaufman, M.; Zurgil, N.; Deutsch, M. Photobleaching of fluorescein as a probe for oxidative stress in single cells. *Journal of photochemistry and photobiology. B, Biology* **2014,** *140*, 306-14.
174. Xu, J.; Li, Q.; Yue, Y.; Guo, Y.; Shao, S. A water-soluble BODIPY derivative as a highly selective "Turn-On" fluorescent sensor for H2O2 sensing in vivo. *Biosensors and Bioelectronics* **2014,** *56*, 58-63.
175. Martin, M. M.; Lindqvist, L. The pH dependence of fluorescein fluorescence. *Journal of Luminescence* **1975,** *10* (6), 381-390.

Chapter 5

NEW BODIPY-BASED PROBES FOR THE DETECTION OF HYDROGEN PEROXIDE

Research is what I'm doing when I don't know what I'm doing.

Wernher von Braun

STATEMENT OF AUTHORSHIP

Title of Paper	Aryl boronate and benzil BODIPY-based fluorescent probes for hydrogen peroxide
Publication Status	☐ Published ☐ Accepted for Publication ☐ Submitted for Publication ☑ Publication Style
Publication Details	Purdey, M. S.; McLennan, H. J.; Sutton-McDowall, M. L.; Abell, A. D., New BODIPY-based probes for the detection of hydrogen peroxide. **2015**, *In Preparation*

Principal Author

Name of Principal Author (Candidate)	Malcolm S. Purdey		
Contribution to the Paper	Synthesis of fluorescent probes, fluorescence assays and selectivity testing of probes with reactive oxygen species, assistance with fluorescence oocyte studies and writing of the manuscript.		
Overall percentage (%)	65%		
Signature		Date	29/10/2015

Co-Author Contributions

By signing the Statement of Authorship, each author certifies that:

i. the candidate's stated contribution to the publication is accurate (as detailed above);

ii. permission is granted for the candidate in include the publication in the thesis; and

iii. the sum of all co-author contributions is equal to 100% less the candidate's stated contribution.

Name of Co-Author	Hannah J. McLennan		
Contribution to the Paper	Assistance with *in vitro* maturation of oocytes.		
Signature		Date	30/10/15

Name of Co-Author	Melanie L. Sutton-McDowall		
Contribution to the Paper	Fluorescence oocyte studies and analysis of data.		
Signature		Date	30.10.15

Name of Co-Author	Andrew D. Abell		
Contribution to the Paper	Project direction and editing of manuscript.		
Signature		Date	29/10/15

Chapter 5: Aryl boronate and benzil BODIPY-based probes for hydrogen peroxide††

Malcolm S. Purdey[a,b,c], Hanna J. McLennan[a,b,d], Melanie L. Sutton-McDowall[a,b,d] and Andrew D. Abell[a,b,c]

[a] ARC Centre of Excellence for Nanoscale BioPhotonics, Australia

[b] Institute for Photonics & Advanced Sensing, The University of Adelaide, North Terrace, Adelaide 5005, Australia

[c] Department of Chemistry, School of Physical Sciences, The University of Adelaide, North Terrace, Adelaide 5005, Australia

[d] Robinson Research Institute, School of Medicine, The University of Adelaide, Medical School, Adelaide 5005, Australia

5.1 ABSTRACT

The detection of hydrogen peroxide (H_2O_2) is critical in the study of oxidative stress in biological environments. This paper presents a comparison of two new cell-permeable boron-dipyrromethene (**BODIPY**) based fluorescent probes for the detection of H_2O_2. The aryl boronate PeroxyBODIPY-1 (**PB1**) gives a greater change in fluorescence upon reaction with H_2O_2 and was able to detect H_2O_2 in denuded bovine oocytes. However the benzil, nitrobenzoylBODIPY (**NbzB**), exhibits exclusive selectivity for H_2O_2 over other ROS. This crucial comparison reveals the importance of selecting the appropriate fluorophore for a given biological application.

†† Purdey, M.S.; McLennan, H.J.; Sutton-McDowall, M.L.; Abell, A.D.; Aryl boronate and benzil BODIPY-based probes for hydrogen peroxide. **2015** *In Preparation*

5.2 COMMUNICATION

Hydrogen peroxide (H_2O_2) is an important reactive oxygen species (ROS) that acts as both an cell signaller[176] and a causative of oxidative stress.[19] Such cellular stress can have serious consequences to cell function, for example it is known to result in defective sperm function[5] and compromised embryonic development[7] in reproductive biology. The detection of H_2O_2 is thus of real importance in understanding both the mechanisms of oxidative stress and a range of important cellular signalling processes.

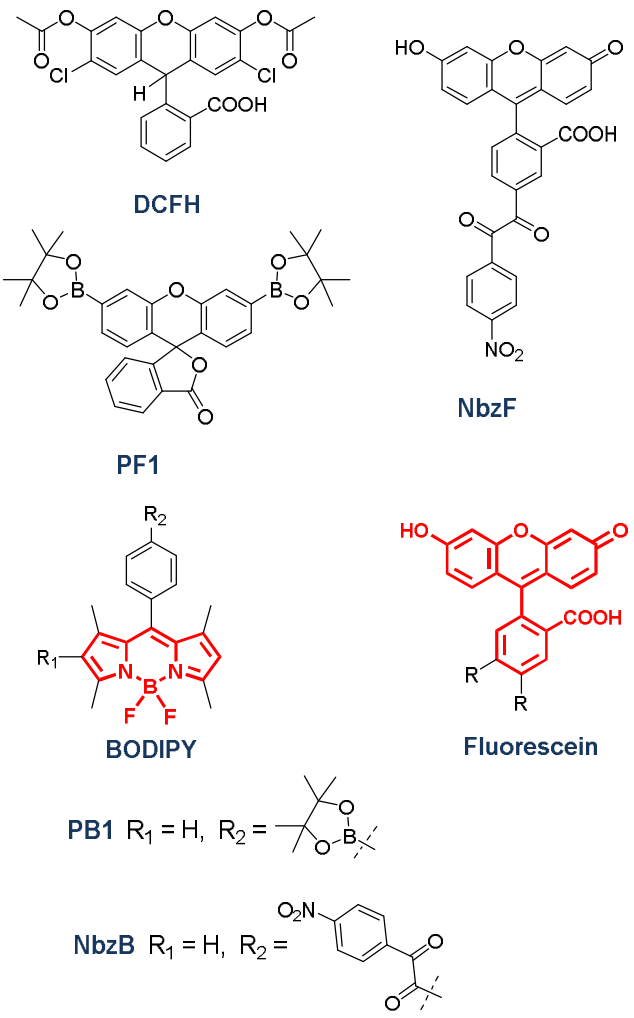

Figure 48. Fluorescent probes. 2',7'-dichlorohydrofluorescein diacetate (**DCFH**) is a general ROS probe, **PF1** is an aryl boronate probe that selectively targets H_2O_2 and **NbzF** is a benzil that shows selectivity for H_2O_2 over all other ROS. Highlighted in red are the **fluorescein** and **BODIPY** cores.

Fluorescent probes, such as those shown in **Figure 48** are commonly used for *in situ* detection of H_2O_2 and real-time monitoring of associated processes within a cell. In each case, the fluorophore functions by giving a measurable change in fluorescence on reaction with H_2O_2, Many of these probes (e.g. 2',7'-dichlorohydrofluorescein diacetate **DCFH**, see **Figure 48**) react with a range of ROS, however the aryl boronates[30,153,177] (e.g. peroxyfluor-1, **PF1**) and benzil-based probes[103,104] (e.g. **NbzF**) exhibit selectivity for H_2O_2 over other

ROS.[124] The aryl boronates react with H_2O_2 to form a phenol;[30,100] e.g. the weakly fluorescent probe **PF1** is irreversibly oxidized to give a fluorescent fluorescein derivative (**Figure 48**).[94,96,99] The nitro-benzyl group of **NbzF** quenches fluorescence by donor-excited photo-induced electron transfer (d-PET), an effect that is lost after reaction with H_2O_2, giving a measurable increase in fluorescence.[103]

Although many studies have reported new aryl boronate[30] or benzil probes,[104] to date no meaningful comparison has been made between the two classes of probes. As detection of H_2O_2 is vital in many applications, there is a real need to directly compare aryl boronate and benzil fluorescent probes with regards to their reaction for H_2O_2.

Two new probes, peroxyBODIPY-1 (**PB1**) and nitrobenzoyl-BODIPY (**NbzB**) are reported here that allow a direct and meaningful comparison of an aryl boronate (**PB1**) with a benzil (**NbzB**) (**Figure 48**). The boron-dipyrromethene (**BODIPY**) fluorescent core structure was selected for this comparative study because of its stability under physiological conditions and an ability to tune its excitation and emission properties with minor structural modifications.[48] H_2O_2-sensitive boronate and para-nitrophenyl diketone groups were attached at R_2 of the common **BODIPY** core (see **Figure 48**) of **PB1** and **NbzB**, respectively. **PB1** and **NbzB** were also designed to allow future chemical modification of the **BODIPY** core. For example, it is known that substituents at R_1 can affect excitation and emission wavelengths,[178] and photostability.[62]

PB1 and **NbzB** were synthesised from a common intermediate **16**, which was itself readily prepared on reaction of 2,4-dimethylpyrrole **14** with 4-iodobenzoic acid **15**, see **Scheme 13**. Reaction of **16** with bis(pinacolato)diboron under Suzuki conditions gave **PB1** in a 48 % yield. Alternately, reaction of intermediate **16** with 4-ethynyl-1-nitrobenzene **17**, under Sonigashira conditions, gave **18** as an immediate precursor to **NbzB**. The alkyne of compound **18** was oxidized with DMSO and $PdCl_2$ to give **NbzB** in 54 % yield over two steps from intermediate **16**.

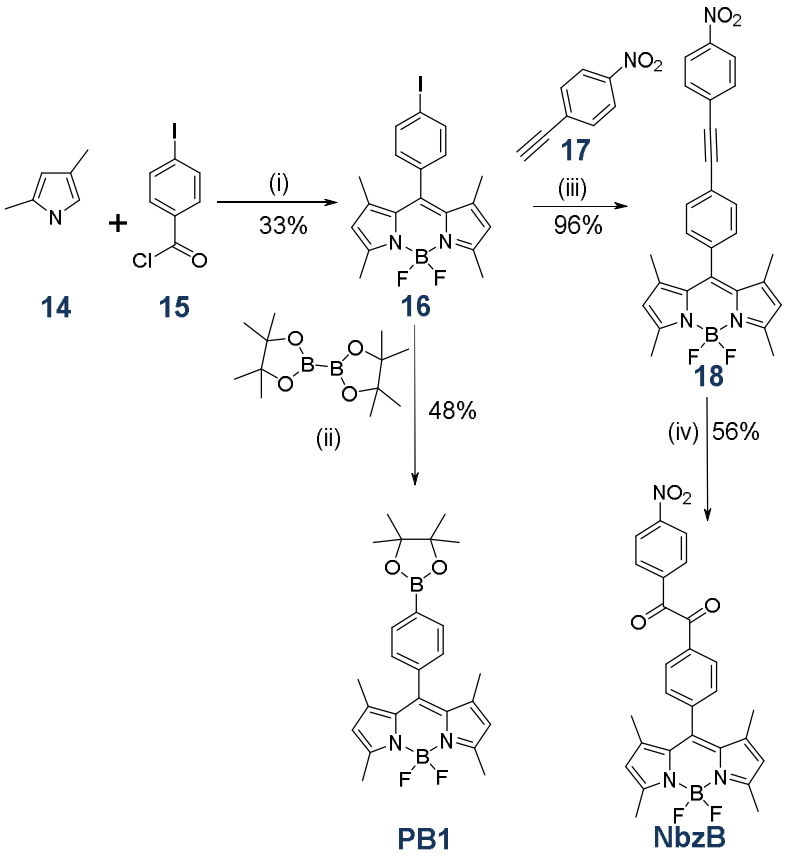

Scheme 13. Synthesis of BODIPY-based H_2O_2 sensors. (i) 1.$CHCl_3$, r.t., 72 h; 2.Et_3N, $BF_3.Et_2O$, r.t., 24h. (ii) $Pd(dppf)Cl_2$, KOAc, DMF, 100 °C, 2h. (iii) $PdCl_2(PPh_3)_2$, CuI, Et_3N, THF, r.t., 16h. (iv) $PdCl_2$, DMSO, 145 °C, 4h.

A direct comparison of **PB1** with **NbzB** chiefly involves determining the response of each to H_2O_2. **PB1** was reacted with five different concentrations of H_2O_2 (ranging from 5 to 100 μM) and the fluorescent responses were measured after 50 min. The resultant plots shown in **Figure 49A** clearly reveal that fluorescence decreases as the concentration of H_2O_2 increases. A significant reduction in fluorescence was evident at the lowest concentration (5 μM) of H_2O_2, a level of detection consistent with reports on other aryl boronate probes.[54] The absorption spectrum of **PB1** was also measured over the course of the above experiment, and does not change for all concentrations of H_2O_2 (see Supplementary Information **Figure 52**).

The second probe, benzil **NbzB**, gave an increase in fluorescence with increasing concentrations of H_2O_2 (from 5 μM to 100 μM) as shown in **Figure 49B**. Again, **NbzB** was sensitive to 5 μM H_2O_2, as per the literature fluorescein-based benzil probe **NbzF**.[103] **NbzB** presents approximately 1.75-fold increase in fluorescence on incubation with 100 μM H_2O_2 (**Figure 49B**). This contrasts the change in fluorescence shown by **PB1**, that was a >5-fold decrease in fluorescence (**Figure 49A**). The fluorescent responses of **PB1** and **NbzB** incubated with lower concentrations of H_2O_2 also reflected this trend.

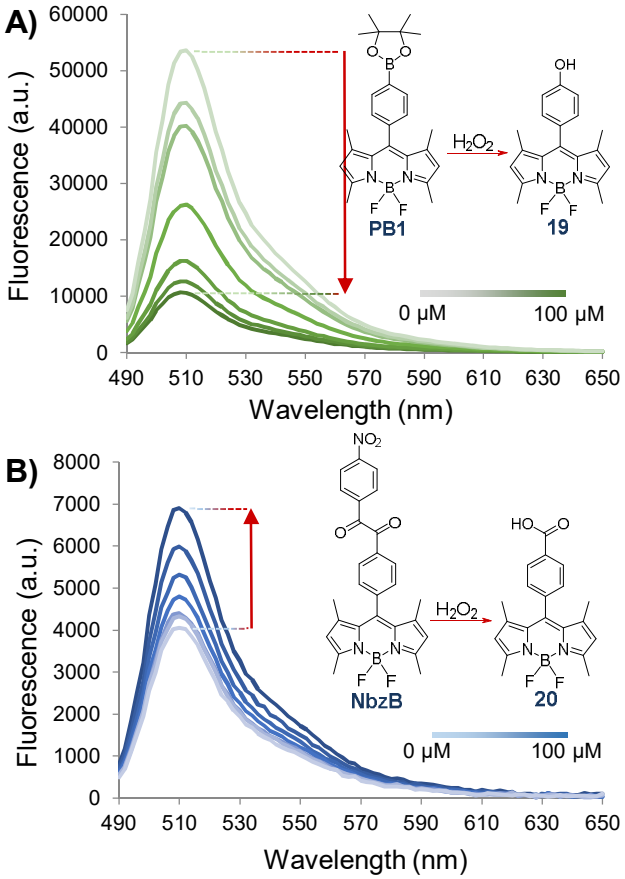

Figure 49. Response of **PB1** and **NbzB** to 0, 5, 10, 25, 50, 75 and 100 μM of H_2O_2 over 50 min in 100 mM phosphate buffer at pH 7.4. (A) Decrease in fluorescent spectra of **PB1** when incubated with H_2O_2 (excitation 470 nm). **PB1** is oxidized by H_2O_2 to give the alcohol **19** as shown. (B) Increase in fluorescent spectra of **NbzB** when incubated with H_2O_2 (excitation 470 nm). **NbzB** is oxidized by H_2O_2 to give the acid **20** as shown.

The selectivity of **PB1** to a range of other ROS [hydroxyl radicals ($^{\bullet}OH$), hypochlorite (^{-}OCl), tert-butyl hydroperoxide (TBHP), nitric oxide (NO), superoxide ($O_2^{\bullet-}$) and peroxynitrite ($ONOO^{-}$)] was also investigated. Each ROS (100 μM) was incubated with separate samples of **PB1** and the resultant fluorescent responses measured. The results shown in **Figure 50A** clearly show that **PB1** is more sensitive to H_2O_2 compared to the other six ROS, with some decrease in fluorescence observed for $ONOO^{-}$ and $^{\bullet}OH$ but not ^{-}OCl, TBHP, NO and $O_2^{\bullet-}$. Thus **PB1** has good selectivity for H_2O_2 over most ROS with the exception of $ONOO^{-}$.

NbzB was also incubated with 100 μM solutions of $^{\bullet}OH$, ^{-}OCl, TBHP, NO^{+}, $O_2^{\bullet-}$ and $ONOO^{-}$ and the resultant fluorescence spectra compared in order to define the probes selectivity profile (see **Figure 50B**). Little difference in fluorescence was apparent for samples incubated with $^{\bullet}OH$, ^{-}OCl, TBHP, NO^{+}, $O_2^{\bullet-}$ and $ONOO^{-}$. Thus **NbzB** shows high selectivity for H_2O_2, similar to probe **NbzF** that has the same benzil-activating group,[103] and is more selective for H_2O_2 than **PB1**. This observation is supported by literature, which suggests that benzil-based probes[103,104] generally exhibit a higher selectivity for H_2O_2 over other ROS than

do the aryl boronate counterparts.[100] Benzil-based probes such as **NbzB** are therefore well suited to applications where a high degree of selectivity for H_2O_2 is required.

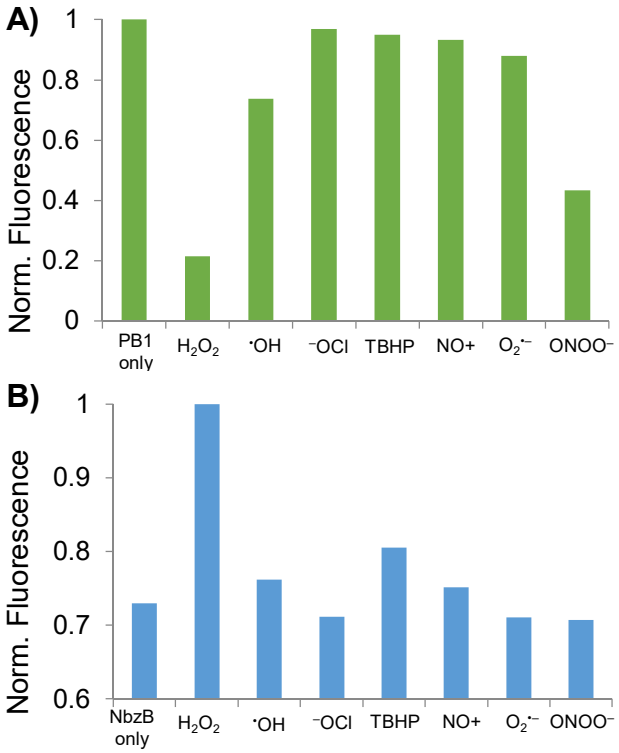

Figure 50. Response of **PB1** and **NbzB** to H_2O_2 and hydroxyl radicals (•OH), hypochlorite ($^-$OCl), tert-butyl hydroperoxide (TBHP), nitric oxide (NO^+), superoxide ($O_2^{\bullet-}$) and peroxynitrite ($ONOO^-$). Samples were exposed to 100 µM ROS over 50 min in 100 mM phosphate buffer at pH 7.4. Excitation was set at 470 nm, and emission was collected at 510 nm. (A) Fluorescent quenching of **PB1** when incubated with 100 µM ROS. (B) Fluorescent quenching of **NbzB** when incubated with ROS.

PB1 and **NbzB** were then tested *in vitro* with bovine oocytes, a species noted for poor permeability of fluorophores into the cell. Oocytes were matured *in vitro* and denuded of cumulus cells before incubating in the absence or presence of 1 mM H_2O_2 for 30 min at 38°C. The oocytes were washed and then stained with either **PB1** or **NbzB** and incubated for a further 30 min. Confocal microscopy was used to image the oocytes, with representative results shown in **Figure 51** (see supplementary information, **Figure 53**, for population average). Both **PB1** and **NbzB** clearly permeate into the oocytes. The fluorescence intensity of oocytes stained with **PB1** decreased significantly from absence of H_2O_2 (**Figure 51A**) compared to in the presence of H_2O_2 (**Figure 51B**). Conversely, oocytes stained with **NbzB** only showed a minor increase in fluorescence when treated with H_2O_2 (**Figure 51C** and **D**). Thus **PB1** is more sensitive to H_2O_2 than **NbzB** *in vitro*. The confocal images of oocytes (**Figure 51**) also reveal that **NbzB** is localised close to the cell membrane, whereas **PB1** exhibits higher fluorescence across the diameter of the cell.

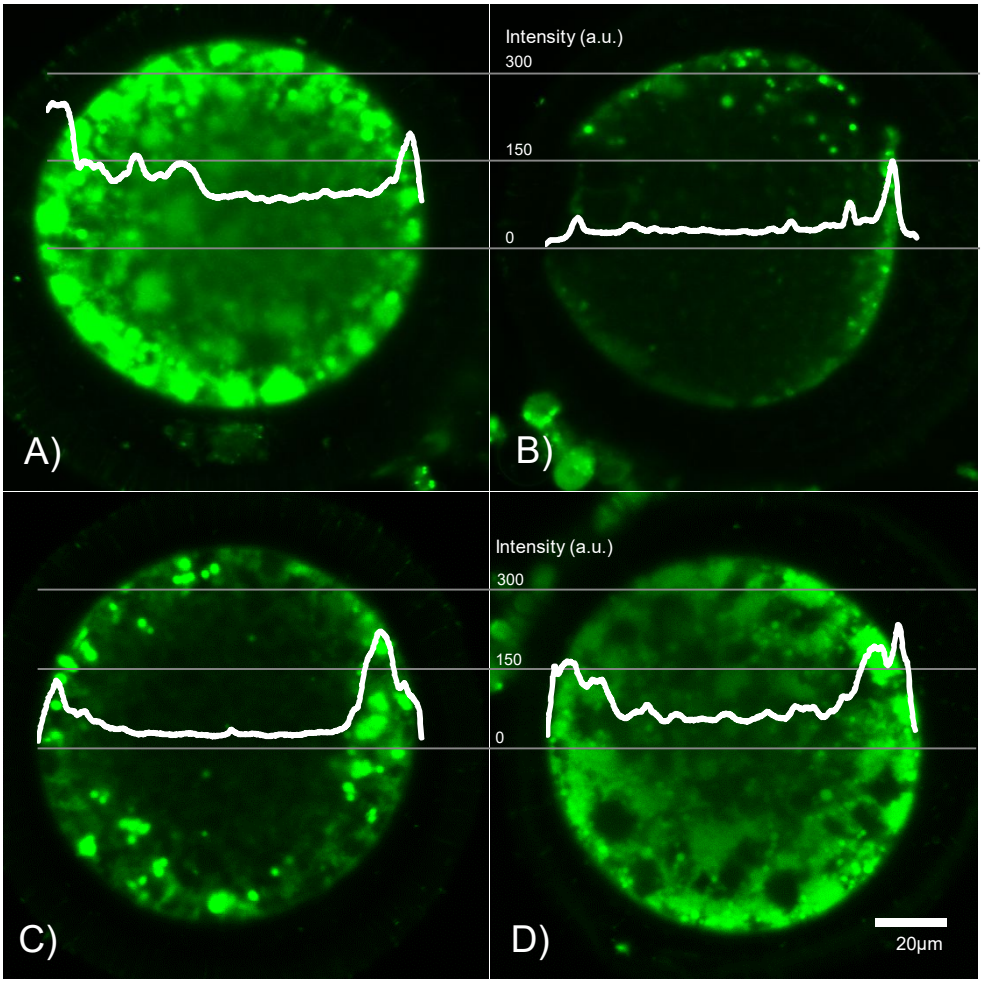

Figure 51. Confocal microscope images of denuded bovine oocytes stained with **PB1** and **NbzB** (exc. 490 nm, em. 509 nm). The intensity of fluorescence across the diameter of each oocyte is plotted for comparison. A) **PB1** stain in absence of H_2O_2. B) **PB1** stain after H_2O_2 treatment. C) **NbzB** stain in absence of H_2O_2. D) **NbzB** stain after H_2O_2 treatment.

5.3 CONCLUSIONS

The aryl boronate-based **PB1** and benzil-based **NbzB** show good selectivity for H_2O_2 over other ROS, with a sensitivity limit of at least 5 µM of H_2O_2. **NbzB** has the advantage of showing enhanced selectivity for H_2O_2 over other ROS. However, **PB1** has somewhat higher sensitivity with a greater fluorescent response and is as such effective at detecting H_2O_2 in bovine oocytes. This crucial comparison presents the advantages of these two probes for given biological applications and suggests aryl boronates show greater sensitivity to H_2O_2 than benzils in bovine oocytes.

5.4 ACKNOWLEDGEMENTS

This research was supported in part by Cook Medical Pty Ltd and Australian Research Council linkage grant LP 110200736 and the ARC Centre of Excellence in Nanoscale BioPhotonics (CNBP) CE140100003. This work was performed in part at the OptoFab node of the Australian National Fabrication Facility (ANFF) utilizing Commonwealth and SA State

Government funding. This research was also undertaken in part on the NCI National Facility in Canberra, Australia, which is supported by the Australian Commonwealth Government.

5.5 SUPPLEMENTARY INFORMATION

5.5.1 Materials

All reagents were purchased from Sigma-Aldrich unless otherwise stated. Tetrahydrofuran (THF) was purchased from Scharlau and dried using an Innovative Technology Pure-Solv solvent purification system. Davsil silica gel (40-63 μm) was used for column chromatography. ^{1}H and ^{13}C NMR spectra were recorded in $CDCl_3$ (Cambridge Isotope Laboratories, Cambridge, MA) at 26 °C on an Agilent Technologies 500 MHz NMR with DD2 console, then analysed using Bruker TopSpin 3.2. FTIR spectra were recorded using a Perkin Elmer Spectrum 400 FT-IR/FT-FIR Spectrometer. High resolution mass spectrometry (HRMS) samples were recorded using an Agilent 6230 TOF LC-MS. All analytical reverse-phase HPLC was performed using an Agilent 1260 Infinity Analytical HPLC, using a Phenomenex Luna 5u C18(2) 100A column. Samples were run in a gradient of 10-100% acetonitrile in water over 15 min. Bovine IVF medium was prepared using VitroFert from IVF Vet Solutions (Adelaide, Australia); 4 mg/ml fatty acid free BSA (ICPBio Ltd; Auckland, New Zealand); 10 IU/ml heparin, 25 μM penicillamine, 12.5 μM hypotaurine and 1.25 μM epinephrine.

5.5.2 Calibration of PB1 and NbzB in Hydrogen Peroxide

A stock solution of approximately 100 mM H_2O_2 in Milli-Q water was prepared from a 30% H_2O_2 solution in water and the exact concentration was determined by UV absorption at 240 nm (ε_{240} = 43.6 $M^{-1}cm^{-1}$) using a Cary UV-Vis-NIR 5000 Spectrophotometer. **PB1** and **NbzB** were separately added to a 96-well plate in 100 mM phosphate buffer at pH 7.4 to give a final concentration of 10 μM of each probe. Samples were treated with 0, 5, 10, 25, 50, 75 or 100 μM of H_2O_2 in a 96-well plate. The resultant absorption and/or fluorescent spectra were monitored using a Biotek Synergy H4 fluorescence plate reader (fluorescence excitation 490 nm) over 50 min. All experiments were performed in triplicate and the results averaged.

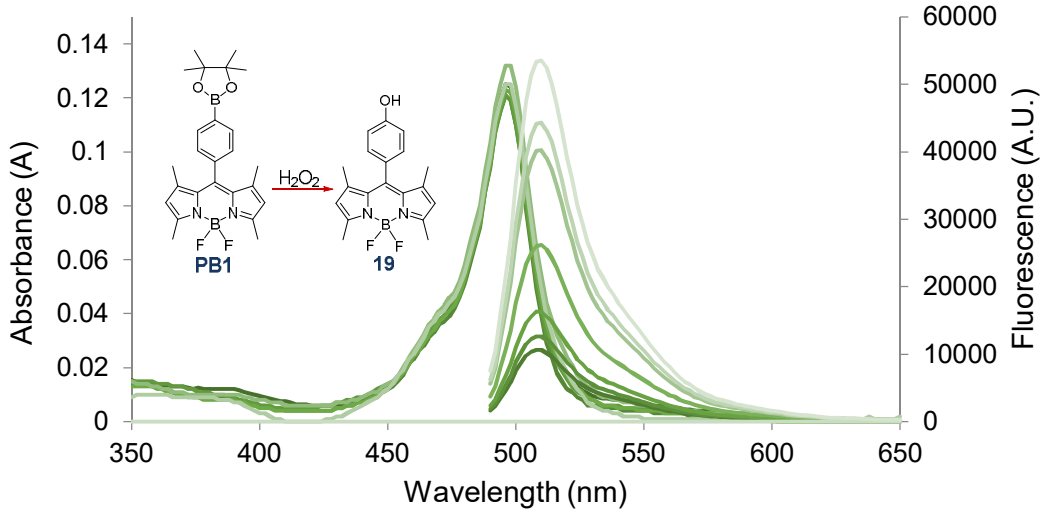

Figure 52. Oxidation of **PB1** to **11** with H_2O_2 after 50 min in 100 mM phosphate buffer at pH 7.4. Absorption (left) and fluorescence (right) spectra of **PB1** when incubated with 0, 5, 10, 25, 50, 75 and 100 µM H2O2 (fluorescence excitation 470 nm). This shows the clear quenching of fluorescence with increasing H_2O_2, however there is no change in the absorption spectrum.

5.5.3 ROS Selectivity Study

Solutions of **PB1** and **NbzB** in 100 mM phosphate buffer at pH 7.4 were treated with 100 µM of ROS: H_2O_2, $ONOO^-$, ^-OCl, $^{\bullet}OH$, $O_2^{\bullet-}$, NO, and *tert*-butyl hydroperoxide (TBHP). A stock solution of approximately 100 mM H_2O_2 in Milli-Q water was prepared from a 30% H_2O_2 solution in water and the exact concentration was determined by UV absorption at 240 nm (ε_{240} = 43.6 $M^{-1}cm^{-1}$) using a Cary UV-Vis-NIR 5000 Spectrophotometer. A stock solution of NaOCl was similarly prepared and the ^-OCl concentration determined by UV absorption at 292 nm (ε_{292} = 350 $M^{-1}cm^{-1}$). A solution of $ONOO^-$ was prepared by a known method,[79] and its concentration determined using UV absorption at 302 nm (ε_{302} = 1670 $M^{-1}cm^{-1}$). $^{\bullet}OH$ was produced by the Fenton reaction of 100 µM H_2O_2 with 1 mM $FeClO_4$. $O_2^{\bullet-}$ was also produced by a known method,[95] using a xanthine/xanthine oxidase system for production of $O_2^{\bullet-}$ and catalase as a scavenger for any H_2O_2 produced. NO was generated from S-nitrosoglutathione, and TBHP was diluted from a stock solution. The ROS were added to each probe and the fluorescence was monitored using a Biotek Synergy H4 fluorescence plate reader (excitation 490 nm, emission 510 nm) over 50 min. All experiments were performed in triplicate and the results averaged.

5.5.4 Detection of H_2O_2 in Bovine Oocytes

Bovine oocytes were denuded of cumulus cells and matured *in vitro* for 24 h at 38 °C in bovine IVF media according to literature procedures. Half of the oocytes were then treated with 1 mM H_2O_2 and then incubated for a further 30 min. Oocytes were then transferred to solutions containing either **PB1** or **NbzB** at a concentration of 10 µM in Bovine IVF media.

These were then incubated for 30 min, before transferring oocytes from each treatment group into 5μL drops in glass-bottom confocal dishes (Cell E&G; Houston, TX). These droplets were overlaid with oil and the fluorescence from each oocyte was captured using a FluoView FV10i confocal microscope and accompanying software (Olympus; Tokyo, Japan). Both **PB1** and **NbzB** were measured using 490 nm excitation and 509 nm emission filters. Microscope settings, including laser intensity and image size were kept constant while imaging. Quantification of the fluorescence was calculated using ImageJ software (National Institutes of Health, Bethesda, MD). The fluorescence intensity across the diameter of the oocyte was calculated, and an average for each treatment group is presented in **Figure 53**. Representative graphs and images are presented in the manuscript in **Figure 51**.

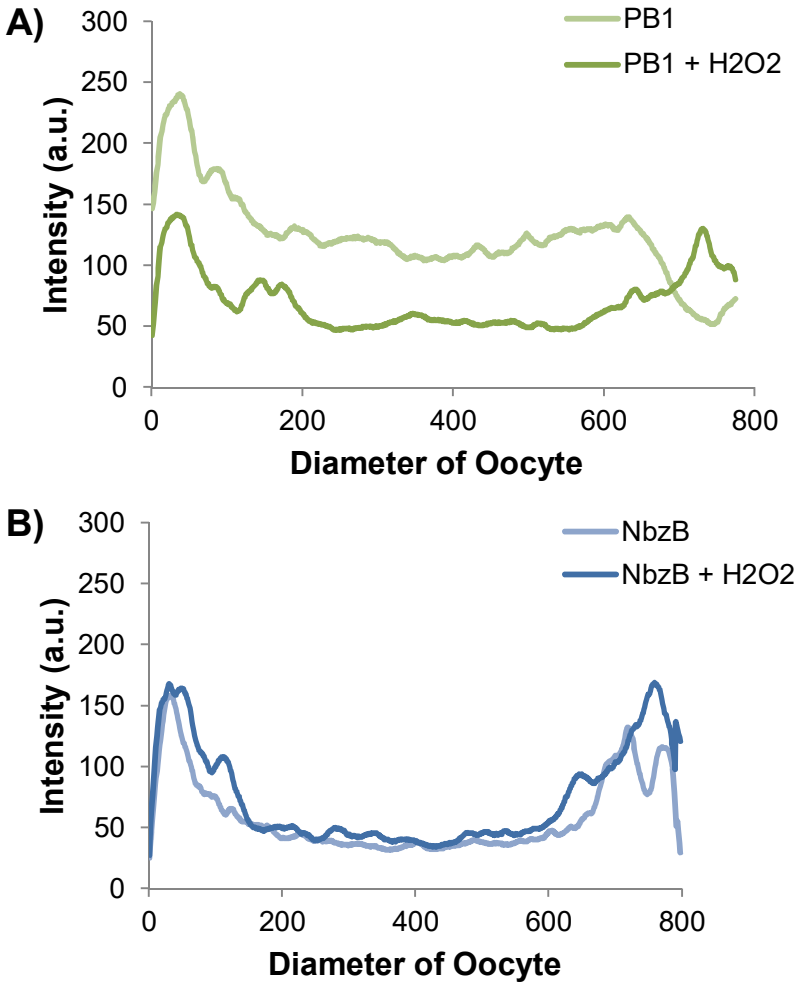

Figure 53. Average of the fluorescence intensity across the oocyte populations of each treatment group. A) **PB1** with and without treatment of H_2O_2 – a significant decrease was shown after treatment, which agreed with fluorescence studies in the absence of cells. B) **NbzB** with and without treatment of H_2O_2 – no significant increase was seen, although a slight increase is suggested. This agrees with solution based studies shown in **Figure 49**.

5.5.5 Synthesis

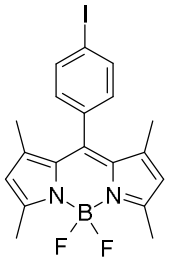

Compound **16**: (Synthesised as per literature[65]) 4-Iodobenzoic acid (496 mg, 2 mmol) was dissolved in anhydrous $CHCl_3$ (20 mL) under argon atmosphere. Thionyl chloride (4 mL) was added whilst stirring and the resultant solution was refluxed for 1 h. The reaction mixture was evaporated to dryness to produce crude 4-iodobenzoyl chloride which was used without further purification. Crude 4-iodobenzoyl chloride was dissolved in $CHCl_3$ (25 mL), and 2,4-dimethylpyrrole (412 µL, 4 mmol) was added under N_2 and the reaction mixture was stirred at room temperature for 3 days. Triethylamine (1.5mL) and $BF_3.Et_2O$ (2mL) were added dropwise and the solution was stirred for a further 24 h. The crude product was eluted through a silica column using 3:1 PET ether:$CHCl_3$ to afford **3** as an orange solid (298 mg, 33 %) **^{1}HNMR** ($CDCl_3$, 500MHz): δ(ppm) 7.84 (2H, d, J = 8.0 Hz), 7.04 (2H, d, J = 7.5Hz), 5.99 (2H, s), 2.55 (6H, s), 1.41 (6H, s).

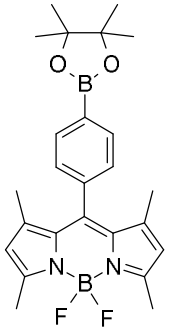

PeroxyBODIPY-1 (**PB1**): BODIPY phenyl iodide **16** (54 mg, 0.12 mmol), bis(pinacolato)diboron (121 mg, 0.48 mmol), potassium acetate (107 mg, 1.12 mmol) and $Pd(dppf)_2Cl_2$ were combined in a heavy-walled microwave reaction vial. The solution was dissolved in dry DMF (2 mL) and sealed with a Teflon cap in an inert N_2 atmosphere. The vial was heated under microwave irradiation at 100 °C for 2 h. The resultant dark brown solution was poured into saturated sodium bicarbonate (15 mL), and extracted with DCM (15 mL, 2 x 10 mL). The combined organic layers were dried over $MgSO_4$ and solvent removed under reduced pressure. The crude product was eluted through a silica column using 1:1

PET ether:$CHCl_3$ to afford **PB1** as a light orange solid (54 mg, 48 %). **^{1}HNMR** ($CDCl_3$, 500MHz): δ(ppm) 7.90 (2H, d, J = 7 Hz), 7.29 (2H, d, J = 7 Hz), 5.96 (2H, s), 2.55 (6H, s), 1.38 (12H, s), 1.36 (6H, s). **^{13}CNMR** ($CDCl_3$, 125MHz): δ(ppm) 155.5, 143.2, 141.6, 137.9, 135.4, 131.2, 127.3, 121.2, 84.15, 25.0, 14.6 (t, J = 10 Hz), 14.5. **HRMS-ESI**: calculated 451.2539, found 451.2521. **IR** (dry film) ν_{max}: 2978 (CH, aliphatic), 1543, 1511 (C=C), 1470, 1398, 1360, 1307, 1260, 1194, 1157, 1144, 1084, 982, 858, 835, 719. **HPLC** retention time 25.1 min; purity 94%.

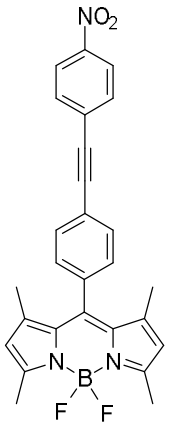

Compound **18**: BODIPY phenyl iodide (42 mg, 0.095 mmol), 4-nitroethynyl benzene **17** (17 mg, 0.11 mmol), $PdCl_2(PPh_3)_2$ (4.5 mg, 0.006 mmol) and copper (I) iodide (3 mg, 0.015 mmol) were placed in a dry vial in an inert N_2 glovebox. Triethylamine (0.1 mL) and THF (3 mL) were added and stirred overnight. The reaction mixture was then evaporated to dryness, then purified by eluting through a silica column with 2:1 PET ether:$CHCl_3$ to afford an orange solid, **5** (43 mg, 96 %) **^{1}HNMR** ($CDCl_3$, 500MHz): δ(ppm) 8.24 (2H, d, J = 8.5 Hz), 7.71-7.69 (4H, d, J = 7.5 Hz), 7.34 (2H, d, J = 8.0 Hz), 6.00 (2H, s), 2.56 (6H, s), 1.43 (6H, s). **^{13}CNMR** ($CDCl_3$, 125MHz): δ(ppm) 156.0, 147.2, 142.9, 140.3, 136.1, 132.5, 132.3, 131.1, 129.7, 128.5, 123.7, 123.0, 121.4, 93.7, 88.7, 14.6 (t, J = 10 Hz), 14.6. **HRMS**: [M+H] calculated 471.1930, found 471.1956. **IR** (dry film) ν_{max}: 2921 (CH, aliphatic), 2220 (-C≡C-), 1593, 1539, 1508 (C=C), 1468, 1436, 1405, 1370, 1339, 1302, 1187, 1158, 1079, 1047, 971, 854, 833, 810, 765, 748, 704.

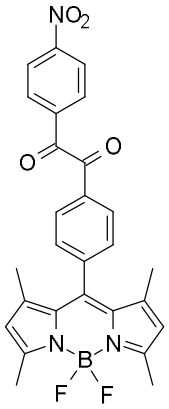

NitrobenzoylBODIPY (**NbzB**): **18** (24 mg, 0.051 mmol) and $PdCl_2$ were dissolved in DMSO (0.5 mL) and heated to 145 °C for 4 h. The solvent was removed under reduced pressure, and the crude solid was purified by eluting through a silica column using 1:1 PET ether:$CHCl_3$ to afford an orange powder, **NbzB** (14 mg, 55 %) **^{1}HNMR** ($CDCl_3$, 500 MHz): δ(ppm) 8.39 (2H, d, J = 8.0 Hz), 8.23 (2H, d, J = 8.5 Hz), 8.15 (2H, d, J = 8 Hz), 7.53 (2H, d, J = 8 Hz), 6.01 (2H, s), 2.56 (6H, s), 1.38 (6H, s) **^{13}CNMR** ($CDCl_3$, 125 MHz): δ(ppm) 191.6, 191.2, 156.5, 151.3, 142.6, 142.5, 139.1, 137.1, 132.7, 131.1, 130.7, 129.4, 124.2, 121.7, 14.6, 14.6 (t, J = 9.6 Hz). **MS**: [M+H] calculated 503.18, found 503.17. **IR** (dry film) ν_{max}: 2920, 2851 (CH, aliphatic), 1712, 1676 (C=O, ketone), 1544, 1519 (C=C), 1408, 1406, 1346, 1307, 1195, 1157, 1084, 982, 897, 833, 776, 738, 709. **HPLC** retention time 23.0 min; purity 95%.

5.5.6 Spectra

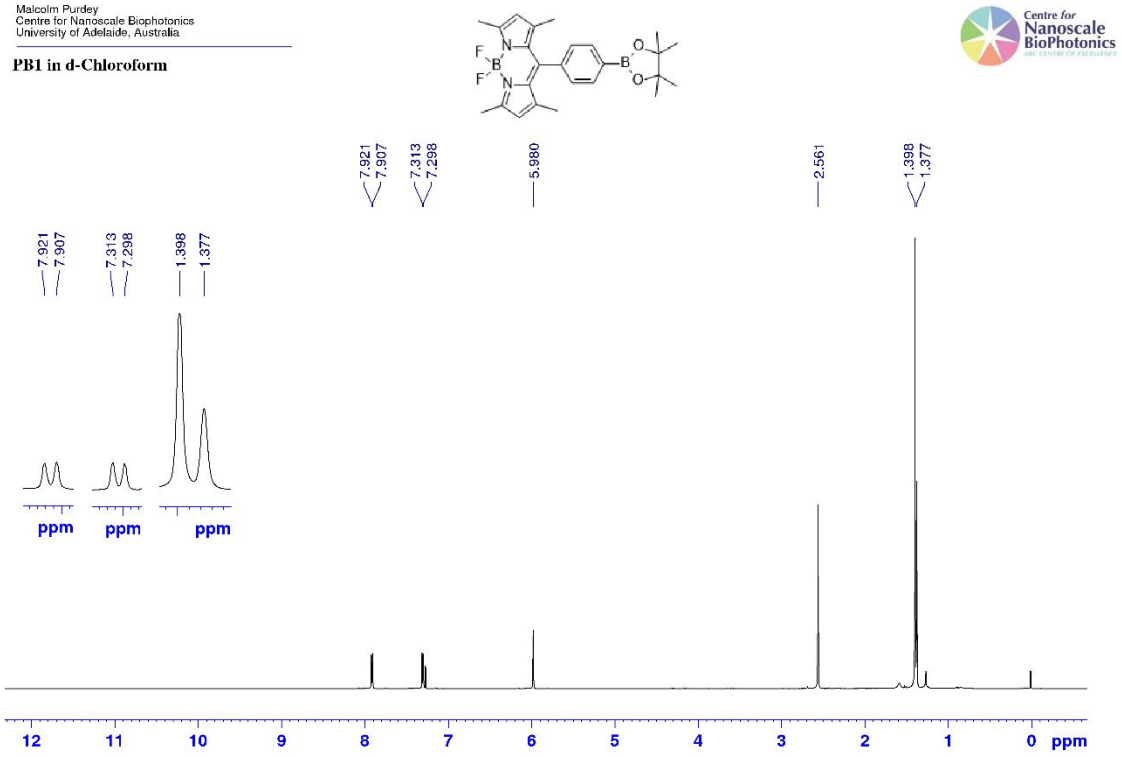
Malcolm Purdey
Centre for Nanoscale Biophotonics
University of Adelaide, Australia
PB1 in d-Chloroform
Centre for Nanoscale BioPhotonics
7.921
7.907
7.313
7.298
5.980
2.561
1.398
1.377
ppm
12
11
10
9
8
7
6
5
4
3
2
1
0
ppm

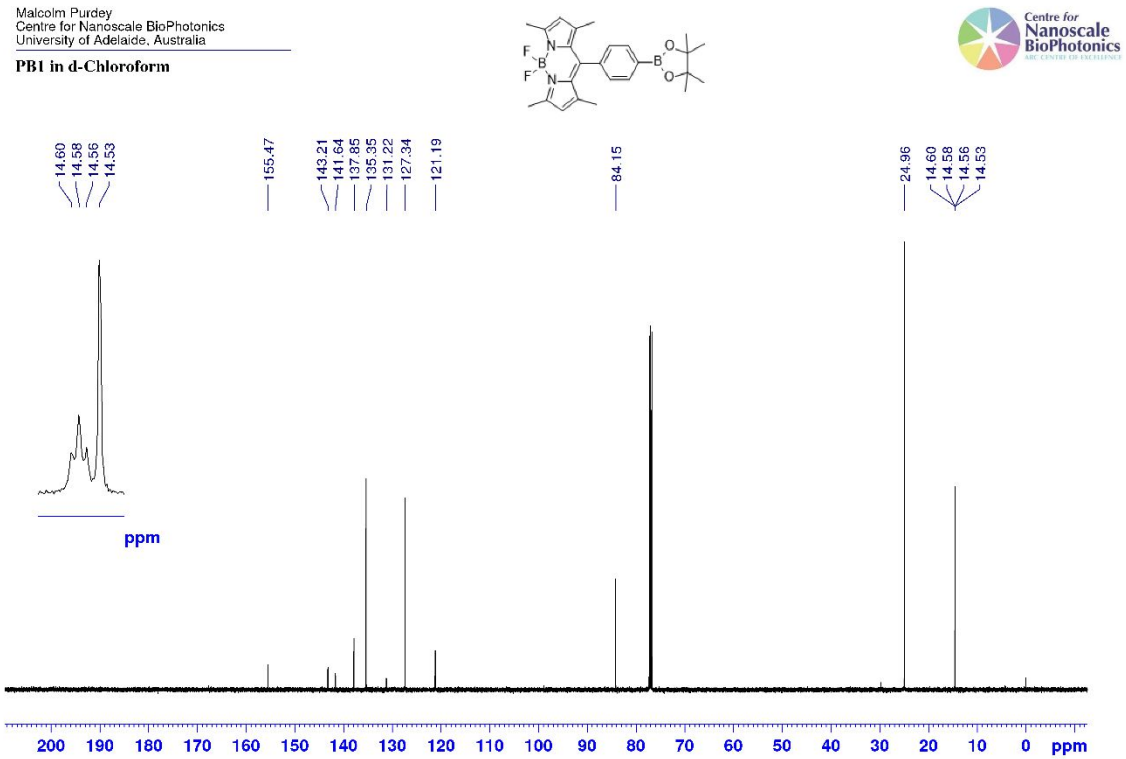
Malcolm Purdey
Centre for Nanoscale BioPhotonics
University of Adelaide, Australia
PB1 in d-Chloroform
Centre for Nanoscale BioPhotonics
14.60
14.58
14.56
14.53
155.47
143.21
141.64
137.85
135.35
131.22
127.34
121.19
84.15
24.96
14.60
14.58
14.56
14.53
ppm
200
190
180
170
160
150
140
130
120
110
100
90
80
70
60
50
40
30
20
10
0
ppm

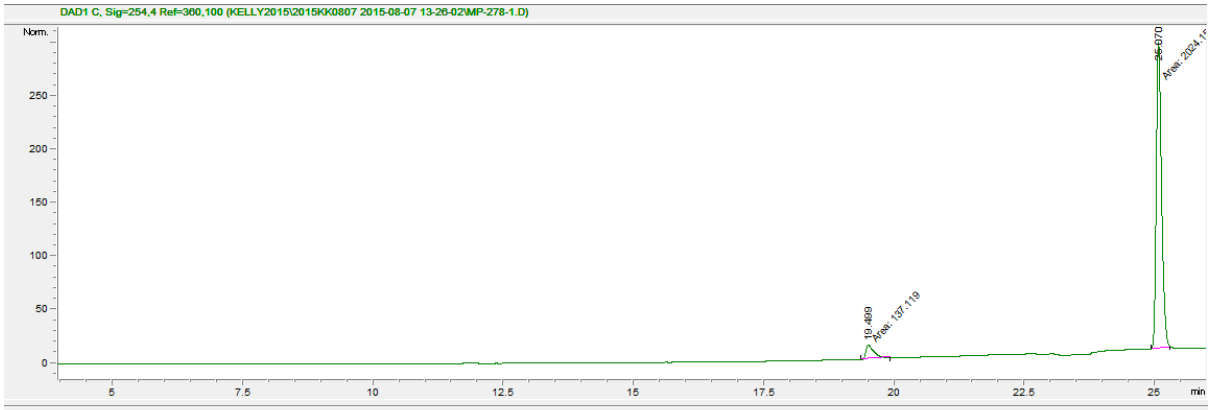

File Information	
LC-File	MP-278-1.D
File Path	C:\CHEM32\1\DATA\KELLY2015\2015KK0807 2
Date	07-Aug-15, 16:51:58
Sample	MP-278-1
Sample Info	
Barcode	
Operator	Kelly
Method	NKLA10_100_15MIN_1ML.M
Analysis Time	28 min
Sampling Rate	0.0067 min (0.402 sec), 4201 datapoints

#	Time	Area	Height	Width	Area%	Symmetry
1	19.499	137.1	12.9	0.1772	6.344	0.409
2	25.07	2024.1	287.7	0.1173	93.656	0.709

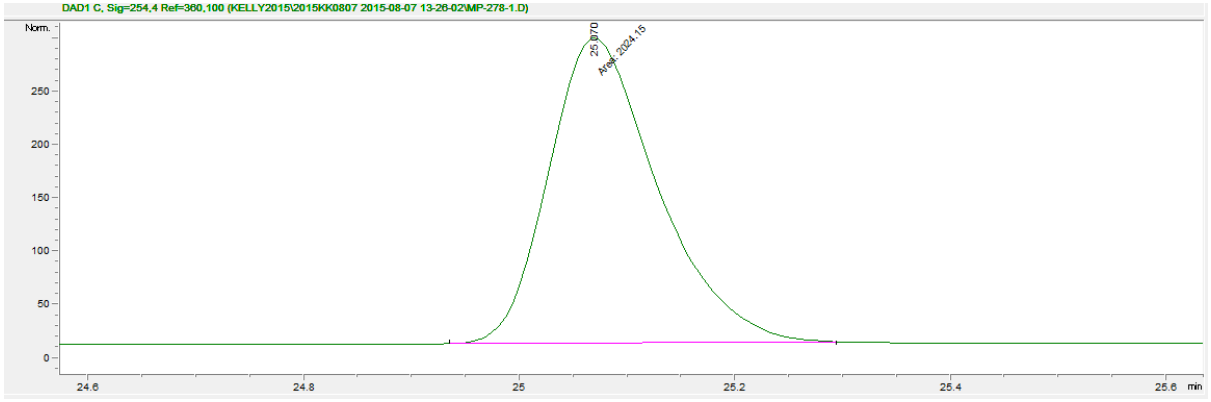

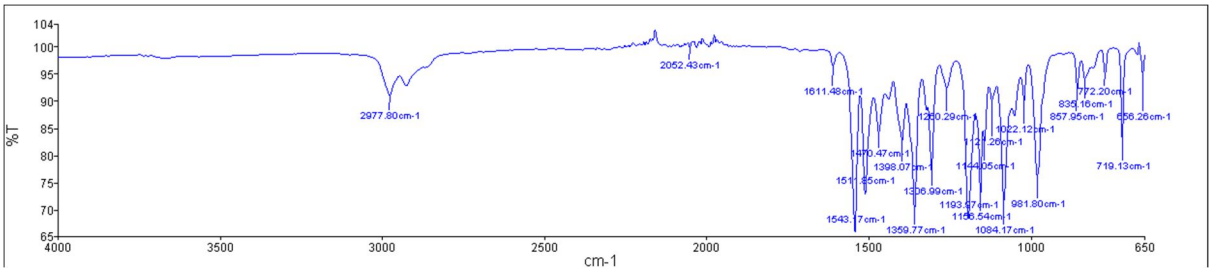

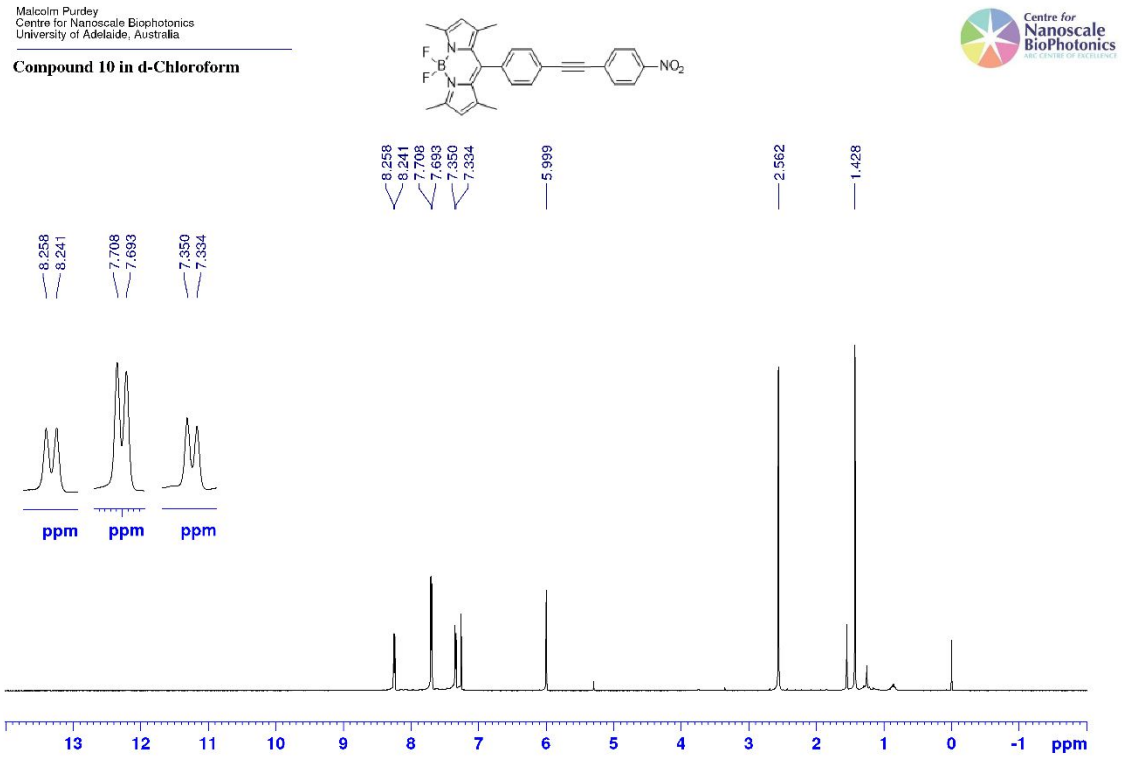
Malcolm Purdey
Centre for Nanoscale Biophotonics
University of Adelaide, Australia
Compound 10 in d-Chloroform
Centre for Nanoscale BioPhotonics
8.258
8.241
7.708
7.693
7.350
7.334
5.999
2.562
1.428
ppm
ppm
ppm
13 12 11 10 9 8 7 6 5 4 3 2 1 0 -1 ppm

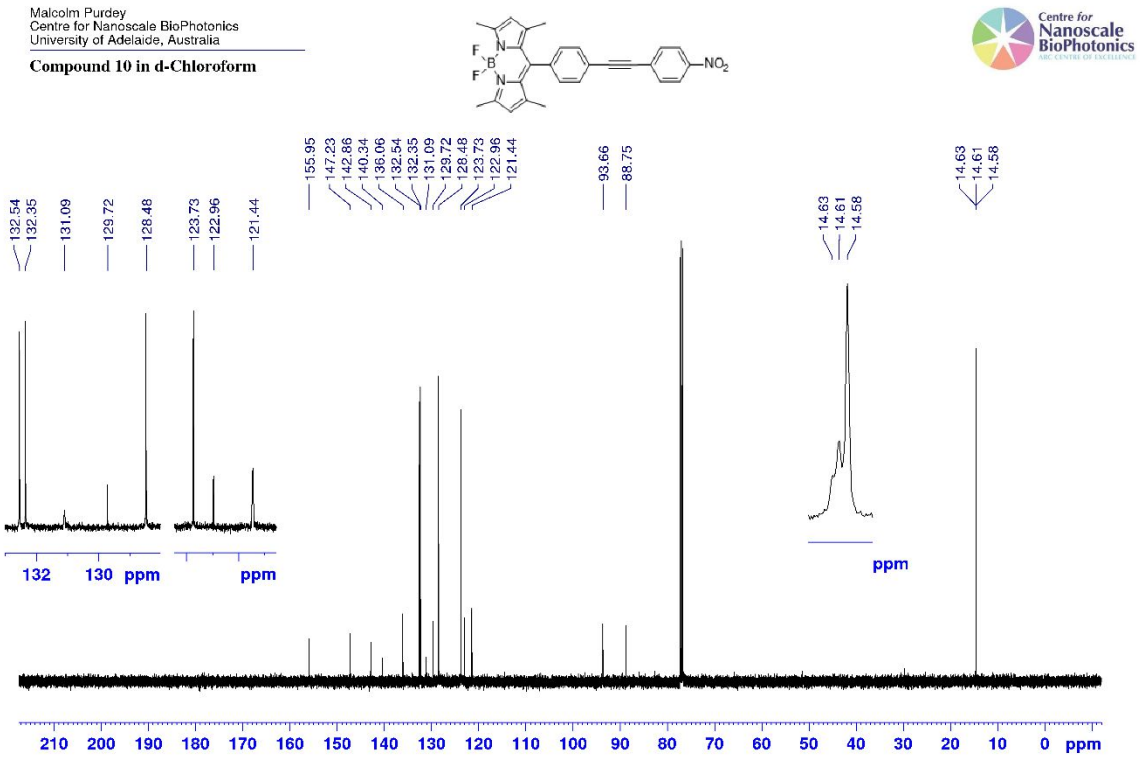
Malcolm Purdey
Centre for Nanoscale BioPhotonics
University of Adelaide, Australia
Compound 10 in d-Chloroform
Centre for Nanoscale BioPhotonics
155.95
147.23
142.86
140.34
136.06
132.54
132.35
131.09
129.72
128.48
123.73
122.96
121.44
93.66
88.75
14.63
14.61
14.58
132 130 ppm
ppm
ppm
210 200 190 180 170 160 150 140 130 120 110 100 90 80 70 60 50 40 30 20 10 0 ppm

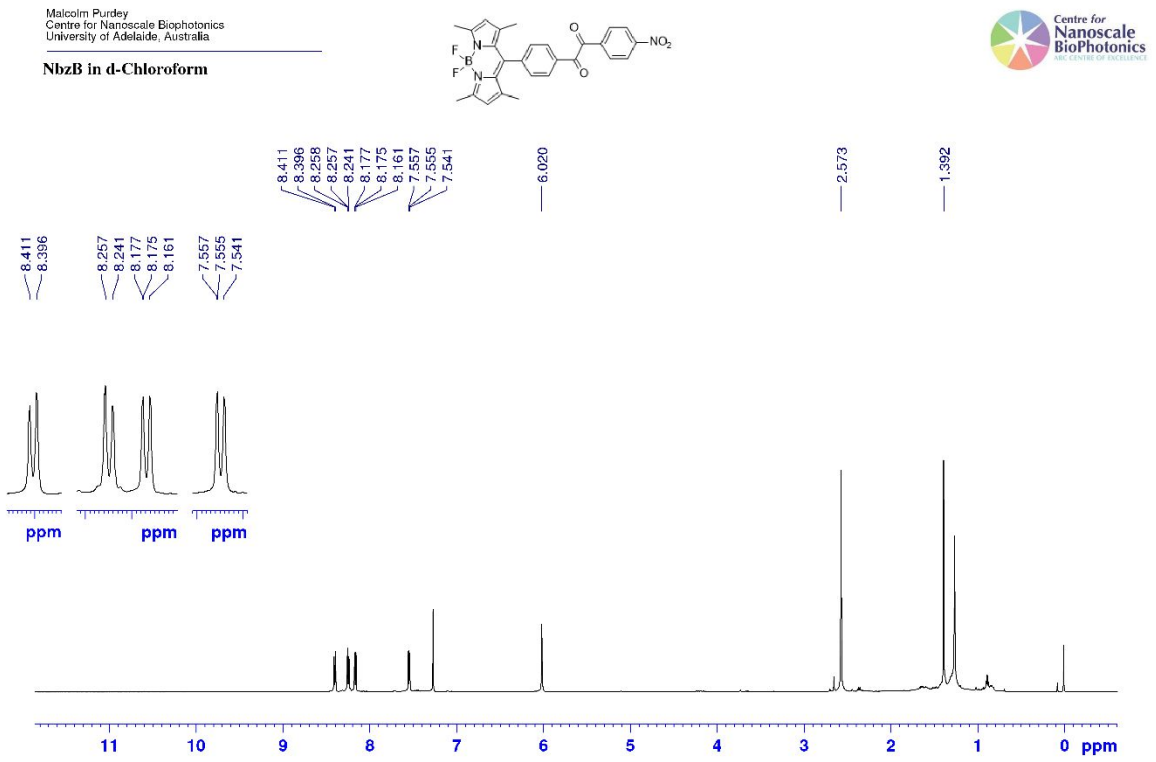
Malcolm Purdey
Centre for Nanoscale Biophotonics
University of Adelaide, Australia
NbzB in d-Chloroform
Centre for Nanoscale BioPhotonics
8.411
8.396
8.258
8.257
8.241
8.177
8.175
8.161
7.557
7.555
7.541
6.020
2.573
1.392
ppm
11
10
9
8
7
6
5
4
3
2
1
0 ppm

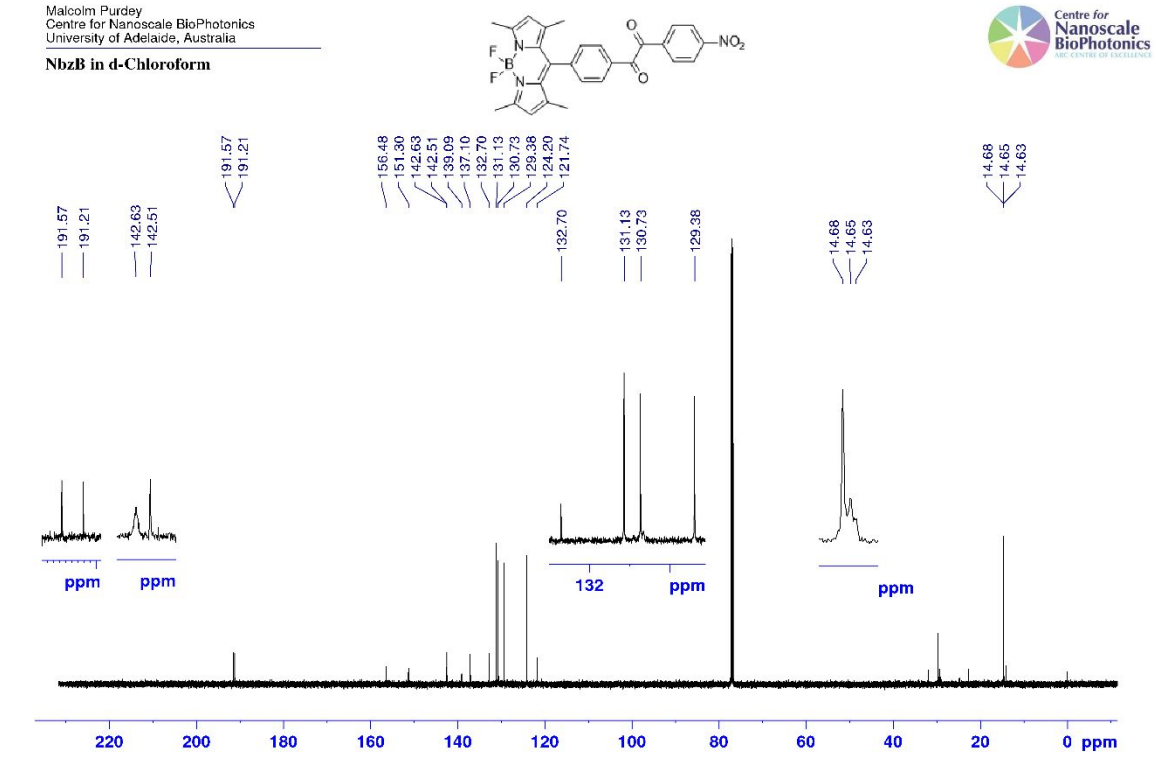
Malcolm Purdey
Centre for Nanoscale BioPhotonics
University of Adelaide, Australia
NbzB in d-Chloroform
Centre for Nanoscale BioPhotonics
191.57
191.21
156.48
151.30
142.63
142.51
139.09
137.10
132.70
131.13
130.73
129.38
124.20
121.74
14.68
14.65
14.63
132
ppm
220
200
180
160
140
120
100
80
60
40
20
0 ppm

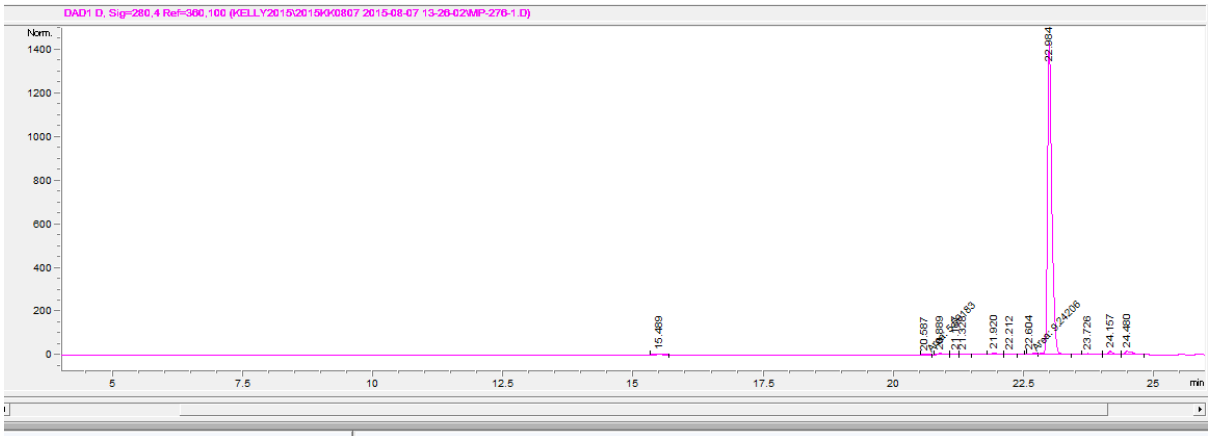

File Information	
LC-File	MP-276-1.D
File Path	C:\CHEM32\1\DATA\KELLY2015\2015KK0807 2
Date	07-Aug-15, 16:22:07
Sample	MP-276-1
Sample Info	
Barcode	
Operator	Kelly
Method	NKLA10_100_15MIN_1ML.M
Analysis Time	27.993 min
Sampling Rate	0.0067 min (0.402 sec), 4200 datapoints

#	Time	Area	Height	Width	Area%	Symmetry
1	15.489	34.1	5.1	0.0977	0.395	0.783
2	20.587	5.6	8E-1	0.1164	0.065	0.397
3	20.889	51.2	7.6	0.1002	0.593	0.579
4	21.187	20.4	3.6	0.0857	0.236	0.744
5	21.328	15.3	2.2	0.1017	0.177	0.617
6	21.92	52.3	8.8	0.0873	0.607	0.613
7	22.212	12.6	2.2	0.0871	0.146	0.684
8	22.604	9.2	1.6	0.0959	0.107	0.539
9	22.984	8154.6	1433.5	0.0948	94.501	0
10	23.726	33.7	4.5	0.1101	0.391	0.511
11	24.157	98	13.9	0.1063	1.136	0.679
12	24.48	142	15.5	0.1248	1.646	0.374

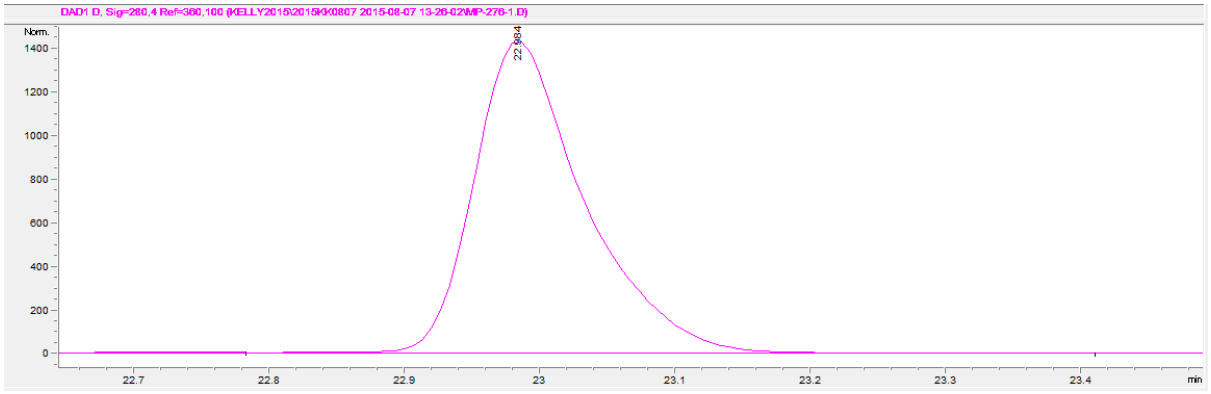

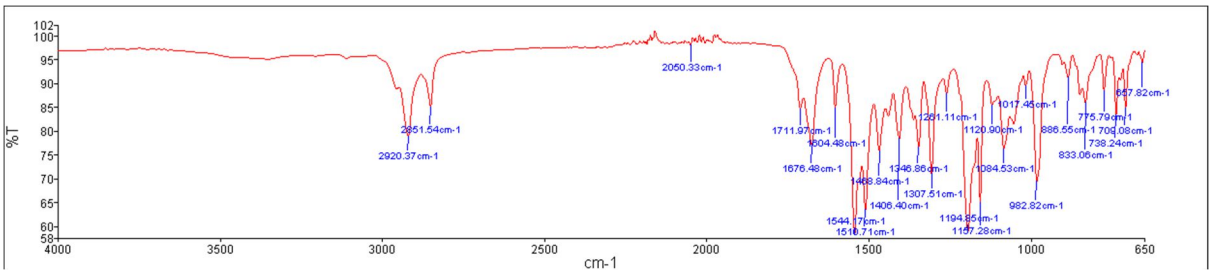

5.6 REFERENCES

5. Aitken, R. J.; Curry, B. J. Redox regulation of human sperm function: from the physiological control of sperm capacitation to the etiology of infertility and DNA damage in the germ line. *Antioxid Redox Signal* **2011,** *14* (3), 367-81.
7. Morado, S.; Cetica, P.; Beconi, M.; Thompson, J. G.; Dalvit, G. Reactive oxygen species production and redox state in parthenogenetic and sperm-mediated bovine oocyte activation. *Reproduction* **2013,** *145* (5), 471-8.
19. Groeger, G.; Quiney, C.; Cotter, T. G. Hydrogen peroxide as a cell-survival signaling molecule. *Antioxid Redox Signal* **2009,** *11* (11), 2655-71.
30. Lippert, A. R.; Van de Bittner, G. C.; Chang, C. J. Boronate Oxidation as a Bioorthogonal Reaction Approach for Studying the Chemistry of Hydrogen Peroxide in Living Systems. *Accounts of Chemical Research* **2011,** *44* (9), 793-804.
48. Loudet, A.; Burgess, K. BODIPY Dyes and Their Derivatives: Syntheses and Spectroscopic Properties. *Chemical Reviews* **2007,** *107* (11), 4891-4932.
54. Miller, E. W.; Albers, A. E.; Pralle, A.; Isacoff, E. Y.; Chang, C. J. Boronate-Based Fluorescent Probes for Imaging Cellular Hydrogen Peroxide. *Journal of the American Chemical Society* **2005,** *127* (47), 16652-16659.
62. Komatsu, T.; Oushiki, D.; Takeda, A.; Miyamura, M.; Ueno, T.; Terai, T.; Hanaoka, K.; Urano, Y.; Mineno, T.; Nagano, T. Rational design of boron dipyrromethene (BODIPY)-based photobleaching-resistant fluorophores applicable to a protein dynamics study. *Chemical communications* **2011,** *47* (36), 10055-7.
65. Ziessel, R.; Ulrich, G.; Haefele, A.; Harriman, A. An artificial light-harvesting array constructed from multiple Bodipy dyes. *J Am Chem Soc* **2013,** *135* (30), 11330-44.
79. Hempel, S. L.; Buettner, G. R.; O'Malley, Y. Q.; Wessels, D. A.; Flaherty, D. M. Dihydrofluorescein diacetate is superior for detecting intracellular oxidants: comparison with 2',7'-dichlorodihydrofluorescein diacetate, 5(and 6)-carboxy-2',7'-dichlorodihydrofluorescein diacetate, and dihydrorhodamine 123. *Free Radical Biology and Medicine* **1999,** *27* (1–2), 146-159.
94. Chang, M. C. Y.; Pralle, A.; Isacoff, E. Y.; Chang, C. J. A selective, cell-permeable optical probe for hydrogen peroxide in living cells. *Journal of the American Chemical Society* **2004,** *126* (47), 15392-15393.
95. Albers, A. E.; Dickinson, B. C.; Miller, E. W.; Chang, C. J. A red-emitting naphthofluorescein-based fluorescent probe for selective detection of hydrogen peroxide in living cells. *Bioorganic & Medicinal Chemistry Letters* **2008,** *18* (22), 5948-5950.
96. Dickinson, B. C.; Huynh, C.; Chang, C. J. A Palette of Fluorescent Probes with Varying Emission Colors for Imaging Hydrogen Peroxide Signaling in Living Cells. *Journal of the American Chemical Society* **2010,** *132* (16), 5906-5915.
99. Dickinson, B. C.; Peltier, J.; Stone, D.; Schaffer, D. V.; Chang, C. J. Nox2 redox signaling maintains essential cell populations in the brain. *Nat Chem Biol* **2011,** *7* (2), 106-112.
100. Sikora, A.; Zielonka, J.; Lopez, M.; Joseph, J.; Kalyanaraman, B. Direct oxidation of boronates by peroxynitrite: Mechanism and implications in fluorescence imaging of peroxynitrite. *Free Radical Biology & Medicine* **2009,** *47* (10), 1401-1407.
103. Abo, M.; Urano, Y.; Hanaoka, K.; Terai, T.; Komatsu, T.; Nagano, T. Development of a Highly Sensitive Fluorescence Probe for Hydrogen Peroxide. *Journal of the American Chemical Society* **2011,** *133* (27), 10629-10637.
104. Abo, M.; Minakami, R.; Miyano, K.; Kamiya, M.; Nagano, T.; Urano, Y.; Sumimoto, H. Visualization of phagosomal hydrogen peroxide production by a novel fluorescent probe that is localized via SNAP-tag labeling. *Anal Chem* **2014,** *86* (12), 5983-90.
124. Setsukinai, K.; Urano, Y.; Kakinuma, K.; Majima, H. J.; Nagano, T. Development of novel fluorescence probes that can reliably detect reactive oxygen species and distinguish specific species. *The Journal of biological chemistry* **2003,** *278* (5), 3170-5.

153. Purdey, M. S.; Connaughton, H. S.; Whiting, S.; Schartner, E. P.; Monro, T. M.; Thompson, J. G.; Aitken, R. J.; Abell, A. D. Boronate probes for the detection of hydrogen peroxide release from human spermatozoa. *Free Radical Biology and Medicine* **2015,** *81* (0), 69-76.
176. Rhee, S. G.; Chang, T. S.; Jeong, W.; Kang, D. Methods for detection and measurement of hydrogen peroxide inside and outside of cells. *Mol Cells* **2010,** *29* (6), 539-49.
177. Lin, V. S.; Dickinson, B. C.; Chang, C. J. Boronate-Based Fluorescent Probes: Imaging Hydrogen Peroxide in Living Systems. *Methods in enzymology* **2013,** *526C*, 19-43.
178. Komatsu, T.; Urano, Y.; Fujikawa, Y.; Kobayashi, T.; Kojima, H.; Terai, T.; Hanaoka, K.; Nagano, T. Development of 2,6-carboxy-substituted boron dipyrromethene (BODIPY) as a novel scaffold of ratiometric fluorescent probes for live cell imaging. *Chemical communications* **2009,** (45), 7015-7.

Chapter 6

EXTENDING CURRENT SENSING TECHNOLOGIES

Not only does God play dice, but… he sometimes throws them where they cannot be seen.

Stephen Hawking

Chapter 6: Extending Current Sensing Technologies

6.1 INTRODUCTION

6.1.1 Autofluorescence background signal

The detection of hydrogen peroxide (H_2O_2) using fluorescent probes is often frustrated by interference from autofluorescence within cells and organisms. Autofluorescence is the intrinsic fluorescence of natural proteins and biomolecules such as NADH, NADPH and FAD^{++}.[179] This provides a significant background signal that can be extremely difficult to separate from emission spectra of fluorescent probes.[180] The autofluorescent signal arises mostly from excitation in the blue region (450-490 nm) and green emission (510-530 nm).[179] These are common excitation and emission regions for fluorescent probes including many of the fluorophores discussed in prior chapters [such as peroxyfluor-1 (**PF1**), carboxyperoxyfluor-1 (**CPF1**, **Figure 54**), 2-ethoxy(2-ethoxyethoxy)peroxyfluor-1 (**EEPF1**), peroxyBODIPY-1 (**PB1**) and nitrobenzoylBODIPY (**NbzB**)]. The interference from autofluorescence reduces the apparent sensitivity of these probes in both *in vitro* and *in vivo* applications. Therefore, it is desirable to avoid autofluorescence in order to improve the detection limit of fluorescent probes in biological environments.

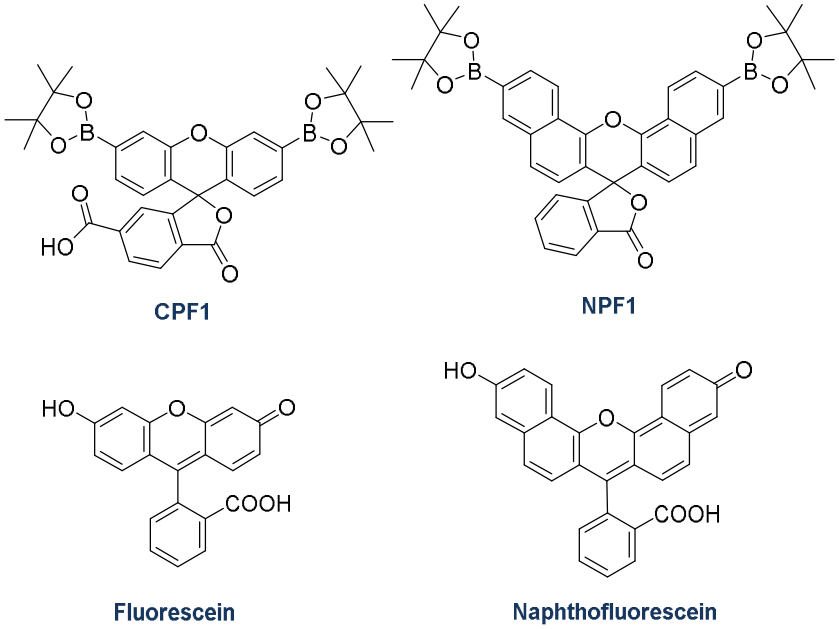

Figure 54. Fluorescent probes, carboxyperoxyfluor-1 (C**PF1**) and naphthoperoxyfluor-1 (**NPF1**). **Fluorescein** and **naphthofluorescein** are shown here for comparison. **Fluorescein** has an emission maximum of 520 nm, and **naphthofluorescein** emits at 650 nm.

One solution to this problem is to use a fluorescent probe with a red emission spectrum. Hence the red emitted light would avoid the autofluorescence background signal in the blue and green regions.[181] This has further advantages, as the excitation spectrum would also be

red-shifted, i.e. the fluorophore would be excited by photons of lower energy. This then decreases the phototoxicity of the excitation light to a biological environment, as higher energy photons such as UV light cause DNA mutations.[182]

The aryl boronate naphthoperoxyfluor-1 (**NPF1**, **Figure 54**) has been reported as a red-emitting probe for H_2O_2 in order to address the issue of autofluorescence.[95] This fluorophore reacts with H_2O_2 to form **naphthofluorescein** (**Figure 54**), with a red emission maximum of 650 nm. Furthermore, **NPF1** is similar to other aryl boronates such as **PF1** as it shows selectivity for H_2O_2 over many reactive oxygen species (ROS).[95] These characteristics present **NPF1** as a promising alternative to green-emitting fluorophores such as **PF1** or **CPF1**. The use of **NPF1** for solution-based *in vitro* studies and immobilisation to optical fibre tips could avoid autofluorescence and therefore improve the detection limit of H_2O_2 compared to the green-emitting probes.

This chapter reports the synthesis of **NPF1** and its comparison to **CPF1** for the detection of H_2O_2.

6.1.2 Reusable Fibre Probes

The reported optical fibre tip probes for H_2O_2 (see **Chapters 3** and **4**) were functionalised with the aryl boronate **CPF1**. However, the reaction of aryl boronates with H_2O_2 is irreversible[30] and these probes therefore cannot detect further H_2O_2 after the **CPF1** has been oxidised. Immobilisation of a reversible ROS probe onto a fibre tip would therefore create a sensor for H_2O_2 that could be re-used for multiple experiments, including performing continuous measurements in dynamic environments.

Naphthalimide Flavin redox sensor 1 (**NpFR1**) and Flavin coumarin redox sensor 2 (**FCR2**) have recently been reported for the detection of ROS (**Figure 55**).[83,84] These fluorescent probes lack selectivity for H_2O_2 compared to other ROS, but reversibly oxidise and reduce in response to the redox state of a biological environment. **NpFR1** is a turn-on fluorescence probe that is non-fluorescent until oxidised by ROS such as H_2O_2. The resultant oxidised compound fluoresces green (550 nm).[83] The compound can then be reduced to re-form the non-fluorescent **NpFR1**. Reduction can take place inside a cell by natural antioxidants, or the compound can be reduced in a fluorescence assay using a reducing agent such as $NaBH_4$.

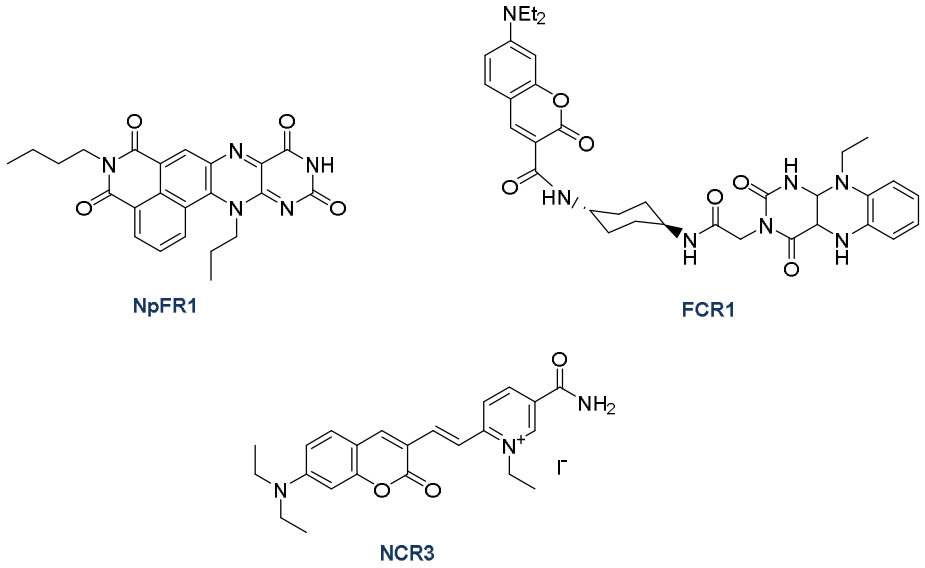

Figure 55. Reversible probes for ROS, naphthalimide Flavin redox sensor 1 (**NpFR1**), Flavin coumarin redox sensor 2 (**FCR2**) and nicotinamide coumarin redox sensor 3 (**NCR3**).

FCR2 is a Förster resonance energy transfer (FRET)-based ratiometric probe (see discussion in section **1.2.4**).[84] **FCR2** fluoresces blue (470 nm) until it reacts with ROS such as H_2O_2, and emits green fluorescence (510 nm). This improves upon **NpFR1**, as the fluorescence of **FCR2** is visible within a cell either in oxidised or reduced form. However, the shift in emission upon oxidation is minor (less than 50 nm). This complicates the analysis of obtained spectra, as the blue and green emission peaks overlap significantly. Therefore another reversible ROS probe, nicotinamide coumarin redox sensor 3 (**NCR3**, **Figure 55**) was synthesised by Kaur et al.[183] This new probe is based on nicotinamide, in contrast to the Flavin-inspired **NpFR1** and **FCR2**. **NCR3** exhibited an excellent spectral shift of greater than 100 nm upon oxidation by H_2O_2, with emission peaks at 500 nm and 635 nm in its reduced and oxidised forms respectively (**Figure 56**). As such, **NCR3** has ideal spectral properties for use on a fibre tip sensor.

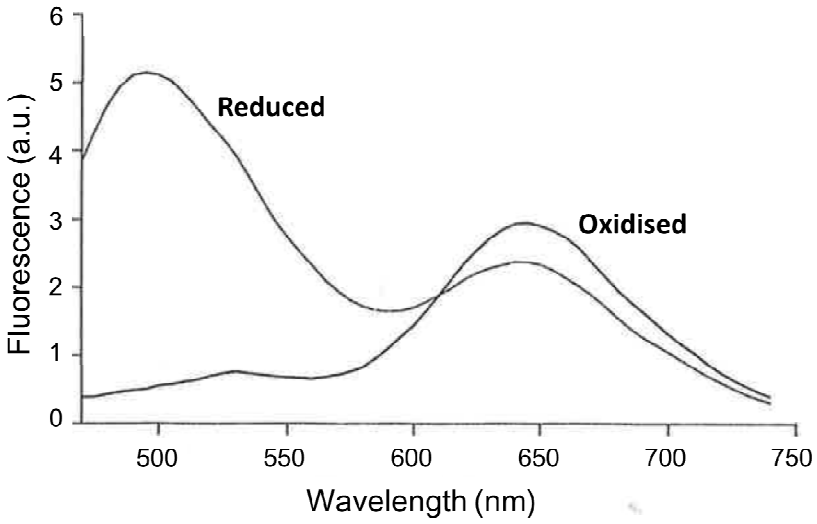

Figure 56. Emission spectra of **NCR3** in reduced and oxidised form. Excitation maxima are 458 nm for both forms.[183]

This chapter reports the functionalisation of **NCR3** in polyacrylamide to an optical fibre tip to create a reversible sensor for H_2O_2.

6.2 NAPHTHOPEROXYFLUOR-1

NPF1 was synthesised with minimal modifications to procedures reported in literature (**Scheme 14**).[95] 1,6-Dihydroxy naphthelene (**40**) and phthalic anhydride (**41**) were heated in methanesulfonic acid to give **naphthofluorescein**. **Naphthofluorescein** was then triflated with N-phenyl bis(trifluoromethanesulfonimide) to give the triflated compound **42**. Intermediate **42** was then reacted with bis(pinacolato) diboron under Suzuki conditions as shown (**Scheme 14**) to give **NPF1** in a yield of 81 %.

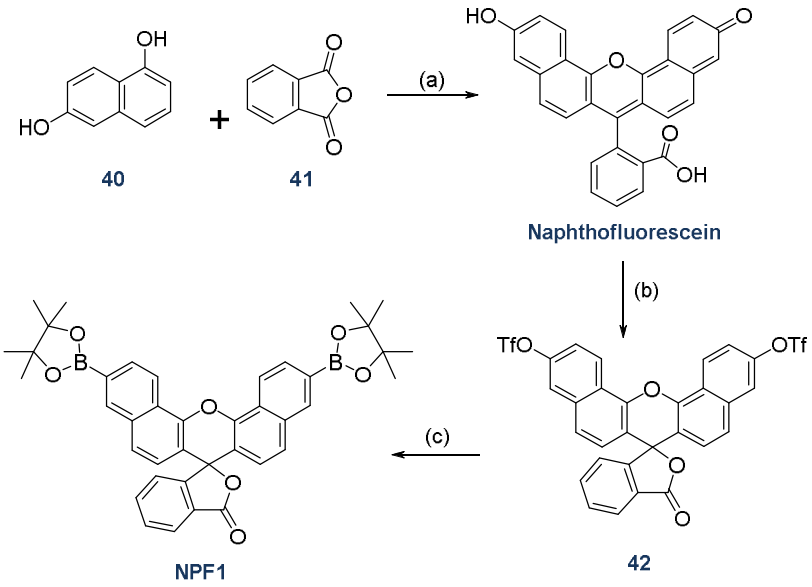

Scheme 14. Synthesis of **NPF1**. (a) $MeSO_3H$, 135 °C, 48 h. (b) N-phenyl-bis(triflate), DIPEA, DMF, r.t., 24 h. (c) bis(pinacolato)diboron, $Pd(dppf)_2Cl_2$, KOAc, dioxane, 100 °C, 24 h.

For **NPF1** to be used in a cell or on a fibre tip, it must detect H_2O_2 with similar sensitivity to the fluorophores previously described in this thesis. Therefore, **NPF1** and **CPF1** were both incubated with H_2O_2 and the fluorescent responses compared. **NPF1** was dissolved to give a 2 mM solution in DMSO. This was then diluted to 10 μM in α-MEM buffer solution containing different concentrations of H_2O_2. These solutions of **NPF1** were prepared with 0, 1, 50 or 100 μM of H_2O_2, and the resultant fluorescence measured by a Cary Eclipse Fluorescence Spectrometer at 37 °C. **Figure 57A** shows the fluorescence from samples in H_2O_2 after 40 min. Only a slight increase in fluorescence was observed, even in solutions with 50 or 100 μM H_2O_2. These results were then compared to **CPF1** as reported in **Chapter 3** (reprinted here in **Figure 57B**). The previously obtained fluorescent response of **CPF1** to 20 μM of H_2O_2 was 20-fold greater than the response of **NPF1** to 100 μM of H_2O_2 (**Figure 57A**). This lower fluorescent response indicates that **NPF1** is far less sensitive to H_2O_2 than **CPF1**.

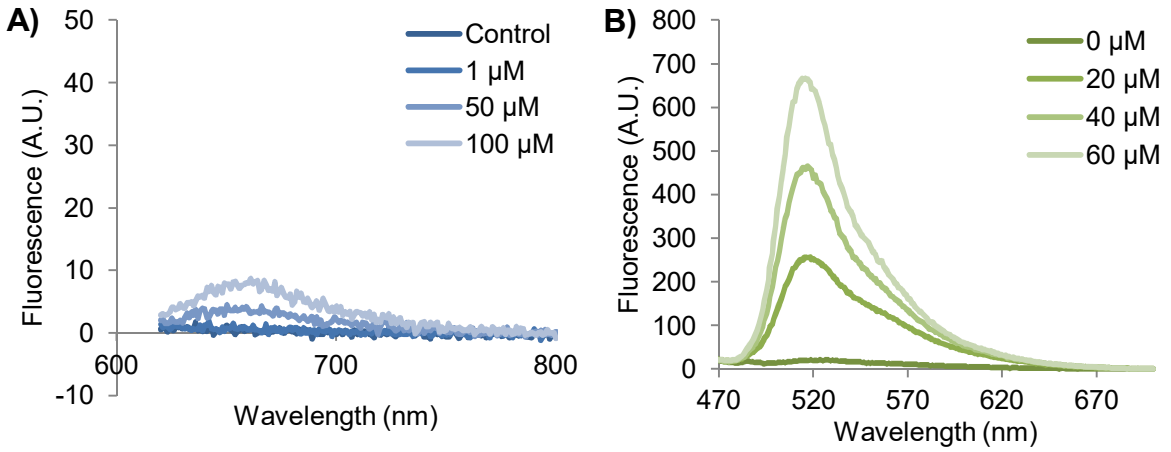

Figure 57. Response of (A) NPF1 to 0, 1, 50 and 100 μM H_2O_2 after 40 min at 37 °C in α-MEM media. (B) CPF1 to 0, 20, 40 and 60 μM H_2O_2 after 40 min at 37 °C in α-MEM media.

These results hence suggest that **NPF1** will not be able to detect biologically relevant concentrations of H_2O_2 <100 μM *in vitro*, due to this poor fluorescent response. Furthermore, this response also suggests that **NPF1** is not a good candidate for functionalisation to optical fibre tips. As there is a low fluorescent signal from **NPF1**, a higher excitation power would be required to improve the emission signal for detection by a spectrometer. However, increasing the power of excitation would also increase the photobleaching of **NPF1** on the fibre tip, thus reducing the recorded fluorescence. This counteracts the increase in fluorescence that would be observed upon reaction with H_2O_2, again reducing its effectivity in detection H_2O_2. Hence, **NPF1** is less suitable than **CPF1** for use *in vitro* or immobilised to optical fibres, and was not investigated further.

6.3 REVERSIBLE FIBRE-TIP SENSOR FOR HYDROGEN PEROXIDE

The reversible ROS sensor **NCR3**[⌗⌗] (**Figure 58**) was functionalised to optical fibre tips using the polyacrylamide method described in **Chapters 3** and **4**. The distal end of the fibre was then coupled to a 473 nm light source for excitation, and the emission collected by a spectrometer (see Experimental section **6.5.4**, **Figure 61**). These functionalised fibre tips were washed in pH 7.4 buffer, then dipped in a 1 mM solution of H_2O_2. After removal from solution, the fluorescence was recorded in air before being dipped into a reducing solution of 1 mM $NaCNBH_3$. The fibre was removed from solution and the fluorescent signal recorded again. This process was repeated, alternately immersing in oxidising, then reducing solutions, in order to examine the reversibility of the fibre sensor. The ratio of the two emission peaks at 500 nm and 635 nm was then calculated. A similar fluorescent ratio was observed for all seven cycles after oxidation of the probe by H_2O_2 (**Figure 59**). However, the

⌗⌗ **NCR3** was used as provided by Amandeep Kaur and Elizabeth New at the University of Sydney, Sydney, NSW. The author wishes to thank them for the design, synthesis and provision of a sample of **NCR3**.

ratio shown by the reduced form of the probe was less consistent across the cycles, as a decrease of the ratio was observed in cycle one and six. This error may have been caused by a slight difference in time the fibre tip was dried in air before the fluorescent ratio was measured or the time in the reducing solution ($NaCNBH_3$). These differences thus could have led to a lower fluorescent ratio. Despite this, a clear difference was observed between the fluorescent ratio of the oxidised and reduced forms of the probe (**Figure 59**). These results clearly indicate that the sensor can be cycled multiple times between the oxidised form of **NCR3** to the reduced form. This implies that **NCR3** may be used on a fibre tip to create a reversible sensor for H_2O_2 and other ROS.

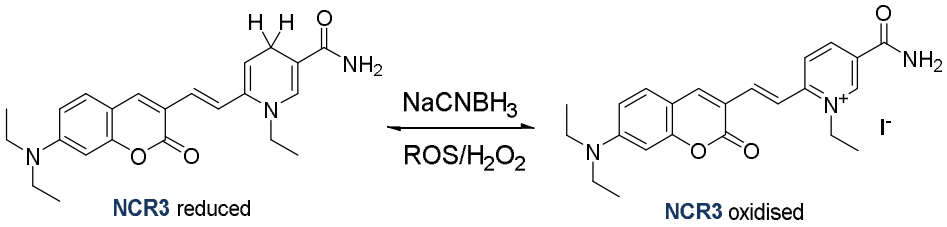

Figure 58. Oxidation and reduction of **NCR3** by H_2O_2 and $NaCNBH_3$ respectively.

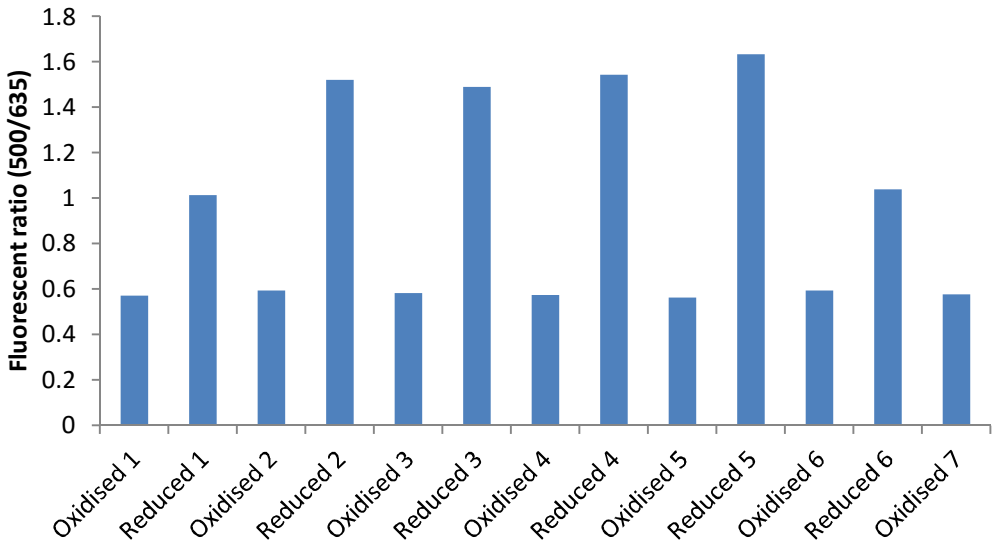

Figure 59. Fluorescent ratio of **NCR3** in air after treatment with $NaCNBH_3$ (reduced), or H_2O_2 (oxidised). This graph shows very little change in fluorescent ratio after 7 cycles.

Furthermore, these results also demonstrate that the reversibility of a redox probe such as **NCR3** can be rapidly measured on a fibre tip. Standard solution-based measurement of reversibility requires the oxidant and reductant to be added sequentially. Multiple cycles requires the tedious addition of exact amounts of oxidant and reductant. Moreover, the number of cycles that can be tested in solution is limited by the volume of liquid added to the cuvette each cycle. In contrast, this fibre sensor can simply be moved between oxidising/reducing solutions as many times as is desired, allowing longer trials to test many

iterations of oxidation and reduction. This would also enable the determination of the maximum number of redox cycles before the fluorophore is degraded.

Although the fluorescent ratios in **Figure 59** indicated reversible oxidation and reduction of the sensor; **Figure 60** shows a drop in the fluorescence intensity from the sensor over 2 min in buffer solution. This drop was initially thought to be due to photobleaching of the **NCR3**. However, attenuation of the laser excitation power revealed the same decrease in fluorescent signal over multiple trials. Therefore the decrease in fluorescence intensity can be explained by the leaching of **NCR3** out of the polymer and into the buffer solution. This explanation is supported by the structure of **NCR3**, as there are multiple polar groups, including a formal positive charge in its oxidised state (**Figure 58**). The hydrophilicity of the oxidised form of **NCR3** allows ionic and ion-dipole interactions with the polar buffer solution, while it maintains much weaker interactions with the more hydrophobic polyacrylamide backbone. This explains the rapid diffusion of **NCR3** from the polymer that results in the observed decrease in fluorescence.

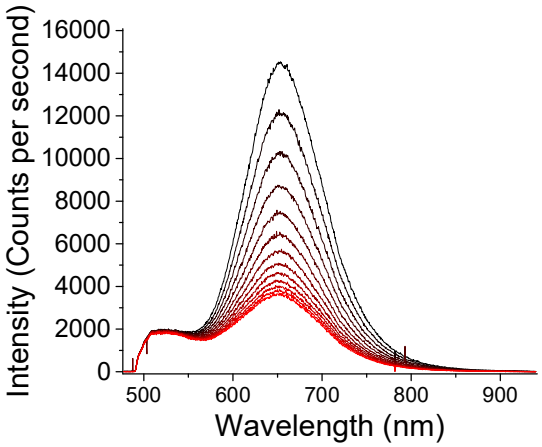

Figure 60. Fluorescence of **NCR3** (oxidised) on a fibre tip over 2 min in pH 7.4 phosphate buffer.

Therefore, the leaching of **NCR3** from the polymer limits its ultimate use as a tip-sensor, despite its ability to reversibly detect oxidation and reduction. Structural modification of **NCR3** could include more hydrophobic groups in order to reduce the interactions with the buffer solution. Thus the new fluorophore would not leach from the polymer, and the sensor could be used for reversible detection of H_2O_2 without loss of fluorescence intensity.

6.4 CONCLUSION AND OUTLOOK

NPF1 was found to be much less sensitive to H_2O_2 than **CPF1** that had been used in previous chapters. The benefit from **NPF1** competing with less autofluorescent background

does not compensate for the greater than 20-fold loss in relative to **CPF1**. Therefore, **NPF1** should not be used for detection of H_2O_2 in solution or on optical fibre tips.

NCR3 was effective at reversibly detecting H_2O_2 on an optical fibre tip. This fibre tip functionalised with **NCR3** showed potential as a re-useable optical sensor for H_2O_2. However, the apparent diffusion of **NCR3** from the polyacrylamide matrix into the buffer solution limits its use as a re-usable H_2O_2 sensor. Further improvements to this system could include the addition of a hydrophobic group to **NCR3** in order to anchor the compound within the polymer network. The suggested modification should hence produce a re-usable, reversible sensor for H_2O_2.

6.5 EXPERIMENTAL

6.5.1 Materials

All chemicals were purchased from Sigma-Aldrich unless otherwise stated. Bis(acrylamide) was purchased from Polysciences (Warrington, PA). 200 µm core diameter multimode fibre was purchased from Thorlabs (USA). α-MEM bovine IVF medium was prepared using VitroFert from IVF Vet Solutions (Adelaide, Australia); 4 mg/ml fatty acid free BSA (ICPBio Ltd; Auckland, New Zealand); 10 IU/ml heparin, 25 µM penicillamine, 12.5 µM hypotaurine and 1.25 µM epinephrine.

6.5.2 Synthesis

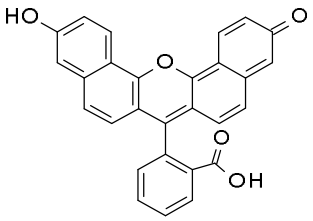

Modification of a literature procedure.[95] Dihydroxynaphthelene (3.2 g, 20.0 mmol) and phthalic anhydride (1.48 g, 10.0 mmol) were suspended in methanesulfonic acid (25 mL) under N_2 atmosphere. The mixture was heated to 135 °C for 48 h, then cooled and poured into an ice/water slurry (250 mL). The crude product was then eluted through a silica column with 5 % DCM in methanol to afford a red solid, **naphthofluorescein** (450 mg, 11 %) **^{1}HNMR** ($CDCl_3$, 300MHz): δ(ppm) 10.15 (s, 2H), 8.69 (d, 2H, J = 9 Hz), 8.09 (dd, 1H, J_1 = 6.3 Hz, 2.7 Hz), 7.78-7.74 (m, 2H), 7.45 (d, 2H, J = 8.7 Hz), 7.35 (dd, 2H, J_1 = 9.0 Hz, J_2 = 2.4 Hz), 7.31 (dd, 1H, J_1 = 5.4 Hz, J_2 = 3 Hz), 7.20 (d, 2H, J = 2.7 Hz), 6.70 (d, 2H, J = 8.7 Hz).

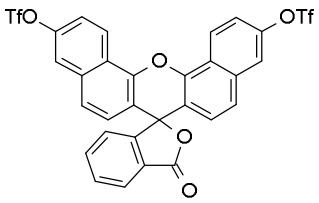

Modification of a literature procedure.[95] **Naphthofluorescein** (217 mg, 0.5 mmol) was dissolved in anhydrous DMF (3 mL) and DIPEA (495.9 µL, 3.0 mmol) was added dropwise whilst stirring. N-phenyl-bis(triflate) in anhydrous DMF (3 mL) was added dropwise over 5 min, the reaction was then stirred for 24 h. Diluted with ethyl acetate (100 mL), washed with water (2 x 50 mL), then brine (50 mL), was dried on Na_2SO_4 and the solvent was removed *in vacuo*. The sample was then eluted through a silica column with neat DCM as eluent to yield the desired off-white solid **42**. (205 mg, 59 %) **^{1}HNMR** ($CDCl_3$, 300MHz): δ(ppm) 8.77 (d, 2H, J = 9.6 Hz), 8.16 (d, 1H, J = 6.6 Hz), 7.71-7.64 (m, 5H), 7.55 (dd, 2H, J_1 = 9.3 Hz, J_2 = 2.4 Hz), 7.40 (d, 2H, J = 8.7 Hz), 7.03 (d, 1H, J = 6.9 Hz), 6.82 (d, 2H, J = 8.7 Hz).

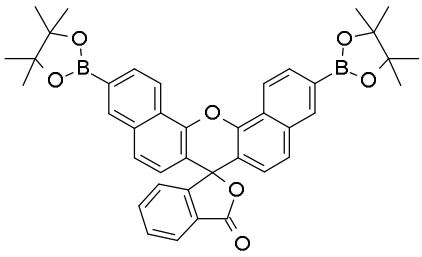

Modification of a literature procedure. **42** (160 mg, 0.23 mmol), Pd(dppf)Cl_2•CH_2Cl_2 (57 mg, 0.072 mmol), dppf (38.7 mg, 0.072 mmol), potassium acetate (228.5 mg, 2.33 mmol) and bis(pinacolato)diboron (295 mg, 1.17 mmol) were dried overnight under vacuum. Under a nitrogen atmosphere, 1,4-dioxane (10 mL) was added dropwise by cannula, and reaction mixture was stirred at 100 °C for 24 h. The solvent was removed *in vacuo* and the sample was eluted through a silica column using neat DCM as eluent. The resultant light yellow solid was then triturated with diethyl ether (3x3 mL) to give the desired bone-white solid **NPF1**. (122 mg, 81 %) **^{1}HNMR** ($CDCl_3$, 300MHz): δ(ppm) 8.76 (2H, d, J=8.4Hz), 8.37 (2H, s), 8.16-8.08 (3H, m), 7.69-7.61 (2H, m), 7.57 (2H, d, J=8.4Hz), 7.17-7.12 (1H, m), 6.86 (2H, d, J=9.0Hz).

6.5.3 Fluorescence Assay

The response of **NPF1** and **CPF1** to H_2O_2 was compared using a Cary Eclipse Fluorescence Spectrometer. **NPF1** and **CPF1** were each dissolved in DMSO to a concentration of 2 mM, then diluted to a final concentrations of 10 µM in separate α-MEM buffer solutions. H_2O_2 was

added to give final concentrations of either 0, 1, 20, 40, 50, 60 and 100 μM. Fluorescence spectra were measured after 40 min of incubation at 37°C.

6.5.3.1 Polyacrylamide Photopolymerisation on Optical Fibre Tips

A solution of 3-(trimethoxysilyl)propyl methacrylate in pH 3.5 adjusted Milli-Q water was mixed and sonicated until clear. Multi-mode fibre (200 μm diameter) was cut to length and the end face was cleaved in order to provide a clean surface, then immersed in the methacrylate solution for 1 h. The fibre tip was then dried under N_2, rinsed with Milli-Q water and dried under N_2 again. The distal end of the fibre was then coupled into the fibre setup shown in **Figure 61** below. A monomeric stock solution comprising of 3% bisacrylamide, 27% acrylamide and 70% pH 6.5 phosphate buffer solution was dissolved under sonication. **NCR3** (0.2 mg) was dissolved in the monomeric solution (400 μL) with triethylamine (10 μL) and 200 μL of this was pipetted into a small Eppendorf tube. The functionalised fibre tip was immediately immersed in this solution, and irradiated under 405 nm light for 2s to form a polymeric coating on the fibre tip.

6.5.4 Fibre Setup

A schematic of the optical setup is shown in **Figure 61**, for both photopolymerisation of the polymer using the 405 nm source, and optical measurements using the 473 nm source.

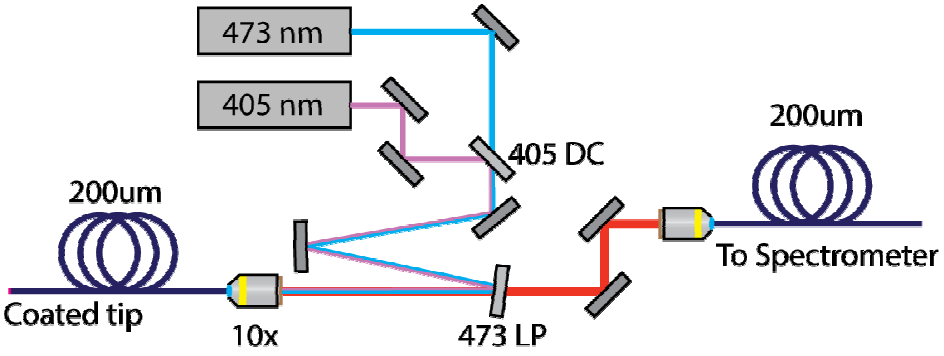

Figure 61. Experimental configuration for photopolymerisation, and optical measurements.

For excitation of the fluorophore for both direct attached and polymer embedded methods, the 473 nm laser (Toptica iBeam Smart) was coupled into the distal end of the probe fibre, with the 405 nm arm blocked. The coupled laser light then excites the fluorophore-doped probe tip, and a portion of this fluorescent light is then captured into a back-propagating mode in the fibre. This then passes through a 473 nm long-pass filter (Semrock EdgeBasic) to remove excess pump light, before being coupled into a spectrometer (Horiba iHR320) via a 200 μm optical fibre patch cable.

The same experimental configuration was used to induce photopolymerisation on the fibre tips, with the 473 nm path blocked, and a timed shutter used on the 405 nm source to control the deposition time of the polymer.

6.5.5 NCR3 Oxidation and Reduction on Fibre Tips

Fibres tips were functionalised with **NCR3** and coupled into excitation sources and detectors as above. The fibre tip was dipped into a solution of H_2O_2 (1 mM in pH 7.4 phosphate buffer) for 2 min, then removed and air dried for 2 min. The emission spectrum was recorded in air, and the fibre tip inserted into a pH 7.4 phosphate buffer for 2 min. The fibre tip was removed from solution, air dried for 2 min, and the fluorescence spectrum recorded. The fibre tip was then dipped into a solution of $NaCNBH_3$ (1 mM in pH 7.4 phosphate buffer) for 2 min, then removed from solution and air dried for a further 2 min. The fluorescence was recorded, and the fibre was again washed in pH 7.4 buffer as above. This process of oxidation and reduction of the fluorophore in H_2O_2 and $NaCNBH_3$ was repeated to give a total of seven cycles.

6.6 REFERENCES

30. Lippert, A. R.; Van de Bittner, G. C.; Chang, C. J. Boronate Oxidation as a Bioorthogonal Reaction Approach for Studying the Chemistry of Hydrogen Peroxide in Living Systems. *Accounts of Chemical Research* **2011,** *44* (9), 793-804.
83. Yeow, J.; Kaur, A.; Anscomb, M. D.; New, E. J. A novel flavin derivative reveals the impact of glucose on oxidative stress in adipocytes. *Chemical communications* **2014,** *50* (60), 8181-8184.
84. Kaur, A.; Haghighatbin, M. A.; Hogan, C. F.; New, E. J. A FRET-based ratiometric redox probe for detecting oxidative stress by confocal microscopy, FLIM and flow cytometry. *Chemical communications* **2015,** *51* (52), 10510-10513.
95. Albers, A. E.; Dickinson, B. C.; Miller, E. W.; Chang, C. J. A red-emitting naphthofluorescein-based fluorescent probe for selective detection of hydrogen peroxide in living cells. *Bioorganic & Medicinal Chemistry Letters* **2008,** *18* (22), 5948-5950.
179. Dumollard, R.; Ward, Z.; Carroll, J.; Duchen, M. R. Regulation of redox metabolism in the mouse oocyte and embryo. *Development* **2007,** *134* (3), 455-465.
180. Smith, C. A.; Pollice, A.; Emlet, D.; Shackney, S. E. A simple correction for cell autofluorescence for multiparameter cell-based analysis of human solid tumors. *Cytometry Part B: Clinical Cytometry* **2006,** *70B* (2), 91-103.
181. Lord, S. J.; Conley, N. R.; Lee, H.-l. D.; Nishimura, S. Y.; Pomerantz, A. K.; Willets, K. A.; Lu, Z.; Wang, H.; Liu, N.; Samuel, R.; Weber, R.; Semyonov, A.; He, M.; Twieg, R. J.; Moerner, W. E. DCDHF Fluorophores for Single-Molecule Imaging in Cells. *ChemPhysChem* **2009,** *10* (1), 55-65.
182. Müller, L.; Gocke, E. The rise and fall of photomutagenesis. *Mutation Research/Reviews in Mutation Research* **2013,** *752* (2), 67-71.
183. Kaur, A.; New, E. J. Unpublished Work. University of Sydney: 2015.

Chapter 7

APPLICATIONS AND CONCLUSIONS

One never notices what has been done; one can only see what remains to be done.

Marie Curie

Chapter 7: Applications and Conclusions

7.1 APPLICATIONS

Thus far in this thesis I have reported only the work undertaken that addresses the development of hydrogen peroxide sensors for reproductive health, as outlined in **Chapter 1**. However, I have applied the described research in broader contexts with collaborators in the disciplines of optics, oncology, geology, embryology and andrology. These applications arise from compounds, ideas or technology written within this thesis.

7.1.1 pH Sensor for Tumour Margin Detection

pH probes (such as in **Chapter 4**) have uses in other biological environments and as medical diagnostics. For example, tumours have a lower pH than the surrounding healthy tissue. Detection of this pH margin, however, is frustrated by the high autofluorescence from the tissue. A "lift-off" method for an optical pH probe was developed with collaborators Dr. Erik Schartner and Dr. Matt Henderson*. This allowed the pH probe to detect tumour margins and avoid the autofluorescence of the tissue by lifting the probe off the sample before recording the fluorescence spectrum (**Figure 62**). Rationalisation of the effectiveness of this "lift-off" method was provided by the author. This implication from use of the "lift-off" is that the dual pH and H_2O_2 probe (**Chapter 4**) could also be used for detection of pH and H_2O_2 in such applications.

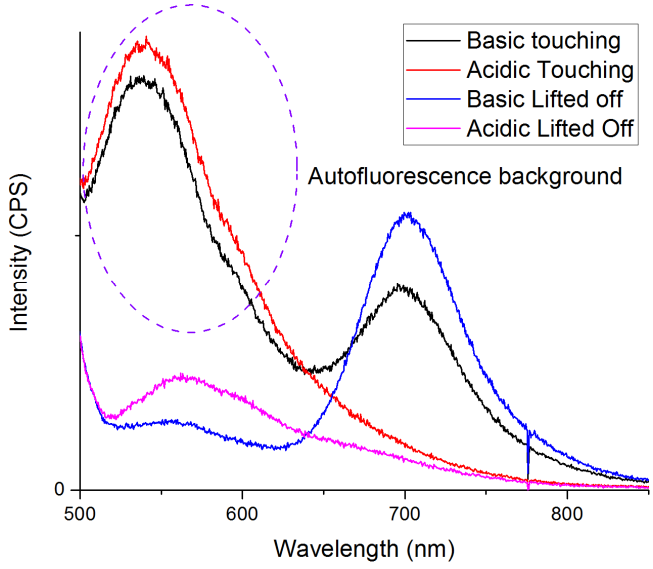

Figure 62. Demonstration of the lift-off method to remove the autofluorescence background. The fluorescence spectrum of a pH probe is shown in acidic and basic solutions, both before and after lifting the probe off the sample.

* Schartner, E. P.; Henderson, M. R.; Purdey, M. S., Dhatrak, D.; Monro, T. M.; Gill, P. G.; Callen, D. F., Tumour detection in human tissue samples using a fibre tip pH probe. **2016**, *In preparation*.

7.1.2 Detection of Redox States and Oxidative Stress in Bovine Oocytes

Samples of **PF1** (**Chapter 2**) synthesised by the author have been used to identify oxidative stress in oocytes. For example, a study was undertake of cumulus oocyte complexes that were treated with bone morphogenic protein 15 and follicle stimulating hormone to assess the effect of each on NADPH production (see **Appendix 1**)[†]. NADPH is a reducing agent, therefore the redox state of the cell was examined by imaging the reduced glutathione and H_2O_2 levels (**Figure 63**). This study found that stimulation with follicle stimulating hormone alone showed a decrease in the ability of the oocyte to regulate oxidative stress. Another study examined the role of non-esterified fatty acids in oxidative stress of endoplasmic reticulum[‡]. **PF1** was again used to detect H_2O_2 production within the cell. This work using bovine oocytes was performed in collaboration with Dr. Melanie Sutton-McDowall and Assoc. Prof. Jeremy Thompson in the Robinson Research Institute.

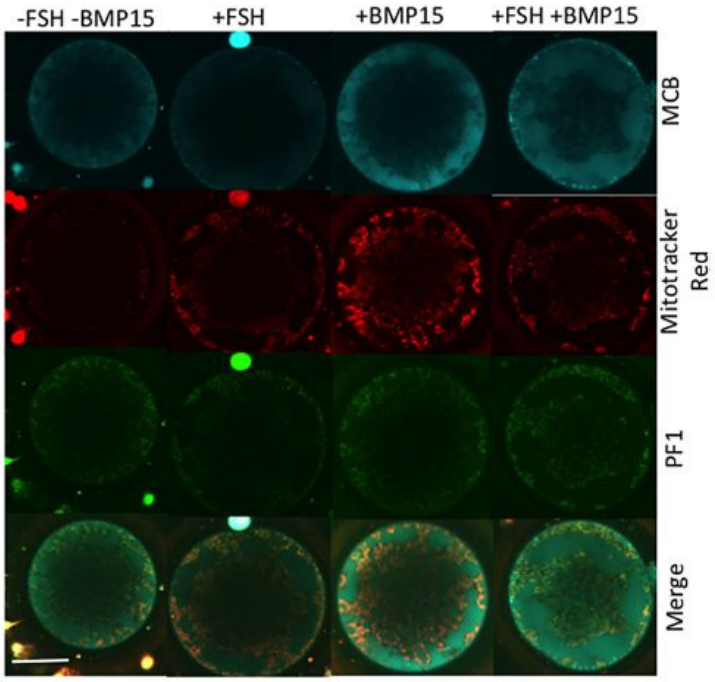

Figure 63. Oocytes with different treatments of follicle stimulated hormone and bone morphogenic protein 15. **PF1** indicates H_2O_2 production, mitrotracker red shows the location of the mitochondria, and MCB is a reduced glutathione probe.

[†] Sutton-McDowall, M. L.; Purdey, M. S.; Brown, H. M.; Abell, A. D.; Mottershead, D. G.; Cetica, P. D.; Dalvit, G. C.; Goldys, E. M.; Gilchrist, R. B.; Gardner, D. K.; Thompson, J. G., Redox and anti-oxidant state within cattle oocytes following in vitro maturation with bone morphogenetic protein 15 and follicle stimulating hormone. *Molecular Reproduction and Development* **2015,** *82* (4), 281-294

[‡] Sutton-McDowall, M. L.; Wu, L.; Purdey, M.; Brown, H. M.; Abell, A. D.; Goldys, E. M.; MacMillan, K. L.; Robker, R. L.; Thompson, J. G., Non-Esterified Fatty Acid-Induced Endoplasmic Reticulum Stress in Cattle Cumulus Oocyte Complexes Alters Cell Metabolism and Developmental Competence. *Biology of Reproduction* **2015**, *Available online*, doi:10.1095/biolreprod.115.131862.

7.1.3 Hydrogen Peroxide Monitoring in Spermatozoa

PF1 and **EEPF1** (**Chapter 2**) are continuing to be utilised in human spermatozoa by ongoing collaboration with Dr. Mariana Neves under the supervision of Prof. John Aitken at the University of Newcastle. This project aims to monitor H_2O_2 production in sperm (e.g. **Figure 64**) with respect to mitochondrial ROS production and characterise this relationship in healthy sperm. Furthermore, factors present in the female reproductive tract such as cytokines will be explored for their role in sustained H_2O_2 release during capacitation of spermatozoa. Other trials in spermatozoa will examine the capacitation of equine sperm cells to increase the success rate for equine *in vitro* fertilisation (IVF).

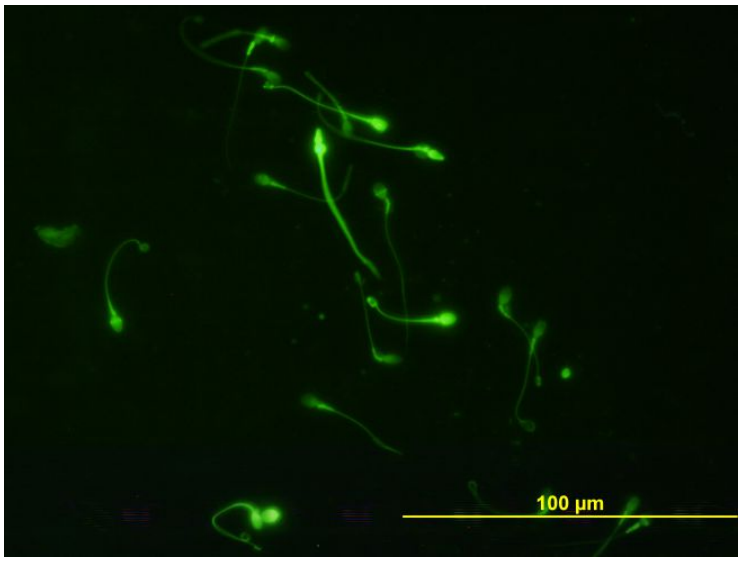

Figure 64. Sperm incubated with **EEPF1** fluoresce to reveal oxidative stress.

7.1.4 Detection of Gold Nanoparticles for Mining Industry

Another area of interest is the detection of gold nanoparticles. This is extremely important in the mining industry as new techniques for nanoparticle detection are required to explore underground gold deposits. The author thus synthesised a diiodo-BODIPY probe (**I-BODIPY**) for gold nanoparticles. **I-BODIPY** is similar in structure to the fluorophores peroxyBODIPY-1 (**PB1**) and nitrobenzoylBODIPY (**NbzB**) reported in **Chapter 5**. The fluorescent response of **I-BODIPY** to gold nanoparticles was then tested by Dr. Agnieszka Zuber in cuvette and microstructured optical fibres. This method using **I-BODIPY** was found to improve upon previously known detection limits[§]. The author would also like to

[§] Zuber, A.; Purdey, M.; Schartner, E.; Forbes, C.; van der Hoek, B.; Giles, D.; Abell, A.; Ebendorff-Heidepriem, H., Detection of gold nanoparticles with different sizes using absorption and fluorescence based method. *Sensors and Actuators B: Chemical* **2016**, *227*, 117-127.

Australian patent application 2015902890 – "Detection of Gold Nanoparticles" (Deep Exploration Technologies CRC Limited) – 21 July 2015

acknowledge that this work was supported by the Deep Exploration Technologies Cooperative Research Centre whose activities are funded by the Australian Government's Cooperative Research Centre Program.

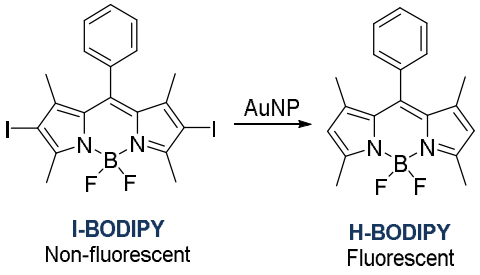

Figure 65. Reaction of non-fluorescent **I-BODIPY** with gold nanoparticles to form the fluorescent **H-BODIPY**.

7.2 CONCLUSIONS

This thesis has presented a range of work on the detection of hydrogen peroxide (H_2O_2) for reproductive health. H_2O_2 is fundamental to biological processes such as oxidative stress and embryo development. The examined literature summarised the chemistry of fluorescent probes for H_2O_2 and outlined the physics of non-invasive optical fibre probes.

Three aryl boronates, [peroxyfluor-1 (**PF1**), carboxyperoxyfluor-1 (**CPF1**) and a novel probe 2-ethoxy(2-ethoxyethoxy)peroxyfluor-1 (**EEPF1**)] were synthesised, and detected H_2O_2 in artificially stimulated and poor quality human spermatozoa. These aryl boronates were shown to be more effective than commercially available probes in this biological system. Furthermore, **PF1** detected H_2O_2 in bovine oocytes, indicating the redox state of the cumulus oocyte complex. Aryl boronate and benzil-based borondipyrromethene (**BODIPY**) probes were synthesised and compared, with aryl boronate peroxyBODIPY-1 (**PB1**) showing a greater fluorescent response to H_2O_2 than nitrobenzoylBODIPY (**NbzB**). Thus the aryl boronates selected for use throughout this thesis were more sensitive to H_2O_2 than benzil counterparts. A red emitting fluorophore, naphthoperoxyfluor-1 (**NPF1**) was also examined to address autofluorescence within biological environments. However, **NPF1** was found to be insufficiently sensitive for H_2O_2, thus the other aryl boronates such as **CPF1** were suggested for use in preference to **NPF1**.

CPF1 attached to glass confocal microscope dishes was characterised by confocal microscopy and typhoon imaging. This model system indicated that **CPF1** detected H_2O_2 effectively on a glass surface as per in solution. The light-catalysed formation of a polyacrylamide matrix was found to be the most effective method for functionalising **CPF1** to optical fibre tips. This produced a functional tip probe for H_2O_2. This work was expanded by functionalising fibre tips with **CPF1** and seminaphthorhodofluor-2 (**SNARF2**) to give a fibre tip probe for H_2O_2 and pH. The probe detected H_2O_2 at biologically relevant concentrations

and reproducibly sensed pH 6.5-8.4, suggesting this probe would be useful for non-invasive detection of H_2O_2 and pH near embryos. Furthermore, this study revealed the importance of combining H_2O_2 and pH sensing, as accurate detection of H_2O_2 is affected by the pH of the solution. The described "lift-off" method for pH detection of tumour margins also suggested this dual probe could find applications in other biological environments. Finally, a reversible fibre tip sensor for H_2O_2 was explored by functionalising a redox probe, nicotinamide coumarin redox sensor 3 (**NCR3**) onto an optical fibre tip. The fibre tip sensor was shown to detect multiple cycles of oxidation and reduction. However, the fluorescence intensity was reduced over time due to leaching of **NCR3** from the polymer on the fibre tip. This first example of a reversible H_2O_2 fibre probe shows promise for the use of redox probes to construct a re-useable optical sensor for H_2O_2.

In conclusion, aryl boronates **PF1**, **CPF1**, **PB1**, **NbzB** and **EEPF1** were used effectively in reproductive biology. **CPF1** was then used to create an optical fibre tip probe for H_2O_2, and this was combined with the pH sensor **SNARF2** to give the first example of a dual probe for H_2O_2 and pH. These outcomes are promising for the non-invasive detection of H_2O_2 in reproductive biology. Moreover, this research achieved the goal set by the industry partners, Cook Medical, to create an optical fibre probe for H_2O_2 that could be used within an embryo incubator. This would allow real-time monitoring of H_2O_2 near human embryos in order to improve embryo health and potentially better clinical outcomes for patients undergoing IVF.

Appendices

There's a way to do it better – find it.

Thomas Edison

Appendix 1: Free Radical Biology and Medicine Paper

Free Radical Biology and Medicine 81 (2015) 69–76

Contents lists available at ScienceDirect

Free Radical Biology and Medicine

journal homepage: www.elsevier.com/locate/freeradbiomed

Original Contribution

Boronate probes for the detection of hydrogen peroxide release from human spermatozoa

Malcolm S. Purdey [a], Haley S. Connaughton [b], Sara Whiting [b], Erik P. Schartner [a], Tanya M. Monro [a], Jeremy G. Thompson [c], R. John Aitken [b,*], Andrew D. Abell [a,*]

[a] ARC Centre of Excellence for Nanoscale BioPhotonics, Institute for Photonics & Advanced Sensing, and School of Physical Sciences, The University of Adelaide, Adelaide, SA 5005, Australia

[b] Discipline of Biological Sciences and Priority Research Centre in Reproductive Science, Faculty of Science and IT, University of Newcastle, Callaghan, NSW 2308, Australia

[c] ARC Centre of Excellence for Nanoscale BioPhotonics, The Robinson Research Institute, and School of Paediatrics and Reproductive Health, The University of Adelaide, Adelaide, SA 5005, Australia

ARTICLE INFO

Article history:
Received 4 September 2014
Received in revised form
23 December 2014
Accepted 13 January 2015
Available online 30 January 2015

Keywords:
Hydrogen peroxide
Reactive oxygen species
Human spermatozoa
Organic synthesis
Aryl boronate
Free radicals

ABSTRACT

Human spermatozoa are compromised by production of reactive oxygen species (ROS), and detection of ROS in spermatozoa is important for the diagnosis of male infertility. The probes 2′,7′-dichlorohydrofluorescein diacetate (DCFH), dihydroethidium (DHE), and MitoSOX red (MSR) are commonly used for detecting ROS by flow cytometry; however, these probes lack sensitivity to hydrogen peroxide (H_2O_2), which is particularly damaging to mammalian sperm cells. This study reports the synthesis and use of three aryl boronate probes, peroxyfluor-1 (PF1), carboxyperoxyfluor-1, and a novel probe, 2-(2-ethoxyethoxy)ethoxyperoxyfluor-1 (EEPF1), in human spermatozoa. PF1 and EEPF1 were effective at detecting H_2O_2 and peroxynitrite ($ONOO^-$) produced by spermatozoa when stimulated with menadione or 4-hydroxynonenal. EEPF1 was more effective at detection of ROS in spermatozoa than DCFH, DHE, or MSR; furthermore it distinguished poorly motile sperm as shown by greater ROS production. EEPF1 should therefore have a significant role in the diagnosis of oxidative stress in male infertility, cryopreservation, age, lifestyle, and exposure to environmental toxicants.

Reactive oxygen species (ROS) produced by human spermatozoa compromise sperm function [1–5], and as such their detection is important for the diagnosis of male infertility [6]. ROS are typically detected in human spermatozoa using fluorescent probes such as dihydroethidium (DHE), MitoSOX red (MSR), and 2′,7′-dichlorohydrofluorescein diacetate (DCFH) (Fig. 1) [7]. DHE is an intracellular ROS probe that fluoresces within both the head and the mitochondrial midsection of the spermatozoon upon oxidation. It is most commonly used for detection of superoxide ($O_2^{\bullet-}$), although it also reacts with hydrogen peroxide (H_2O_2) in the presence of peroxidases and with oxidases and cytochromes [8]. MSR is a charged variant of DHE that localizes in the mitochondrial matrix to predominantly respond to and measure the generation of $O_2^{\bullet-}$. DCFH is a fluorescein-based nonspecific probe that reportedly reacts with H_2O_2 [9] and other ROS, particularly hydroxyl radicals ($^{\bullet}OH$) and peroxynitrite ($ONOO^-$) [10]. This probe has some disadvantages, because it requires the concomitant presence of peroxidases to react with H_2O_2 [11], can undergo autoxidation, and is known to catalyze $O_2^{\bullet-}$ production [9]. An aryl boronate probe reported by Chang et al. [12], peroxyfluor-1 (PF1), reacts with both H_2O_2 and $ONOO^-$, but not $^{\bullet}OH$, $O_2^{\bullet-}$, nitric oxide (NO), or hypochlorite (^-OCl) [12,13]. This class of probe has found wide use in the in vivo detection of H_2O_2 [14], including research into ROS production in cryopreserved mouse spermatozoa [15]. The ability of aryl boronates to detect the low levels of ROS generated by mammalian spermatozoa suggests this class of probe as a potential diagnostic tool for the selective detection of ROS, particularly H_2O_2 in sperm cells. This would be of clinical significance as several independent studies have indicated that H_2O_2 is particularly damaging to mammalian sperm function [16–18].

A number of aryl boronates have been developed for use in a range of biological applications [14]. We chose to use PF1, carboxy-PF1 (CPF1), and a new probe, 2-(2-ethoxyethoxy)ethoxy-PF1 (EEPF1), for the study as they are structurally similar, to allow for direct and meaningful comparison, while being relatively easy to prepare on both small and larger scales. This is an important consideration for future work in this area. CPF1 is a variant of PF1

* Corresponding authors.
E-mail addresses: john.aitken@newcastle.edu.au (R.J. Aitken), andrew.abell@adelaide.edu.au (A.D. Abell).

http://dx.doi.org/10.1016/j.freeradbiomed.2015.01.015
0891-5849/

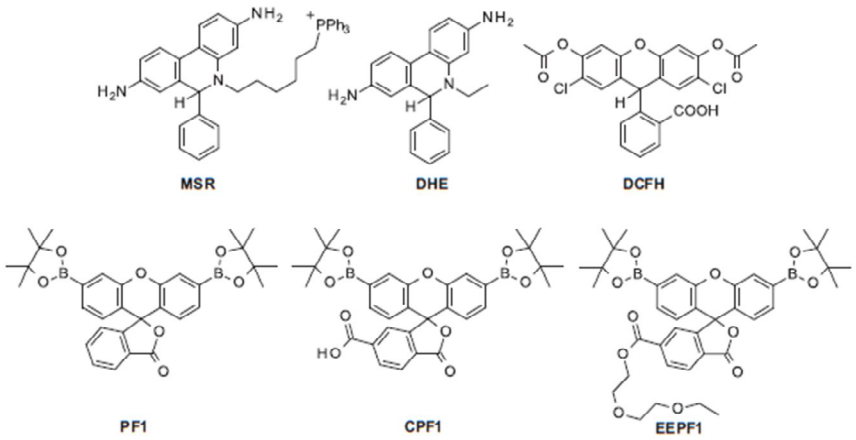

Fig. 1. Chemical structures of the ROS sensors used in this study. MSR, DHE, and DCFH are oxidized by removal of the indicated hydrogens to produce a fluorescent aromatic structure. PF1, CPF1, and EEPF1 are oxidized by the deprotection of the pinacolatoboron groups to produce highly fluorescent structures.

originally synthesized for attachment to other functional groups [19,20]. EEPF1 contains a truncated polyethylene glycol (PEG) group with increased hydrogen bond acceptors to enhance the aqueous solubility relative to PF1. A series of comparative studies were performed to define the relative ability of all three probes to detect ROS generation by human spermatozoa in a sensitive and selective manner. This study examines the relative capacities of these probes to detect H_2O_2 and $ONOO^-$ spontaneously generated by human spermatozoa exhibiting impaired motility. The results have important diagnostic implications for the facilitated detection of oxidative stress in mammalian spermatozoa exhibiting signs of impaired functionality.

Materials and methods

Materials

Unless otherwise stated all chemicals were purchased from Sigma Aldrich. *N*-(3-dimethylaminopropyl)-*N′*-ethylcarbodiimide hydrochloride (EDC-HCl) was obtained from GL Biochem (Shanghai). 4-Hydroxynonenal (4HNE) was from Sapphire Biosciences; MitoSOX red, dihydroethidium, and Live/Dead fixable FAR red stain were from Life Technologies. 2′,7′-Dichlorofluorescein diacetate was from Molecular Probes. Freshly prepared Biggers, Whitten, and Whittingham (BWW) medium was used for all experiments, supplemented with 1 mg/ml polyvinyl alcohol (PVA), 5 units/ml penicillin, and 5 mg/ml streptomycin, and the osmolarity was kept between 290 and 310 mOsm/kg [21].

Semen samples

The University of Newcastle Human Ethics Committee and the NSW State Minister for Health approved the use of semen samples for research. A cohort of unselected, normozoospermic donors, mainly university students of unknown fertility status, supplied semen samples for this study. Semen samples were produced into a sterile container and delivered to the laboratory within 1 h of ejaculation.

Sample preparation

Spermatozoa were isolated by discontinuous Percoll gradient centrifugation using a simple two-step design incorporating 44 and 88% Percoll as described previously [22]. Purified spermatozoa were recovered and washed with Hepes-buffered BWW medium supplemented with 1 mg/ml PVA [21], centrifuged at 500*g* for 5 min, and resuspended at a concentration of 2×10^7 cells/ml.

Leukocyte removal

Where indicated, all residual traces of leukocyte contamination in the sperm suspensions were removed using magnetic beads (Dynabeads, Dynal, Oslo, Norway) coated with a monoclonal antibody against the common leukocyte antigen CD45 (Invitrogen, Carlsbad, CA, USA). After Percoll isolation, 5×10^6 cells in 100 μl BWW medium were added to prewashed antibody-bound Dynabeads and then placed on a rotor for 30 min. After incubation, each sample was placed in a magnetic holder to separate leukocyte-bound Dynabeads from purified sperm cells in BWW medium. Luminol-peroxidase-mediated chemiluminescence was then used to confirm the removal of leukocytes from each sperm suspension; for this purpose 20 μl of zymosan opsonized with autologous serum was added to each 400-μl sample, 5 min after the beginning of the luminometry run [7].

Treatments

Spermatozoa were treated with menadione (0–50 μM), arachidonic acid (AA; 0–50 μM), and H_2O_2 (0–4 mM) for 15 min at 37 °C. Treatments with 4HNE (0–400 μM) were for 30 min at 37 °C. Stock solutions of menadione were made up fresh daily in dimethyl sulfoxide (DMSO), with a minimum dilution of 1/100 in BWW medium before being added to spermatozoa.

Staining

After spermatozoa were treated they were incubated with PF1, CPF1, and EEPF1 for 30 min at 37 °C at a final concentration of 10 μM. Stock solutions were made up using DMSO at a concentration of 10 mM.

Flow cytometry

A FACS-Canto flow cytometer (Becton–Dickinson) was employed using a 488-nm argon laser coupled with emission measurements using the 530/30 band pass (green) FITC channel. Ten thousand sperm events were recorded after nonsperm events

were gated out. Data were analyzed using BD Diva software (Becton–Dickinson).

Statistical analysis

All graphed results are expressed as the mean ± standard error of the mean. Experiments were replicated at least three times with independent samples. Data were then analyzed by one-way analysis of variance using GraphPad Prism 6, followed by post hoc comparison by Fisher's least significant difference test.

ROS selectivity study

Solutions of PF1, CPF1, EEPF1, and DCFH in 20 mM Hepes buffer at pH 7.4 were treated with 100 μM ROS: H_2O_2, $ONOO^-$, ^-OCl, $^{\bullet}OH$, $O_2^{\bullet-}$, NO, and *tert*-butylhydroperoxide (TBHP). A stock solution of approximately 100 mM H_2O_2 in Milli-Q water was prepared from a 30% H_2O_2 solution in water and the exact concentration was determined by UV absorption at 240 nm (ε_{240}=43.6 M^{-1} cm^{-1}) using a Cary UV–Vis–NIR 5000 spectrophotometer. A stock solution of NaOCl was similarly prepared and the ^-OCl concentration determined by UV absorption at 292 nm (ε_{292}=350 M^{-1} cm^{-1}). A solution of $ONOO^-$ was prepared by a known method [23], and its concentration was determined using UV absorption at 302 nm (ε_{302}=1670 M^{-1} cm^{-1}). $^{\bullet}OH$ was produced by the Fenton reaction of 100 μM H_2O_2 with 1 mM $FeClO_4$. $O_2^{\bullet-}$ was also produced by a known method [24], using a xanthine/xanthine oxidase system for the production of $O_2^{\bullet-}$ and catalase as a scavenger for any H_2O_2 produced. NO was generated from *S*-nitrosoglutathione, and TBHP was diluted from a stock solution. The ROS were added to each probe and the fluorescence was monitored using a Biotek Synergy H4 fluorescence plate reader (excitation 450 nm, emission 520 nm) over 40 min.

Fluorescence controls for menadione, AA, and 4HNE

Solutions of PF1, CPF1, and EEPF1 in BWW medium were treated with menadione (0–50 μM), arachidonic acid (0–50 μM), or 4-hydroxynonenal (0–400 μM) to give a final probe concentration of 10 μM. Samples were incubated for 15 min (30 min for 4HNE) at 37 °C, then fluorescence emission was quantified using a Fluostar Optima (BMG Labtech), with settings of excitation filter 485 ± 10 nm and emission filter at 520 nm.

Synthesis

PF1 was prepared as described [12] using microwave irradiation in place of conventional heating: 3′,6′-diiodofluoran [12] (89 mg, 0.16 mmol), bis(pinacolato)diboron (160 mg, 0.63 mmol), potassium acetate (141 mg, 0.63 mmol), and $Pd(dppf)Cl_2$ (14 mg, 0.02 mmol), predried in vacuo, were dissolved in DMF (4 ml) under N_2 atmosphere in a sealed microwave vial fitted with a Teflon cap. The light brown mixture was reacted in a CEM Discover microwave synthesizer (Matthews, NC, USA) at 80 °C for 2 h. The solvent was removed under reduced pressure to give a dark brown powder, which was purified by column chromatography eluting with 4:1 hexane:ethyl acetate to give PF1 as a white solid (40 mg, 45%). The sample was characterized by 300-MHz proton nuclear magnetic resonance spectroscopy (^{1}H NMR) in deuterated chloroform. ^{1}H NMR: δ 8.03 (1H, m), 7.74 (2H, s), 7.60 (2H, m), 7.43 (2H, dd, J_1=7.8 Hz, J_2=1.1 Hz), 7.06 (1H, m), 6.86 (2H, d, J=7.8 Hz), 1.35 (24H, s).

CPF1 [19] was similarly prepared: 3′,6′-diiodo-6-carboxyfluoran pyridinium salt [25] (109 mg, 0.16 mmol), bis(pinacolato)diboron (160 mg, 0.63 mmol), potassium acetate (142 mg, 0.63 mmol), and $Pd(dppf)Cl_2$ (13.9 mg, 0.017 mmol) were dissolved in dry DMF (4 ml) in an anhydrous N_2 atmosphere. The resultant solution was reacted in a microwave vial sealed with a Teflon cap at 100 °C for 3 h in a CEM Discover microwave synthesizer. The solution was evaporated under reduced pressure to give a dark brown powder, which was purified by flash column chromatography eluting with neat ethyl acetate to give CPF1 as a light brown solid (55 mg, 58%). The sample was similarly characterized. ^{1}H NMR ($CDCl_3$, 300 MHz): δ 8.29 (dd, 1H, J_1=7.8 Hz, J_2=1.4 Hz), 8.11 (d, 1H, J=7.8 Hz), 7.79–7.73 (m, 3H), 7.43 (dd, 2H, J_1=7.8 Hz, J_2=1.1 Hz), 6.81 (d, 2H, J=7.8 Hz), 1.35 (s, 24 H).

EEPF1 was prepared as follows: CPF1 (50 mg, 0.08 mmol), *N*-hydroxysuccinimide (11 mg, 0.08 mmol), and EDC-HCl (26 mg, 0.13 mmol) were added to DMF (1 ml) in a dry N_2 glove box and stirred for 1 h. 2-(2-Ethoxyethoxy)ethanol (23 μl, 0.17 mmol) in dry DMF (0.5 ml) was added and the solution stirred for a further 2 h. The solvent was removed under reduced pressure, and the resultant solid was purified by column chromatography eluting with ethyl acetate to give EEPF1 as a white powder (28 mg, 47%). The sample was similarly characterized by ^{1}H NMR ($CDCl_3$, 500 MHz): δ 8.28 (1H, dd, J_1=8.0 Hz, J_2=1.0 Hz), 8.09 (1H, d, J_1=8.0 Hz), 7.76 (2H, s), 7.71 (1 H, s), 7.44 (2H, d, J_1=8.0 Hz), 6.82 (2H, d, J=7.5 Hz), 4.42 (2H, t, J=4.5 Hz), 3.76 (2H, t, J=4 Hz), 3.61 (2H, t, J=2.75), 3.52 (2H, t, J=4.5 Hz), 3.45 (2H, q, J=7 Hz), 1.35 (24H, s), 1.14 (3H, t, J=7 Hz). This new boronate probe was also characterized by 125-MHz carbon 13 nuclear magnetic resonance spectroscopy (^{13}C NMR) and high-resolution mass spectrometry (HRMS). ^{13}C NMR ($CDCl_3$, 125 MHz): δ 168.6, 164.9, 154.0, 150.5, 136.5, 131.2, 130.0, 129.7, 129.4, 129.0, 128.8, 126.9, 125.3, 125.1, 123.8, 120.5, 84.2, 70.6, 69.8, 68.9, 64.8, 24.9, 15.1. HRMS: calcd, 712.3226; found, 712.3237. The synthesis of CPF1 and EEPF1 is shown in Scheme 1.

Results and discussion

ROS characterization of probes

The sensitivity of EEPF1 to H_2O_2 was defined by incubating separate samples with 0–100 μM H_2O_2 and monitoring the resultant fluorescence (see Fig. 2A). A clear, dose-dependent response is evident, with an emission maximum at 525 nm. EEPF1 was also incubated with each individual ROS at 100 μM to determine the selectivity of EEPF1 for various ROS, and the reactivity profiles are summarized in Fig. 2B. For comparison, the reaction of DCFH with each ROS was also characterized and the results are shown in Fig. 2C. Similar reactivity profiles for PF1 and CPF1 are reported in the supplementary material. EEPF1 showed good reactivity with H_2O_2, and although there was a significant initial fluorescence response from $ONOO^-$, a greater overall fluorescence was observed for H_2O_2 over 40 min. This is probably due to the more transient nature of $ONOO^-$ compared with H_2O_2. Limited fluorescence was observed for the reaction of EEPF1 with all other ROS studied, with a similar result for the other aryl boronates (Supplementary Fig. S1). By contrast, DCFH reacts best with both $ONOO^-$ and $^{\bullet}OH$ (Fig. 2C) and to a lesser extent with ^-OCl and $O_2^{\bullet-}$, but not H_2O_2, as shown in Fig. 2C. This lack of reactivity to H_2O_2 is consistent with some literature [10], but contrasts with other reports that infer the detection of H_2O_2 using this probe [9]. However, DCFH is able to detect other ROS, such as $^{\bullet}OH$ produced from H_2O_2 in vivo and also H_2O_2 in the presence of peroxidases [11]. Thus, the aryl boronates have a clear advantage over DCFH for the detection of H_2O_2 in the absence of any external catalyst.

Comparative study on ROS production in human spermatozoa

The ability of the aryl boronates PF1, CPF1, and EEPF1 and other probes described in the literature (the dihydrofluorescein DCFH

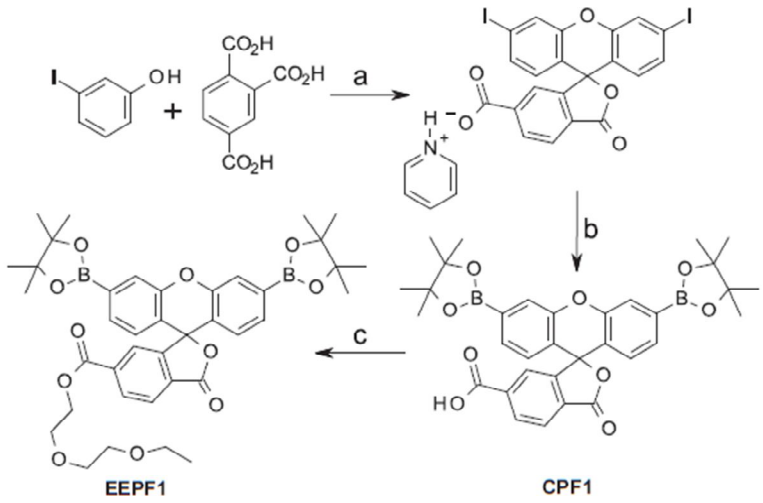

Scheme 1. Synthesis of CPF1 and EEPF1. (a) $MeSO_3H$, 140 °C, 72 h; then recrystallization 2:1 acetic anhydride:pyridine [25]. (b) Bis(pinacolato)diboron, $Pd(dppf)Cl_2$, KOAc, DMF, mic. synth., 100 °C, 3 h. (c) *N*-hydroxysuccinimide, EDC-HCl, DMF, 1 h; then 2-(2-ethoxyethoxy)ethanol, 2 h.

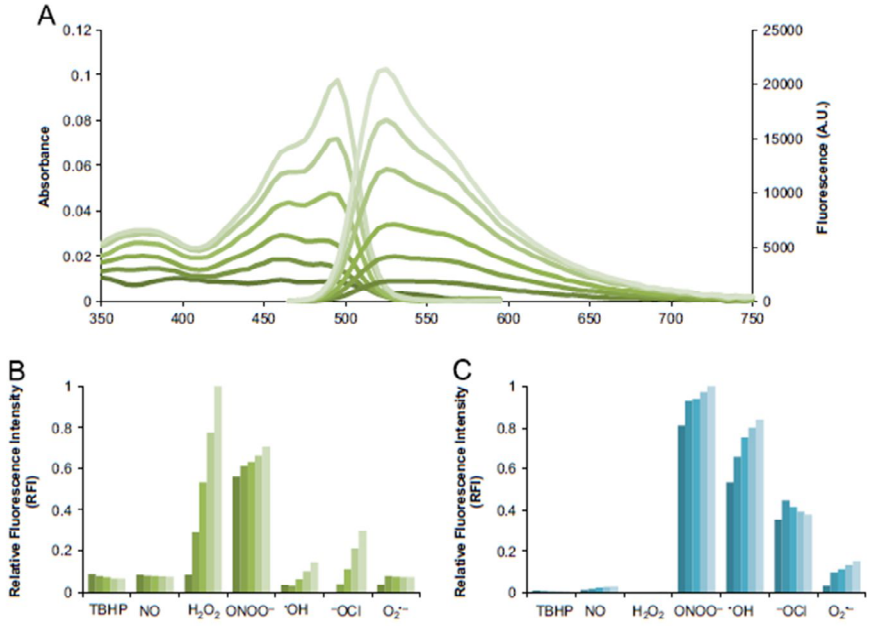

Fig. 2. Fluorescence characterization of EEPF1 and comparison with DCFH for selectivity to ROS. (A) Absorption and emission spectra of EEPF1 when treated with 0, 10, 25, 50, 75, and 100 μM H_2O_2 and incubated at 37 °C for 40 min in 20 mM Hepes buffer (excitation at 450 nm). (B) EEPF1 and (C) DCFH selectivity data, each incubated at 37 °C with 100 μM ROS and measured at 0, 10, 20, 30, and 40 min (excitation 450 nm, emission 520 nm).

and the hydroethidiums DHE and MSR) to detect ROS in spermatozoa was then studied in populations of human spermatozoa, with a view to defining their relative abilities to detect cellular ROS generation. ROS production in human spermatozoa was induced by treating samples with three different compounds, menadione, AA, and 4HNE [7]. Menadione is a redox-cycling quinone known to produce significant oxidative stress due to quinone oxidoreductase activity [26,27]. AA is a *cis*-unsaturated fatty acid associated with the production of $O_2^{\cdot-}$ by sperm mitochondria [28,29], and 4HNE is a lipid-derived aldehyde responsible for the induction of mitochondrial ROS generation in senescent spermatozoa [30]. Further samples were also treated with 4 mM H_2O_2 as a positive control for probes sensitive to H_2O_2 (DCFH, PF1, CPF1, EEPF1). The ROS-producing compounds were incubated separately with each probe (DCFH, DHE, MSR, PF1, CPF1, and EEPF1) and the resulting fluorescence response was measured by flow cytometry.

Fig. 3 shows the percentage of fluorescent spermatozoa, indicating the percentage of spermatozoa that generated ROS as measured by each probe. MSR showed the largest background fluorescence in the negative control samples (Fig. 3A), with

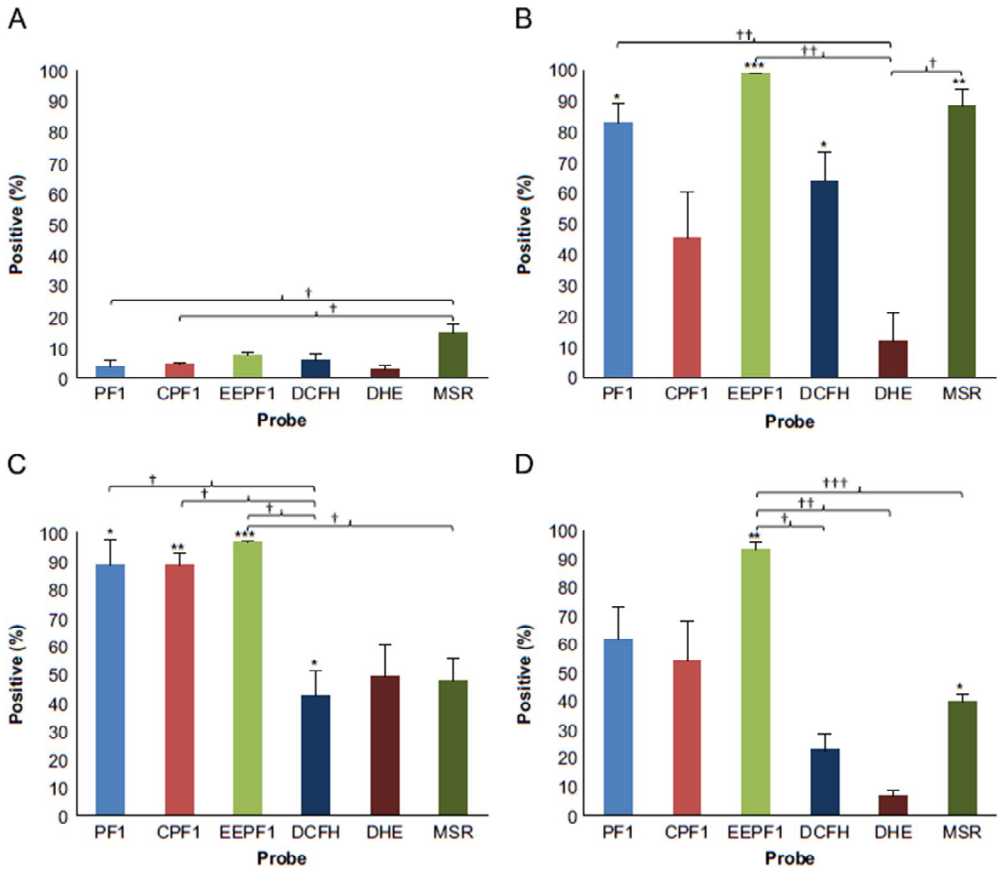

Fig. 3. Analysis of flow cytometry results, showing the percentage of human sperm populations that indicated a fluorescent response. (A) Negative control sample with no external stimulus. Samples exposed to stimuli: (B) 50 μM menadione for 15 min, (C) 50 μM AA for 15 min, and (D) 200 μM 4HNE for 30 min. Significance levels: $^{*}P<0.05$, $^{**}P<0.01$, $^{***}P<0.001$ compared with untreated sample. †$P<0.05$, ††$P<0.01$, †††$P<0.001$ compared on graph.

significantly higher fluorescent populations ($P<0.05$) than aryl boronates PF1 and CPF1, presumably reflecting the active generation of mitochondrial ROS by populations of human spermatozoa, as previously described [31]. For the treated sperm samples, those incubated with DHE exhibited the smallest fluorescent populations for all stimuli (Fig. 3B–D). Conversely, those stained with EEPF1 consistently showed the largest fluorescent populations, with over 90% responding positively after treatment with the ROS-generating reagents (Fig. 3B–D). PF1 also showed readily measurable fluorescent responses to the stimuli, with comparable or larger fluorescent populations than DCFH, DHE, and MSR (Fig. 3B–D). Staining spermatozoa with CPF1 gave the lowest fluorescent populations of all three aryl boronates. Nevertheless, treated sperm were more fluorescent with CPF1 than with DHE and DCFH within the sperm groups treated with AA (Fig. 3C) and 4HNE (Fig. 3D).

Thus the aryl boronates PF1 and EEPF1 were the most broadly sensitive of the probes to ROS produced by spermatozoa on stimulation with menadione, AA, and 4HNE (Fig. 3B–D), with the latter clearly being the most sensitive. The third aryl boronate (CPF1), although sensitive, gave less consistent results. Of the other probes, MSR gave the greatest response to each stimulus (Fig. 3B–D), and DHE was the least sensitive.

The fluorescent populations shown in Fig. 3 also provide some insights into which ROS are produced by spermatozoa on treatment with menadione and 4HNE (results for AA are discussed separately, see Fig. 4). Thus for samples stained with MSR, a smaller proportion of fluorescent cells was apparent for 4HNE treatments (Fig. 3D) compared to menadione (Fig. 3B), suggesting that the latter is the more efficient stimulator of $O_2^{\bullet-}$ production. In contrast, fluorescence of the aryl boronates PF1, CPF1, and EEPF1 were similar between menadione and 4HNE treatments (Fig. 3B and D), indicating similar levels of H_2O_2/$ONOO^-$ production. This suggests an efficient conversion of $O_2^{\bullet-}$ (detected by MSR) to H_2O_2

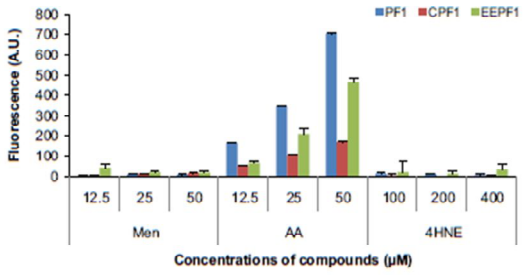

Fig. 4. Fluorescence response of PF1, CPF1, and EEPF1 to menadione, AA, and 4HNE in the absence of spermatozoa. Fluorescence readings were recorded in BWW solution after 30 min of incubation at 37 °C by a microplate reader. Excitation wavelength was 485 nm, emission recorded at 520 nm. Each probe gave a dose-dependent response upon exposure to AA; however, no significant response was recorded when incubated with either menadione or 4HNE.

or $ONOO^-$ (detected by the aryl boronates) in those samples treated with 4HNE. However, similar to MSR, DCFH showed a lack of sensitivity for the ROS produced in response to 4HNE (Fig. 3D) compared with the menadione (Fig. 3B) treatments. Yet DCFH is also known to react with H_2O_2 and $ONOO^-$, as do the aryl boronates, suggesting that DCFH should have similar sensitivities to the 4HNE and the menadione treatments. This incongruity could be due to the production of $^{\bullet}OH$ in samples treated with menadione and not those treated with 4HNE. The $^{\bullet}OH$ radical reacts with DCFH but not with the aryl boronates, which would result in the more positive populations observed for DCFH in samples treated with menadione than with 4HNE (Fig. 3B and D). Another likely explanation is the need for oxidation of DCFH to be facilitated by peroxidase, which may not be trivial owing to the highly compartmentalized nature of the spermatozoon, limiting the distribution and hence the catalytic availability of the peroxidase. This again highlights the significant advantage of the aryl boronates over DCFH in this regard, as no external catalysis is required to produce a fluorescent response.

We next investigated the fluorescence of PF1, CPF1, and EEPF1 on incubation with menadione, AA, and 4HNE in the absence of spermatozoa, to directly assess the reactivity of the probes to these compounds. Menadione (12.5, 25, 50 μM), AA (12.5, 25, 50 μM), and 4HNE (100, 200, 400 μM) were separately incubated with PF1, CPF1, and EEPF1 and the resulting fluorescence was measured. A fluorescent response was not observed when PF1, CPF1, or EEPF1 was incubated with menadione or 4HNE (see Fig. 4). However, AA did cause a dose-dependent response with PF1 ($r=0.9999$), CPF1 ($r=0.9898$), and EEPF1 (0.9994), as shown in Fig. 4. This is possibly due to autoxidation of AA, generating a hydroperoxide [32] capable of deprotecting the aryl boronates of the probes, thus leading to a fluorescent response. This may explain the observed increase in fluorescent population for PF1, CPF1, and EEPF1 in the presence of AA compared to those populations stained with DCFH, DHE, and MSR. AA was not used to induce ROS production in further experiments using spermatozoa with PF1, CPF1, and EEPF1.

Sensitivity of aryl boronates to ROS production in human spermatozoa

Dose-dependent studies were subsequently carried out to further define the sensitivity of the three new aryl boronates PF1, CPF1, and EEPF1 in spermatozoa stimulated with menadione, 4HNE, and H_2O_2. Diphenylene iodonium (DPI), an inhibitor of NO and $O_2^{\bullet-}$ production by flavoproteins, was used to further test the sensitivity of the probes for ROS generation.

Menadione

Populations of spermatozoa treated with menadione and incubated with EEPF1 show the largest fluorescent populations (see Fig. 5A). This result is consistent with the earlier study comparing the aryl boronates to previously studied probes, in which EEPF1 gave the greatest fluorescent response of the six probes as shown in Fig. 3. However, the populations stained with EEPF1 (Fig. 5A) were over 90% positive at even the lowest concentration of menadione (12.5 μM), significantly larger than with PF1 ($P<0.05$). Populations stained with PF1 also revealed a dose-dependent increase in activity when treated with 12.5–50 μM menadione (Fig. 5A, $r=0.937$). In contrast, the fluorescent responses of populations stained with CPF1 were not statistically significant even at 50 μM menadione (Fig. 5A). Thus it appears that the new probe EEPF1 is the most effective of the probes for ROS production in spermatozoa on stimulation with menadione. The existing aryl boronate PF1 is significantly less effective, and CPF1 is the least effective of all three. Microscope images of spermatozoa stained with CPF1 and EEPF1 were obtained (see supplementary material). ROS produced by both the head and the mitochondria-rich midpiece can be seen, indicating that neither CPF1 nor EEPF1 stained specifically for a location inside the cell.

Co-incubation of DPI with 50 μM menadione did not significantly decrease the positive population for EEPF1 and, although suggested, no statistically significant reduction in signal was recorded in the presence of PF1 and CPF1 (Fig. 5A) when treated with DPI. Overall, incubation with menadione indicated greater sensitivity of EEPF1 over PF1 and CPF1, suggesting that it may be a particularly useful probe for the detection of intracellular ROS.

4HNE

Fig. 5B shows the fluorescent responses for spermatozoa treated with 4HNE. Samples stained with PF1 or EEPF1 revealed significant fluorescent populations at 100, 200, and 400 μM treatments with 4HNE. However, those samples incubated with CPF1 did not produce a significant fluorescent response as a consequence of the large variation associated with these measurements. The signal generated in the presence of PF1 was significantly reduced ($P<0.05$) in the presence of DPI. However, incubating with DPI did not reduce the fluorescent response for samples treated with EEPF1, again suggesting an increased efficacy over PF1. From these results it is clear that both PF1 and EEPF1 were capable of detecting significant H_2O_2 or $ONOO^-$ production by 4HNE-stimulated spermatozoa.

H_2O_2

EEPF1 gave the greatest fluorescent response to ROS in populations of spermatozoa treated with H_2O_2 (see Fig. 5C). These fluorescent populations correlated with the concentration of H_2O_2 added ($r=0.946$, $P<0.01$). Fig. 5C also shows that in contrast, samples stained with PF1 gave only a limited increase in positivity at 250 and 500 μM H_2O_2, whereas CPF1 generated a negligible fluorescence response, even for samples treated with up to 500 μM H_2O_2. These results again indicate a greater efficacy of EEPF1 over PF1 and CPF1 for the detection of ROS produced by human spermatozoa stimulated with H_2O_2.

The mechanism by which H_2O_2 stimulates enhanced ROS generation by human spermatozoa is thought to involve the induction of lipid peroxidation followed by the covalent binding of lipid aldehydes such as 4HNE to proteins in the mitochondrial electron transport chain (ETC), particularly, succinic acid dehydrogenase [23]. The adduction of proteins within the ETC is, in turn, thought to lead to electron leakage and sustained ROS generation. The fact that DPI, an inhibitor of flavoproteins involved in mitochondrial electron transport such as succinic acid dehydrogenase, could significantly impair the ROS response to H_2O_2 as detected by EEPF1 is in good agreement with this model.

In light of these results, EEPF1 is clearly able to sense ROS produced by human spermatozoa more effectively than PF1, CPF1, DCFH, DHE, or MSR. Hence, we suggest that EEPF1 should be used in preference to DCFH, DHE, or PF1, particularly for detection of low concentrations (0–100 μM) of H_2O_2 or $ONOO^-$ in human spermatozoa.

The different fluorescent responses of PF1, CPF1, and EEPF1 to ROS produced by spermatozoa (Figs. 3 and 5) also provide some preliminary insights into structure–activity relationships for the aryl boronate class of probe. CPF1 consistently detected lower numbers of reactive spermatozoa than PF1 and EEPF1. As fluorescein-based probes are susceptible to photobleaching, 10 μM solutions of CPF1 and PF1 were irradiated with a 100-mW 488-nm argon laser to ensure that the cause of differing fluorescent responses was not photobleaching. CPF1 and PF1 showed comparable rates of photobleaching; as such, the reduced CPF1

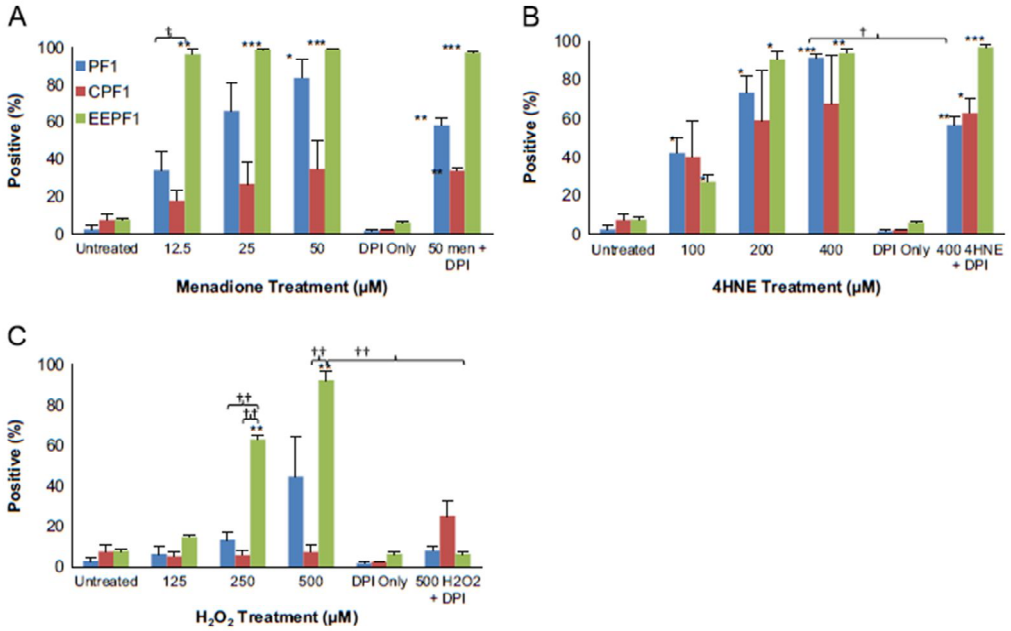

Fig. 5. Analysis of flow cytometry results for menadione-, 4HNE-, and H_2O_2-treated spermatozoa. (A) Menadione-treated spermatozoa exhibit dose–response correlation with PF1 and CPF1; however, EEPF1 shows large positive populations to 12.5, 25, and 50 μM treatments. (B) PF1, CPF1, and EEPF1 all exhibit dose–response correlations to sperm stimulated with 4HNE. (C) EEPF1 shows a dose–response correlation to spermatozoa treated with H_2O_2 concentrations of 0–500 μM. Significance levels: $^*P<0.05$, $^{**}P<0.01$, $^{***}P<0.001$ compared with untreated sample. $\dagger P<0.05$, $\dagger\dagger P<0.01$ compared on graph.

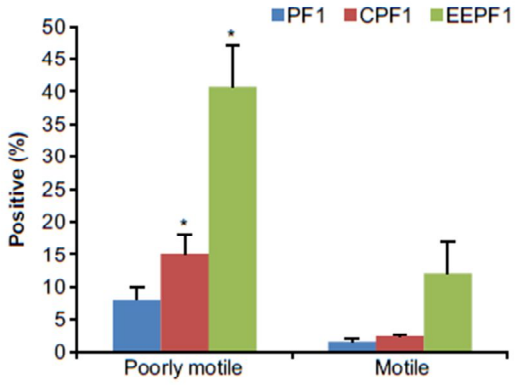

Fig. 6. Analysis of flow cytometry results showing the percentage of poorly motile and motile samples of human spermatozoa populations indicating a fluorescent response. EEPF1 provides a greater fluorescent response to the ROS produced in poorly motile sperm. Significance level relative to motile sample: $^*P<0.05$.

positive populations observed in Fig. 5 are not the results of differences in rates of photobleaching. However, for spermatozoa to be analyzed by flow cytometry, the probe must be able to cross the plasma membrane to react with intracellular ROS and generate a fluorescent signal. It is therefore likely that the impaired cellular uptake of CPF1 is responsible for its lack of activity. Any localized fluctuation in pH would affect the ionization of the carboxyl group of CPF1, which would, in turn, be expected to influence cell permeability and hence the intracellular concentration of this probe. By contrast, EEPF1 is esterified with a truncated PEG (see Scheme 1) so it would be expected to possess a higher capacity for intracellular penetration. Furthermore, hydrolysis of the PEG ester by intracellular esterases may enhance cellular retention of the active species, as reported for a similar aryl boronate probe, PF6-AM [33].

Spontaneous ROS generation by human spermatozoa

Finally, the use of PF1, CPF1, and EEPF1 to detect spontaneous ROS generation by human spermatozoa was investigated to validate the use of these probes for detecting the increased ROS production associated with poorly motile sperm. To this end, the spermatozoa were separated on discontinuous Percoll gradients into subpopulations exhibiting high and low levels of motility [7] (see Materials and methods for details). These sperm populations were then separately incubated with PF1, CPF1, or EEPF1. Fig. 6 clearly demonstrates the increased generation of ROS by poorly motile spermatozoa compared with their more motile counterparts. A relative increase in the proportion of ROS-generating cells was detected in the poorly motile cells with PF1, CPF1, and EEPF1. The largest increase was seen with EEPF1, which detected ROS generation in around 40% of the poorly motile cells compared with $<15\%$ with PF1 and CPF1. These results confirm EEPF1 as the most effective of these probes for the detection of released ROS in human spermatozoa. As such, EEPF1 is recommended for use as an intracellular probe for detection of ROS in human spermatozoa.

Conclusion

The aryl boronate probes discussed here react directly with H_2O_2 and therefore present a distinct advantage over DCFH, which we show to be insensitive to H_2O_2. PF1 and EEPF1 were also shown to be effective fluorescent probes for the detection of both H_2O_2 and $ONOO^-$ in human spermatozoa. Both PF1 and EEPF1 were significantly more effective at detection of ROS by flow cytometry compared to DCFH and DHE when stimulated using menadione and 4HNE. In particular, EEPF1 was the most effective of the

studied probes for externally stimulated and spontaneously generated ROS produced by human spermatozoa. This particular probe should therefore have a significant role to play in the diagnosis of oxidative stress in spermatozoa in the context of a variety of circumstances including spontaneous male infertility, cryopreservation, age, lifestyle, and exposure to environmental toxicants.

Acknowledgments

This research was supported in part by Cook Medical Pty Ltd and Australian Research Council Linkage Grant LP 110200736 and the ARC Centre of Excellence in Nanoscale BioPhotonics for the Adelaide laboratory and DP 110103951 in the case of Newcastle. T. M. acknowledges the support of an ARC Georgina Sweet Laureate Fellowship, FL130100044.

Appendix A. Supporting information

Supplementary data associated with this article can be found in the online version at http://dx.doi.org/10.1016/j.freeradbiomed.2015.01.015.

References

[1] Jones, R.; Mann, T.; Sherins, R. Peroxidative breakdown of phospholipids in human spermatozoa, spermicidal properties of fatty acid peroxides, and protective action of seminal plasma. *Fertil. Steril.* **31**:531–537; 1979.
[2] Aitken, R. J.; Clarkson, J. S. Cellular basis of defective sperm function and its association with the genesis of reactive oxygen species by human spermatozoa. *J. Reprod. Fertil.* **81**:459–469; 1987.
[3] Alvarez, J. G.; Touchstone, J. C.; Blasco, L.; Storey, B. T. Spontaneous lipid peroxidation and production of hydrogen peroxide and superoxide in human spermatozoa superoxide dismutase as major enzyme protectant against oxygen toxicity. *J. Androl.* **8**:338–348; 1987.
[4] Aitken, R. J.; Curry, B. J. Redox regulation of human sperm function: from the physiological control of sperm capacitation to the etiology of infertility and DNA damage in the germ line. *Antioxid. Redox Signaling* **14**:367–381; 2011.
[5] Gong, S.; Gabriel, M. C. S.; Zini, A.; Chan, P.; O'Flaherty, C. Low amounts and high thiol oxidation of peroxiredoxins in spermatozoa from infertile men. *J. Androl.* **33**:1342–1351; 2012.
[6] Aitken, R. J.; Iuliis, G.; Baker, M. Direct methods for the detection of reactive oxygen species in human semen samples. In: Agarwal, A., Aitken, R. J., Alvarez, J. G., editors. *Studies on Men's Health and Fertility*. Totowa (NJ): Humana Press; 2012. p. 275–299.
[7] Aitken, R. J.; Smith, T. B.; Lord, T.; Kuczera, L.; Koppers, A. J.; Naumovski, N.; Connaughton, H.; Baker, M. A.; De Iuliis, G. N. On methods for the detection of reactive oxygen species generation by human spermatozoa: analysis of the cellular responses to catechol oestrogen, lipid aldehyde, menadione and arachidonic acid. *Andrology* **1**:192–205; 2013.
[8] Robinson, K. M.; Janes, M. S.; Pehar, M.; Monette, J. S.; Ross, M. F.; Hagen, T. M.; Murphy, M. P.; Beckman, J. S. Selective fluorescent imaging of superoxide in vivo using ethidium-based probes. *Proc. Natl. Acad. Sci. USA* **103**:15038–15043; 2006.
[9] Murphy, M. P.; Holmgren, A.; Larsson, N. -G.; Halliwell, B.; Chang, C. J.; Kalyanaraman, B.; Rhee, S. G.; Thornalley, P. J.; Partridge, L.; Gems, D.; Nystroem, T.; Belousov, V.; Schumacker, P. T.; Winterbourn, C. C. Unraveling the biological roles of reactive oxygen species. *Cell Metab.* **13**:361–366; 2011.
[10] Setsukinai, K.; Urano, Y.; Kakinuma, K.; Majima, H. J.; Nagano, T. Development of novel fluorescence probes that can reliably detect reactive oxygen species and distinguish specific species. *J. Biol. Chem.* **278**:3170–3175; 2003.
[11] Myhre, O.; Andersen, J. M.; Aarnes, H.; Fonnum, F. Evaluation of the probes 2′,7′-dichlorofluorescin diacetate, luminol, and lucigenin as indicators of reactive species formation. *Biochem. Pharmacol.* **65**:1575–1582; 2003.
[12] Chang, M. C. Y.; Pralle, A.; Isacoff, E. Y.; Chang, C. J. A selective, cell-permeable optical probe for hydrogen peroxide in living cells. *J. Am. Chem. Soc.* **126**:15392–15393; 2004.
[13] Sikora, A.; Zielonka, J.; Lopez, M.; Joseph, J.; Kalyanaraman, B. Direct oxidation of boronates by peroxynitrite: mechanism and implications in fluorescence imaging of peroxynitrite. *Free Radic. Biol. Med.* **47**:1401–1407; 2009.
[14] Lippert, A. R.; Van de Bittner, G. C.; Chang, C. J. Boronate oxidation as a bioorthogonal reaction approach for studying the chemistry of hydrogen peroxide in living systems. *Acc. Chem. Res.* **44**:793–804; 2011.
[15] Gray, J. E.; Starmer, J.; Lin, V. S.; Dickinson, B. C.; Magnuson, T. Mitochondrial hydrogen peroxide and defective cholesterol efflux prevent in vitro fertilization by cryopreserved inbred mouse sperm. *Biol. Reprod.* **89**:17; 2013.
[16] Aitken, R. J.; Buckingham, D.; Harkiss, D. Use of a xanthine oxidase free radical generating system to investigate the cytotoxic effects of reactive oxygen species on human spermatozoa. *J. Reprod. Fertil.* **97**:441–450; 1993.
[17] Armstrong, J. S.; Rajasekaran, M.; Chamulitrat, W.; Gatti, P.; Hellstrom, W. J.; Sikka, S. C. Characterization of reactive oxygen species induced effects on human spermatozoa movement and energy metabolism. *Free Radic. Biol. Med.* **26**:869–880; 1999.
[18] Baumber, J.; Ball, B. A.; Gravance, C. G.; Medina, V.; Davies-Morel, M. C. G. The effect of reactive oxygen species on equine sperm motility, viability, acrosomal integrity, mitochondrial membrane potential, and membrane lipid peroxidation. *J. Androl.* **21**:895–902; 2000.
[19] Srikun, D.; Albers, A. E.; Chang, C. J. A dendrimer-based platform for simultaneous dual fluorescence imaging of hydrogen peroxide and pH gradients produced in living cells. *Chem. Sci* **2**:1156–1165; 2011.
[20] He, F.; Tang, Y.; Yu, M.; Wang, S.; Li, Y.; Zhu, D. Fluorescence-amplifying detection of hydrogen peroxide with cationic conjugated polymers, and its application to glucose sensing. *Adv. Funct. Mater.* **16**:91–94; 2006.
[21] Biggers, J.; Whitten, W. K.; Whittingham, D. G. The culture of mouse embryos in vitro. In: Daniel, J., editor. *Methods of Mammalian Embryology*. San Francisco: Freeman; 1971. p. 86–118.
[22] Aitken, R. J.; Harkiss, D.; Knox, W.; Paterson, M.; Irvine, D. S. A novel signal transduction cascade in capacitating human spermatozoa characterised by a redox-regulated, cAMP-mediated induction of tyrosine phosphorylation. *J. Cell Sci.* **111**:645–656; 1998.
[23] Hempel, S. L.; Buettner, G. R.; O'Malley, Y. Q.; Wessels, D. A.; Flaherty, D. M. Dihydrofluorescein diacetate is superior for detecting intracellular oxidants: comparison with 2′,7′-dichlorodihydrofluorescein diacetate, 5(and 6)-carboxy-2′,7′-dichlorodihydrofluorescein diacetate, and dihydrorhodamine 123. *Free Radic. Biol. Med.* **27**:146–159; 1999.
[24] Albers, A. E.; Dickinson, B. C.; Miller, E. W.; Chang, C. J. A red-emitting naphthofluorescein-based fluorescent probe for selective detection of hydrogen peroxide in living cells. *Bioorg. Med. Chem. Lett.* **18**:5948–5950; 2008.
[25] Albers, A. E.; Okreglak, V. S.; Chang, C. J. A FRET-based approach to ratiometric fluorescence detection of hydrogen peroxide. *J. Am. Chem. Soc.* **128**:9640–9641; 2006.
[26] Hughes, L. M.; Griffith, R.; Carey, A.; Butler, T.; Donne, S. W.; Beagley, K. W.; Aitken, R. J. The spermostatic and microbicidal actions of quinones and maleimides: toward a dual-purpose contraceptive agent. *Mol. Pharmacol.* **76**:113–124; 2009.
[27] Mitchell, L. A.; De Iuliis, G. N.; Aitken, R. J. The TUNEL assay consistently underestimating DNA damage in human spermatozoa and is influenced by DNA compaction and cell vitality: development of an improved methodology. *Int. J. Androl.* **34**:2–13; 2011.
[28] Aitken, R. J.; Wingate, J. K.; De Iuliis, G. N.; Koppers, A. J.; McLaughlin, E. A. Cis-unsaturated fatty acids stimulate reactive oxygen species generation and lipid peroxidation in human spermatozoa. *J. Clin. Endocrinol. Metab.* **91**:4154–4163; 2006.
[29] Koppers, A. J.; Garg, M. L.; Aitken, R. J. Stimulation of mitochondrial reactive oxygen species production by unesterified, unsaturated fatty acids in defective human spermatozoa. *Free Radic. Biol. Med.* **48**:112–119; 2010.
[30] Aitken, R. J.; Whiting, S.; De Iuliis, G. N.; McClymont, S.; Mitchell, L. A.; Baker, M. A. Electrophilic aldehydes generated by sperm metabolism activate mitochondrial reactive oxygen species generation and apoptosis by targeting succinate dehydrogenase. *J. Biol. Chem.* **287**:33048–33060; 2012.
[31] Koppers, A. J.; De Iuliis, G. N.; Finnie, J. M.; McLaughlin, E. A.; Aitken, R. J. Significance of mitochondrial reactive oxygen species in the generation of oxidative stress in spermatozoa. *J. Clin. Endocrinol. Metab.* **93**:3199–3207; 2008.
[32] Porter, N. A.; Wolf, R. A.; Yarbro, E. M.; Weenen, H. The autoxidation of arachidonic acid: formation of the proposed SRS-A intermediate. *Biochem. Biophys. Res. Commun.* **89**:1058–1064; 1979.
[33] Dickinson, B. C.; Peltier, J.; Stone, D.; Schaffer, D. V.; Chang, C. J. Nox2 redox signaling maintains essential cell populations in the brain. *Nat. Chem. Biol.* **7**:106–112; 2011.

Appendix 2: Sensors Paper

sensors

MDPI

Article

A Dual Sensor for pH and Hydrogen Peroxide Using Polymer-Coated Optical Fibre Tips

Malcolm S. Purdey [1,2,3,*], Jeremy G. Thompson [1,2,4], Tanya M. Monro [1,2,5], Andrew D. Abell [1,2,3] and Erik P. Schartner [1,2]

Received: 28 October 2015; Accepted: 11 December 2015; Published: 17 December 2015
Academic Editor: W. Rudolf Seitz

1 ARC Centre of Excellence for Nanoscale BioPhotonics, Adelaide 5005, SA, Australia; jeremy.thompson@adelaide.edu.au (J.G.T.); tanya.monro@unisa.edu.au (T.M.M.); andrew.abell@adelaide.edu.au (A.D.A.); erik.schartner@adelaide.edu.au (E.P.S.)
2 Institute for Photonics and Advanced Sensing (IPAS), The University of Adelaide, North Terrace, Adelaide 5005, SA, Australia
3 Discipline of Chemistry, School of Physical Sciences, The University of Adelaide, North Terrace, Adelaide 5005, SA, Australia
4 Robinson Research Institute, School of Medicine, The University of Adelaide, North Terrace, Adelaide 5005, SA, Australia
5 University of South Australia, North Terrace, Adelaide 5001, SA, Australia
* Correspondence: malcolm.purdey@adelaide.edu.au; Tel.: +61-883-132-390

Abstract: This paper demonstrates the first single optical fibre tip probe for concurrent detection of both hydrogen peroxide (H_2O_2) concentration and pH of a solution. The sensor is constructed by embedding two fluorophores: carboxyperoxyfluor-1 (CPF1) and seminaphtharhodafluor-2 (SNARF2) within a polymer matrix located on the tip of the optical fibre. The functionalised fibre probe reproducibly measures pH, and is able to accurately detect H_2O_2 over a biologically relevant concentration range. This sensor offers potential for non-invasive detection of pH and H_2O_2 in biological environments using a single optical fibre.

Keywords: optical fibre; hydrogen peroxide probe; pH sensor; dual sensor; fibre tip sensor

1. Introduction

Hydrogen peroxide (H_2O_2) and pH play vital combined roles in cellular signalling [1–3], tumour development [4–7] and reproductive health science [8–11]. For example, the unregulated production of H_2O_2 by an embryo is a hallmark of embryonic stress [12], while pH fluctuations during embryo culture can negatively affect embryonic development [13]. The simultaneous detection of pH and H_2O_2 would therefore provide significant benefit in monitoring the associated cellular processes. H_2O_2 and pH can be detected in cells by specific fluorophores, measuring either an increase in fluorescence intensity [14,15], or a change in emission spectra respectively [16,17]. However the use of these fluorescent probes in applications such as *in vitro* fertilisation (IVF) poses significant scientific and ethical questions, as their effect on the development of embryos is unknown. As such, direct contact of fluorophores with an embryo is ethically unsound and not allowable in most regulatory jurisdictions.

Optical fibre-based probes offer an attractive and non-invasive approach. Here a fluorophore of interest can be attached to the fibre surface for localised measurement without being released into the solution [18–20]. Various configurations of optical fibres have been examined for development of such fluorescent sensors, specifically; functionalized end-faces (tip sensors) [21,22], exposed core [23] and microstructured fibres [24,25]. Although microstructured fibre based sensors can be more

Sensors **2015**, *15*, 31904–31913

sensitive than tip sensors [26], filling of the air holes with analyte is required in order to perform a measurement. This typically restricts microstructured fibres to single temporal measurements, unless microfluidics or external flushing systems are employed, and these may impede on the cell culture environment. Exposed-core fibre sensors are ideal for environmental sensing and do not require microfluidics or external flushing and offer advantages in distributed sensing. However, tip-based sensors offer potential for temporal measurements in a single location rather than distributed along the length, or can be repositioned to obtain a spatial map of the sample as desired. Tip sensors often have reduced sensitivity compared to microstructured fibres [26], especially as conventional attachment of a single layer of fluorophore to a fibre tip results in a low signal intensity [27]. However, the signal intensity can be improved by increasing the density of fluorophore on the fibre tip.

H_2O_2 can be detected by aryl boronate-based fluorophores such as peroxyfluor-1 (PF1) [28] and carboxyPF1 (CPF1, Figure 1) [29]. These aryl boronates have been shown as particularly effective fluorescent probes for detection of H_2O_2 in human spermatozoa and bovine oocytes [29,30]. pH can be detected using a range of fluorophores, with seminaphthorhodofluor-2 (SNARF2, Figure 1) offering some advantages over alternative probes, as the ratiometric emission from this probes changes its spectral features over the physiological pH range, with a pK_a of 7.5 [31]. This minimises potential errors which could arise from using a solely intensity-based probe. Additionally, its emission spectrum overlaps minimally with the emission of CPF1 [32], allowing the separate interrogation of each fluorophore.

This paper reports the first dual probe for sensing pH and the detection of H_2O_2 by immobilising two separate fluorophores (CPF1 and SNARF-2) onto a single optical fibre tip in a polyacrylamide matrix. The two fluorophores are attached to a multi-mode fibre tip by a light-catalysed polymer coating [33], to allow for greater control of fluorophore surface density and thus subsequent signal intensity. This then allows detection of both H_2O_2 and pH within a single system.

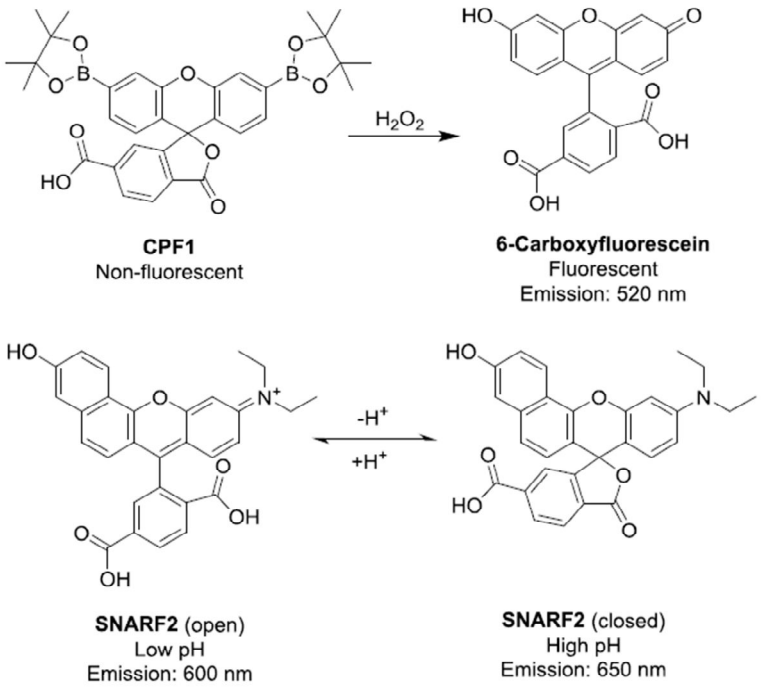

Figure 1. Chemical structures of fluorescent probes used in this study. Carboxyperoxyfluor-1 (CPF1) reacts with H_2O_2 to form the fluorescent 6-carboxyfluorescein. Seminaphthorhodofluor-2 (SNARF2) is found in the protonated (open) form and lactone (closed) at low and high pH respectively.

Sensors **2015**, *15*, 31904–31913

2. Experimental Section

2.1. Materials

All chemicals were purchased from Sigma-Aldrich unless otherwise stated. Bis(acrylamide) was purchased from Polysciences (Warrington, PA, USA). HPLC grade acetonitrile was purchased from Scharlau. 100 mM Phosphate buffer solutions were prepared from monosodium phosphate and disodium phosphate in Milli-Q water. Multimode fibre (200 µm core diameter, FG200UCC) was purchased from Thorlabs (Newton, NJ, USA), with one end connectorised for attachment to the optical setup.

2.2. Polyacrylamide Photo-Polymerisation on Optical Fibre Tips

A solution of 3-(trimethoxysilyl)propyl methacrylate (5 µL) in 10% acetic acid solution (30 µL) and ethanol (1 mL) was mixed and sonicated until clear. Multi-mode fibre was cleaved and each segment immersed in the methacrylate solution for 1 h. The fibre tip was then dried under N_2, rinsed with Milli-Q water and re-dried under N_2. The distal end of the fibre was coupled into a 405 nm source (Crystalaser 405 nm) using a 10× microscope objective. A monomeric stock solution comprising of 3% bisacrylamide, 27% acrylamide and 70% pH 6.5 phosphate buffer solution was dissolved under sonication. CPF1-NHS (0.2 mg), and SNARF2-NHS (0.2 mg) were added to this solution (400 µL) and 200 µL of the resulting solution was pipetted into a small Eppendorf tube. Triethylamine (10 µL/mL) was added to the mixture, and the fibre tip was immersed in this solution exactly 60 s after addition of the triethylamine and immediately irradiated under 405 nm light for 10 s at 13.4 mW, to form a polymeric coating on the fibre tip.

2.3. Optical Measurements

The experimental configuration used for optical measurements is shown in Figure 2 below.

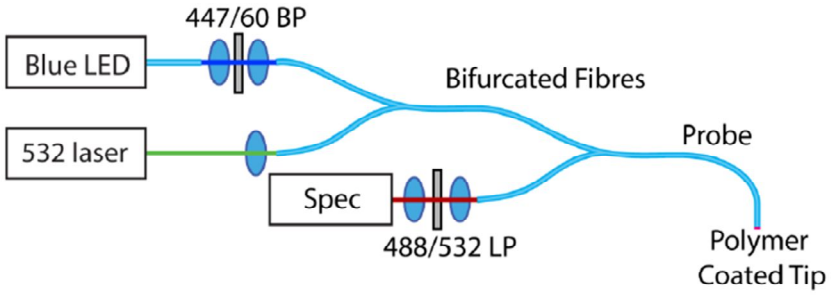

Figure 2. Experimental configuration for optical measurements of the combined pH/peroxide sensor. The blue LED source was used to illuminate the peroxide sensitive carboxyperoxyfluor-1 (CPF1) fluorophore, while the green excites the pH sensitive seminaphtharhodafluor-2 (SNARF).

A 470 nm blue LED source (Thorlabs M470F1, Newton, NJ, USA) with an appropriate bandpass filter (Semrock Brightline 447/60, Rochester, NY, USA) was coupled into one input of a bifurcated fibre (Ocean Optics 200 µm, UV/VIS). Attached CPF1 was then excited with light from a 532 nm green laser (Crystalaser 25 mW, Reno, NV, USA) coupled into the other input for excitation of the SNARF. An additional bifurcated fibre was used to connect the excitation sources to the sensing fibre, with the remaining input connected to the input of the spectrometer (Horiba iHR550, Synapse detector, Kyoto, Japan). Long-pass filters were inserted directly into the spectrometer input cage, with 488 nm (Semrock 488 nm Edgebasic) and 532 nm (Semrock 532 nm Razoredge) used for peroxide and pH respectively.

The two excitation channels were controlled independently, with only one excitation wavelength used at any particular time to excite either the peroxide or pH channel. The corresponding emission

Sensors **2015**, *15*, 31904–31913

filter was used with each excitation source to attenuate residual pump light from the fibres. The use of connectorised fibres and multi-mode fibres greatly simplifies the measurement procedure, as no adjustments or realignment are required when swapping between pH and peroxide measurements.

3. Results and Discussion

3.1. Hydrogen Peroxide Detection

3.1.1. Detection of Biologically Relevant H_2O_2 Concentrations

CPF1 and SNARF2 immobilised on fibre tips were tested in solutions containing H_2O_2 to establish the sensitivity of this surface configuration. Fibre tips were first functionalised with 3-(trimethoxysilyl)propyl methacrylate, then dipped into a solution of acrylamide/bisacrylamide with N-hydroxysuccinimide esters of CPF1 and SNARF2. The N-succinimide esters of CPF1 and SNARF2 increase solubility in the acrylamide solution to provide a more reproducible density of fluorophores embedded in the polymer matrix. Excitation light (405 nm) was coupled into the distal end of the fibre and the tip irradiated for 10 s to form a polymer layer on the tip containing the fluorophores. The functionalised fibres were dipped into a range of concentrations of H_2O_2 (0, 50, 75 and 100 μM) in pH 7.5 phosphate buffer, and the emission peaks from CPF1 at 520 nm and SNARF at 600 and 660 nm were observed under 473 nm excitation. A low excitation power was used (27 μW) for these trials to minimise any potential effects of photobleaching. The entire spectrum was then integrated and normalised to the initial peak of CPF1 at 520 nm. This was necessary because each probe has slightly different initial fluorescence values and hence raw intensity values cannot be directly compared. Furthermore, each fibre probe was only used once for detection of H_2O_2 to ensure maximum consistency between trials. Figure 3 shows an increase in normalised integrated fluorescence due to CPF1 over a 20 min exposure to H_2O_2. This time interval was dictated by the reaction rate of aryl boronates such as CPF1 with H_2O_2 [34].

Normalised fluorescence of CPF1 in the presence of 100 μM H_2O_2 is greater than for the control, which lacked H_2O_2 (Figure 3A). This increase in fluorescence is consistent with CPF1 reacting with H_2O_2 on the fibre tip. Furthermore, a plot of the rate of increase in fluorescence vs concentration of H_2O_2 (Figure 3B) clearly shows this rate increasing as the concentration of H_2O_2 increases from 0 μM to 50 μM, 75 μM and 100 μM of H_2O_2. A similar increase was observed in our previous studies on the detection of H_2O_2 with CPF1 in solution [27], and we have also shown that CPF1 is able to detect relevant H_2O_2 concentrations in reproductive biology [29]. Hence, this probe exhibits sufficient sensitivity for this biological environment.

An initial drop in fluorescence was observed for some probes (see Figure 3A), particularly the probe immersed in a 50 μM H_2O_2 solution. This is likely due to a change in emission properties of the fluorophores as the probe is moved from air into the solution. A more rapid increase in fluorescence was observed in the first 5 min, suggesting the probe is equilibrating in the new medium. After 5 min the probes show a near linear increase in fluorescence intensity. Thus, an incubation time of greater than 5 min is required to give an accurate indication of the rate of increase in fluorescence due to H_2O_2. A plateau was not observed over the time course of the experiment, suggesting quantitative data should be obtained from the rate of increase in fluorescence rather than the overall increase in fluorescence.

It is also important to note that an increase in the integrated fluorescent signal was evident, even in the absence of H_2O_2 (Figure 3A). A decrease in fluorescence would be expected if photobleaching or leaching of the fluorophore from the polymer occurred over the course of the experiment. The effect of photobleaching on CPF1 was of particular interest, since CPF1 is oxidised by H_2O_2 to give 5-carboxyfluorescein. 5-carboxyfluorescein is known to photobleach [35], a process which occurs more rapidly in the presence of reactive oxygen species such as H_2O_2 [36]. In order to accurately sense H_2O_2 with CPF1, low rates of photobleaching must be achieved. An increase in fluorescence in the absence of H_2O_2 suggests that photobleaching was not occurring on the fibre during the experiment.

Sensors **2015**, *15*, 31904–31913

This is an important observation for the practical use of the probe since the fibre's ability to sense accurately would be reduced by photobleaching of the fluorophores on the fibre tip.

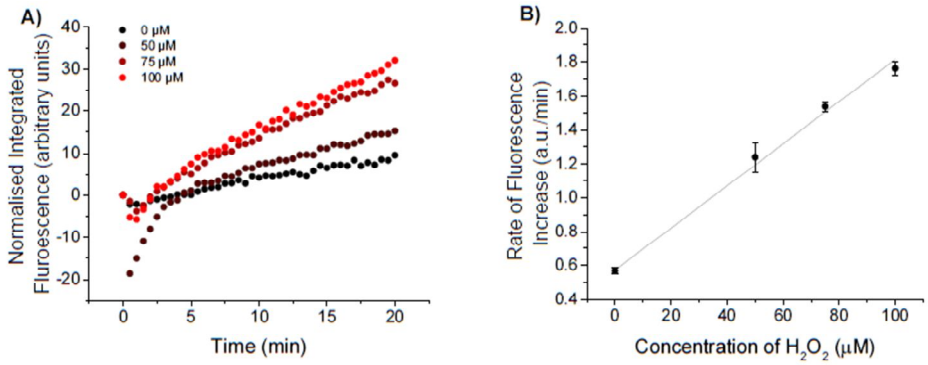

Figure 3. (A) Integrated fluorescence intensity from CPF1 using blue excitation with varied peroxide concentration in pH 7.5 buffer; 100 µM H_2O_2 shows an increased fluorescent response from the fibre without H_2O_2; (B) Slope of integrated fluorescence for increasing concentrations of H_2O_2 (0, 50, 75 and 100 µM). Error bars indicate the standard error of the calculated slope.

3.1.2. Effect of Change in pH on Detection of H_2O_2

The effect of pH on the detection of H_2O_2 in fibre was next investigated by immersing functionalised fibre tips in solutions of H_2O_2 of differing pH. Fibre tips were functionalised with CPF1 and SNARF2 as before and separately immersed in 100 µM separate solutions of H_2O_2 at a pH of 7.05, 7.55 or 8.05. A 470 nm light source was coupled into the fibre for excitation and the increase in fluorescence was recorded over 20 min. All spectra were integrated and normalised as before, with the results shown in Figure 4A. The rate of increase in fluorescence was calculated as depicted in Figure 4B. The observed rate at pH 8.05 was 1.5 times greater than the rate observed at pH 7.05 (Figure 4B).

The reaction rate of aryl boronates (such as CPF1) with H_2O_2 is higher in more basic solutions [37]. CPF1 reacts with the conjugate base of H_2O_2 (hydroperoxide ion HOO^-) [15] to give fluorescent 5-carboxyfluorescein. As the pH increases, more H_2O_2 dissociates into its conjugate base, HOO^-. The concentration of HOO^- available to react with CPF1 will therefore be higher in more basic solutions, accounting for the observed upward trend in rates due to increasing pH (Figure 4B). Furthermore, the product of CPF1 with H_2O_2 is a carboxyfluorescein, and fluorescein exhibits different quantum yields of fluorescence at differing pH [38]. Thus, the pH of the solution is highly pertinent to the accurate detection of H_2O_2. This is further highlighted by a comparison of rates of increase in fluorescence at different pH and H_2O_2 concentration, shown in Figures 3B and 4B. A rate of approximately 1.2 a.u./min was calculated for a 100 µM solution of H_2O_2 in pH 7.05 (Figure 4B). However, a similar rate was calculated for a 50 µM solution of H_2O_2 at a pH of 7.55 (Figure 3B). The observed rate in these experiments is clearly dependent on the pH, in addition to the concentration of H_2O_2. It is hence necessary that the pH of a solution must be known in order to calculate an unknown concentration of H_2O_2 resulting from an increase in fluorescence. Therefore, it is critical that the probe also incorporates a pH sensitive component to accurately determine the H_2O_2 concentration. This improves upon many systems for detection of H_2O_2 that do not simultaneously measure pH, despite the reported effect on H_2O_2 detection [15].

Sensors **2015**, *15*, 31904–31913

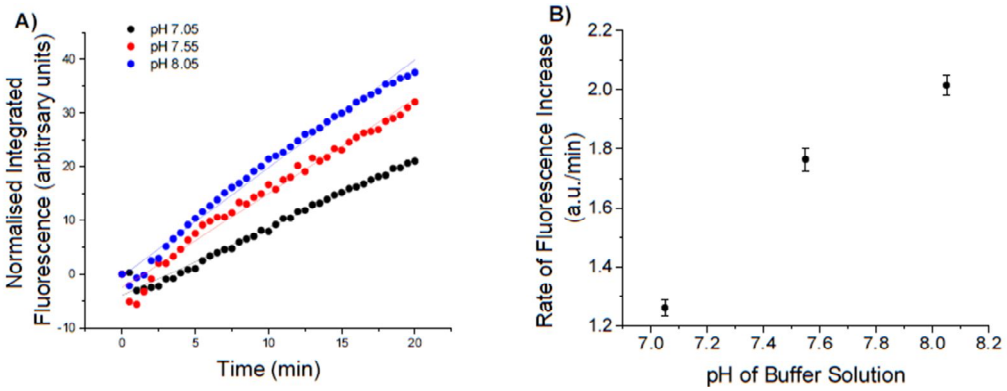

Figure 4. Response of CPF1 to 100 μM H_2O_2 in solutions that varied in pH. (A) Integrated fluorescent responses of probes to 100 μM H_2O_2 in pH 7.05, 7.55 and 8.05 over 20 min using blue excitation; (B) Rate of increase in fluorescence of each probe with H_2O_2 in each of the 3 pH solutions. Error bars indicate the standard error of the calculated slope.

3.2. *pH Sensing*

3.2.1. Initial pH Sensing

The sensitivity of these functionalised fibre tips was defined across a series of solutions of differing pH, ranging from 6.5 to 8.5. Fibres functionalised with CPF1 and SNARF2 as before were dipped into phosphate buffer solutions of each pH. 532 nm light attenuated to 13 μW was coupled into the fibre for excitation, and the fluorescent signal from immobilised SNARF2 was collected after 1 min equilibration time. The fibre was removed from solution, dried, and immersed in a subsequent buffer solution. Two fibre probes were calibrated in this way using sixteen buffer solutions ranging from pH 6.5 to 8.5 as shown in Figure 5. This broad pH range (6.4–8.5) was chosen in order to demonstrate the potential of the probe in biological applications beyond the narrower constraints of an embryo. Five additional probes were then calibrated in selected solutions across this range (see fibres 3–7 in Figure 5B). The fluorescence spectra were recorded as shown in Figure 5A. The probe exhibits a decrease in intensity of fluorescence at 600 nm as the pH increases, with an increase in intensity at 660 nm.

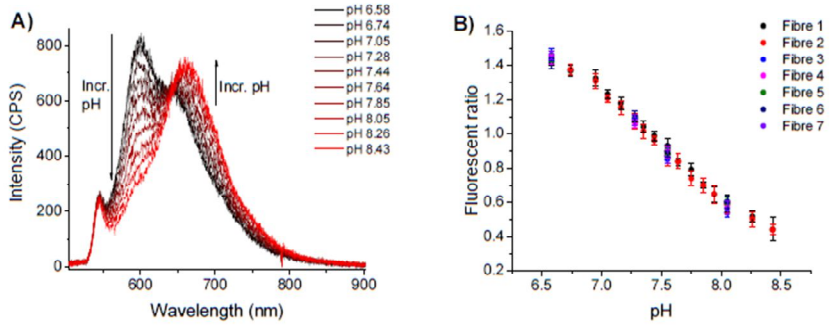

Figure 5. pH response of SNARF-2 embedded in polyacrylamide on fibre tip to varied pH. (A) Emission spectra of SNARF in various pH buffers; (B) Ratio of emission peak intensities 600/660nm shown with over multiple trials. The effect of noise was reduced by taking the mean of eight values between 598–602 nm and 558–662 nm. Error bars represent the standard deviation of these values.

Sensors **2015**, *15*, 31904–31913

The pH of the buffer was correlated with the observed fluorescent signal by calculating the ratio of intensities at 600 nm and 660 nm for each spectrum (Figure 5B). This analysis revealed an inverse correlation between this fluorescent ratio and pH of the solution. The plot also shows a linear trend over the pH range 7.0 to 8.0 and indicates that the sensor should be of use for determining the pH of a biological sample near physiological pH. Moreover, multiple fibre trials produced similar pH calibration curves (Figure 5B) showing good reproducibility between fibres. This data also indicates that SNARF2 bound to a fibre tip behaves as in solution [32]. Therefore, SNARF2 effectively senses the pH of a buffer solution when embedded in polyacrylamide on a fibre tip.

3.2.2. pH Sensing before and after Detection of Hydrogen Peroxide

The functionalised fibre probes were used to sense pH before and after immersion in H_2O_2, in order to determine if this affected the pH sensing capability. Each fibre was functionalised with CPF1 and SNARF2 and calibrated in phosphate buffer solutions of known pH as described in Section 3.2.1. The fibre tips were then immersed for 20 min in one of three H_2O_2 solutions: 100 µM solution of H_2O_2 in pH 7.55 buffer, 50 µM H_2O_2 in pH 7.55 buffer or 100 µM H_2O_2 in pH 7.05 buffer. These conditions represent the range of conditions that the probe may experience in unknown samples. Each probe was calibrated again in phosphate buffer solutions as above. The resulting pH calibration curves were plotted for each probe both before and after immersion in H_2O_2 (Figure 6).

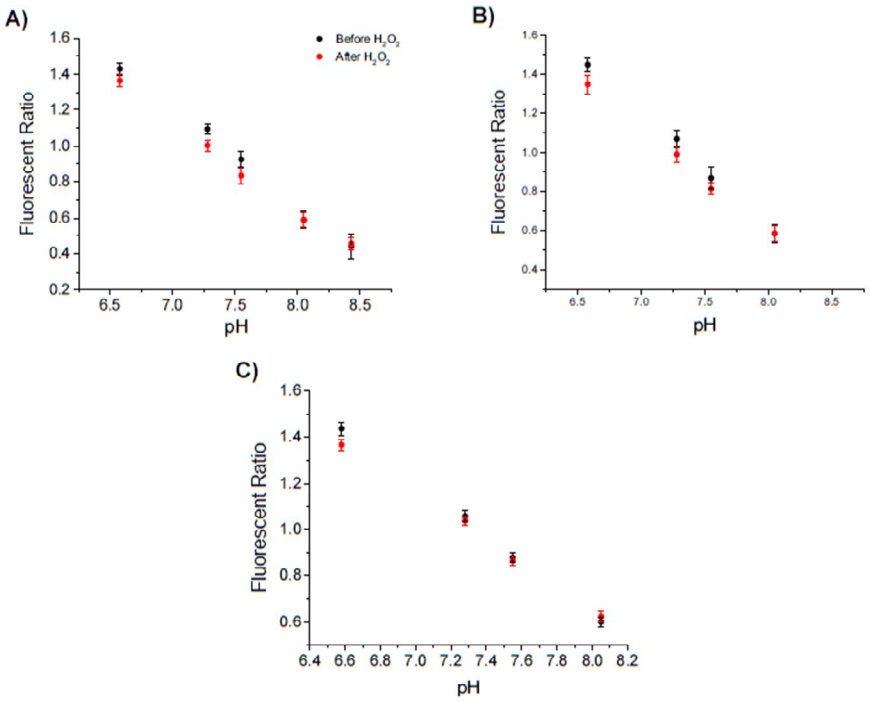

Figure 6. Sensing of pH before and after immersion in H_2O_2. Each graph plots the ratio of emission peaks of SNARF2 at 600/660 nm with the pH of the buffer solution tested, before and after solutions: (A) 100 µM solution of H_2O_2 in pH 7.55 buffer; (B) 50 µM H_2O_2 in pH 7.55 buffer; (C) 100 µM H_2O_2 in pH 7.05 buffer. Three different samples were trialled before and after H_2O_2 solutions to demonstrate the independence of the result to concentration of H_2O_2 or the pH of the H_2O_2 solution. To reduce any effect of noise, the mean of eight values between 598–602 nm and 558–662 nm is given. Error bars represent the standard deviation of these values.

Sensors **2015**, *15*, 31904–31913

The fluorescent ratios shown in Figure 6A show minimal changes before and after immersion in 100 μM H_2O_2 in pH 7.55. This indicates that reaction of H_2O_2 with CPF1 does not affect the sensing of pH by SNARF2. Figure 6B reveals similar fluorescent ratios before and after immersion in 50 μM H_2O_2 in pH 7.55 buffer. H_2O_2 again does not affect the sensing of pH over the tested concentration range, 50 μM to 100 μM H_2O_2. Figure 6C shows the fluorescent ratios of SNARF on fibre tips before and after immersing in 100 μM H_2O_2 in pH 7.05 buffer. As per the previous results, the fluorescent ratio curves did not change significantly after immersion in H_2O_2. Importantly, immersing the probe into a solution containing H_2O_2 does not affect the pH sensing capability of the probe. This demonstrates that SNARF2 can be used on optical fibre tips for sensing pH independent of the detection of H_2O_2 by CPF1.

4. Conclusions/Outlook

The tip of an optical fibre has been functionalised with two separate fluorophores, CPF1 and SNARF2 embedded in polyacrylamide, in order to allow measurement of the H_2O_2 concentration and pH respectively. The probe is demonstrated to effectively detect H_2O_2 over a physiological pH range. The probe shows a minimum detectable concentration of 50 μM H_2O_2 at pH 7.5, and pH was measured repeatedly over the range 6.5–8.5 with resolution of 0.1 pH units. Each fluorophore was used in tandem by alternating excitation sources, *i.e.*, blue excitation to interrogate CPF1 for H_2O_2 detection, and green excitation for SNARF2 to sense pH, with minimal cross-talk. The combination of pH and H_2O_2 detection also addressed the crucial issue of accurate measurement of H_2O_2 in solutions with varying or unknown pH, where the pH of the solution alters the apparent H_2O_2 concentration. This is the first example of a dual pH and H_2O_2 probe and is an important proof of concept for the detection of pH and H_2O_2 in ethically complex biological environments such as found in an IVF laboratory.

This probe could find potential application if placed near the cumulus cells of an oocyte for monitoring of extracellular pH and H_2O_2 fluxes during fertilisation and during early embryonic development. Tapering of the fibre tip could also increase the resolution from 200 μm to a few microns if required [39]. This fibre probe may offer potential not only in embryology, but a range of biological applications whereby the system must remain isolated from any external agents such as organic fluorophores.

Acknowledgments: This research was supported in part by Cook Medical Pty Ltd and Australian Research Council linkage grant LP 110200736 and the ARC Centre of Excellence for Nanoscale BioPhotonics (CNBP). This work was performed in part at the OptoFab node of the Australian National Fabrication Facility (ANFF) utilising Commonwealth and SA State Government funding. T.M. acknowledges the support of an ARC Georgina Sweet Laureate Fellowship FL130100044.

Author Contributions: M.S.P., E.P.S., T.M.M. and A.D.A. conceived and designed the experiments; J.G.T. provided biological specifications for the probe; M.S.P. performed the experiments and analysed the data; E.P.S. and A.D.A. assisted with analysis; M.S.P wrote the paper with contributions from E.P.S., A.D.A, J.G.T. and T.M.M.

Conflicts of Interest: The authors declare no conflict of interest.

References

1. Gough, D.R.; Cotter, T.G. Hydrogen peroxide: A Jekyll and Hyde signalling molecule. *Cell Death Dis.* **2011**, 2. [CrossRef] [PubMed]
2. Neill, S.J.; Desikan, R.; Clarke, A.; Hurst, R.D.; Hancock, J.T. Hydrogen peroxide and nitric oxide as signalling molecules in plants. *J. Exp. Bot.* **2002**, *53*, 1237–1247. [CrossRef] [PubMed]
3. Thannickal, V.J.; Fanburg, B.L. Reactive oxygen species in cell signaling. *Am. J. Physiol. Lung Cell. Mol. Physiol.* **2000**, *279*, L1005–L1028.
4. Szatrowski, T.P.; Nathan, C.F. Production of large amounts of hydrogen peroxide by human tumor cells. *Cancer Res.* **1991**, *51*, 794–798. [PubMed]
5. Burdon, R.H. Superoxide and hydrogen peroxide in relation to mammalian cell proliferation. *Free Radic Biol. Med.* **1995**, *18*, 775–794. [CrossRef]

6. Gerweck, L.E.; Seetharaman, K. Cellular pH gradient in tumor *versus* normal tissue: potential exploitation for the treatment of cancer. *Cancer Res.* **1996**, *56*, 1194–1198. [PubMed]
7. Engin, K.; Leeper, D.B.; Cater, J.R.; Thistlethwaite, A.J.; Tupchong, L.; McFarlane, J.D. Extracellular pH distribution in human tumours. *Int. J. Hyperth.* **1995**, *11*, 211–216. [CrossRef] [PubMed]
8. Bize, I.; Santander, G.; Cabello, P.; Driscoll, D.; Sharpe, C. Hydrogen peroxide is involved in hamster sperm capacitation *in vitro*. *Biol. Reprod.* **1991**, *44*, 398–403. [CrossRef] [PubMed]
9. Nasr-Esfahani, M.H.; Aitken, J.R.; Johnson, M.H. Hydrogen peroxide levels in mouse oocytes and early cleavage stage embryos developed *in vitro* or *in vivo*. *Development* **1990**, *109*, 501–507. [PubMed]
10. Armstrong, J.S.; Rajasekaran, M.; Chamulitrat, W.; Gatti, P.; Hellstrom, W.J.; Sikka, S.C. Characterization of reactive oxygen species induced effects on human spermatozoa movement and energy metabolism. *Free Radic. Biol. Med.* **1999**, *26*, 869–880. [CrossRef]
11. Baumber, J.; Ball, B.A.; Gravance, C.G.; Medina, V.; Davies-Morel, M.C.G. The Effect of Reactive Oxygen Species on Equine Sperm Motility, Viability, Acrosomal Integrity, Mitochondrial Membrane Potential, and Membrane Lipid Peroxidation. *J. Androl.* **2000**, *21*, 895–902. [PubMed]
12. Morado, S.; Cetica, P.; Beconi, M.; Thompson, J.G.; Dalvit, G. Reactive oxygen species production and redox state in parthenogenetic and sperm-mediated bovine oocyte activation. *Reproduction* **2013**, *145*, 471–478. [CrossRef] [PubMed]
13. Ocon, O.M.; Hansen, P.J. Disruption of Bovine Oocytes and Preimplantation Embryos by Urea and Acidic pH. *J. Dairy Sci.* **2003**, *86*, 1194–1200. [CrossRef]
14. Chan, J.; Dodani, S.C.; Chang, C.J. Reaction-based small-molecule fluorescent probes for chemoselective bioimaging. *Nat. Chem.* **2012**, *4*, 973–984. [CrossRef] [PubMed]
15. Lippert, A.R.; Van de Bittner, G.C.; Chang, C.J. Boronate Oxidation as a Bioorthogonal Reaction Approach for Studying the Chemistry of Hydrogen Peroxide in Living Systems. *Acc. Chem. Res.* **2011**, *44*, 793–804. [CrossRef] [PubMed]
16. Lin, J. Recent development and applications of optical and fiber-optic pH sensors. *TrAC Trends Anal. Chem.* **2000**, *19*, 541–552. [CrossRef]
17. Han, J.; Burgess, K. Fluorescent Indicators for Intracellular pH. *Chem. Rev.* **2009**, *110*, 2709–2728. [CrossRef] [PubMed]
18. Heng, S.; Nguyen, M.-C.; Kostecki, R.; Monro, T.M.; Abell, A.D. Nanoliter-scale, regenerable ion sensor: Sensing with a surface functionalized microstructured optical fibre. *RSC Adv.* **2013**, *3*, 8308–8317. [CrossRef]
19. Foo, H.T.C.; Ebendorff-Heidepriem, H.; Sumby, C.J.; Monro, T.M. Towards microstructured optical fibre sensors: surface analysis of silanised lead silicate glass. *J. Mater. Chem. C* **2013**, *1*, 6782–6789. [CrossRef]
20. Heng, S.; Mak, A.M.; Stubing, D.B.; Monro, T.M.; Abell, A.D. Dual Sensor for Cd(II) and Ca(II): Selective Nanoliter-Scale Sensing of Metal Ions. *Anal. Chem.* **2014**, *86*, 3268–3272. [CrossRef] [PubMed]
21. Tan, W.; Shi, Z.Y.; Smith, S.; Birnbaum, D.; Kopelman, R. Submicrometer intracellular chemical optical fiber sensors. *Science* **1992**, *258*, 778–781. [CrossRef] [PubMed]
22. Schartner, E.; Monro, T. Fibre Tip Sensors for Localised Temperature Sensing Based on Rare Earth-Doped Glass Coatings. *Sensors* **2014**, *14*, 21693–21701. [CrossRef] [PubMed]
23. Palmisano, T.; Prudenzano, F.; Warren-Smith, S.C.; Monro, T.M. Design of exposed-core fiber for methadone monitoring in biological fluids. *J. Non Cryst. Solids* **2011**, *357*, 2000–2004. [CrossRef]
24. Smolka, S.; Barth, M.; Benson, O. Highly efficient fluorescence sensing with hollow core photonic crystal fibers. *Opt. Express* **2007**, *15*, 12783–12791. [CrossRef] [PubMed]
25. Wolfbeis, O.S. Fiber-optic chemical sensors and biosensors. *Anal. Chem.* **2008**, *80*, 4269–4283. [CrossRef] [PubMed]
26. Schartner, E.P.; Tsiminis, G.T.; Henderson, M.R.; Monro, T.M. *A Comparison Between Multimode Tip and Suspended Core Fluorescence Optical Fibre Sensors*; Optical Society of America: Munich, Germany, 2015.
27. Purdey, M.S.; Schartner, E.P.; Sutton-McDowall, M.L.; Ritter, L.J.; Thompson, J.G.; Monro, T.M.; Abell, A.D. Localised hydrogen peroxide sensing for reproductive health. *Proc. SPIE* **2015**, *9506*. [CrossRef]
28. Chang, M.C.Y.; Pralle, A.; Isacoff, E.Y.; Chang, C.J. A selective, cell-permeable optical probe for hydrogen peroxide in living cells. *J. Am.Chem. Soc.* **2004**, *126*, 15392–15393. [CrossRef] [PubMed]
29. Purdey, M.S.; Connaughton, H.S.; Whiting, S.; Schartner, E.P.; Monro, T.M.; Thompson, J.G.; Aitken, R.J.; Abell, A.D. Boronate probes for the detection of hydrogen peroxide release from human spermatozoa. *Free Radic. Biol. Med.* **2015**, *81*, 69–76. [CrossRef] [PubMed]

30. Sutton-McDowall, M.L.; Purdey, M.; Brown, H.M.; Abell, A.D.; Mottershead, D.G.; Cetica, P.D.; Dalvit, G.C.; Goldys, E.M.; Gilchrist, R.B.; Gardner, D.K.; *et al.* Redox and anti-oxidant state within cattle oocytes following *in vitro* maturation with bone morphogenetic protein 15 and follicle stimulating hormone. *Mol. Reprod. Dev.* **2015**, *82*, 281–294. [CrossRef] [PubMed]
31. Whitaker, J.E.; Haugland, R.P.; Prendergast, F.G. Spectral and photophysical studies of benzo[c]xanthene dyes: Dual emission pH sensors. *Anal. Biochem.* **1991**, *194*, 330–344. [CrossRef]
32. Srikun, D.; Albers, A.E.; Chang, C.J. A dendrimer-based platform for simultaneous dual fluorescence imaging of hydrogen peroxide and pH gradients produced in living cells. *Chem. Sci.* **2011**, *2*, 1156–1165. [CrossRef]
33. Song, A.; Parus, S.; Kopelman, R. High-Performance Fiber-Optic pH Microsensors for Practical Physiological Measurements Using a Dual-Emission Sensitive Dye. *Anal. Chem.* **1997**, *69*, 863–867. [CrossRef] [PubMed]
34. Sikora, A.; Zielonka, J.; Lopez, M.; Joseph, J.; Kalyanaraman, B. Direct oxidation of boronates by peroxynitrite: Mechanism and implications in fluorescence imaging of peroxynitrite. *Free Radic. Biol. Med.* **2009**, *47*, 1401–1407. [CrossRef] [PubMed]
35. Song, L.; Hennink, E.J.; Young, I.T.; Tanke, H.J. Photobleaching kinetics of fluorescein in quantitative fluorescence microscopy. *Biophys. J.* **1995**, *68*, 2588–2600. [CrossRef]
36. Platkov, M.; Tirosh, R.; Kaufman, M.; Zurgil, N.; Deutsch, M. Photobleaching of fluorescein as a probe for oxidative stress in single cells. *J. Photochem. Photobiol. B Biol.* **2014**, *140*, 306–314. [CrossRef] [PubMed]
37. Xu, J.; Li, Q.; Yue, Y.; Guo, Y.; Shao, S. A water-soluble BODIPY derivative as a highly selective "Turn-On" fluorescent sensor for H_2O_2 sensing *in vivo*. *Biosens. Bioelectron.* **2014**, *56*, 58–63. [CrossRef] [PubMed]
38. Martin, M.M.; Lindqvist, L. The pH dependence of fluorescein fluorescence. *J. Lumin.* **1975**, *10*, 381–390. [CrossRef]
39. Leung, A.; Shankar, P.M.; Mutharasan, R. A review of fiber-optic biosensors. *Sens. Actuators B Chem.* **2007**, *125*, 688–703. [CrossRef]